MECHANISMS OF LIQUID EXTRACTION IN A PILOT PLANT SIEVE PLATE COLUMN

BY

FOLASEGUN ANTHONY DAWODU

A thesis submitted to the
University of Aston in Birmingham
for the degree of
Doctor of Philosophy

Department of Chemical Engineering
The University of Aston in Birmingham

JUNE 1983

ACKNOWLEDGEMENTS

The author wishes to express his sincere thanks to,

Professor G. V. Jeffreys
Head of the Department of Chemical Engineering
for his constant advice and interest

Dr. C. J. Mumford
in the Department of Chemical Engineering for his stimulating guidance and interest.

The technical staff of the Department of Chemical Engineering for their willingness to help.

Special thanks are extended to Miss J. Whitmore and Mrs. H. Turner for their kind help in typing this thesis.

This research is dedicated to my mother
for her continued support, encouragement and
unyielding confidence.

THE UNIVERSITY OF ASTON IN BIRMINGHAM

MECHANISMS OF LIQUID EXTRACTION IN A PILOT PLANT SIEVE PLATE COLUMN

by

Folasegun Anthony Dawodu

A thesis submitted to
The University of Aston in Birmingham
for the degree of Doctor of Philosophy
June 1983

Summary

The literature pertinent to droplet hydrodynamics and mass transfer in perforated (sieve) plate liquid-liquid extractor columns has been reviewed.

An experimental investigation was conducted in a 450 mm diameter perforated plate extractor with four plates using four different designs with holes of 1.588 mm, 3.175 mm, 4.763 mm and 6.350 mm, each with adjustable downcomers.

Hydrodynamics were studied with the system Clairsol 350 (dispersed) and water. The parameters investigated included jet length, dispersed phase hold-up, coalesced dispersed phase and flocculation zone height beneath the plates, mean drop size and drop size distribution as a function of phase velocities. The results have been compared with the published correlations based on data from laboratory scale perforated plate columns or single ground glass nozzles; a wide divergence was found. The experimental data were therefore correlated independently to predict the jet length, dispersed phase hold-up, flocculation zone height and mean drop size. The correlation for mean drop size was modified to include terms involving column dimensions. The mean drop size was correlated within ±10%. Drop size distributions were obtained by analysis of photographic prints. Mugele-Evans upper-limit function gave a better fit compared to the log-normal.

Mass transfer operation was with the system Clairsol (dispersed)-acetone-water. Both directions of transfer were investigated. In the calculation of the overall experimental mass transfer coefficient $(K_{OD})_{expt.}$ the mean driving force was determined from the concentration profile along the column using Simpson's Rule. A novel method was developed to calculate the theoretical overall mass transfer coefficient using the drop size distribution diagram to determine the volume percentage of stagnant, circulating and oscillating drops in the sample population. Individual mass transfer coefficients were estimated for the corresponding droplet states using published single nozzle drop mass transfer models. A fairly wide divergence was found between the experimental and theoretical overall mass transfer coefficients based on the other workers' models.

Recommendations for industrial column design include: (i) using drilled and punched plate to obtain effective use of all orifices and (ii) reduction in plate spacing to reduce back mixing.

Key Words

LIQUID EXTRACTION, SIEVE PLATE COLUMN

CONTENTS

CHAPTER 1

INTRODUCTION

1. INTRODUCTION

1.1 APPLICATION OF LIQUID-LIQUID EXTRACTION

Liquid-liquid extraction is one of the most important diffusional processes for the separation and purification of compounds from mixtures. It is used as an adjunct to distillation in the manufacture of organic chemicals and in the processing of crude petroleum.

Unlike distillation, the application of liquid-liquid extraction is not limited to volatile, thermally stable materials. The separation of a liquid mixture into well defined fractions, the recovery of a volatile solute or removal of impurities from solution by contacting with a partially, or completely, immiscible solvent may offer economic advantages over distillation or evaporation. Examples of the use of liquid-liquid extraction include nitration and sulphonation processes in the manufacture of intermediates, dyes, medicinal products and explosives. It is also used in the recovery of acetic acid from dilute solutions of cellulose acetate using ethyl acetate as solvent (109).

Traditional liquid-liquid extraction operations may simply be classified as:

(1) Single contact operation;

(2) Co-current (cross-flow) multiple contact

operation;

(3) Countercurrent operation, including multiple stage or continuous contacting.

In single contact operation, mixing is carried out in a single operation; the two liquids, one containing solute, are thoroughly contacted and allowed to approach equilibrium whereby solute is transferred from one phase to the other. The two phases are then separated; this is generally by gravity settling, but centrifuges may be used. The operation may be carried out either batchwise or continuously. In co-current multiple contact operation, mixing and separation of the two liquids as in the previous method, is followed by contact of treated liquid after separation, that is the extract, with fresh solvent. This operation is repeated as often as required. The process may be batch or semi-continuous in operation. This method is mostly used in the laboratory or small scale work because large volumes of solvent will be required to ensure satisfactory extraction.

In countercurrent contact operations, the two liquids are made to flow countercurrently, usually by virtue of their density difference, through some suitable form of equipment. If the equipment is a vertical column, the dense phase is introduced into the top of

the column and the light phase into the bottom; countercurrent flow of the phases is thus assisted by gravity. Continuous operation is most effective. Application of this technique includes countercurrent multiple contact operation with reflux, used for the separation of homologous substances where both the separation factor and the distribution coefficient are low. The use of reflux serves to reduce the large number of theoretical stages which would be necessary to obtain the desired purity of extract. In the case of a differential countercurrent contact process, there is no intermediate separation of the two phases. One of the phases remains as the dispersed (droplet) phase through the contactor as the phases pass in countercurrent flow. The dispersed phase is then allowed to coalesce at the end of the device before being discharged. This mode of operation is extensively used in industry.

1.2 EQUIPMENT DESIGN AND OPERATION

There is considerable variety of equipment available for liquid-liquid extraction. Industrial equipment may simply be classified (1,112,153) as follows:

(1) Equipment in which two phases are mixed to create a dispersion of one in the other with subsequent separation in discrete stages. This includes mixer-settlers. Mixer settlers

are commonly used where only a few, for example, five with a maximum of ten, contact stages are required. They are used extensively in the mineral extraction industry where fairly high flowrates are encountered. Mixer settlers are also in common use for phase reactions or neutralizations which require a residence time of 0.5 to 2 minutes or longer to reach equilibrium.

(2) Equipment in which contact between two immiscible phases is made with one phase dispersed as droplets which travel through a continuum of the other. This may be subdivided into the following groups.
Two phases separated by gravity:

(i) No additional mechanical agitation is required to maintain dispersion or redispersion.

(a) Spray columns

(b) Baffle plate columns

(c) Perforated (sieve) plate columns

(d) Packed columns

(ii) Additional mechanical agitation is required to redisperse or maintain dispersion.

(a) Rotary agitated columns, e.g. the R.D.C., Oldshue-Rushton, Wirz or Scheibel columns.

(b) Pulsed columns, e.g. the pulsed plate column or pulsed (packed) column.

(3) Equipment in which centrifugal force is used, both to create dispersion of the phases and to separate the dispersed phase, i.e. centrifugal extractors such as the Podbielniak contactor. Centrifugal extractors are used where a very short residence time and low hold-up is essential, for example in pharmaceuticals processing, or when there is a small density difference between the phases. Liquids which tend to emulsify severely can also be separated. Centrifugal extractors have relatively high capital and operating costs and the number of stages which can be accommodated in a single unit is limited.

The present work forms part of a continuing study of hydrodynamics and mass transfer efficiencies of gravity operated columns on a laboratory and pilot plant scale (5, 57, 143). Since,

(i) Many sieve plate extraction columns are in

use commercially under conditions for which phases cannot be observed and with uncertainty as to their mode of operation

and (ii) sieve plate columns appear increasingly attractive with escalating energy costs, compared with rotary agitated columns.

the present investigation is concerned with this specific design. Attention was drawn to its topicality by industry (13) since studies reported in the literature are restricted to laboratory columns, from which data are not amenable to scale up; or investigations involving single drops which take no account of the distribution of drop sizes in the swarm and the inter-drop effects in practical columns.

The objective is to further knowledge of the hydrodynamics and mass transfer characteristics of large perforated plate columns of traditional design and to improve the design procedure for specific applications.

CHAPTER 2

GRAVITY OPERATED EXTRACTION COLUMNS

2. GRAVITY OPERATED EXTRACTION COLUMNS

2.1 PRINCIPLE OF OPERATION

Liquid-liquid extraction columns are operated with the two liquid phases flowing countercurrently. The heavy phase is introduced at the top of the column and flows downward countercurrent to the light phase which is fed into the bottom, generally via a distributor. In this type of extractor, phase flows are assisted by gravity.

Spray columns are the simplest type of device. They comprise empty columns without packing or baffles as illustrated in Figure 2-1. Heavy liquid fills the whole cross section of the column and the light phase is dispersed throughout the continuous phase by injection via a perforated plate distributor, or an arrangement of nozzles. Alternatively the light liquid may be continuous in which case the distributor is located at the top. The major problem with large spray columns arises from recirculation of continuous phase (51), coalescence of the dispersed phase and incomplete mixing. Thus an increase in height equivalent of a theoretical stage (H.E.T.S.) is associated with increase in column diameter.

Baffle plate columns, illustrated in Figure 2-2, incorporate horizontal baffles to direct the liquid

GRAVITY OPERATED EXTRACTION COLUMNS

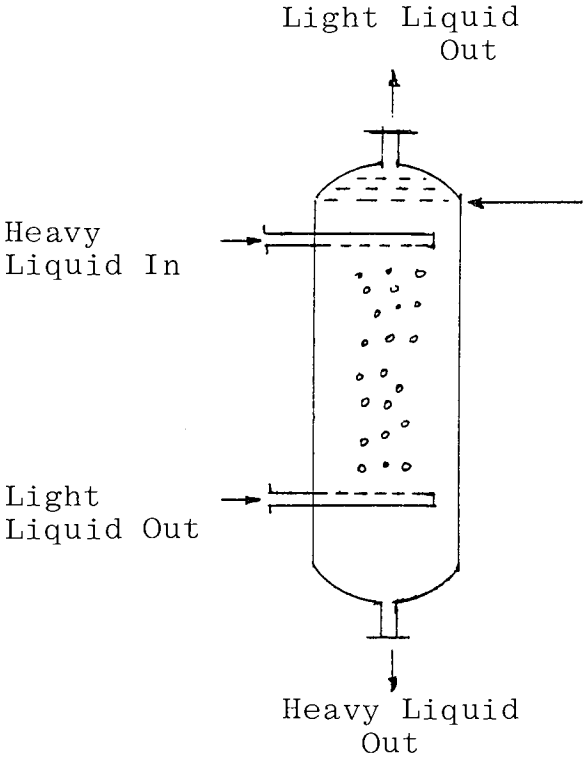

Fig. 2-1 Spray Column

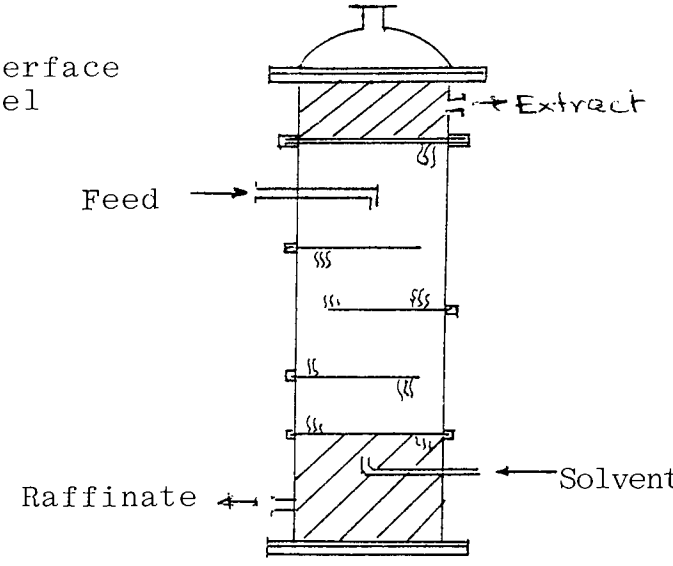

Fig. 2-2 Baffle Plate Column

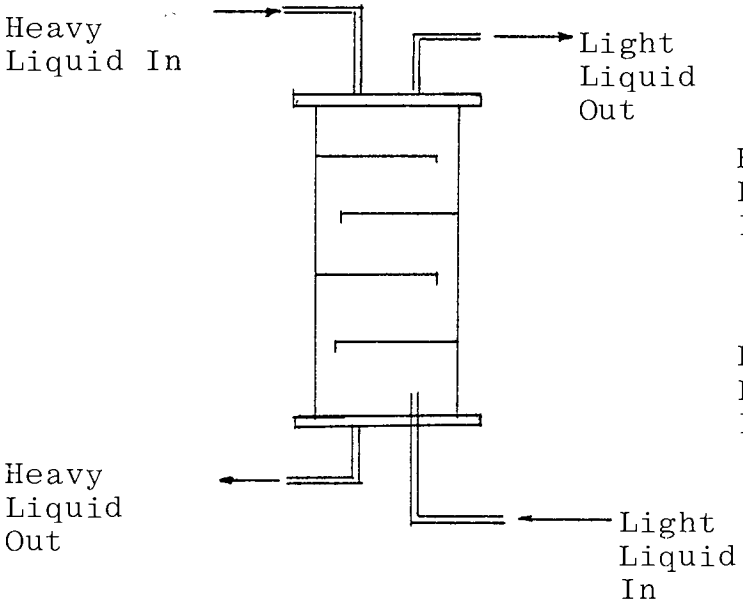

Fig. 2-3 Perforated Plate Column

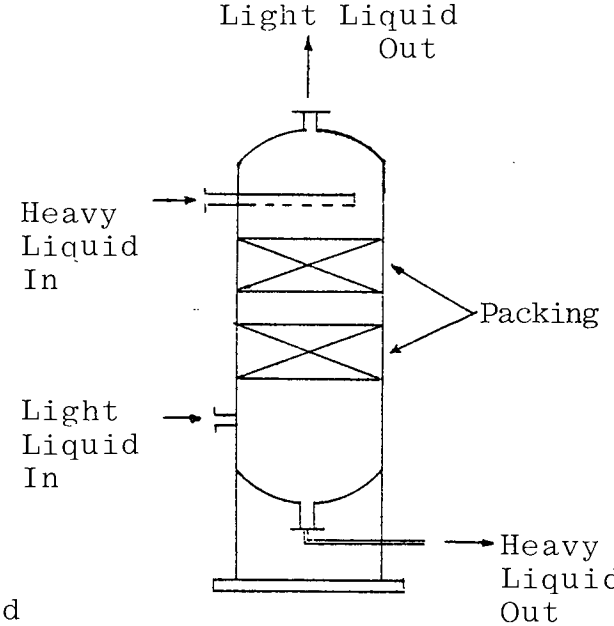

Fig. 2-4 Packed Column

flows. The purpose of internal baffling is to provide uniform mixing of the phases and thus eliminate the tendency for H.E.T.S. to increase with increasing column diameter. The simplest design of baffle column employs side-to-side flow or centre to centre-to-side flow of liquid phases.

Packed columns are simple vertical columns provided with grids to support the packing as shown in Figure 2-4. Typical packings are Raschig rings, which are randomly packed (the ratio of column diameter to packing diameter is maintained at between 8 and 10 to 1 and packing support provided every 1.83m to 2.44m of packed height) or stacked for larger sizes, or simple grids. The use of packing serves to increase the interfacial area between the phases, to improve drop size mass-transfer by inducing turbulence and also to reduce the recirculation of the continuous phase. The height equivalent to a theoretical plate varies widely and may range from 1.5m to 6m in industrial size units of 1.05m to 4.20m diameter.

The perforated plate column is one of the most widely used types of column. The dispersed phase is made to flow through a series of perforated plates mounted in the column and which, under normal operation, cause successive coalescence and redispersion of this phase. As shown in Figure 2-3, a downspout is provided

to convey the continuous phase thereby preventing recirculation. In the simplest design, the perforations are in the horizontal plane, however, a number of modified forms of perforated plate design are described by Morello and Poffenberger (109).

The use of jet-type holes with a projecting lip above the plate surface prevents wetting of the plate by the dispersed liquid (104). These columns are very effective with respect to the handling capacity and efficiency of extraction, particularly for systems of low interfacial tension. Details of practical operation are given in Section 5.

2.2 DESIGN FUNDAMENTALS

Liquid-liquid extraction processes require equipment capable of operating continuously at high contact efficiency and large phase throughputs. These criteria depend mainly on the internal structure of the contacting equipment and upon the physical properties of the liquid systems. Analysis suggests that continuous redispersion improves the contacting efficiency of an extractor. Design fundamentals should therefore involve for continuous contactors, the evaluation of:

(i) The number of transfer units for the required degree of extraction.

(ii) Height of a transfer unit (H.T.U.).

(iii) Column volumetric capacity.

(iv) System characteristics.

The concept of the theoretical stage has been used in substitution for (i) and (ii) but is only strictly applicable to discrete stage contacting. The preferred approach is, in fact, from a consideration of droplet mass transfer mechanisms and hold up as discussed in 3.2-1.

The number of equilibrium stages may be computed by simultaneously solving the material balance for the stage together with the equilibrium relationships for a given system or by graphical mass balance (153). The height of a transfer unit, or stage efficiency, is determined from pilot scale experiments or predicted from experience. Capacity may be predicted from calculation of the onset of flooding derived by empirical correlation of equations from dimensionless analysis as discussed in 3.2-2.

Wettability of the column internals has an important effect on efficiency. For optimum performance any plate, and indeed the column shell or packing, should be preferentially wetted by the continuous phase to prevent reduction in interfacial area due to coalescence

of the dispersed phase into globules or, in the extreme, channelling of the dispersed phase as jets or by wall flow. This has been investigated in a perforated plate column by Haynes et al (66) and Garner et al (38) and the effect noted by others in spray columns (153) and packed columns (71). This tendency can be avoided by using jet or nozzle type trays (i.e. in a perforated plate column). The application of a suitable hydrophobic or hydrophilic lining to the column internals may also be considered depending on which phase is dispersed.

Transfer of solute across the interface between the two immiscible liquids occurs due to the deviation from equilibrium. The rate of mass transfer is governed by an equation of the form

$$N_A = KA(\Delta C_m) \qquad 2.2\text{-}1$$

where A is the interfacial area and ΔC_m the driving force. The overall coefficient K is defined in terms of three resistances, viz. the reciprocals of the dispersed and continuous phase film coefficients k_d and k_c, plus an interfacial resistance; the latter is usually very small and may be neglected. Hence:

$$\frac{1}{K} = \frac{1}{k_d} + \frac{1}{mk_c} \qquad 2.2\text{-}2$$

where m is the distribution coefficient.

The choice of the use of k_d or k_c depends on the driving force chosen in Equation 2.2-1, i.e. whether it is referred to the continuous or dispersed phase. Generally, a high interfacial area will give a high rate of mass transfer. This is obtained by dispersing one phase as fine drops in a continuum of the other. The diffusional resistance in both phases can be minimised by maintaining a high level of turbulence in the liquids. Thus as discussed later there is, quite apart from phase separation requirements, a drop size at which A, k_c and k_d are at their optimum values.

In addition to determining the mode of solute transfer the distribution of drop sizes governs the frequency of droplet-droplet coalescence, if present, and also the extent of axial mixing. That is, the smaller an individual drop the longer it will be in the contact zone compared to the average drop and it may be highly back-mixed by any gross eddy motions in the continuous phase since it has small inertia. The balance between the optimum droplet size distribution for mass transfer and the tendency for axial mixing to increase with smaller drop sizes are significant factors in the design of gravity columns. The driving force in terms of concentration difference may also be significantly reduced by axial mixing effects. In practice the effect

of axial mixing is dependent on the characteristics and diameter/length ratio of the particular contactor and is therefore greater in large industrial columns. For example, fixed stators or packings will generally reduce axial mixing, albeit at the expense of volumetric capacity.

2.3 SELECTION OF EXTRACTOR EQUIPMENT

The choice of an extractor can involve many factors including the reliability of scale up, the number of actual stages required, flow rates, floor space available, maintenance, turn down flexibility, permissible liquid residence times and emulsification tendencies. Treybal (153) and Mumford (112) have presented reviews on this subject. Generally, the least complicated contactor which will perform the extraction with low maintenance requirements is preferred for an industrial process. Therefore the various gravity operated columns are important.

The gravity columns are generally preferred to mixer-settlers when large throughputs are to be handled since they offer economies in agitation and power requirement costs, floor space and reduced solvent inventory. They operate with relatively small amounts of hold-up of raffinate and extract. This is important when processing radio-active, flammable, expensive or

low stability materials. In extraction processes it is necessary as a final step, or in multicontact stagewise equipment, at intermediate steps, to separate the two phases. Rapid coalescence is desirable otherwise an excessive residence time is required or some of the continuous phase will be removed with the bulk dispersed phase, resulting in reduced efficiency, capacity and loss of solvent.

The gravity columns with no mechanical agitation require no moving parts and are utilized extensively in petroleum refining applications which require only a few theoretical stages, i.e. up to 12 theoretical stages. They are particularly economical devices for systems of low interfacial tension and large density difference; they are not suited to systems difficult to disperse, i.e. of high interfacial tension. Agitation by rotors or pulsing is then necessary.

In practice, spray columns are generally too inefficient for most extractions; therefore the choice may lie between a conventional packed column or a perforated plate column (assuming the special characteristics of agitated designs are not required).

Despite the fact that packing will reduce the axial mixing to much lower values than are found in spray columns, packed columns are still subject to it. In

packed columns, suitable dispersed phase hold-up and interfacial area are difficult to establish when the ratio of flow rates to the column is outside the range 0.5 to 2.0. Furthermore, mass transfer rates would generally be low for systems of low or high interfacial tension. Also packed columns are prone to liquid segregating towards the walls and the dispersed liquid flowing in the centre of the column (channelling). Therefore, redistribution of the liquid is necessary at intervals varying from three to ten times the column diameter. Furthermore, repeated impact of drops on the packing elements can result in an increase in the proportion of small drops as the dispersed phase trasverses through the column (since pairs of equi-sized drops do not result from each impact).

With regard to the drop size attained in packed columns, Pratt et al (99) demonstrated the existence of an equilibrium droplet size distribution, attained after passage through a packed section. Therefore, during their passage through the packings the droplets undergo some process, viz. breakdown of larger droplets and growth of smaller droplets, which results in an equilibrium exit droplet size distribution.

To clarify these phenomena Thornton (150) examined the size distribution of toluene droplets in an aqueous

continuous phase as they passed through 45.72cm packed section of 1.91cm Raschig rings in a column of 183.0cm high x 7.62cm diameter. The distribution became progressively skewed with column height and could be represented approximately by means of a log-normal distribution function. A stable distribution was only reached after the droplets had passed through several centimetres of packing. Consequently, the Sauter mean droplet diameter, d_{32}, became progressively smaller with column height and only approached an equilibrium value towards the top of the column. The change in d_{32} with column height could be represented by an exponential equation:

$$d_{32} = d_{32(eq)} + 0.27\exp(-0.0157h) \qquad 2.3\text{-}1$$

The equilibrium value of the mean droplet size d_{32} was found to have a value of 0.45cm for toluene dispersed in water.

Thornton (149) also examined the impact of single droplets travelling at their terminal velocity on fixed baffles representing packing elements. It was demonstrated that a critical drop size existed, below which breakdown on impact did not occur. In an energy balance, before and after symmetrical collision with a packing element an equation was derived which could be solved for the critical droplet size:

$$1.79\ (d_c^2 \Delta\rho g) + (d_c U_t^2 \rho_D) = 3.12\sigma \qquad 2.3\text{-}2$$

where U_t is the terminal velocity of the droplet on impact with the baffle, i.e. the terminal velocity in an infinite medium. However, this equation is based upon a symmetrical collision producing two equal sized 'daughter' droplets; unsymmetrical collisions are equally probable, resulting in only a small portion of the original droplet being sheared. This would produce a greater spread in the droplet size distribution.

For liquids likely to deposit 'films' plates are presumably better than packings (since wettability of packings and the vital filming by the continuous phase would be affected). In addition plates would be preferable with a 'viscous' continuous phase. However, packed columns may be preferred when solids are present in materials being handled which may block holes in the plates. Also for corrosive materials packings are cheaper than special metal plates.

CHAPTER 3

PERFORATED PLATE COLUMN CHARACTERISTICS

3. PERFORATED PLATE COLUMN CHARACTERISTICS

3.1 FUNDAMENTALS

3.1-1 DROP FORMATION AND GROWTH FROM WETTED AND NON-WETTED ORIFICES/NOZZLES

It is clear from 2.2 that a meaningful prediction of mass transfer rate and hence column design requires accurate knowledge of the interfacial area to be created between the dispersed droplets and the continuous phase, i.e. the hold-up and drop size distribution. Moreover, the settling or rising velocity of the drops and hence the volumetric capacity depends upon drop size. Thus a knowledge of the factors influencing drop sizes will have a significant bearing upon the ability to design and evaluate the performance of liquid-liquid extractors. Consideration will be limited here to drop formation phenomena at sieve plates.

Drop formation depends upon the orifice construction and the degree of wettability of the construction material by the dispersed liquid. Typically an orifice is a hole drilled through a flat plate of material. However, if the material is preferentially wetted by the dispersed phase and the injection velocity is low, the dispersed phase tends to spread over a wider surface than the hole perimeter. This may result in drops of dispersed liquid breaking away from a reservoir of liquid around the hole at irregular intervals. Thus the

drop size will be large and variable. At higher dispersed phase velocities the characteristics change to resemble those with non-wetted plate materials.

If the orifice plate is not preferentially wetted by the dispersed liquid, or if the orifice is punched in the direction of dispersed phase flow, that is, of the projected nozzle type shown in Figure 3.1-1, the drop size is more uniform. Since wetting conditions are difficult to predict and may change in service due to grease or scum deposition, projected nozzles are preferred in all cases.

Figure 3.1-2 illustrates the changes that occur as the flowrate through the nozzle varies. At low velocities (U_N = 1 - 10cm/sec), drops form individually at the nozzle tip. They grow in size and eventually break away as single uniform drops when the buoyancy force overcomes interfacial tension. As the velocity is increased (U_N = 3 - 12cm/sec), a cylindrical neck of dispersed liquid extends from the nozzle and drops form by jet disintergration. Increasing the velocity further (U_N = 16 - 25cm/sec), lengthens the jet which appears as a smooth column of liquid with occasional transient lumps. Finally the jet takes on a ruffled appearance at the downstream and the drops formed are less uniform than in the earlier stages. This behaviour occurs at or near the maximum jet length corresponding to the critical

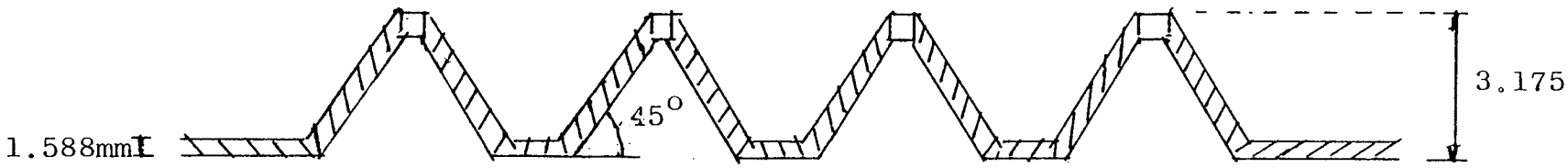

Fig. 3.1-1 Drilled and Punched Plate Orifice - with Typical Dimensions (104)

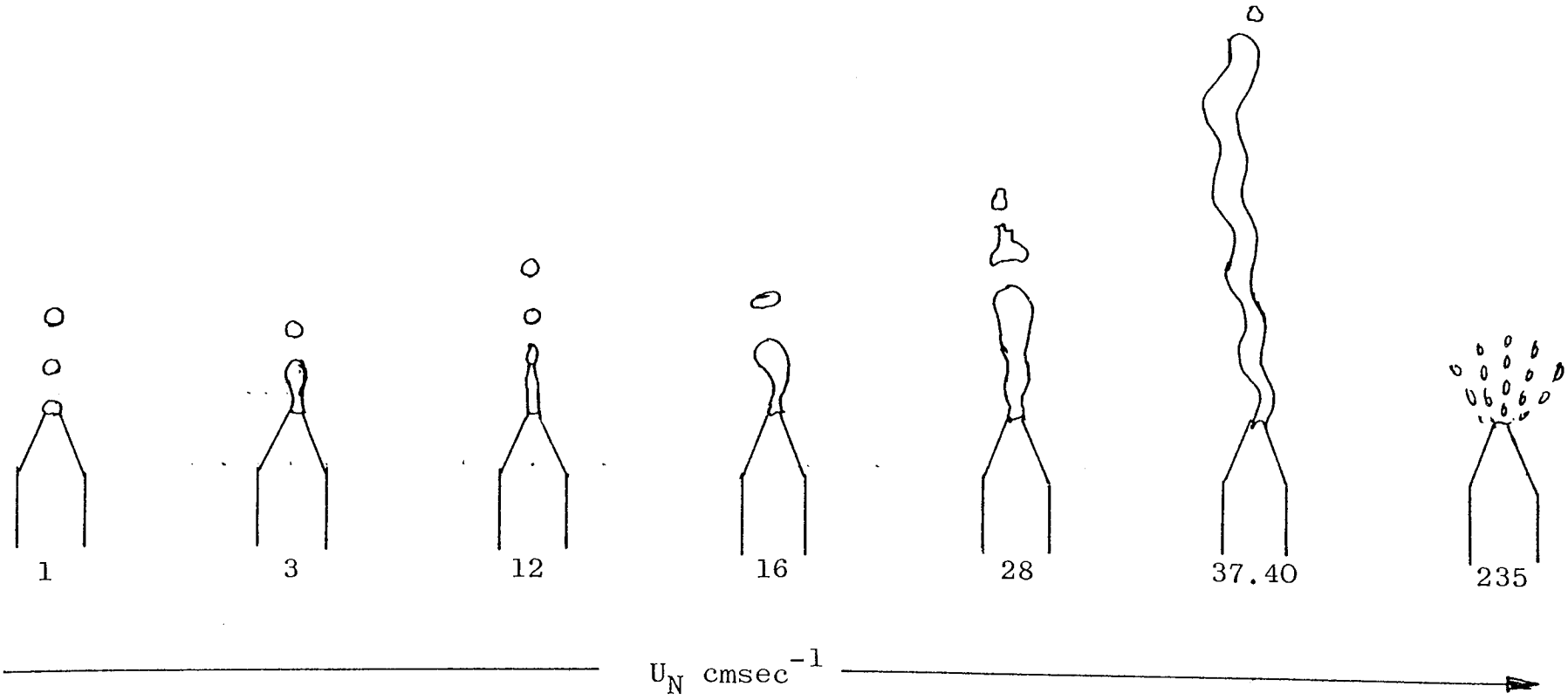

Fig. 3.1-2 Jetting Characteristics

velocity. Increasing the velocity still further decreases the jet length and the uniformity of drop size, the jet break up point retreats to the nozzle tip and a non-uniform spray of very small drops is produced.

On a laboratory scale ground glass nozzles of close tolerance or diameter, and meticulously cleaned, have been used for single drop and drop swarm studies (67, 83, 105, 119, 156). However, these are impracticable on a pilot or industrial scale. To obtain reproducible performance in practical extraction columns it is desirable for the plate to be wetted by the continuous phase. Furthermore, the range of orifice velocities of interest, a control parameter in the present work, is between the two extremes discussed above. Velocities in this range are commonly encountered in industrial equipment.

Whilst most workers are in general agreement with the above qualitative description their results differ quantitatively. Among the correlations for drop size from wetted nozzles and orifices those of Hayworth and Treybal (67), and Null and Johnson (119) are widely accepted; both sets of researchers present photographs which illustrate the drop formation processes.

At low injection velocities, the drop volume V may be obtained by equating buoyant and interfacial forces.

Harkins and Brown introduced a correction coefficient which accounts for the drop fraction that remains at the nozzle when the drop detaches;

$$V_o = \frac{\pi D_N \sigma}{g\Delta\rho} \cdot f \qquad 3.1\text{-}1$$

f was shown to be a function of the ratio $\frac{D_N}{2a}$, a being Laplace constant,

$$a = \left(\frac{2\sigma}{g\Delta\rho}\right)^{0.5} \qquad 3.1\text{-}2$$

For cases where the velocity effect is important, Hayworth and Treybal (67) extended the analysis of Harkins and Brown (60) by adding correction terms to equation 3.1-1 to allow for inertial or viscous forces. Their proposed correlation is

$$V + 4.11 \times 10^{-4} V^{2/3} \left(\frac{\rho D U_N^2}{\Delta\rho}\right) = 21 \times 10^{-4} \left(\frac{\sigma D_N}{\Delta\rho}\right) + 1.069 \times 10^{-2} \left[\frac{D_N^{0.747} U_N^{0.365} \mu_c^{0.186}}{\Delta\rho}\right]^{1.5} \qquad 3.1\text{-}3$$

They also presented a nomogram from which the drop diameter could be obtained without long iterations.

Null and Johnson (119) derived a correlation for drop volume using a geometrical approach, but based on actual observation of drops during formation. Two phases

of drop formation were considered, that is (i) the period during which the drop is growing but has not begun to break away from the nozzle and (ii) the period during which the process of breaking away is actually occuring. Their model appears to describe liquid-liquid drop formation satisfactorily and predicts drop volumes for flow rates in the range of

$$0 \lesssim \left(\frac{D_N U_N^2 \rho_D}{g_c \sigma}\right)^{0.5} \lesssim 1.4 \qquad 3.1\text{-}4$$

Keith and Hixson (83) presented plots of drop volume and jet length versus flowrate for selected systems but did not provide any generalized correlation.

Meister and Scheele (105) predicted the drop volume based upon a two stage drop formation process. In the static stage, the buoyancy force due to density difference between the two phases and the kinetic force associated with the liquid flowing out of the nozzle is assumed to separate the drop from the nozzle; whilst the interfacial tension force at the nozzle tip and the drag force exerted by the continuous phase tends to retain the drop on the nozzle. During the second stage, when the lifting force exceeds the restraining force, the drop begins to break away from the nozzle. This theoretical consideration led to a correlation equivalent to

$$V = V_o \left[\frac{1+5\mu_c U_N D_N^2}{\sigma D_F^2} - \frac{\rho_D D_N U_N^2}{3\sigma} + 1.22 D_N \left(\frac{g\Delta\rho U_N^2 \rho_D}{\sigma^2} \right)^{1/3} \right] \qquad 3.1\text{-}5$$

For liquid-liquid systems Funijawa et al (36) found that jetting velocity could be correlated by

$$U_j = 4.4\sigma^{0.2} D_N^{-0.5} \qquad 3.1\text{-}6$$

where U_j is jetting velocity, cm sec^{-1}.

Meister and Scheele (106) later modified their correlation to predict formation under jetting conditions. This modification leads to

For $U_N = U_j$

$$V = V_o \left[\frac{D_j}{D_N} + \frac{5\mu_c U_N D_N D_j}{\sigma D_F^2} - \frac{\rho_D U_N^2 D_N^3}{3\sigma D_j^2} + 1.22 \left(\frac{U_N^2 D_N D_j^2 \rho_D g\Delta\rho}{\sigma^2} \right)^{1/3} \right] \qquad 3.1\text{-}7$$

D_j is the average jet diameter which may be different from the hole diameter D_N. These authors also suggest a mechanism of jet formation based on jetting velocity. It is assumed that a jet will form if there is sufficient downward force at the nozzle exit ($\rho_d > \rho_c$). For a drop not large enough for detachment the liquid velocity leaving the nozzle will enlarge the drop or

lower it to form an enlongated imperfect cylinder of liquid, thus forming a jet. Several correlations to evaluate the jetting velocity are available in the literature (30, 36, 21, 141, 142).

Rayleigh (127) attributed the instability of a cylindrical liquid jet to disturbances of wavelength initiated at the nozzle exit as a result of density and pressure flu ctuations. By neglecting the viscosities of both fluids, the disturbance of maximum amplitude was shown to have a wavelength λ given by

$$\lambda = 4.508 D_j \qquad 3.1\text{-}8$$

Other investigators took account of jet viscosities or of the two fluid viscosities (107, 151, 160).

From a theoretical consideration of correlations of dropsize, Christiansen and Hixson (21) related the nozzle velocity U_N at which the maximum velocity occurs with the system properties for binary liquid pairs. By direct observation of jet disturbances and measuring drop and jet diameter they obtained results of the form

$$U_{NM} = 2.69 \left(\frac{\sigma/D_j}{0.5137\rho_D + 0.4179\rho_c}\right)^{\frac{1}{2}} \left(\frac{D_j}{D_N}\right)^2 \qquad 3.1\text{-}9$$

The nozzle/jet diameter is given empirically by the following equations

$$\frac{D_N}{D_j} = 0.485 \left[\frac{D_N}{(\sigma/g\Delta\rho)^{0.5}} \right]^2 + 1, \text{ for } \frac{D_N}{(\sigma/g\Delta\rho)^{0.5}}$$

$$< 0.785 \qquad 3.1\text{-}10$$

$$\frac{D_N}{D_j} = \frac{1.51 D_N}{(\sigma/g\Delta\rho)^{0.5}} + 0.124 \text{ for } \frac{D_N}{(\sigma/g\Delta\rho)^{0.5}} > 0.785$$

$$3.1\text{-}11$$

The effect of masstransfer on drop formation is difficult to quantify, but by analogy with the effects of solute transfer discussed in 4.1-1, the effects would be expected to depend upon the rate and direction of transfer.

It is inherent in the application of any of the above correlations to the prediction of drop sizes from multi-orifice plates that there is no interference between drops forming from adjacent orifices. For this purpose the experimental data are compared with the above correlations, so as to equate the fundamental studies on single drops and interfaces during mass-transfer with the behaviour of drop populations in a large scale sieve plate column.

3.1-2 DROP SHAPE

The shape of a drop moving in a liquid continuous

phase deviates to some extent from a perfect sphere. At low droplet Reynolds number ($Re = \frac{d_p U \rho}{\mu} \leq 200$), the droplet shape approximates to a sphere. However, at higher Reynolds numbers the droplet is distorted from a spherical shape.

The shape of the drop is of primary importance in the development of a theoretical model for mass transfer, since the change in shape affects both the interfacial area and the continuous phase mass transfer coefficient. Consequently, the dynamics of drops will be reviewed here, prior to discussing mass transfer during drop formation.

Bashforth and Adams (8), theoretically established the shape for a stationary bubble or a pendant drop by balancing pressure inside and outside the surface. Using a numerical method, they prepared tables from which the shape could be drawn.

Licht and Pansing (100) in deriving a theoretical expression for masstransfer during drop formation, assumed the drop to grow as a uniform sphere. For this simple case they obtained the surface area as a function of time as

$$A_s = 4.834\ V_{f,t}^{2/3}\ t^{2/3} \qquad 3.1\text{-}12$$

However, Hughes and Gilliland (73) considered it

impossible to calculate the theoretical shape of a deformed drop, because the local static pressure exerted on the outside of the drop is itself a function of the drop shape and is not exactly even for a sphere. A numerical solution may therefore be required.

Satapathy and Smith (132) give a detailed description of the relationship between drop formation and Reynolds numbers. They described the mechanism of a vortex formation and break-up as the drop Reynolds numbers increased from 4 to 300.

From photographic records of drop distortion, Licht and Naresumaharmurty (101) observed that small drops, i.e. < 0.2cm were less deformed and more spherical than larger ones.

Heertjes and De Nie (68) measured the surface area of growing drops from still photographs and found a linear relationship between the surface area and volume. Angelo et al (4) confirmed the above findings photographically; for a constant feedrate, both the volume and surface area increased linearly with time.

Krisma et al (89) studied the fall of drops of several different immiscible liquids in water. They observed that for each dispersed phase liquid, there were characteristic ranges of diameter in which the drop was spherical, oblate spheroidal or indefinable in

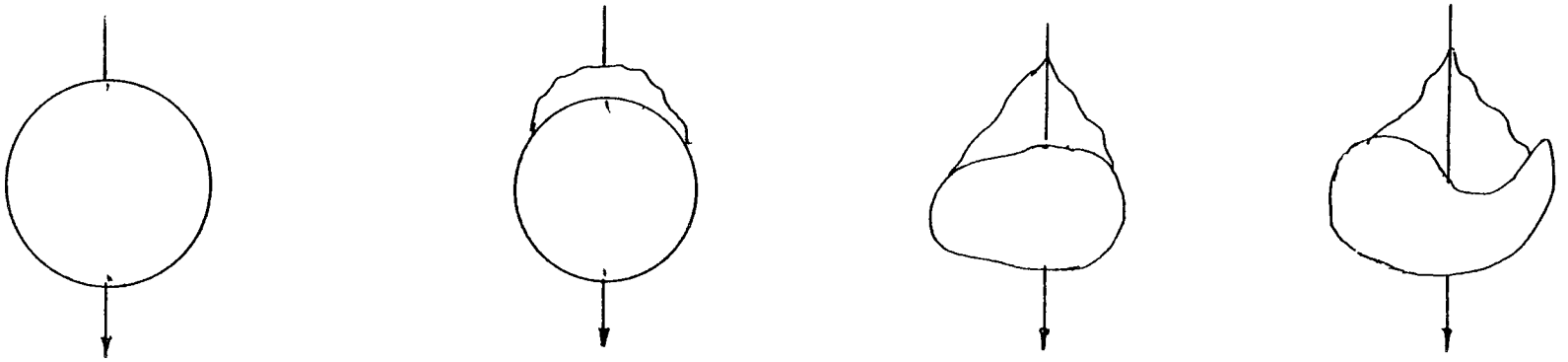

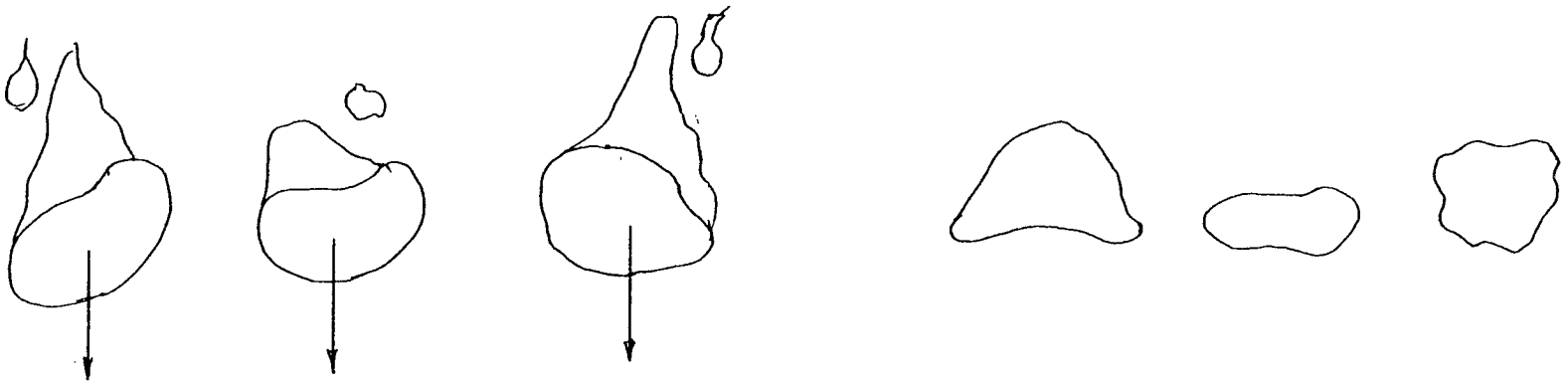

Fig. 3.1-3 Relationship between Drop Shapes and Reynolds Number - for falling droplets (132).

shape.

It is clear from the above that knowledge of drop shapes would result in more accurate estimation of interfacial area and of the resistance to mass transfer in the continuous phase flowing past deformed droplets for sieve plate column design.

3.1-3 INTERNAL CIRCULATION IN DROPS

Circulation in drops and bubbles may arise naturally or result from the action of some external forces. A high initial rate of circulation in a drop can be caused by the break-away of the drop from the nozzle; or natural circulation inside the falling drop can occur by a direct transfer of momentum across the interface. If the viscosity of the continuous phase is high, circulation within the drop can concievably occur due to this. Circulation has been observed even at a Reynolds number of 0.0003. Thus it is evident that circulation within the drop becomes appreciable whenever skin friction is a major portion of the surface forces.

Hadamard (58) postulates that the drag on the surface of fluid droplets moving in a fluid medium causes internal circulation. Consequently, droplets should fall more quickly than solid spheres in the same fluid medium,

since the resistance to motion is less, as there is drag. Boussinesq (10) modified this theory on the basis that there are two surface layers present on the droplet and this surface viscosity causes a resistance to motion of the surface, and thus the velocity of internal circulation.

The above two theories, however, indicate that there is circulation in fluid droplets in all circumstances. Garner and Skelland (44) studied the effect of internal circulation within droplets on liquid mixing. They found that circulation depends largely on the diffusion occuring in the drop and takes place only above a fairly closely defined Reynolds number.

Garner and Skelland (47) investigated the fall of nitrobenzene drops in water with mass transfer taking place. It was pointed out that internal circulation is not necessarily restricted to systems where mass transfer is taking place but occurs in any event. They found that the transition from a stagnant to circulating condition is not sharp but takes place over a two-fold increase in drop diameter. It was also observed that at a critical Reynolds number transition from stagnancy to circulation occurred with the droplets.

$$Re_{critical} = \frac{100}{\mu_c}\, 4/3 \qquad \mu_D = 1\text{-}1.5cp \qquad \sigma = 1\text{-}8 dynes/cm \qquad 3.1\text{-}12a$$

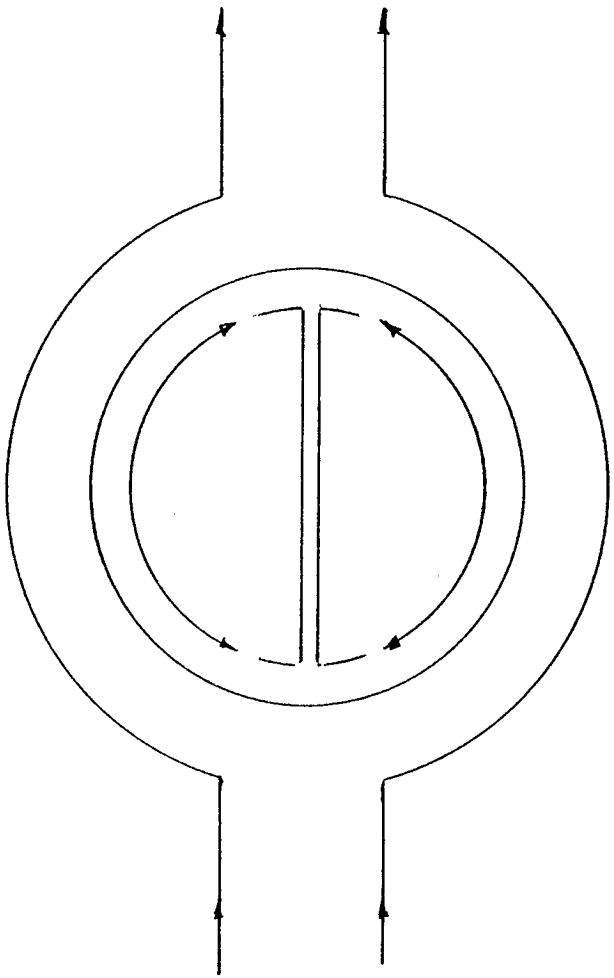

(a)

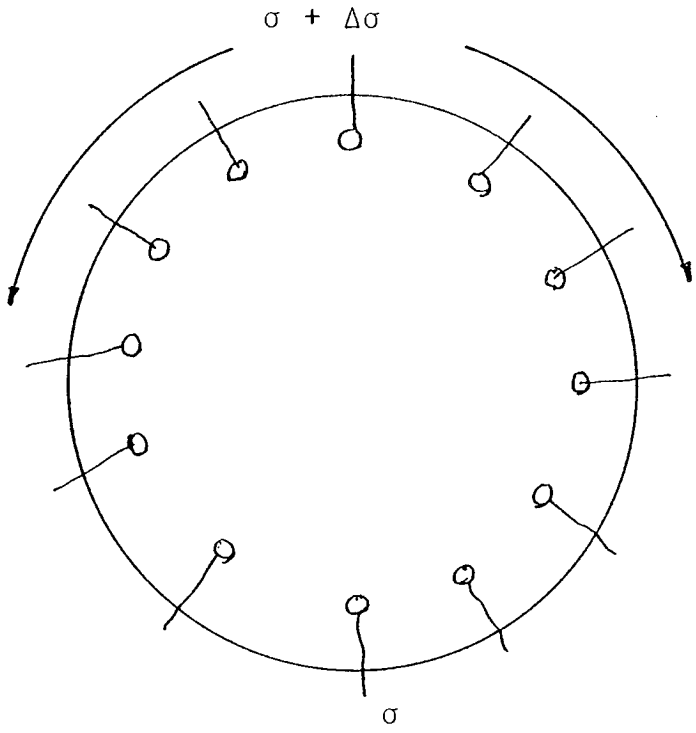

(b)

Opposing Effect on Surface Tension Gradient

Fig. 3.1-4 Circulation Patterns within a Falling Drop

Heertjes et al (69) demonstrated the presence of internal circulation in rapidly growing drops. Isobutanol drops coloured blue with cobalt chloride were formed in water; above a certain water content in the drop the blue colour changed to pink. By means of this colour change they observed that drops formed in 1.3 sec. or less showed a very marked circulation and no circulation occurred for formation times larger than 1.5 sec.

Elzinga and Bachero (32) investigated several liquid-liquid systems and suggested the most likely mechanism underlying the observed reduction in internal circulation caused by surface active agents. Surface active matter accumulates on the downstream surface of the drop since on reaching the interface at the upstream portion it is dragged by passing fluid to the downstream location. Then, because of the composition gradient created, an interfacial tension gradient also exists and the latter gradient opposes the surface flow.

The relevance of the phenomena discussed above to plate column operation may be summarised:

(i) It renders possible a combination of the hydrodynamic equations with appropriate equations governing mass transfer in the drops so that the resulting mass transfer

model would be more realistic.

(ii) It demonstrates that effective diffusivity in liquid drops in a counterflow column is likely to be increased compared with co-current.

(iii) It may explain deviations between experimental and theoretical mass transfer data if trace surface-active impurities enter, or accumulate in, large scale, e.g. industrial columns.

3.1-4 TERMINAL VELOCITY AND DRAG COEFFICIENT

In column operation with countercurrent phase flow the settling or rise velocity of individual drops or drop swarms is of importance. These velocities depend not only on drop size, but also on the phenomena occuring at the phase boundary. Therefore, knowledge of the drag coefficient is necessary to determine the rise, or settling velocity of the drops.

It has been shown (80, 86, 132) that drop resistance to flow decreases with increasing Reynolds number until a certain value is reached then begins to rise sharply as shown in Figure 3.1-5. This increase in resistance depends upon the drops losing their spherical shape and taking up an ellipsoidal shape. The resistance then

increases until the inertial forces acting on the drops cause them to disintegrate. The lower the surface tension, the smaller the force needed to deform and rupture the drops. Hu and Kintner (72) on the basis of numerous measurements presented a correlation curve shown in Figure 3.1-6, which can be used directly to predict terminal velocity, drag coefficient, Reynolds number and Weber number for any equivalent drop size. All the systems studied to derive this correlation were of high interfacial tension (σ > 20 dynes cm^{-1}) and low density difference. The effects of elevated field phase viscosity and low interfacial tension were not covered. However, Warshay et al (159) later reported that the correlation will also predict velocities in systems where σ < 20 dynes cm^{-1}, if the field viscosity was similar to that of water. Their generalised correlation, a plot of $C_D We Z^{0.15}$ Vs $Re Z^{-0.15}$ was capable of bringing together all the data in a single curve. The relationship for the peak velocity is

$$U_t = \frac{1.23(\frac{\sigma}{\mu_c})}{Z^{0.238}} \qquad 3.1\text{-}13$$

$$\text{where } Z = \frac{\sigma^3 \rho_c^2}{g \Delta\rho \mu_c^4} \qquad 3.1\text{-}14$$

and demonstrates that the velocity is dependent only upon the physical properties.

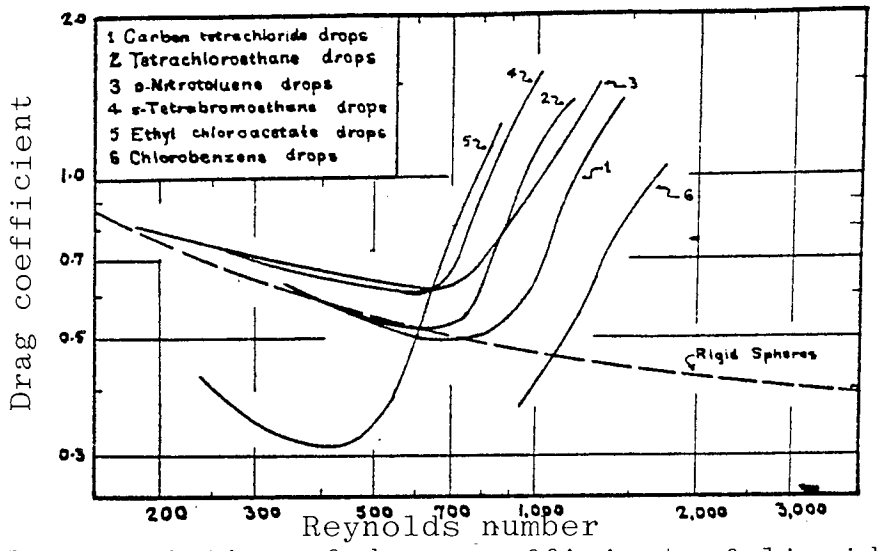

Fig. 3.1-5 Variation of drag coefficient of liquid droplets with Reynolds number (101)

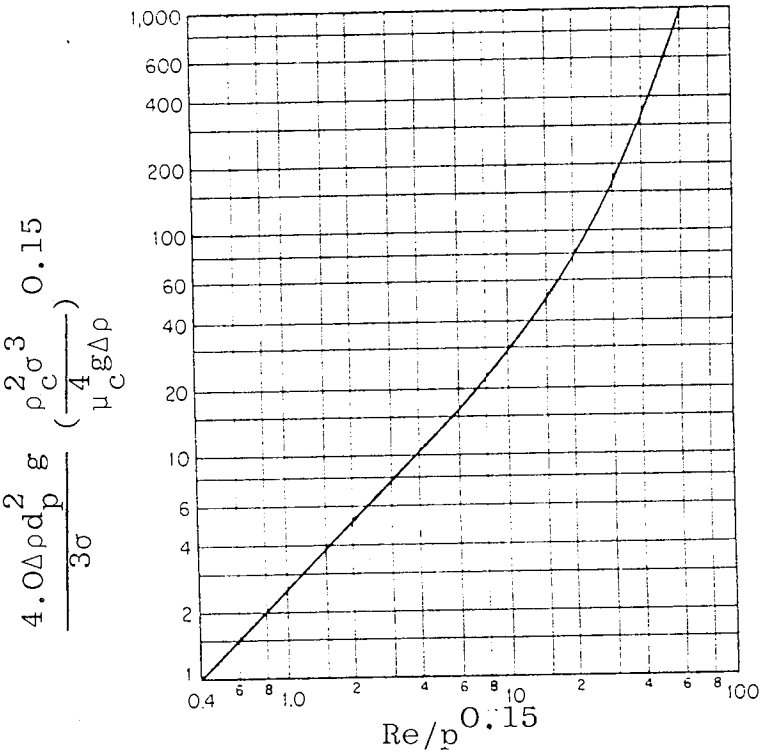

Fig. 3.1-6 General correlation of the Hu and Kintner (72)

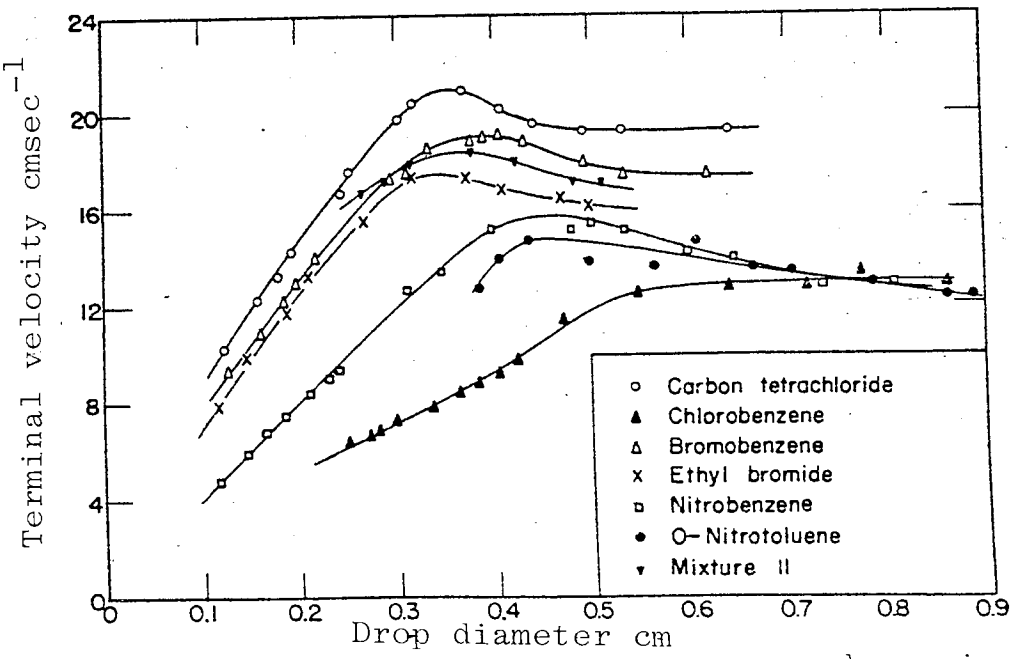

Fig. 3.1-7 Variation of terminal velocity with drop size (101)

Johnson and Braida (79) worked with liquids having viscosities up to 30 centipoise and found that their data lay parallel to the correlation curve of Hu and Kintner (72). By multiplying the group $C_D We Z^{0.15}$ by the viscosity correlation $(\frac{\mu_w}{\mu_c})^{0.14}$ they found that their data points fell directly on the curve of Hu and Kintner (72). Johnson and Braida (79) also found that by increasing the viscosity of the continuous phase to a high enough value, oscillation ceased and consequently they obtained no values at the upper end of their plot.

Licht and Narasimharmurty (101) presented drop velocity data and a correlation which permits a computation of the velocity in the region of large drops where the velocity is nearly constant as shown in Figure 3.1-7. The rise of their curve above that for rigid spheres indicates that the drops studied commenced to circulate internally at a smaller drop size than usual. This may well have been due to a higher purity of materials compared to those of others.

Klee and Treybal (86) presented two dimensional correlations for predicting drop velocity from drop diameter and the pertinent physical properties of the system. They divided the velocity-size curve into two regions and arrived at an equation for each. One of these applied to small drops, for which velocity increased rapidly with increase in drop size, and the other

for the region in which velocity was nearly constant and independent of drop-size.

$$\text{REGION 1:} \quad U_t = \frac{38.3\ d^{0.70}\ \Delta\rho^{0.58}}{\mu_c^{0.11}\ \rho_c^{0.45}} \qquad 3.1\text{-}15$$

$$d < d_t = 7.25\ \left(\frac{\sigma}{g\Delta\rho Z^{0.15}}\right)$$

where d_t is drop diameter at terminal velocity, cm and d is drop diameter or equivalent spherical diameter, cm.

$$\text{REGION 2:} \quad U_t = \frac{17.6\ \mu_c^{0.10}\ \sigma^{0.18}\ \Delta\rho^{0.28}}{\rho_c^{0.55}} \qquad 3.1\text{-}16$$

$$d > d_t$$

The peak velocity between the two regions was not accounted for, and many of the systems exhibited a low interfacial tension (σ = 0.3 to 42 dynes cm^{-1}), but none were of high field viscosity. These two equations were confirmed reasonably well by the data of Hu and Kintner (72) but less closely by that of Licht and Narasimharmurty (101) whose materials were of commercial grade and unpurified.

Elzinga and Bachero (32) investigated the effect of surface active agents on terminal velocities and found that the velocity of uncontaminated drops was considerably higher than that for contaminated drops.

They reported terminal velocities higher than those of Klee and Treybal (86) and Hu and Kintner (72) for the uncontaminated drops. Elzinga and Banchero (32) also noted that after drops formed and broke away there was a short period in which they accelerated to their terminal velocity. It was found that these drops, in the size range 1 to 10mm, had reached at least 95% of their terminal velocity after travelling 5cm.

Levich (96) studied the changes in drop behaviour resulting from small amounts of surface active agents adsorbed at the liquid-liquid interface. He suggested that during the fall of a drop, the adsorbed material is swept towards the rear of the drop and the surface concentration of the surface active molecules on the upstream part of the drop is less than the surface concentration on the downstream part. This results in a gradient of the surface pressure which resists further compression of the film and produces an immobile surface at the rear of the drop. The reduction in the surface flow causes a shift in the position of flow separation towards the front of the drop and this increases the drag coefficient and also alters the wake structure.

Griffith (54) related the terminal velocity of drops and bubbles at low Reynolds number to the cap size and then to the type and amount of surfactant. Experimental data were obtained which agreed well with

the theory except in two instances.

Lochiel (103) presented an equation for the drag coefficient at high Reynolds numbers by using Chao's (17) analysis for flow inside and outside a fully spherical drop and then included the effect of an adsorbed surface active agent to modify the interfacial shear balance.

From the above correlations and results it is clear that liquid drops do not always behave like a rigid sphere or as an ellipsoid. This discrepancy should, therefore, be anticipated when designing a sieve plate column in as much as the nature of liquid interface is not the same as that of a liquid-solid boundary and the shape of the drop is not always rigid and spherical or ellipsoidal. Allowance for the effects would provide more accurate and reliable information with regard to interfacial area, residence time distribution, hold-up and hence column throughput.

3.2 COLUMN HYDRODYNAMICS

3.2-1 PERFORATED PLATE GEOMETRY

The mixing process between two given phases is largely a function of geometry and also the flow behaviour of both phases. Therefore extractor design is necessarily based upon consideration of the internals. With agitated columns such as the Rotating Disc Contactor which have the additional variable of agitator speed, design is mostly based on factors such as vertical and horizontal baffle geometries and upon agitator size and shape. In an unagitated gravity column such as the perforated plate column, internal design includes the size, arrangement, number and type of perforations in each plate; plate spacing; and downspout size and positioning.

Perforations are usually 1.587 to 6.35 mm in diameter and they are arranged on the corners of triangles or squares 12.71 to 19.05 mm apart (153). The smaller hole size is preferred in the case of systems of high interfacial tension (σ<20 dynes.cm^{-1} or 0.02 Nm^{-1}).

Tray spacing of 15.24 to 60.96 cm are common (132) and they are set by a number of considerations. In general experiments have shown that mass transfer rates

will usually be higher and flow capacities smaller, the smaller the tray spacing. For successful operation of a large column, where periodic cleaning may be necessary, a minimum tray spacing of 40.64 to 45.72 cm is reasonable. This allows for man-ways or handholes in the shell.

Downspouts are considered to be best set flush with the plate from which they lead, with no weir (113). This prevents pools of dispersed phase from forming on the plate and interfering with the discrete drop formation from the performations. The downspouts should also extend beyond the accumulated layer of coalesced dispersed phase under each plate. Their cross-sectional areas should be such that the linear velocity of the continuous liquid in the downspout will not exceed the terminal settling velocity of some arbitrary small droplet of dispersed liquid, e.g. 0.793 or 1.587 mm in diameter, for the range of liquid-liquid systems normally encountered. The latter considerations help prevent recycling of large amounts of entrained dispersed liquid which might result in premature flooding. The free area for flow of continuous

liquid between the end of the downspout and the plate to which is leads should be larger than the downspout cross-section. This tends to reduce the linear velocity of flow across the plate and hence past the drops, thereby increasing the contact time during the period of drop formation and initial acceleration.

3.2-2 HOLD-UP

Efficient dispersion to generate a large interfacial area is of prime importance for mass transfer in liquid-liquid systems. A knowledge of the fractional hold-up of the dispersed phase x, together with the drop size distribution, for a given system and plate provides a means of calculating the interfacial contact area below loading rates. Thus,

$$a = 6 \frac{x}{d_{32}} \qquad 3.2\text{-}1$$

where a = interfacial area per unit volume.

$$d_{32} = \frac{\Sigma\ nd^3}{\Sigma\ nd^2} \qquad 3.2\text{-}2$$

where n = number of drops

d_{32} = Sauter mean drop diameter.

d = drop diameter, cm

In the operation of perforated plate columns, three types of hold-up may be identified; static hold-up, operational hold-up and total hold-up. Static hold-up may be defined as the volume of the dispersed phase coalesced under the plates, and the operational hold-up is the volume of the dispersed drops suspended in the continuous field phase during steady state operation of the column. The total hold-up is given by the sum of static and operational hold-ups

$$\phi_t = \phi_{op} + \phi_s \qquad 3.2\text{-}3$$

where ϕ_t is the total hold-up.

The coalesced volume (static hold-up) under each plate would be expected to make little contribution towards mass transfer performance but a knowledge of this will be useful in showing the minimum amount of solvent

required to operate the column, and also in the estimation of the minimum compartment height. The interfacial area of contact between the dispersed phase droplets and the continuous phase depends on the operational hold-up and the mean size of the dispersed phase droplets.

$$A = aV \qquad 3.2\text{-}4$$

where a = interfacial area per unit volume.

Bussolari et al (15) have presented a design method for hold-up applicable to any system in which certain physical properties of the liquids are known. They outline procedures for calculating the individual effects of interfacial tension, orifice effect and frictional effects in the downspout and these are discussed in Section 8. It was shown that the total depth of light liquid below the plate consists of the sum of the separable effects of the dispersed and continuous liquids.

$$h_t = h_{disp} + h_{cont} \qquad 3.2\text{-}5$$

where h_t = total depth of dispersed phase below the top surface of the plate.

Thornton (147) correlated the hold-up and the superficial velocities of the two phases in a spray column by the equation

$$\frac{U_D}{X} + \frac{U_c}{1-X} = \bar{U}_o \ (1-X) \qquad 3.2\text{-}6$$

where $\bar{U}_o$ is the characteristic velocity, obtained by extropolating the mean relative velocity of the drops to zero flow rates.

In the region of constant hold-up, the forces acting on the drop, that is drag, gravity and surface forces are at dynamic equilibrium and the drops move at constant velocities. In the region of changing hold-up the forces acting on the drops are not at equilibrium and both the drops and the continuous phase are accelerating in their respective directions of flow.

On the basis of the above explanation Letan and Kehat (95) correlated the local hold-up as a function of equilibrium slip velocity. These authors defined the equilibrium slip velocity U_s^* as the velocity in the constant hold-up region of the column and calculated U_s^* by the equation

$$U_s^* = \frac{U_D}{H'} + \frac{U_c}{1-H'} \qquad 3.2\text{-}7$$

where H' is the local hold-up. Their experimental data was plotted in the form of an empirical exponential function of the equilibrium slip velocity against the corresponding hold-up;

$$U_s^* = U_s^0 \exp(-aH') \qquad 3.2\text{-}8$$

where U_s^0 is the equilibrium slip velocity extrapolated to zero hold-up and a is an empirical constant. Both U_s^0 and a are functions of the physical properties of the liquids employed and the drop size.

3.2_3 FLOODING

The limiting condition of flow in a perforated plate column is identified by flooding. Flooding is a typical hydrodynamic phenomena particularly associated with any gravity operated column due to which for each flowrate of one phase, there is a corresponding maximum practical flowrate of the other phase. This maximum depends upon the system properties and certain design and operating parameters of the contactor, for example, the free flow area and the extent of backmixing. Flow in excess of the maximum causes either phase to be rejected from the equipment. For example, in the case of the dispersed phase an accumulation of a dense packed layer of drops occurs somewhere in the equipment.

The study of dispersed phase hold-up for the characterisation of column hydrodynamics has shown (49, 148) that hold-up is related to the superficial phase velocities U_d and U_c by

$$\frac{U_d}{x} + \frac{U_c}{1-x} = \bar{U}_p\ (1-x) \qquad 3.2\text{-}9$$

where $\bar{U}_p$ is the characteristic velocity, defined as the mean relative velocity of the droplets extrapolated to essentially zero flowrates. In the present case this will be regarded as the mean vertical component of velocity of the droplets with respect to the continuous phase and in turn will be a function of the mean droplet diameter associated with a specific column geometry and system.

Re-arranging and differentiating equation 3.2-9

$$U_c = \bar{U}_p\ (1-x)^2 - U_d\ \frac{(1-x)}{x}$$

$$\frac{dU_c}{dx} = 2\bar{U}_p\ (x-1) + \frac{U_d}{x^2} \qquad 3.2\text{-}10$$

$$U_d = \bar{U}_p\ x(1-x) - \frac{x}{1-x}\ U_c$$

$$\frac{dU_d}{dx} = \bar{U}_p\ (1-2x) - \frac{U_c}{(1-x)^2} \qquad 3.2\text{-}11$$

At the flooding point, the flowrates reach their maximum values, hence

$$\frac{dU_c}{dx} = 0 \text{ and } \frac{dU_d}{dx} = 0$$

Therefore, equations 3.2-10 and 3.2-11 can be re-written as

$$U_{d(f)} = 2\bar{U}_p x_f^2 (1-x_f) \qquad 3.2\text{-}12$$

$$U_{c(f)} = \bar{U}_p (1-2_{xf})(1-x_f)^2 \qquad 3.2\text{-}13$$

Equations 3.2-12 and 3.2-13 relate the phase flowrate at flooding to the corresponding hold-up x_f.

Eliminating $\bar{U}_p$ between equations 3.2-12 and 3.2-13 yields a relationship between x_f and the flowrate $U_{d(f)}/U_{c(f)}$

$$x_f = \frac{(F_R^2 + 8F_R)^{0.5} + 3F_R}{4(1-F_R)} \qquad 3.2\text{-}14$$

$$\text{where } F_R = \left(\frac{U_{d(f)}}{U_{c(f)}}\right) \qquad 3.2\text{-}15$$

where the terms are as defined in the Nomenclature.

This is not strictly applicable when the mean drop size is not constant over the entire hold-up range within the column as for example, when mass transfer is taking place and drop size may increase owing to enhanced coalescence. In non-masstransfer studies in a spray column, however, Thornton et al (147) found good agreement between their experimental data and equation 3.2-14 above.

For the purpose of the present study the onset of flooding when the lighter phase is dispersed may be

considered to be the condition when at steady phase inlet flowrates there is an increase in the layer of dispersed phase beneath any plate. Whether this tends to occur at either the top or bottom of the column was, depending upon operating parameters until this study, not known.

There have been numerous studies of flooding in packed columns, which are in some ways analogous to perforated plate columns. Flooding of a packed column is in general, considered to correspond to conditions when drops of the dispersed phase begin to be ejected from the packing (71). However, the published studies were all made in the absence of mass transfer and, in view of the influence of mass transfer direction and rate upon drop size, it would be expected to have some influence on flooding. Most of the flooding correlations are presented as graphs, the coordinates of which are complex functions of liquid properties as well as flowrates. However, a statistical study (98) of the available data with the correlations showed that the correlation of Crawford and Wilke (23) is best. Their correlation may be expressed as

$$\frac{(U_c^{0.5} + U_D^{0.5})^2 \rho_c}{a_p \mu_c} = f\left\{\left(\frac{\rho_c}{\Delta\rho}\right)\left[\frac{\sigma}{\rho_c g\left(\frac{e}{a_p}\right)^2}\right]\left[\frac{\mu_c^2 g(\varepsilon/a)}{\sigma^2}\right]\right\} \qquad 3.2\text{-}16$$

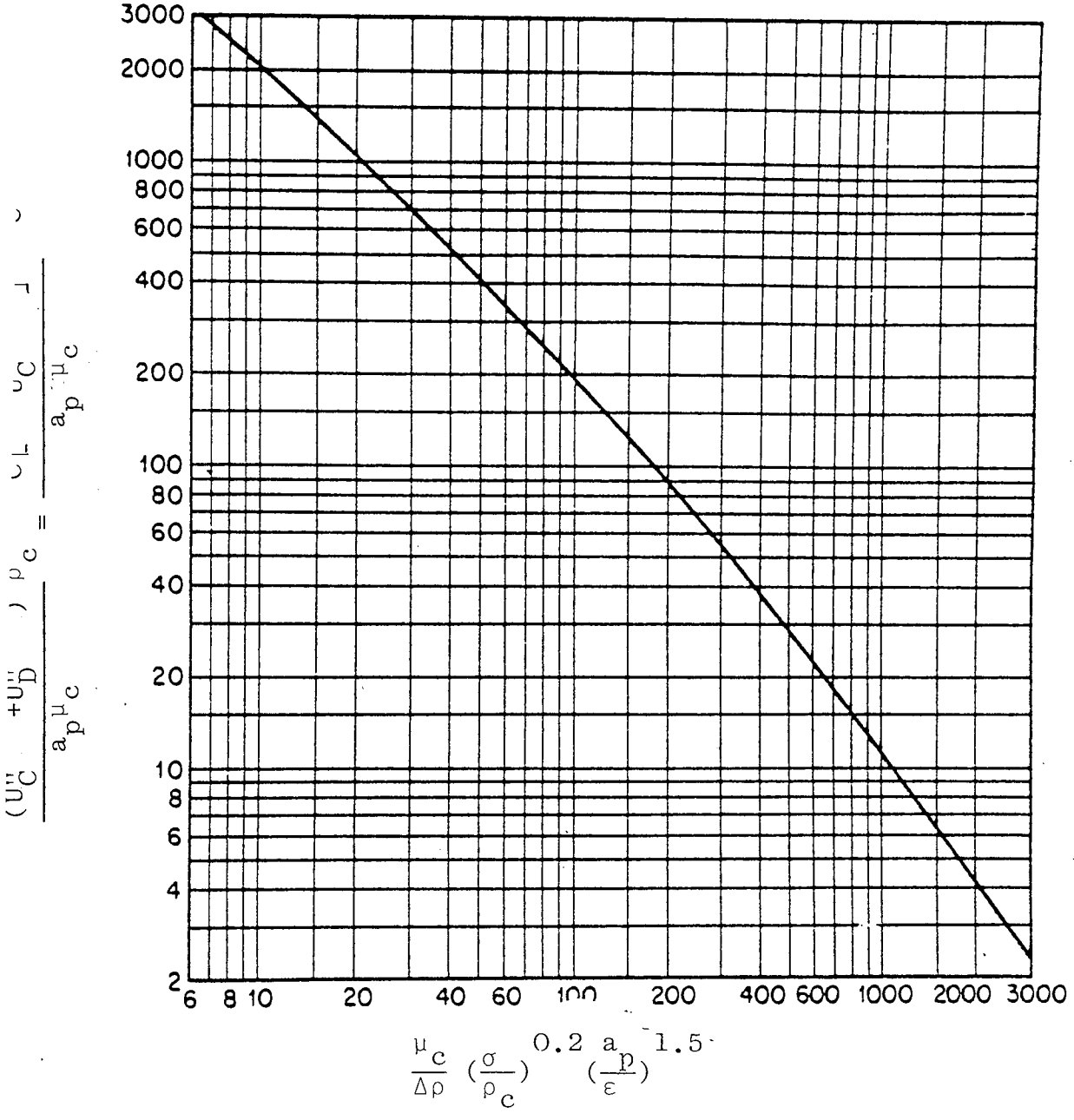

Fig. 3.2-1 Flooding in packed columns (23)

where the notation is as defined in the Nomenclature. The results are shown in Figure 3.2-1. Since the effects of simultaneous mass transfer are uncertain, it is recommended that the design flowrates be no larger than 50 to 60% (113) of the flooding values.

3.2-4 DROP SIZE DISTRIBUTION

3.2-4(1) MEAN DROP SIZE

To estimate the capacity of a perforated plate column requires an accurate knowledge of dropsize distribution. This distribution is dependent upon the method of droplet production and upon their subsequent treatment in the extractor, which depend upon extractor geometry and throughput and on the physical properties of the continuous and dispersed phases. As outlined earlier the conventional method of droplet production involves passing the liquid through holes, e.g. perforations or nozzles.

Two possible extremes of droplet behaviour may be observed for most systemss in perforated plate columns. In one case where mass transfer is occuring so as to induce Marangoni instablities (generally for mass transfer from the dispersed phase), droplets are formed which may have sizes accurately predicted by the existing

correlations but many of which could be much smaller or much larger. Also many satellite drops may be formed. In the other extreme where masstransfer rates are very slow, or impurities are present as surfactant, the drop size distribution differs from those predicted from single nozzle correlations. The result is a dispersion of very small drops with high surface area for mass-transfer but low flooding capacities and a tendency towards entrainment.

Numerous correlations (30, 67, 83, 92, 105, 106, 119) have been proposed for the mean drop size from a single nozzle. Meister and Scheele (105) proposed this correlation

$$V_D = \frac{\pi D_F^3}{6} = F_{HB} \left\{ \frac{\pi \sigma D_N}{g\Delta\rho} + \frac{5\pi\mu D_N^3 U_N}{D_F^2 g\Delta\rho} - \frac{\pi \rho_d D_N^2 U_N^2}{3g\Delta\rho} + 4.5 \left(\frac{\pi^2 D_N^6 U_N^2 \rho_d \sigma}{16(g\Delta\rho)^2} \right)^{0.33} \right\} \qquad 3.2\text{-}17$$

where the terms are as defined in the Nomenclature. This correlation is essentially a force balance on a forming drop and allows the mean drop size D_F formed from a single nozzle to be predicted. Estimates for the correction factor F_{HB} are given by Harkins and Brown (60,105). For continuous phase liquids of viscosity less than $0.01 Nsm^{-2}$ the drag term (i.e. the

TABLE 3.2-1

CORRELATIONS PREDICTING DROP DIAMETER IN THE JETTING REGION

Christensen and Hixson (92)

$$\frac{d}{D_N} = 2.07 \frac{1}{0.485Eö+1} \quad \text{for } Eö < 0.615$$

$$\frac{d}{D_N} = 2.07 \frac{1}{1.51Eö^{\frac{1}{2}}+0.12} \quad \text{for } Eö > 0.615$$

where $Eö = g\Delta\rho D_N^2/\sigma$ (A1)

Perrut and Loutaty (122)

$$\frac{d}{D_N} = 2.07\ (1-0.193Eö) \quad \text{for } 0.011 < Eö < 1.70 \tag{B1}$$

Kumar and Hartland (92)

$$\frac{d}{D_N} = 1.591\ \left(\frac{\Delta\rho D_N U_N^2}{\sigma}\right)^{-0.068} \left(\frac{\Delta\rho D_N^2 g}{\sigma}\right)^{-0.278} \quad \text{for } 0 < \frac{\rho_d D_N U_N^2}{\sigma} < 2$$

$$\frac{d}{D_N} = 1.546\ \left(\frac{\Delta\rho D_N U_N^2}{\sigma}\right)^{-0.021} \left(\frac{\Delta\rho D_N^2 g}{\sigma}\right)^{-0.214} \quad \text{for } 2 < \frac{\rho_d D_N U_N^2}{\sigma} < 8.64 \tag{C1}$$

TABLE 3.2-2

CORRELATIONS PREDICTING THE VOLUME OF SINGLE DROPS PRODUCED FROM SINGLE NOZZLES AT LOW VELOCITIES

Scheele and Meister (105)

$$V = \psi \left(\frac{\sigma\pi D_N}{\Delta\rho g} + \frac{5\mu_c \pi D_N^3 U_N}{d^2 \Delta\rho g} - \frac{\rho_d \pi D_N^2 U_N^2}{3\Delta\rho g} + 4.5 \left(\frac{\sigma\pi^2 \rho_d D_N^6 U_N^2}{16(\Delta\rho)^2 g^2}\right)^{\frac{1}{3}}\right) \text{ where } d = (6v/\pi)^{\frac{1}{3}} \qquad (A2)$$

de Chazal and Ryan (30)

$$V = \frac{\pi D_N \sigma}{\Delta\rho g}\left\{\psi + 1.648 \frac{g\Delta\rho D_N U_N V^{\frac{1}{3}}}{2\sigma U_t} - 0.857 \frac{D_N \rho_d U_N^2}{2\sigma}(1+\beta)\right\} \text{ where } \beta = 0$$

$$\text{for } \left(\frac{\rho_d D_N U_N^2}{2\sigma}\right)^{\frac{1}{2}} < 1.07 - 0.75 \left(\frac{\Delta\rho g D_N^2}{4\sigma}\right)^{\frac{1}{2}} \qquad (B2)$$

$$\text{otherwise, } = 0.286 \left(\frac{\Delta\rho g D_N^2}{4}\right)^{\frac{1}{2}}$$

Izard (92)

$$V = \frac{1}{g\Delta\rho}\left\{\pi D_N \sigma + \frac{\pi D_N U_N \mu_c}{2}\left(\frac{\mu_c + 1.5\mu_d}{\mu_c + \mu_d}\right) - \frac{\pi D_N^2 U_N^2 \rho_d}{3}\left(1 - \frac{2\rho_d}{2\rho_d + \rho_c}\right)\right\} \qquad (C2)$$

Kagan, Kovalev and Zakharychev (81)

$$V = \pi\psi a^3 R \left(1 + 2.39\ W^{\frac{1}{3}} - 0.485\ W\right) \qquad \text{(D2)}$$

where $a = \left(\frac{2\sigma}{g\Delta\rho}\right)^{\frac{1}{2}}$

$$W = \frac{(\rho_c+\rho_d)U_N^2 D_N}{2\sigma}$$

$$R = D_N/2a$$

TABLE 3.2-3

CORRELATIONS PREDICTING THE MINIMUM JETTING VELOCITY

Scheele and Meister (105,106)

$$U_j = \sqrt{3}\ \left(\frac{\sigma}{\rho_d D_N}\right)^{0.5}\ \left(1 - \frac{D_N}{d}\right)^{0.5} \qquad \text{(A3)}$$

de Chazal and Ryan (30)

$$U_j = \sqrt{\ }\ \frac{2\sigma}{\rho_d D_N}\ \left(1.07 - 0.75\ \sqrt{\ }\ \frac{\Delta\rho g D_N^2}{4\sigma}\right) \qquad \text{(B3)}$$

Fujinawa et al (36)

$$U_j = 4.4\ \sigma^{0.2}\ D_N^{-0.5} \qquad \text{(C3)}$$

second term) may be neglected before the correlation is introduced.

Recently, Kumar and Hartland (92) presented correlations to predict the Sauter mean drop size formed at nozzles/orifices in a perforated plate. The liquid-liquid systems studied covered a density range from 880.2 to 994.30 kgm^{-3} and a range of interfacial tension of 30.7 to 5.2 mNm^{-1}. The analysis was restricted to velocities below the critical velocity. The Sauter mean diameter d_{32} of a drop swarm was given by

$$\frac{d_{32}}{D_N} = 1.591 \left(\frac{\Delta\rho D_N U_N^2}{\sigma}\right)^{-0.068} \left(\frac{\Delta\rho D_N^2 g}{\sigma}\right)^{-0.278}$$

$$\text{for } 0 < \frac{\rho_d D_N U_N^2}{\sigma} < 2 \qquad 3.2\text{-}18$$

and

$$\frac{d_{32}}{D_N} = 1.546 \left(\frac{\Delta\rho D_N U_N^2}{\sigma}\right)^{-0.021} \left(\frac{\Delta\rho D_N^2 g}{\sigma}\right)^{-0.214}$$

$$\text{for } 2 < \frac{d D_N U_N^2}{\sigma} < 8.64 \qquad 3.2\text{-}19$$

The results showed an average percentage deviation of 8.7 in the single drop region and 10.8 in the jetting region compared to the data of previous authors (48, 121).

3.2-4(2) HISTOGRAMS

Drop size measurements are generally made to ascertain the true frequency distribution of a drop size. The observed distribution serves as the basic data from which may be derived certain representative constants for example, the mean diameter or the volume-surface mean (Sauter) diameter, and the uniformity parameter.

The simplest way of representing the size distribution in an extraction column is by means of a standard histogram. As illustrated in Figure 7.1-1 this is a plot of the frequency of occurrence as a function of the size range. It gives an immediate indication of the droplet size which constitutes the majority of the distribution.

3.2-4(3) DROP SIZE DISTRIBUTION CHARACTERISTICS

In order to achieve a useful analysis of extraction data from a countercurrent liquid-liquid extractor, such as the sieve plate column, the assumption is often made that drops are spherical and of uniform size. This idealised approach enables the mass transfer coefficient K to be calculated based on the volume surface mean diameter drop, the interfacial area a, and the contact time, from which is obtained the number of transfer units

NTU = Kat. This assumption may lead to serious error when interpreting mass transfer and related processes in discrete drop devices since, as discussed in 4.1-2, the mode of mass transfer into/out of a drop is dependent on drop diameter (i.e. they may be stagnant, circulatory or oscillatry).

As yet, no details of measurements of the drop size distribution in laboratory or industrial sieve plate columns are available in the literature. Previous investigations of droplet size on sieve plates have been confined to the volume surface mean (Sauter) diameter. However, the assumption of some calculated single drop size, however this is weighted, cannot be accurately applied to define the size characteristics or complex behaviour of dispersed phase consisting of a swarm of droplets with a wide distribution of sizes.

Extensive investigations have been carried out by several workers (20,37,108,111,121) using either a spray column or a Rotating Disc Contactor (RDC) on laboratory or pilot scales. These workers (20,37,111,121) have indicated the important features that size distribution might affect in a liquid-liquid extraction process; viz.

1. Residence time distribution of the phase dispersed, i.e. the effect due to drop size dependent velocities.

2. Mass transfer coefficients, generally a lowering of extraction efficiency will result compared to that predicted for the normally assumed mean drop size.

3. Reduction of circulatory and oscillatory effects, i.e. producing stagnant droplets.

Mugele and Evans (111) proposed an upper limit distribution defined in terms of a maximum particle size. The log probability distribution function with two parameters may be expressed as

$$\frac{dV}{dy} = \frac{\delta}{\sqrt{\pi}} e^{-\delta^2 y^2} \qquad 3.2\text{-}4(3)\text{-}1$$

where $y = \text{In} \frac{d}{d_{GM}}$ 3.2-4(3)-2

and d_{GM} is the geometric mean diameter.

The upper-limit function as applied to log probability distribution is given by

$$\frac{dV}{dy} = \frac{\delta}{\sqrt{\pi}} e^{-\delta^2 y^2} \qquad 3.2\text{-}4(3)\text{-}3$$

where $y = \text{In} \frac{ad}{d_m - d}$

d_m is the maximum stable drop size, and the minimum drop size depends upon the prevailing break-up process

and may be dictated by the size that is just entrained by the continuous phase.

$$a = \frac{d_m - d_{50}}{d_{50}} \qquad 3.2\text{-}4(3)\text{-}4$$

a = skewness parameter

$$\delta = \frac{0.394}{\ln \frac{d_{90}}{d_m - d_{90}} \; \frac{d_m - d_{50}}{d_{50}}} \qquad 3.2\text{-}4(3)\text{-}5$$

δ = uniformity parameter

Olney (121) analysed the size distribution of drops in an RDC by adopting the Mugele-Evans (111) log-normal distribution. Wide variations in drop size distribution were measured in the RDC, presumably due to shear or local turbulence in the bulk flow, and to a lesser extent droplet coalescence due to drop interaction effects. Rod (128) proposed model equations for the RDC which included the effect of variable drop size. An approximate solution for a mean height of transfer unit was presented. An experimental distribution function by Gal-Or and Hoelscher (37) was assumed to represent drop size variation. Mumford (113) also showed that the Sauter mean drop diameter d_{32} decreased with vertical distance from the dispersed phase inlet; but did not take into account any influence of the inlet drop size from the distributor on column drop size.

Chartres and Korchinsky (20) have demonstrated quantitatively the very large effect that drop size distribution could have on column performance. A mass-transfer model equation which included the influence of drop size distribution and which was based largely on the previous work of Rod was applied to a Rotating Disc Contactor, utilising distribution data reported by Olney. Predicted extraction efficiencies were found to differ greatly from those based upon Sauter mean drop size. Furthermore, it was found that various experimental size distributions could not be represented by any single defined mean drop size.

Recently, Jeffreys et al (78) analysed the effect of drop size and size distribution on the performance of a 0.45m diameter RDC. These authors proposed equations to extend the range of correlations for drop size up to industrial scale columns and from which the drop size profile can be estimated. Their results gave wide divergencies when compared with those reported previously from small extraction columns.

Clearly then the performance of any gravity operated extractor, such as the perforated plate column, is likely to be correlated more reliably in terms of size distribution than a mean drop size but the distribution is unlikely to be predictable from experiments in small columns.

3.3 MECHANISMS OF FLOCCULATION AND COALESCENCE OF DROPS

3.3-1 DROP FLOCCULATION

As described in 3.2-3, drops of different sizes are formed in a perforated plate column. The small drops rise vertically, albeit with some back mixing, while the large drops follow unpredictable paths along their travel. As the drops collect near the interface, they flocculate into a closely packed mass. Each drop is surrounded by a thin film of the continuous phase and the film between two adjacent drops must rupture before they can combine in the flocculant layer. Drops near the main phase boundary coalesce into it via a drop-interface coalescence mechanism. Coalescence fundamentals are discussed in 3.3-2.

At a given set of phase flow rates the ease with which the flocculated drops coalesce together and subsequently into the interface determines the height of the coalescing zone. The residence time in the flocculation zone takes several minutes and hence a significant depth of flocculation-coalescence zone may exist in any column independent of diameter.

Preliminary observations (29) showed that the flocculation zone comprises three distinct zones, that is, an inlet section where droplets form a close packed arrangement, a larger mid-section where interdrop

coalescence and droplet distortion occur, and an exit section bounded by an interface. The mechanisms differ in each zone but it is their cumulative effect which is of relevance to the prediction of the height of the phase separation section at the top or bottom of the column, and more importantly of the height beneath each plate which is essentially unavailable for mass transfer purposes.

3.3-2 DROP-DROP AND DROP INTERFACE COALESCENCE

Coalescence occurs either between two or more drops of various sizes or between the drops and a plane interface. The ease with which a dispersed phase coalesces can have a marked influence on the performance of an extractor. Coalescence (i) determines the height of flocculation zone beneath each plate. This may vary when mass transfer occurs since the bulk phase properties change with solute concentration; and Marangoni effects may arise and (ii) determines the column height required at the top (or bottom) phase separation zone, equivalent to a height not available for mass transfer or needed for any external settler. Coalescence on the column walls or on the downcomers is undesirable, e.g. due to dirty or dispersed phase wetted walls, as this will result in rapid formation of large drops of dispersed phase. This may lead to a reduction in interfacial

area and drop residence time and consequently a significant reduction in mass transfer.

A drop does not coalesce immediately with its homo-phase on reaching the phase boundary, but entraps a film of the continuous phase between itself and the phase boundary. According to Hartland (61) the shape of the drop when the film is draining is spherical and for viscous liquids its overall dimensions are practically constant during most of the drainage period. Due to the drop weight the liquid in the film starts flowing out until the film attains a critical thickness. Gillespie and Rideal (52) found this critical thickness for a benzene-water system to be between 10^{-5} to 10^{-4}cm. While the film drains unevenly under the influence of gravitational forces, the drop sits on it and the associated time for the drainage of film is termed the 'rest time' period of the drop. Finally, the film becomes so thin that even a small temperature gradient can cause its distortion and eventual rupture leading to the coalescence of the drop.

A number of investigators (14, 19, 76) have observed that drops of identical size and properties and coalescing under identical conditions, exhibit a variation in coalescence time. This has often resulted in a wide distribution in experimentally measured rest times. Cockbain and McRoberts (22) suggested that this

was caused by a displacement of the adsorbed surface active molecules on the interface. However, since this phenomena has also been noticed in pure systems, this explanation is inadequate. Brown and Hanson (14) proposed that the reason lies in the drops having fallen through considerable distances. Thus they entrap different initial thicknesses of the film of the continuous phase. Charles and Mason (19) observed that film rupture could occur in several places and occasionally in two places simultaneously. They explained the wide distribution of the observed rest times as arising since film rupture occurs over a range of thickness, rather than at some critical thickness. The phenomenon is reviewed in terms of a maximum film thickness at which rupture can occur. Drops which exist longer than the minimum rest time, corresponding to the maximum film thickness, are metastable and are liable to coalesce whenever there is a disturbance to rupture the film.

When the film ruptures, the coalescence of the drop is usually not a single-staged process. As the drop drains into its homo-phase, it may give rise to a smaller secondary drop. This smaller secondary drop stays on the phase boundary before coalescing to give rise to yet another, smaller, secondary drop. As many as eight secondary drops have been observed from a single primary drop in some systems. Charles and Mason

(18) studied the formation of secondary drops extensively. They took high speed cine photographs of the phenomenon of partial coalescence and showed that a primary drop at a flat interface drains until it forms a cylindrical column which pinches off at the base to form a secondary drop.

Jeffreys and Hawksley (76) have shown that the phenomenon of secondary drop formation could result from the shock waves caused by rupture of the film. Brown and Hanson (14) proposed that secondary drops could form by the mechanism suggested by Charles and Mason (19) and Jeffreys and Hawksley (76), depending upon the depth to which the primary drop is submerged in the interface. If the drop is submerged to less than 0.20 of its diameter, it is likely to coalesce by the simple drainage process. If, however, it is submerged to more than 0.26 of its diameter, coalescence will occur by the mechanism outlined by Jeffreys and Hawksley (76).

In a practical extraction operation coalescence of one drop with another may happen at an early stage in the drop life while the solute concentration is high. Mixing brought about by the coalescence brings fresh fluid elements to the interface and thus increases the local mass transfer coefficient. However, (in the absence of subsequent redispersion) coalescence also leads to a

reduction in dispersed phase hold-up and interfacial area which may over-ride the effects of the induced mixing. Groothius and Zuiderweg (57), while studying the behaviour of benzene-acetic acid-water system, observed that concentration of solute between the drops was higher when acetic acid was transferred from the dispersed benzene drops to the continuous water phase, than on the rest of the drop surface. When the transfer was from the continuous phase into the drops, coalescence was retarded. These authors obtained the same result irrespective of the phase dispersed.

Smith et al (145) carried out a study of coalescence of liquid drops of several systems in extraction columns. They used a theoretical analysis to formulate a hypothetical mechanism for coalescence proposed by the previous investigators (19,56). Their observation was similar to that of Groothius and Zuiderweg (57); the region between the drops and between drops and the interface was more concentrated in solute than a region remote from these areas when transfer of mass was from the drops to the continuous phase. When the transfer of mass was from the continuous phase into the drops, the regions between the drops and interface were preferentially depleted in solute and coalescence became less likely (see Figure 3.3-1).

In an attempt to obtain a more quantitative

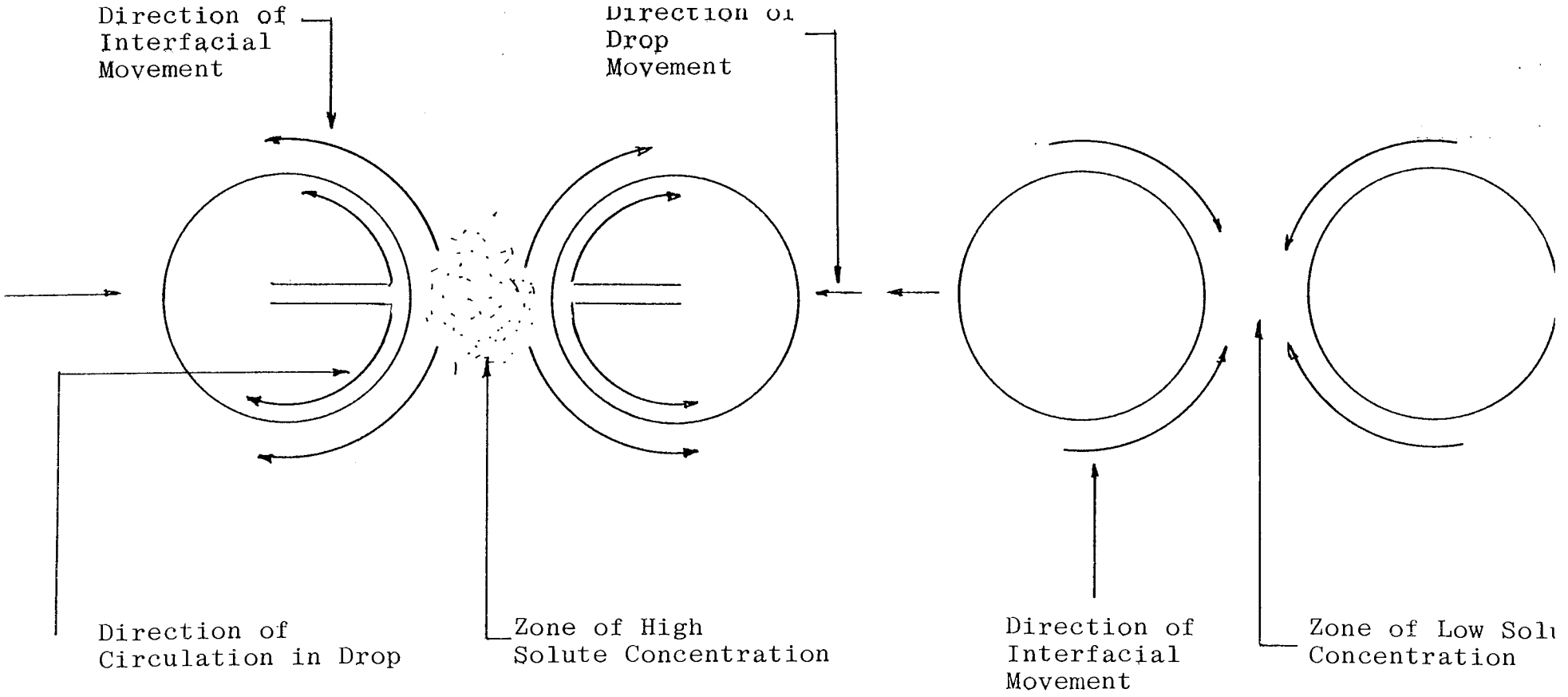

Fig. 3.3-1A: Tranfser of Material from the Dispersed Phase to the Continuous Phase.

Fig. 3.3-1B: Transfer of Material fro Continuous Phase to the Dispersed Phase.

Fig. 3.3-1: Effect of Solute Transfer of Interdrop Coalescence (145)

picture of the phenomenon Groothius and Zuiderweg (57) employed a continuous flow system to simulate industrial conditions. They confirmed that coalescence rate can be greatly increased when mass transfer occurs.

Jeffreys and Lawson (77) studied extensively the behaviour of coalescing single drops with a benzene-acetone-water system. They measured the coalescence times of aqueous drops at an oil-water interface. These authors observed an increase in coalescence rate with transfer of solute from the droplets to the continuous phase. Their results are in general agreement with the findings of Groothius and Zuiderweg (57).

Coalescence rate is sensitive to impurities such as interfacial scum and surfactants. Katalinic (82) found that trace amounts of impurity, such as dirt or grease, will reduce the life time of drops at the interface. If the impurity is surface active in nature, the effect can lead to a marked decrease in the coalescence rate. Nielson et al (118) studied the effect of a surface-active stabilizing agent soluble in either the oil or water phase. They found that the life time of the drops depended upon the cubic root of the surfactant concentration. Clearly, whilst they can be eliminated in small scale laboratory columns with pure liquid systems, the effects of grease or surfactants may be an important factor in any commercial perforated plate column.

3.4 AXIAL MIXING PHENOMENA

Backmixing or axial mixing is a phenomenon which occurs when pockets of fluid move at velocities differing randomly from the mean velocity. This spread of velocities is caused by eddying. In an extraction column it results in a reduction of mean concentration driving force $(\Delta C)_m$ and hence reduces the number of theoretical stages (efficiency). Ideally for maximum efficiency each phase should flow with no axial mixing, that is, it should be in plug flow. In practice, however, there is always some axial mixing. For example, whilst the arrangement of trays in a perforated plate column reduces axial mixing of either phase to much lower values compared with spray columns, they are still subject to it. However, in perforated plate columns, axial mixing is confined to the regions between adjacent trays and does not spread through the column.

The phenomenon of axial mixing may result from the following:

(i) Turbulence inparted by the rising drops.

(ii) Entrainment of field liquid in the wake of the drops.

(iii) Radial diffusion, as a consequence of non-uniform velocity.

(iv) A distribution of residence times for the dispersed phase flow.

(v) True molecular diffusion.

These mechanisms act either separately or in combination, and their effect is to decrease the concentration gradient which is the driving force for mass transfer.

To identify axial mixing effects, Muyauchi (115) suggested three different definitions of the number of transfer units (NTU).

1. True value

$$(NTU)_{ox} = \frac{K_{ox} a_s L}{U_x} \qquad 3.4\text{-}1$$

where a_s is surface area per unit volume.

2. The apparent value of NTU, including axial mixing effects, i.e. the measured value

$$(NTU)_{oxm} = \int_{Cx_0}^{Cx_1} \frac{dC_x}{C_x - (Q+mC_y)} \qquad 3.4\text{-}2$$

3. Piston flow, or plug flow, $(NTU)_{oxp}$ defined as that based upon the logarithmic mean driving force computed from the inlet and outlet concentrations in the column.
In general

$$(NTU)_{ox} \geq (NTU)_{oxm} \geq N_{oxp} \qquad 3.4\text{-}3$$

Entrainment is a form of backmixing, which acts to destroy the concentration changes produced by the trays. Felix and Holder (34) studied extensively the effects of extraction interstage entrainment on extraction efficiency. They used premium grade lubricating oils to extract phenol in multistage plate towers. For no internal entrainment and systems of similar physical properties and solubilities, the number of theoretical stages required was expressed as

$$N_T = \frac{\log \frac{(\phi - 1)}{(\phi \frac{s}{m} - 1)}}{\log (s/m)} \qquad 3.4\text{-}4$$

as $\varepsilon_f = 1.0$, ε_f is the entrainment factor.

If the efficiency of an internally entrained extractor is defined as the ratio of the number of theoretical stages needed for a given feed improvement to those needed when internal entrainment occurs, the efficiency is

$$\eta_a = \frac{N_T}{N} = \frac{\log \left[1 + \frac{1}{\varepsilon_f} (\frac{s}{m} - 1)\right]}{\log (s/m)}, \frac{s}{m} \neq 1.0 \qquad 3.4\text{-}5$$

$$\text{For } \frac{s}{m} = 1.0, \ \eta_a = \frac{1}{\varepsilon_f} \qquad 3.4\text{-}6$$

where the terms are as defined in the Nomenclature.

Numerous authors (73, 79, 82, 144) have pointed out that axial mixing has analogies with diffusion and much has been done to develop such a mathematical treatment.

CHAPTER 4

MASS TRANSFER IN LIQUID-LIQUID SYSTEMS

4. MASS TRANSFER IN LIQUID-LIQUID SYSTEMS

In spray or perforated plate columns there are three distinct stages of mass transfer in the life time of drop swarms. These are:

(1) Formation of the discrete drops at the distributor or perforated plates.

(2) Free rise (or fall) of the drops at a steady state slip velocity.

(3) Movements through the drop flocculation zone and drop-drop/drop interface coalescence at the end of their vertical travel through the column.

In spray columns, droplet formation is followed by unimpeded free rise (or fall) through the entire column and then by drop flocculation and coalescence at the principal interface. In perforated plate columns, however, discrete drop formation is followed by free rise between adjacent plates and then, normally, by complete coalescence and redispersion at each plate (operation with droplets so small, or at such low hold-ups, that droplets pass through plates without coalescence is unrealistic). With regard to mass transfer the drop formation and travel periods would be expected to be important.

In general the mass transfer from a swarm of drops is equated to the sum of that of the individual drops expressed as a mean drop size as discussed in section 4.1-1. Any effects due to drop interaction are hence neglected. This may be unimportant in plate columns, since interdrop coalescence does not occur between plates, although the proximity of other drops would be expected to modify single drop behaviour. However, as discussed in 4.3-1 drop masstransfer is dependent upon drop size so that inaccuracies could be introduced.

4.1-1 MASS TRANSFER DURING DROP FORMATION

The earliest theoretical work upon which all subsequent treatments of unsteady diffusion are based is that by Higbie (70). He developed the penetration theory by solution of the unsteady state diffusion equation in accordance with Fick's law

$$\frac{\partial c}{\partial t} = \mathscr{D} \frac{\partial^2 c}{\partial Z^2} \qquad 4.1\text{-}1$$

The conditions on equation 4.1-1 are

$$c(z,o) = c_o \qquad 4.1\text{-}2$$

$$c(o,t) = c^* \qquad 4.1\text{-}3$$

where the terms are as defined in the Nomenclature. Under these conditions, equation 4.1-1 has the solution

$$c = c_o + \frac{c^* - c_o}{\sqrt{\pi \mathcal{D} t}} \int_z^\infty e^{-\frac{z^2}{4\mathcal{D}t}} dz \qquad 4.1\text{-}4$$

The instantaneous rate of solute transfer at the boundary (z = o) per unit area is given by

$$N' = \mathcal{D} \left(\frac{\partial c}{\partial z}\right)_{z=o} \qquad 4.1\text{-}5$$

The total amount of solute diffusing across the boundary in time t is obtained by combining equations 4.1-4 and 4.1-5 and integrating the resulting expression from o to t

$$N = 2(c^* - c_o)\left(\frac{\mathcal{D}t}{\pi}\right)^{0.5} \qquad 4.1\text{-}6$$

The instantaneous and average individual mass transfer coefficients at time t based on the concentration driving force $(c^* - c_o)$ are respectively

$$k = \left(\frac{\mathcal{D}}{\pi t}\right)^{0.5} \qquad 4.1\text{-}7$$

$$k = 2\left(\frac{\mathcal{D}}{\pi t}\right)^{0.5} \qquad 4.1\text{-}8$$

The above development is based on a constant interfacial area.

Licht and Pansing (100) modified Higbie's approach

and applied it to the case of a growing drop or bubble. It was assumed (i) that the interfacial surface could be simplified to a plane surface and (ii) that a drop is thoroughly mixed by liquid flowing into it so that the entire resistance to mass transfer resides in the continuous phase. For these conditions the following equation defines the overall mass transfer coefficient for extraction out of a drop.

$$k_{cf} = 0.805\left(\frac{\mathcal{D}}{\pi t_f}\right)^{0.5} \qquad 4.1\text{-}9$$

where k_{cf} is the average individual masstransfer coefficient for continuous phase formation. It was observed that the k_{cf}'s of Garner and Skelland (45) were larger than those calculated by the above equation by a factor averaging 1.5.

Heertjes et al (69) also used the Higbie approach but assumed (i) that the velocity of diffusion is small compared with the velocity of the drop, and (ii) that the entire resistance resided within the drop. However, Heertjes et al were unable to correlate their experimental results with theory. Their correlation for the dispersed phase masstransfer coefficient k_{df} based upon the final area of the drop is

$$k_{df} = 3.429\left(\frac{\mathcal{D}}{\pi t_f}\right)^{0.5} \qquad 4.1\text{-}10$$

Groothuis and Kramers (56) developed an expression for mass transfer during drop formation based on a mechanism in which drop growth occurs by formation of fresh elements and no mass transfer occurs laterally between the surface elements of different age. Their treatment is applicable to the case where the dispersed phase resistance is controlling, and other assumptions made are similar to those of previous investigators (68, 69). By expressing volume as a function of time ($V = \phi t$) and basing the mass transfer coefficient (k_{df}) on the final area of the drop, they obtained the expression

$$k_{df} = 1.333 \left(\frac{\mathcal{D}}{\pi t_f}\right)^{0.5} \qquad 4.1\text{-}11$$

Heertjes and De Nie (68) proposed a model for mass transfer to drops at a moderate rate. They compared drops growing by stretching of the surface and used photographic analysis to determine the surface and volume of the drops during formation. By assuming the surface to grow by addition of fresh elements, they obtained the following expression for mass transfer, for continuous drop formation

$$k_{df} = 2 \left(\frac{A_o}{A_r} + \frac{2}{3}\right)\left(\frac{\mathcal{D}_d}{\pi t_f}\right)^{0.5} \qquad 4.1\text{-}12$$

where A_o is the surface area of the rest drop.

A_r is the surface area of the drop at detachment.

For $A_o = 0$, equation 4.1-12 reduces to equation 4.1-11 derived by Groothius and Kramers (56). Their expression for the surface stretch mechanism was

$$k_{df} = 3.055 \left(\frac{A_o}{A_r} + \frac{1}{3}\right)\left(\frac{\mathcal{D}_d}{\pi t_f}\right)^{0.5} \qquad 4.1\text{-}13$$

Several theoretical models have been derived based upon a mechanism in which the growth of surface occurs by stretching, that is the interface is assumed to be uniformly stretched over the drop surface as the drop grows. Ilkovic (74) proposed an equation for the estimation of the diffusion controlled current in a dropping mercury cathode. The equation has been successfully used to describe mass transfer in growing drops (6, 9). According to Ilkovic's development, the total amount of material transfer during formation may be expressed as

$$m_A(t) = (\rho_{Ao} - \rho_{A\infty})D^2(1.714\,\mathcal{D}_d\pi t_f)^{0.5} \qquad 4.1\text{-}14$$

The terms are as defined in the Nomenclature. The corresponding expression for k_{df}, based on the final drop area becomes

$$k_{df} = 1.31\left(\frac{\mathcal{D}}{\pi t_f}\right)^{0.5} \qquad 4.1\text{-}15$$

Popovich et al (124) compared some of the above

models on the basis of a single equation for mass transfer during drop formation

$$N_A = (c_s - c_o)(D\pi)^{0.5} d_f^{2} t_f^{-0.667} t^{1.167} \qquad 4.1\text{-}16$$

where N_A is the mass transferred from a drop in time t.

Angelo et al (5) developed a general theory for the surface stretch model. This generalised penetration theory applies to both forming and oscillating drops. Their theoretical consideration led to the equation

$$k = \frac{2}{\tau} \left(\int_o^t \left[\frac{s(t)}{s_o} \right]^2 \right)^{0.5} dt \qquad 4.1\text{-}17$$

Skelland and Minhas (143) studied mass transfer rates during drop formation for dispersed phase-controlled liquid systems. By statistical analysis they obtained the correlation

$$\frac{k_{df} t_f}{d} = (N_{M1}) = 0.0422 \left(\frac{U_N^2}{dg}\right)^{0.089} \left(\frac{d^2}{\mathcal{D}_d t_f}\right)^{-0.334} \left(\frac{\mu}{\sqrt{\rho_d d\sigma}}\right)^{-0.601} \qquad 4.1\text{-}18$$

Their results, however, showed 25% greater measured rates during drop formation than those predicted by various theoretical models including those by Heertjes et al (69) and Ilkovic (74).

4.1-2 EFFECTS OF SURFACE ACTIVE AGENTS

Any surface active substances present in extraction processes are adsorbed at the liquid-liquid interface. Some of them can, in very small concentrations, reduce the rate of interface mass transfer of an extracting solute to a remarkable degree. For example, Lindland and Terjesen (102) showed that 6×10^{-5}gm of a specific active agent (sodium oleyl-p-anisidinesulphonate) per 100ml liquid reduced mass transfer rates up to 68% in the systems carbon tetrachloride-aqueons iodine-water. Garner and Hale (41) also found that the addition of 0.015% Teepol to the continuous phase reduced the rate of extraction of diethylamine from toluene by water to 45% of its normal value.

When surfactants are present, variations in interfacial tension occur around the drop surface. Experimental observation by Savic (133) suggests that with a moving droplet the action involves an immiscible cap forming over the rest of the sphere while the surface flow over the forward surface remains unimpeded.

However, hydrodynamic effects cannot be neglected since a reduction in internal circulation has been observed due to adsorbed surface active molecules. As a result of this mechanism, at high concentrations of surfactant mass transfer to drops approximates to that to solid spheres.

Levich and Frunkin (97) considered mass transfer in the presence of surfactants from both theory and practical results. They proposed that the surface active agents are adsorbed on the surface of the droplet and swept to its rear by the countercurrent flow of the liquids. This compressed film at the rear of the droplet will have a higher surface pressure and therefore tends to spread backwards opposing flow along the surface between the immiscible fluids.

Skelland and Caenepeel (140) studied the effects of anionic and cationic surface active agents on mass transfer in continuous and dispersed phase controlled systems. They found that contamination resulted in a reduction in mass transfer to 10% with a marked minimum at intermediate concentrations of surfactant. In contrast, the continuous phase coefficient during coalescence was substantially increased by surfactants, with maxima in some cases.

In the light of the above discussion, the effects of surface active substances on mass transfer may be placed into two categories:

(1) Those that form an interfacial barrier of a mechanical, physical or chemical nature (41, 102).

(2) Those which modify the relevant hydrodynamics

(a) by reducing the rate of internal circulation in drops (46, 85)

(b) by damping the interfacial waves or oscillation (12, 28, 32)

(c) by decreasing the terminal velocity of drops (6, 11, 12, 32, 42, 46, 135)

(d) by lowering the interfacial tension (35, 42, 104, 135)

(e) by lessening the transmission of turbulence across the interface (98)

(f) by retarding the rate of coalescence (62, 94).

This discussion indicates that cleanliness is an extremely important factor in obtaining reliable data from experiments on liquid-liquid hydrodynamics and mass transfer. However, some extractions in industrial columns will inevitably be contaminated because of the use of commercial feedstocks. Therefore, this should be taken into consideration when designing columns from single drop data obtained in laboratory columns with pure systems.

4.1-3 EFFECT OF INTERFACIAL TURBULENCE

Interfacial turbulence is a spontaneous activity which may occur at the interface when two liquids, not at equilibrium are in contact. It can bring about a

variety of effects; droplets of a liquid immersed in another may for example be subject to erratic pulsations, eruptions from the surface, violent internal circulation, spontaneous emulsification rippling and twitching of the interface (43, 64, 65, 139). Such activity can be expected to increase the rate of mass transfer over and above that anticipated from the gross hydrodynamic situation. In some cases, rates have been increased as much as tenfold or more (139).

It has frequently been noted that these effects may occur only when the solute is transferred in one direction across an interface but not when it is transferred in the opposite direction and that surface active agents can reduce the effect markedly.

These effects are evidently produced by gradients in interfacial tension resulting from concentration gradients along the surface. This is termed the Marangoni effect (64). Scriven and Sterling (138) treated the hydrodynamics of interfacial instability mathematically using the equations of motion and diffusion. They concluded that some systems may be stable when solute transfer is in one direction, but unstable with transfer in the opposite direction.

Sawistowki and Goltz (134) attempted to relate the mass transfer coefficient to observedbehaviour of

the interface for individual drops when solute transfer was from benzene drops into a continuous aqueous phase. Their results indicated the existence of two main regimes of transfer; the diffusional regrime based on the penetration theory of Higbie (70), and the turbulent regime. Mass transfer coefficients in the latter regime were dependent upon the local interfacial tension and on the concentration of the solute in the dispersed benzene phase.

4.2-1 MASS TRANSFER DURING DROP COALESCENCE

Johnson and Hamielec (80) studied mass transfer during drop coalescence. They proposed a correlation for transfer to or from a drop coalescing immediately as it reaches the phase boundary. It was assumed that as the drop drains, its contents spread out over the entire coalescence surface in a uniform layer. Transient mass transfer then occurs according to the penetration theory with the time of exposure of the layer being equated to the time of formation of the drop. After time t_f the next drop arrives and the mass transfer cycle is repeated. Using the instantaneous transfer rate given by Higbie's (70) equation, Johnson and Hamielec obtained the following equation

$$k_{dc} = 2\left(\frac{\mathcal{D}_d}{t_f}\right)^{0.5} \qquad 4.2\text{-}1$$

Skelland and Minhas (143) derived an expression for the mass transfer coefficient at coalescence K_{dc}. This is given in a simplified form as

$$k_{dc} = \frac{2U_d}{a_c t_f} \left[\frac{2I_{f,c} + (k_{df}/U_d) a_f t_f (I_{f,c} - 4U_d)}{8U_d - 2I_{f,c} - (k_{df}/U_d) a_f t_{f,c} I_{f,c}} \right] \quad 4.2\text{-}2$$

These authors also correlated their experimental results by an expression similar to that proposed for drop formation. The correlation for drop coalescence is

$$\frac{k_{dc} t_f}{d} = 0.1727 \left(\frac{\mu_d}{\rho_d D_d}\right)^{-1.115} \left(\frac{\Delta\rho g d^2}{\sigma}\right)^{1.302} \left(\frac{U_t^2 t_f}{D_d}\right)^{0.146} \quad 4.2\text{-}3$$

where the notation is as defined in the Nomenclature. However, this equation did not satisfy the penetration theory as predicted by Johnson and Hamielec. The average absolute deviation from the data was approximately 25%.

Licht and Pansing (100) briefly investigated the mass transfer of acetic acid from coalescing methyl isobutyl acetone drops into a continuous water phase. They concluded that the amount of transfer was proportional to the concentration of the drop and its diameter.

Treybal (154) modified the work of Licht and Pansing (100) and proposed the following expression

$$k_{df}\ a_f \approx k_{dc}\ a_c \qquad 4.2\text{-}4$$

Studies of both Jeffreys and Lawson (77) and Groothuis and Zuiderweg (57) show that drop coalescence rate increases if accompanied by mass transfer of solute from the droplets to the continuous phase but is retarded when this is from continuous phase to the drops.

4.2-2 MASS TRANSFER DURING DROP RISE (OR FALL)

As mentioned earlier swarms of drops behave differently from single drops, but their motion in counter-currently flowing liquid is a poorly defined area. The motion of a single drop is influenced only by the characteristic of the drop and the fluid immediately surrounding it. In situations involving multi-orifices such as perforated plate columns droplet swarms are produced which move at relatively small distances from each other. The movement of these droplet swarms is affected by the same factors as single drops as well as by the following

(i) drop size distribution

(ii) drop interaction

(iii) coalescence effects caused by closeness of neighbours

(iv) average velocity and local eddy motions of the continuous phase.

Therefore, knowledge of these factors is significant in determining accurate mass transfer coefficients in a perforated plate column.

For small circulating drops of isobutanol in water and nitrobenzene in ethylene glycol Ruby and Elgin (131) correlated mass transfer coefficients for the continuous phase with the following equation

$$k_c = 0.725\left(\frac{dU_s\rho_c}{\mu_c}\right)^{-0.43} (N_{sc})^{-0.58} U_s(1-\phi) \qquad 4.3\text{-}1$$

Rose and Kintner (129) proposed a method of analysis for mass transfer to or from large oscillating liquid drops. They assumed a constant volume for the mass transfer zone, to account for changes in area resulting from the oscillation, and that the local mass transfer coefficient varied in proportion to the thickness of this zone. The correlation takes the form

$$k_d = 0.45\ (\phi_d\omega)^{0.5} \qquad 4.3\text{-}2$$

The frequency of oscillation were predicted using the Schroeder and Kintner (136) modification of Lambs (93) equation

$$\omega^2 = \sigma \frac{b}{r^3} \left[\frac{n(n-1)(n+1))n+2)}{(n+1)\rho_d + n\rho_c} \right] \qquad 4.3\text{-}3$$

and the amplitude coefficient b is equivalent to

$$b = \frac{d_p}{1.242}^{0.225}$$

The terms are as defined in the Nomenclature. Experimentally n was found to be 2.

By modifying Rose and Kintner's (129) model, Angelo et al (5) proposed a correlation for mass transfer to (or from) large drops oscillating during rise or fall. Their surface stretch theory analysis gives the following equations

$$k_d = \left[\frac{4\delta\omega}{\pi} (1 + \delta + 0.375\delta^2) \right]^{0.5} \qquad 4.3\text{-}4$$

$$\text{where } \omega = \frac{1}{2\pi} \left[\frac{192\sigma g_c b}{d_p^3 (3\rho_d + 2\rho_c)} \right]^{0.5} \qquad 4.3\text{-}5$$

$$b = 1.052 d_p^{0.225}$$

δ is a dimensionless amplitude factor characteristic of the oscillation and may be taken as 0.2.

CHAPTER 5

PRACTICAL OPERATION OF PERFORATED PLATE COLUMN

5. PRACTICAL OPERATION OF PERFORATED PLATE COLUMN

5.1 EFFECT OF PLATE SPACING

The effect of plate spacing on the mass transfer efficiency of perforated plate columns was studied in a 90.4mm diameter column using plate spacings of 76.2mm, 152.4mm and 228.6mm by Treybal and Dumoulin (155) with the system toluene - benzoic acid-water. They observed that with this system, and over the concentration range of 0.00012-0.00024gm mole benzoic acid per cm^3 solution correlation by means of (HTU) was reasonable. Decreasing the plate spacing improved the extraction efficiency but decreased the volumetric throughput permissible; this limits the usefulness of spacings less than 152.4mm. These effects and the need to balance efficiency and throughput have been observed by many authors (90, 104, 110, 126) and their results are all in good agreement as shown in Table 5.1-1.

While plate efficiency increases with increasing plate spacing, the effective separating height decreases; thus a tall column would be required for a large plate spacing. Therefore, the economic plate spacing for any specific industrial use could be obtained by balancing the increased cost of pumping and shell construction against the reduced cost of the plates. For large diameter columns, the clearance between the bottom of

TABLE 5.1-1

PLATE SPACING

Dispersed Phase	Continuous Phase	Extracted Solute	Tower dia. cm	Hole dia. cm	No. of Plates	Plate Spacing cm	Efficiency %	References
Toluene	Water	Benzoic Acid	9.22	0.4763	11	12.07	5-10	Allerton, Strom & Treybal (3)
Kerosene	Water	Benzoic Acid	9.22	0.4763	11	12.07	5-10	
Toluene	Water	Diethyla-mine	10.62	0.3175	8	15.24	5-17	Garner, Ellis & Fosbury (38)
Water	Toluene	Diethyla-mine	10.62	0.3175	8	15.24	2-15	Garner, Ellis & Hill (39)
Toluene	Water	Benzoic Acid	6.91	0.1168	1	30.48	13-30	Goldberger & Benenati(53)
Toluene	Water	Benzoic Acid	5.08	0.3175	6	60.96	3-16	Mayfield & Church(104)
Water	Toluene	Benzoic Acid	5.08	0.3175	6	60.96	16.38	
Toluene	Water	Benzoic Acid	7.77	0.3175	8	15.24	2.7	Murall & Rao (114)

Dispersed Phase	Continuous Phase	Extracted Solute	Tower dia. cm	Hole dia. cm	No. of Plates	Plate Spacing cm	Efficiency %	References
Toluene	Water	Benzoic Acid	22.23	0.3175	10	15.24	3-10	Row, Koffolt & Withrow (130)
Toluene	Water	Benzoic Acid	8.89	0.4763 0.4763 0.4763	17 9 6	7.62 15.24 22.86	3-6 5-9 7-13	Treybal & Dumoulin (155)

the downspout and the plate below fixes the minimum plate spacing.

5.2 EFFECT OF HOLE SIZE

For a constant hole area, increase in hole diameter in a plate decreases the number of drops formed at the plate at any instant, for a given throughput. Within the normal range of drop diameter there is consequently a decrease in interfacial area for mass transfer and thus a decrease in the mass transfer efficiency.

Nandi and Ghosh (50) studied this effect of hole size on mass transfer, with the systems, benzene-acetone-water and kerosene-acetone-water. Their results showed that when the hole size was changed from 1.587mm to 3.175mm, keeping the hole area constant, higher efficiencies were obtained with 1.587mm holes than with 3.175mm holes for the system kerosene-acetone-water. The effect was less pronounced with the system benzene-acetone-water.

Krisna et al (89) used methods similar to those of Nandi and Ghosh (50) to find the hole size effect in a 122mm diameter perforated plate column, using the system pegasol-butyric-acid-water, with pegasol dispersed. Their results also showed a decrease in mass transfer coefficient with an increase in the plate hole diameter.

Pyle et al (126) also studied this effect using plates with 3.34% free area and the system ethyl ether-acetic acid-water. Their results showed that at normal operating rates, there was little effect of hole size on plate efficiency between size limits of 1.613mm and 5.11mm. However, the smaller holes showed a higher efficiency.

5.3 EFFECT OF HOLE AREA

From the fundamental theory of diffusional processes, increasing the area of contact between two phases will result in increased values of the diffusional coefficients. This effect has been studied by Pyle et al (126) and Nandi and Ghosh (50). The results of Pyle et al (126) showed that the plate efficiency increased with increasing the hole area of flow for the dispersed phase from 1.8 to 5% for a particular hole size. The results of Nandi and Ghosh (50) showed that there was no change in the values of the extraction coefficients when the hole area was increased from 4.5 to 9%. Krishnamurthy and Rao (88) observed a decrease in overall mass transfer coefficients with an increase in hole area for 1.587mm hole diameter.

The conflicting results of these authors, however, indicated that the optimum hole area in perforated plates has not yet been properly defined.

CHAPTER 6

STAGE EFFICIENCY

6. STAGE EFFICIENCY

FACTORS AFFECTING STAGE EFFICIENCY

For systems of relatively low interfacial tension, i.e. $\sigma < 5.0$ dynes cm^{-1}, perforation diameter and total perforation area have been found to have little effect on stage efficiency (126). However, for systems with high interfacial tension, a decrease in drop size produced by smaller holes results in considerable improvement in extraction rates. Increased plate spacing increases stage efficiency owing to the longer times of contact available for the liquids per stage.

MURPHREE STAGE EFFICIENCY

For columns in which contacting is stagewise masstransfer behaviour is normally characterised either in terms of "stage efficiency" or "stage effectiveness". One of the most widely used theories for calculating stage efficiency is that of Murphree (153). The Murphree efficiency is defined as the change in concentration of a given stream in passing through a stage divided by that which would have been obtained if the two exit streams were in equilibrium. Therefore, Murphree stage efficiency may be expressed in terms of extract composition as E_{ME} or in terms of raffinate compositions as E_{MR}. Thus as shown diagramatically in

Figure 6.1-1.

$$E_{MD} = E_{ME} = \frac{y_m - y_{m+1}}{y_m^* - y_{m+1}} \qquad 6.1\text{-}1$$

$$\text{or } E_{MR} = \frac{x_{m-1} - x_m}{x_{m-1} - x_m^*} \qquad 6.1\text{-}2$$

where x_m and y_m represent the actual average effluent compositions and y_{m+1} and x_{m-1} those of the streams entering the stage. The composition x_m^* and y_m^* represent hypothetical liquid systems that would leave the stage in equilibrium with the average composition of the extract or raffinate actually leaving the stage.

Some relation between Murphree efficiencies and mass transfer coefficients are given in Table 6.1-1. These expressions are only correct for the special case where the equilibrium line is straight over the concentration range for the stage in question.

It must, however, be kept in mind that values of effectiveness are also functions of flow conditions as well as mass transfer coefficients. Thus the observed effectiveness of an extractor may be greater than unity if mixed flow is assumed but at least some counterflow actually exists.

In most actual extractors the flow pattern appears

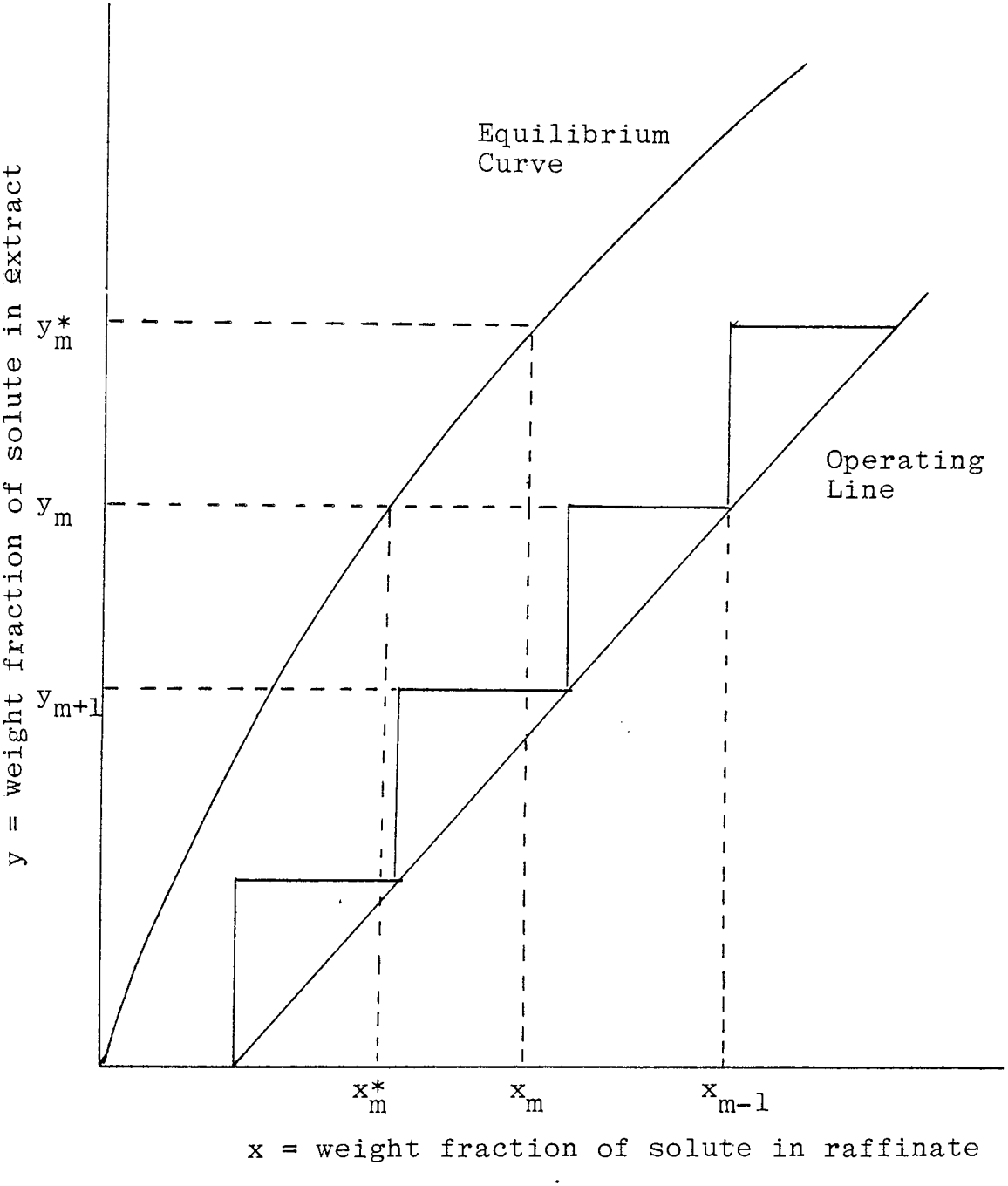

Fig. 6.1-1 Murphree Stage Efficiency

TABLE 6.1-1

CORRELATIONS FOR MASS TRANSFER EFFICIENCY WITH DROPLET SWARMS

PHYSICAL DESCRIPTION	CONDITIONS IMPOSED	EQUATION FOR TRANSFER EFFICIENCY DURING STEADY FALL (RISE) PERIOD	REFERENCE
Stagnant	Finite continuous phase resistance	$E = 1-6 \sum_{n=1}^{\infty} B_n \exp(-4\lambda_n^2 \frac{\mathcal{D}_{AD} t}{D^2})$	Grober (55)
Rigid	No continuous phase resistance, transfer by molecular diffusion	$E = 1 - \frac{6}{\pi 2} \sum_{n=1}^{\infty} \frac{1}{n^2} \exp(\frac{4n^2 \mathcal{D}_{AD} \pi^2 t}{D^2})$	Newman (117)
Rigid	No continous phase resistance	$E = \left[1 - \exp(\frac{-\pi^2 \mathcal{D}_{AD} t}{D^2}) \right]^{\frac{1}{2}}$	Vermeuleu (157)
Circulating Hadernard's Stream Lines	No continuous phase resistance Re < 1, σ = o	$E = 1 - \frac{3}{8} \sum_{n=1}^{\infty} B_n^2 \exp(\frac{-64\tau_n \mathcal{D}_{AD} t}{D^2})$	Kronig & Brink (91)
Circulating Hadernard's Stream Lines	No continuous phase resistance R_e < 1	$E = \left[1 - \exp(\frac{-2.25 \mathcal{D}_{AD} 4\pi^2 t}{D^2}) \right]^{\frac{1}{2}}$	Calderbank & Korchinski (16)

PHYSICAL DESCRIPTION	CONDITIONS IMPOSED	EQUATION FOR TRANSFER EFFICIENCY DURING STEADY FALL (RISE) PERIOD	REFERENCE
Circulating Hadernard's Stream Lines	Finite continuous phase resistance	$E = 1 - \frac{3}{8} \sum_{n=1}^{\infty} B_n^2 \exp\left(\frac{-64\lambda_n \mathcal{D}_{AD} t}{D^2}\right)$	Elizinga & Banchero (32)
Circulating Toriodal Circulating Patterns	No continuous phase resistance $R_e < 1000$	$E = 1-2 \sum_{n=1}^{\infty} B_n \exp\left(\frac{-16\lambda_n \mathcal{D}_{AD} t P_{eD}/(1+\mu_D/\mu_c)}{2048 D2}\right)$	Handlos & Baron (59)
Forming and Oscillating Stretching and Shrinking Motion of the Surface	Finite continuous phase resistance	$E_m = 1 - \exp\left\{ -\sqrt{\frac{4\mathcal{D}_d \omega}{\pi}} (1+\epsilon+\frac{3}{8}\epsilon^2) \frac{A}{V} t_c \right\}$	Angelo et al (5)

to be sufficiently complex that none of the existing flow models would give a realistic basis for correlating stage performance directly with interphase mass transfer coefficients. The situation is still further complicated by the fact that the mass transfer coefficients themselves can vary significantly with position in the extractor stages. For example, in an agitated column they would be expected to be a function of proximity to the agitator, i.e. degree of turbulence; in a perforated plate column they are clearly dependent on the stage in the droplets life. In small laboratory columns overall stage efficiencies as high as 80% have been obtained (113). However, an overall efficiency of 5 to 45% is more common in extraction with the bulk of the data below 20%. Efficiencies of most industrial extractors are not much better.

Treybal (113) correlated overall efficiency data taken from small laboratory sieve plate columns of diameters ranging from 5.1 to 22.23cm and with plate spacing from 7.62 to 60.96cm. The following empirical equation is proposed for estimating overall stage efficiency

$$E = \frac{89500 H_c^{0.5}}{\sigma} \left(\frac{U_D}{U_C}\right)^{0.42} = \frac{0.9(H_c')^{0.5}}{\sigma} \left(\frac{U_D'}{U_C}\right)^{0.42} \qquad 6.1\text{-}3$$

Based on the above correlation, Krishnamurty and Rao (88) suggest that Treybal's correlation could be improved if the right hand side is multiplied by $0.1123/d_o^{0.38}$.

CHAPTER 7

EXPERIMENTAL INVESTIGATION

7. EXPERIMENTAL INVESTIGATION

7.1 INTRODUCTION

As discussed earlier, in plate columns the drops undergo a repetitive cycle of formation from orifices, travel and re-coalescence. The interfacial area is a function of the drop size distribution and dispersed phase hold-up; the mass transfer coefficient depends upon hydrodynamics; the concentration driving force is affected by back-mixing effects. To improve the efficiency of a column design therefore requires a basic understanding of these effects and how they are related to column geometry, for example plate layout, downcomer size, plate spacing and plate hole size.

Although investigations have been reported on the performance of sieve plate columns, there are no reliable design methods. The correlations which do exist are limited in application because they are generally for a specific column, not a column having different structural features, and do not cover a sufficiently wide range of operating variables.

The object of this research programme was therefore to study and correlate hydrodynamic and mass transfer performance using a 450mm pilot plant scale sieve plate column and to develop a design procedure for such columns from laboratory data. For this purpose an ideal system

Clairsol 350 - water with an interfacial tension of 35.50 dynes cm^{-1} was chosen.

7.2 EQUIPMENT DESIGN

The sieve plate extractor comprised a 450mm diameter, 2000mm high glass walled column with a volumetric capacity in excess of 1.67 litres per second for each phase. The perforated plates and the downspouts were supported by four 6.35mm diameter stainless steel tie rods running the length of the column. These rods were threaded at one end to permit fastening to the top end of the column thus preventing the weight of the plate resting on it. The perforated plates were held in position by screwed locking collars. The plates were sealed in the column by means of a 1.588mm thick Viton rubber skirt around each plate. The details of construction are shown in Figure 7.2-1 and the essential dimensions are shown in Table 7.2-1.

Figure 7.2-2 shows a schematic arrangement of the apperatus comprising the column, storage tanks, feed lines, flow controls and other auxillary equipment. The light liquid entered at the bottom and passed through the holes in the distributor and subsequently the perforated plates and left at the top of the column. The heavy liquid entered the top tray via a downspout and left at the bottom of the column. The top tray was

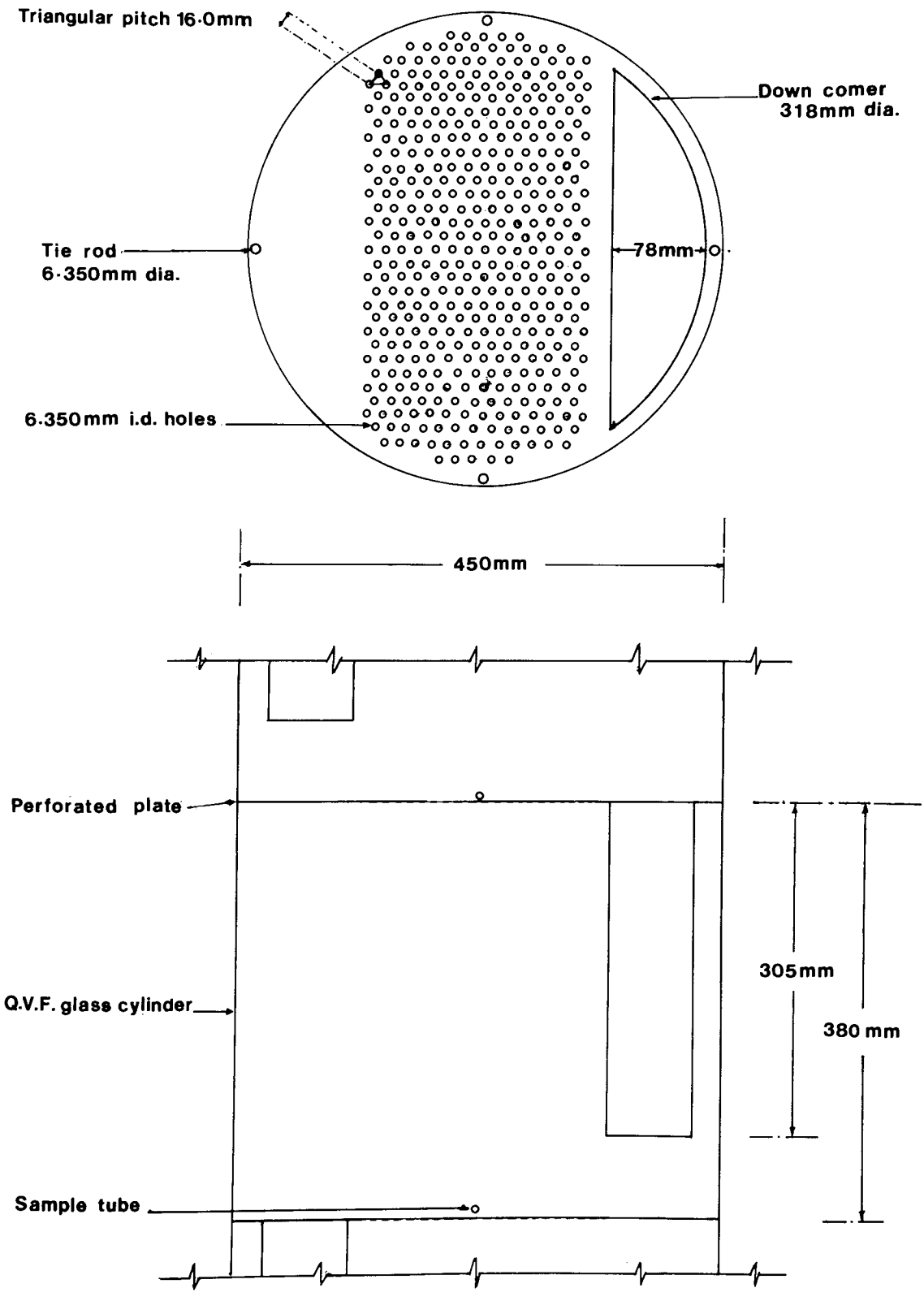

Fig. 7.2-1 Plate Design-6.350mm holes drilled and punched, 409 holes

thus free of entrance effects. The exit lines were of 38.10mm Q.V.F. industrial glass pipe, sufficiently oversized to ensure that they would not limit the capacity of the column.

The gaskets between the glass pipe sections of the column were of inert poly-tetrafluoroethylene (PTFE) rings. The gasket material used between the glass section of the column and the top and bottom section was neoprene sheet which had been found suitable for exposure to Clairsol 350.

Activated carbon filters were used to remove any surfactant contamination from both the light organic and heavy aqueous phase.

The plate layouts selected for investigation are shown in Table 7.2-2 and Figure 7.2-4. These were chosen because industrial columns typically use orifice sizes between 1.588mm and 6.350mm (153). The number of holes per plate were selected to give a dispersed phase superficial velocity in the range 0.28m sec^{-1} to 1.11m sec^{-1}, again typical of published operating conditions. The plate spacing was adjustable between 300mm and 460mm. The downcomer was adjustable to a height of 120mm above the plate. The four reservoirs were each of 1.00m^3 capcity. Each pair of the reservoirs were connected such that any one of two tanks could be used

TABLE 7.2-1

PUMPS

FOR LIGHT PHASE:

PUMP TYPE:	B40 Set A6 (Beresford Pump)
CAT NO.:	GBP/9
SERIAL NO.:	2/707
MOTOR HP:	2.0 BHP Flame proofed (BS229)
PUMP SPEED:	2900 RPM
PHASE:	3

FOR HEAVY PHASE:

PUMP TYPE:	Newman Electric Motors Pump (flame proofed)
FRAME:	F905 FC1216 DB
NO.:	66 421 003
CLASS:	B
MOTOR HP:	0.75
PUMP SPEED:	2850
PHASE:	3

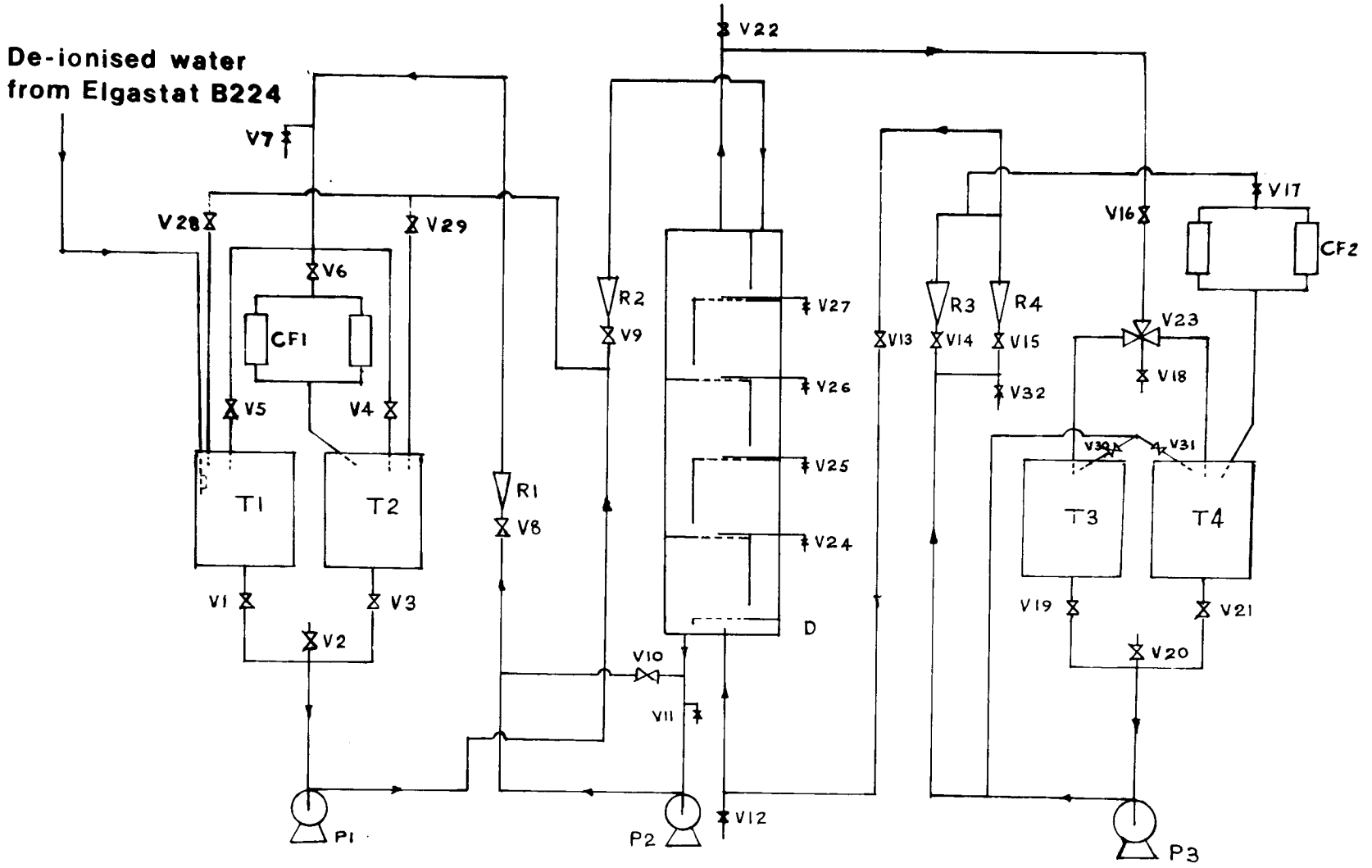

Fig. 7.2-2 Flow diagram of pilot plant sieve plate column

CF1, CF2:	Activated carbon filter tanks for continuous and dispersed phase.
P1, P2:	Inlet and outlet pumps for continuous phase.
P3:	Inlet pump for dispersed phase.
R1, R2:	Inlet and outlet flow measuring rotameters for continuous phase.
R3, R4:	Inlet and outlet flow measuring rotameters for dispersed phase.
T1, T2:	Tanks for continuous phase.
T3, T4:	Tanks for dispersed phase.
V1, V3:	Outlet valves for Tanks T1 and T2.
V19, V21:	Outlet valves for Tanks T3 and T4.
V2:	Drain valve for Tanks T1 and T2.
V20:	Drain valve for Tanks T3 and T4.
V4, V5:	Inlet valves for Tanks T1 and T2.
V23:	3-way inlet valve for Tanks T3 and T4.
V6, V17:	Inlet valves for the carbon filter tanks CF1 and CF2.

V7:	Sample point for Tanks T1 and T2 inlet continuous phase.
V18:	Sample point for Tanks T3 and T4 inlet dispersed phase.
V8, V9:	Control valves for column inlet and outlet continuous phase flow.
V14, V15:	Control valves for column inlet and outlet dispersed phase flow.
V16:	Throttle valve for column outlet dispersed phase.
V10:	Connection valve.
V11, V12:	Column drain valves for continuous and dispersed phases respectively.
V22:	Vent valve.
V24, V25, V26 V27,	Valves for taking samples across the respective trays.
V28, V29	By-pass valves for Tanks T_1 and T_2.
V30, V31	By-pass valves for Tanks T_3 and T_4.
V32,	Sample point for inlet dispersed phase
D	Distributor

TABLE 7.2-2

COLUMN DIMENSIONS

MATERIAL OF CONSTRUCTION:	QVF Transparent Glass
INSIDE DIAMETER:	450mm
THICKNESS:	20mm
HEIGHT:	2000mm
NO. OF STAGES:	5 (Distributor inclusive)

PLATES

MATERIAL OF CONSTRUCTION:	Stainless Steel
DIAMETER:	440mm
DIAMETER WITH VITON RUBBER SHEETING SKIRT ROUND:	458mm
PLATE TYPE:	Punched and Drilled
SETS OF PLATE:	4 sets
NO. OF PLATES PER SET:	5 (Distributor inclusive)

DOWNSPOUT

MATERIAL OF CONSTRUCTION:	Stainless Steel
DIAMETER:	318mm
ARC RADIUS:	78mm
THICKNESS:	10mm
HEIGHT:	305mm

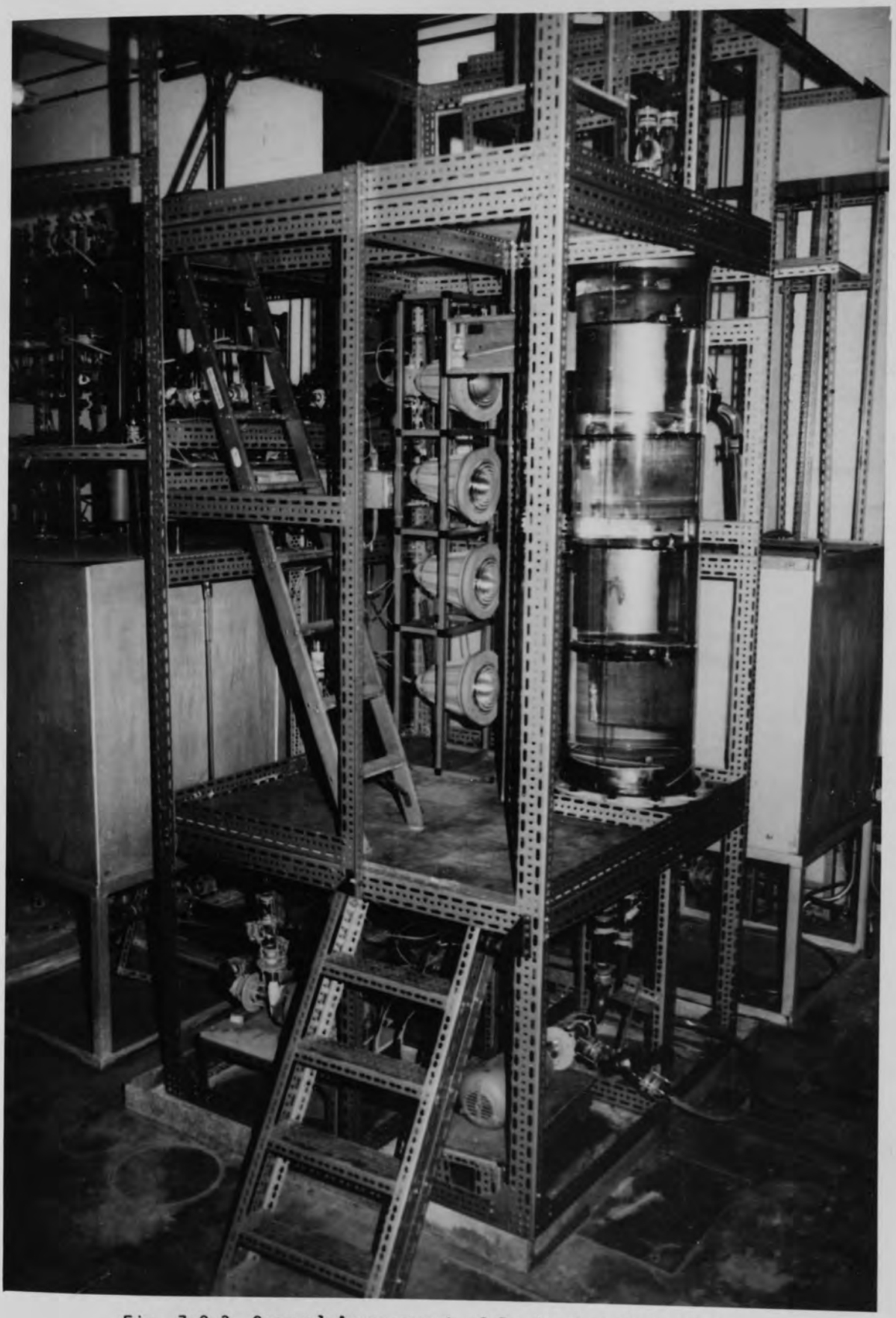

Fig. 7.2-3 General Arrangement of Perforated Plate Column

Lower Access platform at 108 cm elevation with reservoirs in background.

Upper Access platform at 208 cm coincides with top of column section.

TABLE 7.2-3

PLATE LAYOUT

HOLE TYPE	PLATE THICKNESS (mm)	HOLE SIZE (mm)	NO. OF HOLES PER PLATE
DRILLED	3.175	1.587	1517
DRILLED	3.175	3.175	985
PUNCHED	1.587	4.763	550
PUNCHED	1.587	6.350	380

Fig. 7.2-4 Perforated Plate Details

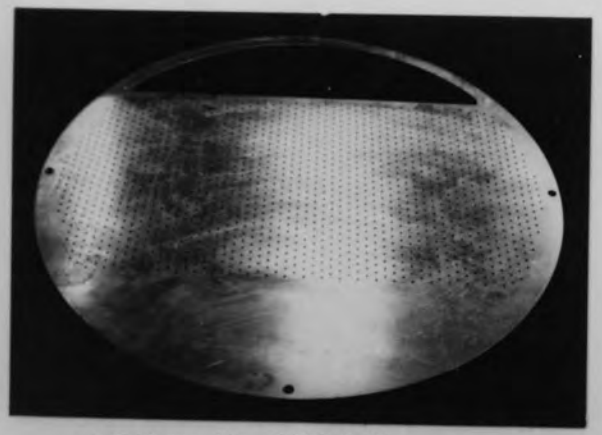

1.588 mm dia. 1517 holes
8.0 mm pitch, drilled only.

4.763 mm dia. 550 holes
13.0 mm pitch, drilled and punched.

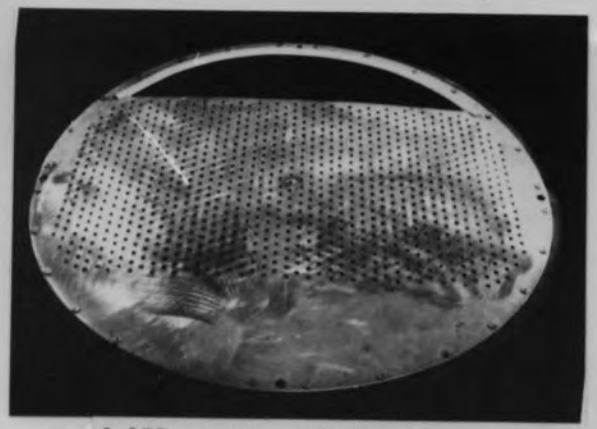

3.175 mm dia. 985 holes
10.0 mm pitch, drilled only

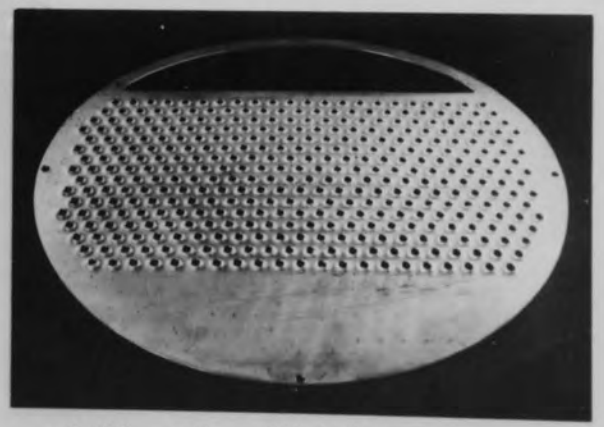

6.350 mm dia. 380 holes
16.0 mm pitch, drilled and punched

TIE ROD

MATERIAL OF CONSTRUCTION:	Stainless Steel
NO. OF THE RODS:	4
DIAMETER:	6.35mm
LENGTH:	2100mm

TANK DIMENSIONS

MATERIAL OF CONSTRUCTION:	Stainless Steel
LENGTH:	913mm
WIDTH:	913mm
HEIGHT:	1223mm
THICKNESS:	12mm
VOLUME:	$1.02m^3$

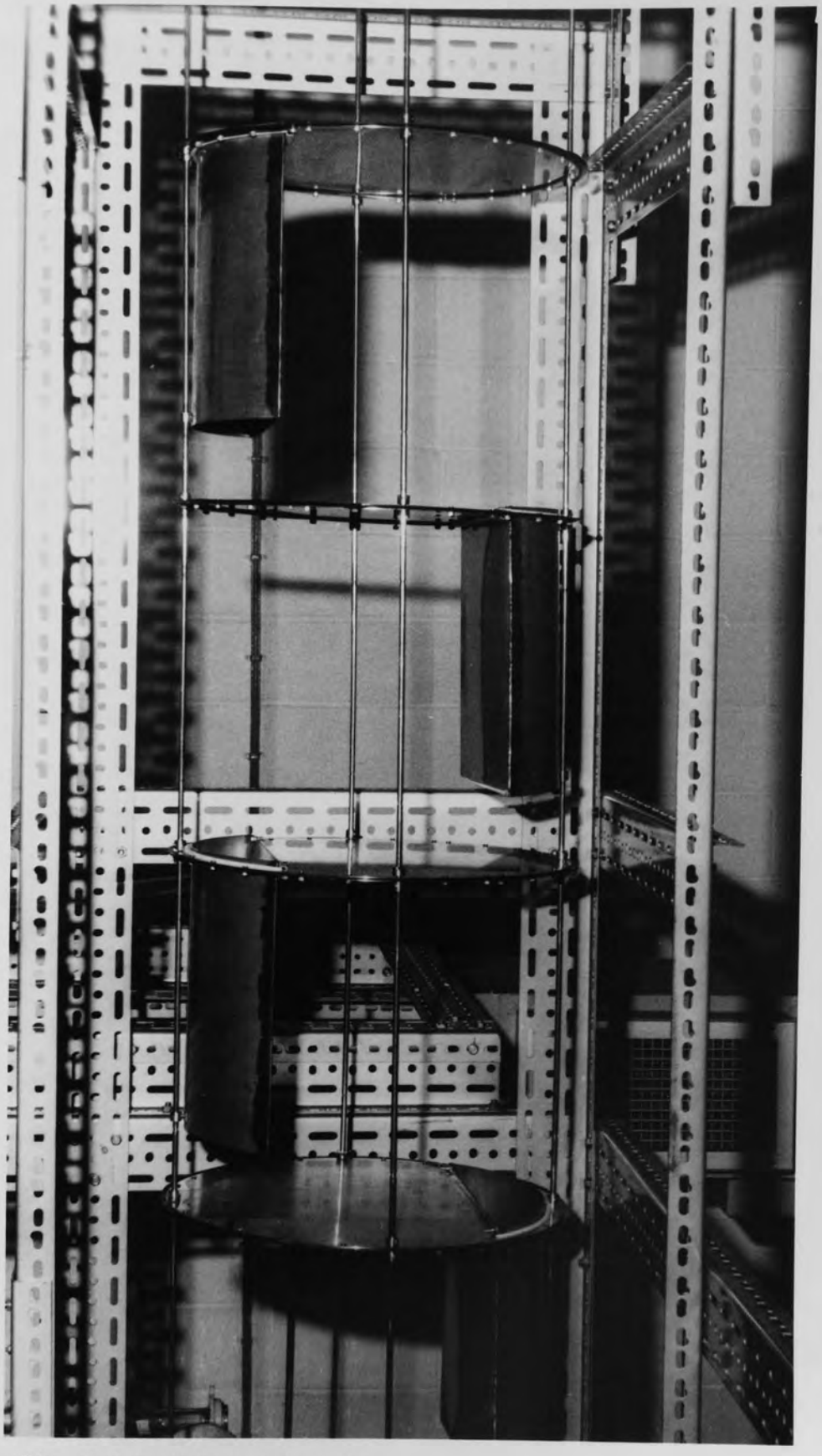

Fig. 7.2-5 Column Internals

4 plates with downcomers (distributor not shown).

Fig. 7.2-5a Detail of bottom distributor plate.
550 holes on 13.0 mm pitch, drilled and punched.
(N.B. plate was perfectly flat; illusion of distortion is due to refraction through glass because of angle of camera).

separately or simultaneously. The dispersed phase was transferred by means of a stainless steel centrifugal pump capable of delivering $0.2m^3\ sec^{-1}$ against 8m head. The continuous phase pump was a Newman, class B type, with 0.75 motor horse power, flame proof and capable of delivering $0.02m^3\ sec^{-1}$ against 4m height. Full pump details are given in Table 7.2-1. The flowrates were indicated on directly calibrated rotameters; the range of the light phase rotameter was 0-3.83 litres sec^{-1} and of the heavy phase rotameters 0-1.67 litres sec^{-1}.

For reasons of safety and economy de-ionised water was used throughout as the continuous phase. This was obtained by passing Birmingham mains water, typical specification for which is given in Appendix 2, through an Elgastat B224 de-ioniser. The specification of this de-ioniser is given in Appendix 3. The dispersed phase was Clairsol 350 specified in Appendix 4.

COALESCENCE ZONE

In any gravity operated column coalescence of the dispersed phase is eventually necessary at the top, or bottom, of the column. Complete coalescence is desirable to avoid continuous phase carry-over. Provision may be made for this, by constructing an external settler. Alternatively, an extension of the column height is required. This extension is sized from a consideration of

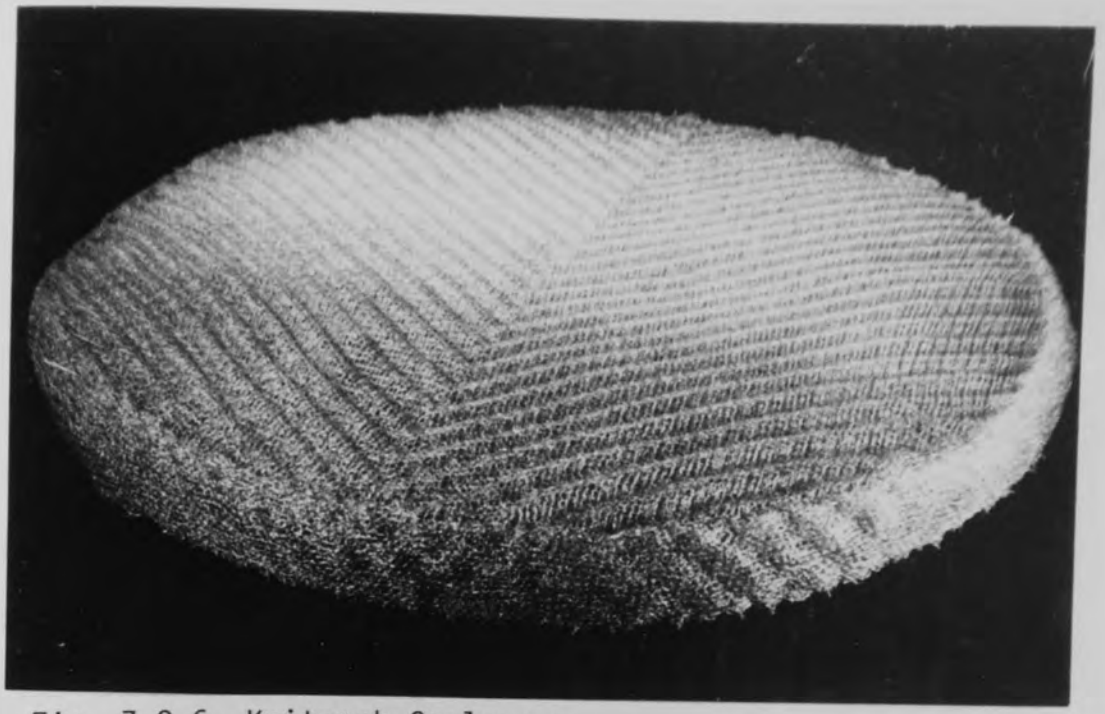

Fig. 7.2-6 Knitmesh Coalescer
Stainless Steel and Polypropyene D.C. Packing
457.2 mm dia x 50.8 mm thick.

Fig. 7.2-7 Top Cover Detail
Knitmesh pad in position for coalescence of outlet dispersion. First downcomer continuous phase input.

the flocculation and coalescence zones which, in practical columns, are sensitive to the presence of contaminants, e.g. interfacial scum or traces of surfactants. Common practice is to increase the cross-sectional area of the column in the disengaging section to assist phase separation.

Coalescing aids may be used to reduce the residence time and hence column volume required, e.g. knitted mesh pads. Selection of this aid depends upon the wetting properties of the dispersed phase. If the dispersed phase wets the surface, drops will coalesce at the solid surface in the form of a liquid film; subsequent drops coalesce readily with this film. If the dispersed phase does not wet the surface, coalescence will occur only if the drops remain in close contact. Generally, there is a significant reduction in coalescence time if the dispersed phase wets the surfaces. Thus, polymer-based packings are preferred if an organic phase is dispersed and stainless steel packings are effective if the aqueous phase is dispersed.

Davies et al (25, 26, 27) have investigated the influence of wettability on coalescence. They used packings composed of more than one material and the result was an effective coalescer. A woven mesh of stainless steel wire and polypropylene fibres resulted in a much more effective coalescence than a one component

packing. This type of multi-component packing system is appropriate for various uses. For example, both a Clairsol-water and a water-Clairsol dispersion can be separated with the same mixed packing. Figure 7.2-6 shows the mixed stainless steel wire and polypropylene fibres; Knitmesh D.C., packing inserted at the top of the column in this work.

7.3-1 MEASUREMENT OF PHYSICAL PROPERTIES

The measurements of the physical properties were made on the dispersed phase, mutually saturated with de-ionised water at 20°c. As outlined in 7.2, this approximated to column operating conditions.

INTERFACIAL TENSION

Interfacial tension was measured on a White Torsion balance equipped with a 4cm circumference ring. Temperature control was within ±0.01°c by means of a Townson and Mercer temperature control system. An average value was taken of the eight observations which gave the highest value of interfacial tension. Lower values were considered unreliable because the film could be ruptured by external disturbances before the maximum tension could be applied on the ring.

VISCOSITY

A Canon Fenske capillary tube viscometer Type BS/1P/CF, number 50 was used to measure viscosity. Using the constant temperature control system, the viscometer was calibrated with distilled water assuming a linear relation between kinematic viscosity and the time needed for the liquid level to fall from one mark to another while the liquid flowed through the capillary tube into another leg.

DENSITY

Density measurements were made using DMA 60 parr digital density meter.

DIFFUSION COEFFICIENT

Diffusion coefficient is an important variable in the general treatment of mass transfer in liquid systems. Several correlations (120, 137, 146) are available for the diffusion of various solutes in a given solvent. These correlations are based upon the two diffusional theories of non-electrolytes, Eyring's theory of absolute reaction rates and the hydrodynamic theory of Stoke Einstein. The correlations most widely used are the ones presented by Wilke and Chang (162), Wagner (158) and King and Mao (84). The last correlation seems to give results of best reproducibility (in a review of these correlations (84)

predictions were compared with 23 experimental values. The standard deviations of these correlations were as follows: Wilke and Chang, 18.5%; Wagner 24.3%; and King and Mao, 21.5%). The first correlation can be quite useful in cases where information on the physical data needed by the other two correlations is not easily available. This correlation was therefore used for estimating the value of the diffusivity for Water-Acetone-Clairsol 350 system. The value of diffusion coefficient of Acetone in Clairsol 350 estimated at $20^{o}c$ was $1.37 \times 10^{-5} cm^{2}\ sec^{-1}$; for Acetone in water $1.10 \times 10^{-5} cm^{2}\ sec^{-1}$.

7.3-2 SYSTEM INVESTIGATED

	DE-IONISED WATER	CLAIRSOL'350'
Density (gm cm^{-3})	0.9982	0.783
Viscosity (kg $^{-1}m^{-1}$)	0.0011	0.0018
Surface Tension (dyne cm^{-1})	71.48	26.73
Interfacial Tension (dyne cm^{-1}) with de-ionised water	-	35.50

7.4 EXPERIMENTAL PROCEDURE

7.4-1 CLEANING THE COLUMN

Cleanliness is an important factor affecting liquid extraction column operation since surfactants, or oil and grease, can easily be dissolved by one of the phases. These result in changes in the physical properties of the system and may lead to inconsistences in the experimental data and results. Suspended solids, e.g. interfacial scum or corrosion products, may act similarly. Therefore, prior to experiments, all the column internals were cleaned using an aqueous solution of Decon 90 at a concentration of 100ml Decon 90 per 20 litres of water. The column was allowed to stand with this solution in it for a minimum of 10 hours; it was then drained and rinsed several times with warm water, care being taken to ensure that no solution remained trapped in any dead ends or low points in the equipment. Finally, it was rinsed through with de-ionised water. The use of de-ionised water for the final wash and in operation was found to reduce the accumulation of interfacial dirt or rag between the two liquid phases. The storage tanks were cleaned in a similar manner.

7.4-2 COLUMN OPERATION

Initial investigation comprised a study of the hydrodynamic behaviour of the column with different plate geometries. Experiments were conducted with the system Clairsol 350-Water without solute being present. Prior to the experiment, the two phases were mutually saturated by allowing the two liquids to flow counter-currently for about 30 minutes or more in order to eliminate any effects due to mass transfer. Since no extraction took place, the physical properties of the solvent remained constant during passage through the column. Since there was no provision for heating/cooling of liquids all runs were made at room temperature. The temperature of the Flameproof Pilot Plant room in which the rig was located and the feeds temperature were found in fact to remain fairly constant at $20^{o}c \pm 0.5^{o}c$.

To start a run, water was admitted to the top of the column via the rotameter at a rate in the range 0 to 1.67 litres per second until it reached the chosen level. The dispersed phase (Clairsol 350) was then slowly introduced via the distributor. The Clairsol 350 which was dispersed into droplets by the plate perforations, rose through the water layer on each plate and normally coalesced into a layer of Clairsol 350 under the plate immediately above. The water flowed across

the plates and descended the column through the downspouts. The principal interface was adjusted and maintained steady at 40cm below the top cover plate for all the hydrodynamic runs. This prevented carry over of the water with the Clairsol phase leaving the top stage when there was a tendency for flooding to occur.

As the Clairsol rate was increased at a fixed water rate, the water outlet required adjustment in order to maintain the principal interface position steady. It was possible to reach a point when further adjustment would not maintain the interface and the column could no longer be operated properly; this corresponded to dispersed phase flow rate of 0.85 litres sec^{-1} and all experiments were necessarily performed below this.

7.4-3 SELECTION OF SYSTEM

Commercial grade Clairsol '350' was selected as the dispersed phase and de-ionised water was selected as the continuous phase. Analar grade acetone was the solute. In order to ensure that the transfer of solute was only in one direction, the dispersed Clairsol was always pre-saturated with continuous water phase.

The following measures were taken to ensure reliable and reproducible results.

(1) The saturation concentration in the aqueous phase was maintained low (Clairsol phase 0.01-0.15gm litre^{-1}; water 0.01-0.10gm litre^{-1}) in order to keep the continuous phase resistance minimal.

(2) The saturation concentration in the solvent phase was maintained large enough to yield a measurable rate of mass transfer.

(3) A sufficient range of the index of refraction of the pure and saturated dispersed phase was obtained to allow for measurement of dispersed phase concentration through its refractive index with good accuracy.

(4) In the range of compositions studied, the index of refraction versus composition curve

as shown in Figure 7.1-2 (in Appendix 5(a) and (b)), did not exhibit a plateau, that is it approximately obeys Beer's Law.

CHAPTER 8

RESULTS - COLUMN HYDRODYNAMICS

8. RESULTS - COLUMN HYDRODYNAMICS

Droplet hydrodynamics in the column were studied over a range of continuous phase throughputs between 0 and 0.70 litres per second (equivalent to U''_C = 0 to 0.44 $cmsec^{-1}$) and dispersed phase throughputs between 0.28 and 0.85 litres per second (equivalent to U_D=2.33 to 2.89 $cmsec^{-1}$, depending on the plate hole size).

For the interpretation of hydrodynamics and drop formation it was found necessary to define several different 'superficial velocities'. These were

U_C - continuous phase superficial velocity based on downcomer area

U_D - dispersed phase superficial velocity based on total plate hole area

U'_D - dispersed phase superficial velocity based on corrected plate hole area

U''_C - continuous phase superficial velocity based on column cross sectional area

U''_D - dispersed phase superficial velocity based on column cross sectional area.

Droplet hydrodynamics in the column were dependent not only on U''_D but upon U_D, determining the injection velocity of the droplets.

At a constant water flow rate with increasing dispersed Clairsol flow rates in the range 0.40 litres sec^{-1} to 0.85 litres sec^{-1} the solvent droplets were generally more nearly spherical, moved faster and coalesced rapidly beneath the plate. A tendency for the drops to become slightly elliptical was observed at the highest dispersed flow rates, i.e. >0.85 litres sec^{-1}.

All the holes in the distributor, or in the plates themselves did not operate at low rates (Fig. 8.1) e.g. U_D <13.31 $cmsec^{-1}$ for the plate hole size 0.1588 cm. This did not appear to interfere significantly with performance of the column i.e. an acceptable drop size distribution, described later in 8.2.1, was produced. With all the plate designs, except that with the smallest holes (d=0.1588cm), jetting occurred from the majority of active holes over the whole range of U_D values. Jetting was only observed with this one plate (d=0.1588 cm) at U_D>13.31 $cmsec^{-1}$.

The phenomena of starved holes resulted in higher nozzle velocities than calculated simply by dividing the volumetric throughput by the total theoretical hole area. A correction was therefore applied for this in calculations, based on experimental observations, as discussed in 8.3; hence the introduction of U_D'.

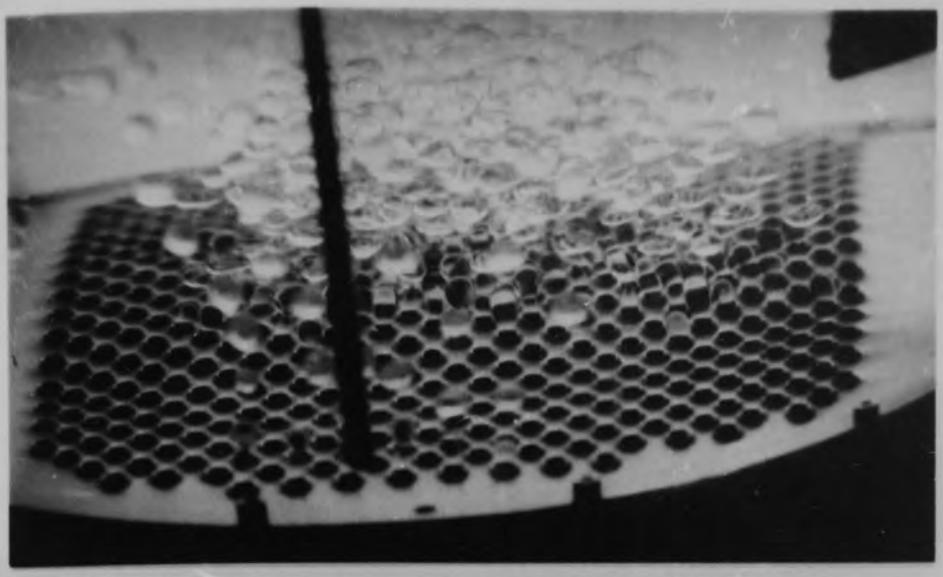

a) Distributor 4.763 mm i.d. hole size

b) Plate 1 6.350 mm i.d. hole size

c) Plate 2 6.350 mm i.d. hole size

Fig 8.1 Droplet formation at low dispersed phase throughputs $U_D = 2.80$ cmsec^{-1} $U''_C = 0.18$ cmsec^{-1}

Measurements were made of

(1) Drop formation from each plate of the four designs.

(2) Mean hold-up over the four plate section.

(3) Flocculation zone height beneath each plate.

(4) Drop size distribution from the distributor and, for different combinations of U_C and U_D, from the second plate.

8.1 SCOPE AND OBSERVATIONS

8.1-1 DROP FORMATION MECHANISMS - PLATES

The most easily observed effect of increasing the dispersed phase flow rate was the varying length of the jets above each plate. At low dispersed phase flow rates, $Q<0.30$ litres sec^{-1}, uniform drops were formed and released individually at the tip of the nozzles on a plate as shown photographically in Figure 8.1-1a. At increased dispersed phase flow rates, $Q>0.38$ litres sec^{-1}, the jets rapidly lengthened and appeared as smooth columns of liquid with occasional, transient lumps. Finally the jets took on a ruffled appearance at their outer ends and the drops formed became less uniform than in the earlier stage, Figure 8.1-1b. This was the maximum jet length obtainable in this experimental work for the plate hole size 0.6350 cm and its corresponding superficial velocity (U_D = 4.40 $cmsec^{-1}$) is the critical velocity. Increasing the flow rate further, Q = 0.85 litre sec^{-1}, equivalent to U_D = 7.06 $cmsec^{-1}$ for the 0.6350 cm plate hole size) caused the jets to oscillate violently from side to side followed by regular periodic disturbance. A mixed regime set in, i.e. drip point and jetting, and the jets began to cross each others flow paths; consequently, there was an

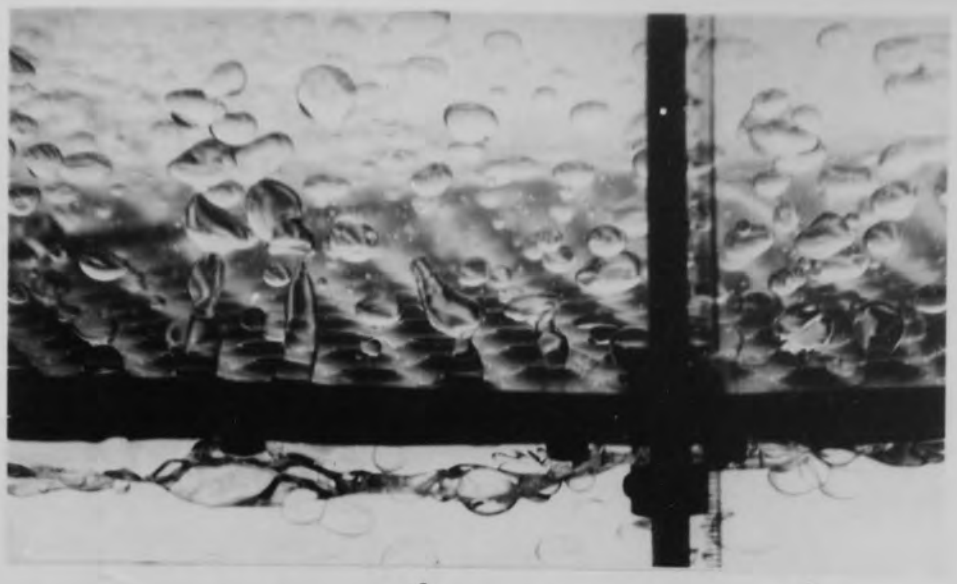

a) U_D = 2.33 $cmsec^{-1}$ U''_C = 0.27 $cmsec^{-1}$

b) U_D = 4.40 $cmsec^{-1}$ U''_C = 0.27 $cmsec^{-1}$

c) Mixed Regime: U_D = 7.06 $cmsec^{-1}$ U''_C = 0.27 $cmsec^{-1}$

Fig. 8.1 -1 Drop Formation by jetting - Plate 2:
6.350 mm i.d. hole size.

increase in the drops' non-uniformity. The corresponding dispersed phase superficial velocity at this point w s considered a 'disruptive' velocity, Figure 8.1-1c.

The effect of increasing U_C was to increase the continuous phase cross flow velocity which disturbed the jets (e.g. as in Fig. 8.1-1c). At high U_D and U_C values this caused side to side oscillation with a tendency to produce smaller drops. This effect was studied quantitatively for the distributor, see section 8.2-5.

8.1-2 HOLD-UP MEASUREMENT

Under steady state conditions of column operation, with the principal interface level maintained at a fixed position, the static hold-up was measured by noting the heights of the coalsced dispersion layer beneath each plate. The steady state height of the zone beneath the principal interface was not included, since in a practical column this takes no part in the extraction process and moreover is independent of the number of plates. Although not included in this determination, flocculation zone heights were also measured; these are discussed in section 8.1-3. Measurement was achieved by reference to graduated tape fixed to the outside wall of the

column. Measurements were made at various points around the column beneath each plate in the column and the results averaged.

The total hold-up was measured by simultaneously cutting off the flow of inlet and outlet liquids to and from the column by rapidly closing the appropriate valves V_{14} or V_{15}, V_8 and V_9. The light phase (Clairsol) was then allowed to settle completely, the heights of coalesced layer under each plate noted, and the total volume calculated.

The effective volume of dispersed phase in the column was obtained by subtraction of the respective static hold-up volume from the total volume of dispersed phase in the column. i.e., effective volume = total volume of dispersed phase - $A \sum_{1}^{n} h$, where n is the number of plates and A is the area of cross section of the column and $\sum_{1}^{n} = (h_1+h_2+h_3+h_4)$ where h_1, h_2, h_3 and h_4 are the individual heights of the coalesced layers under plates 1, 2, 3 and 4.

8.1-3 DROPLET COLLECTION BENEATH PLATES

Figure 8.1-2 shows the relationship between coalescence and flocculation zone height and dispersed phase superficial velocity at a fixed, steady continuous (water) phase rate. The thickness of the coalesced and flocculated layer beneath plates was measured with a transparent tape graduated in centimetres, attached along the length of the outside of the column. Several measurements at various positions around the periphery of the column cross-section were averaged. At high flow rates of water, i.e. $U''_C > 0.44$ cmsec^{-1} and dispersed phase superficial velocity $U''_D > 0.60$ cmsec^{-1} waves of increasing amplitude developed at the interface which made further measurement difficult; also droplets of Clairsol were carried to the downcomer and hence by-passed the plate. In some cases the phenomena shown in Figure 8.1-2(b) was observed i.e. accelerated coalescence beneath one area of a plate. This was attributed to the greatest flocculation height corresponding to the area of plate directly beneath a downcomer i.e. where there were no perforations.

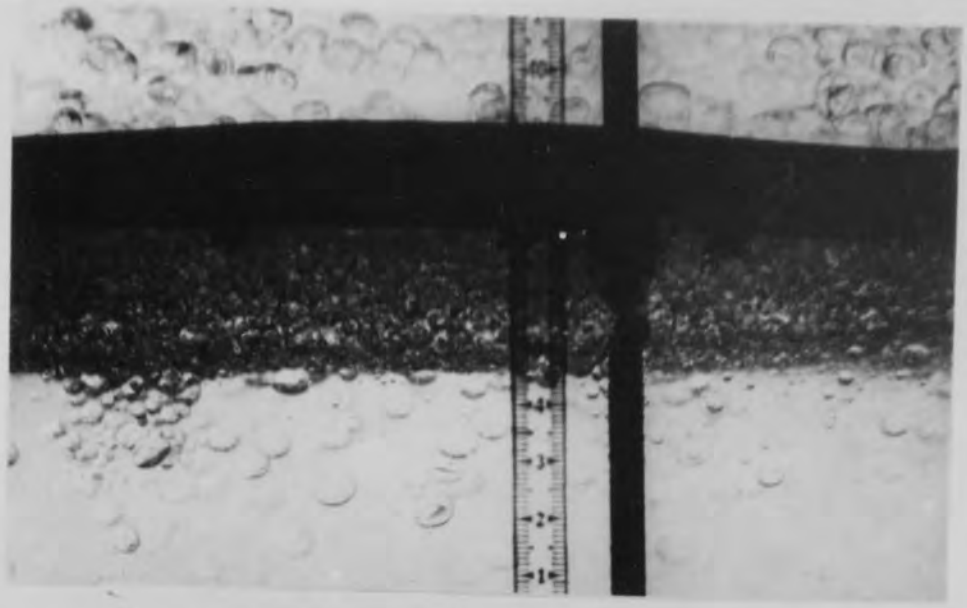

a) U_D = 9.32 cmsec^{-1} U''_C = 0.27 cmsec^{-1}

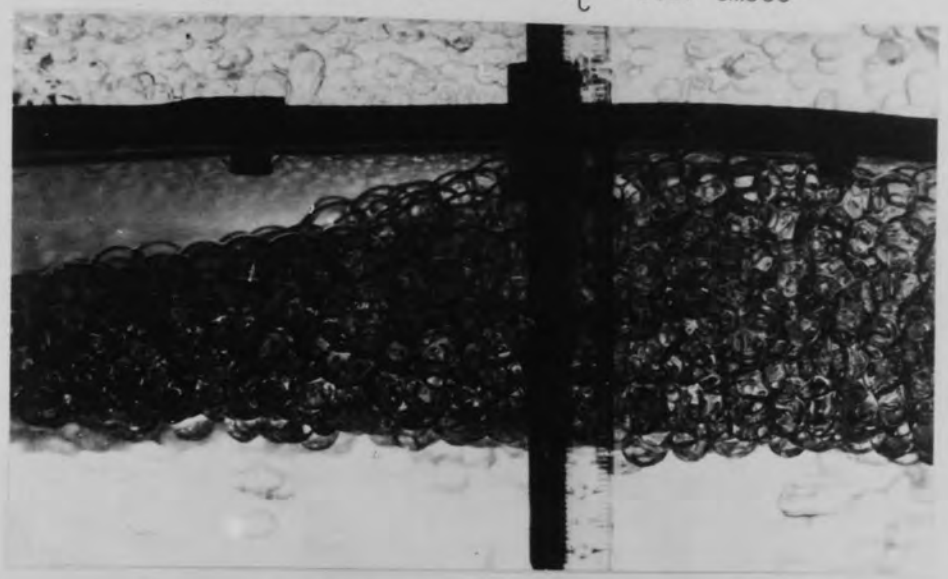

b) U_D = 17.64 cmsec^{-1} U''_C = 0.27 cmsec^{-1}

c) U_D = 28.29 cmsec^{-1} U''_C = 0.27 cmsec^{-1}

Fig 8.1-2 Relationships between flocculation and coalescence height and dispersed phase throughputs.

8.1-4 DROP SIZE MEASUREMENT - PHOTOGRAPHIC ANALYSIS

The photographic study of drop size distribution was carried out using the simple photographic technique suggested by Damon et al.(24) but with improved frontal lighting. Uniform illumination was provided by placing a sheet of white cloth between the floodlights and the column wall, in order to diffuse the light. Thorn Lighting floodlights were used each 30 cm in diameter and of flameproof construction (Simplex Ltd. cat. no. 7791-B). Each contained a 500 watts 'editing screw' reflector lamp. The arrangement is shown in Figure 7.2-3.

Photographs of the drop swarm were taken, when the column was operating under a steady state condition, using a Nikkormat FTN 35 mm camera with a 55 mm Micro-Nikkor lens. Exposures of approximately 0.002 sec were used. This produced sharp droplet outlines at all flow rates. Photographs were taken of drops during their travel through each section of the column.

Correction factors to allow for the effect of the different refractive indices of field liquid and the glass column walls, and for magnification due to curvature of the column, were determined by standardising with a glass marble of a known size inside the column filled with water at the field of focus with respect

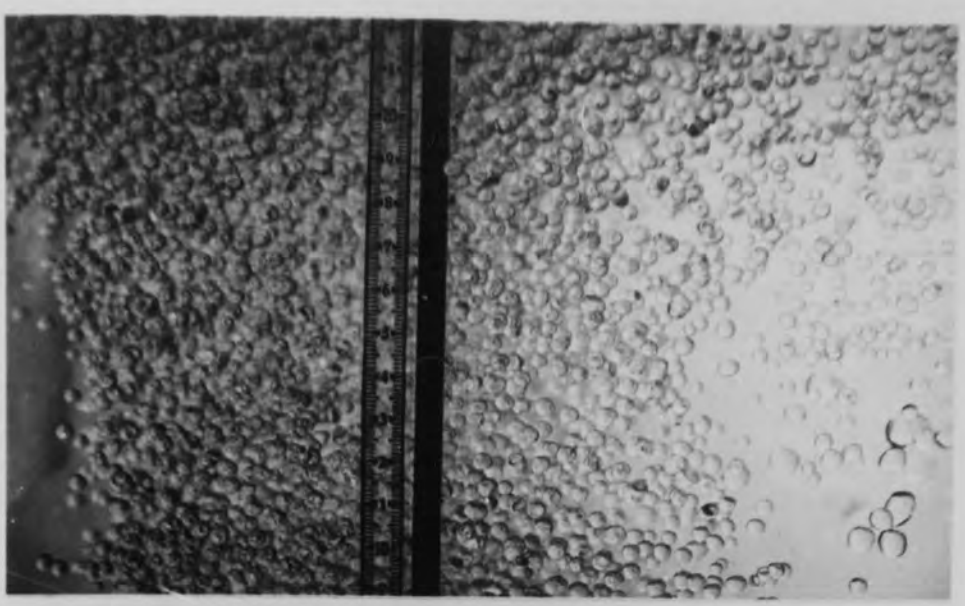

a) U_D = 9.32 cmsec^{-1} U''_C = 0.27 cmsec^{-1}

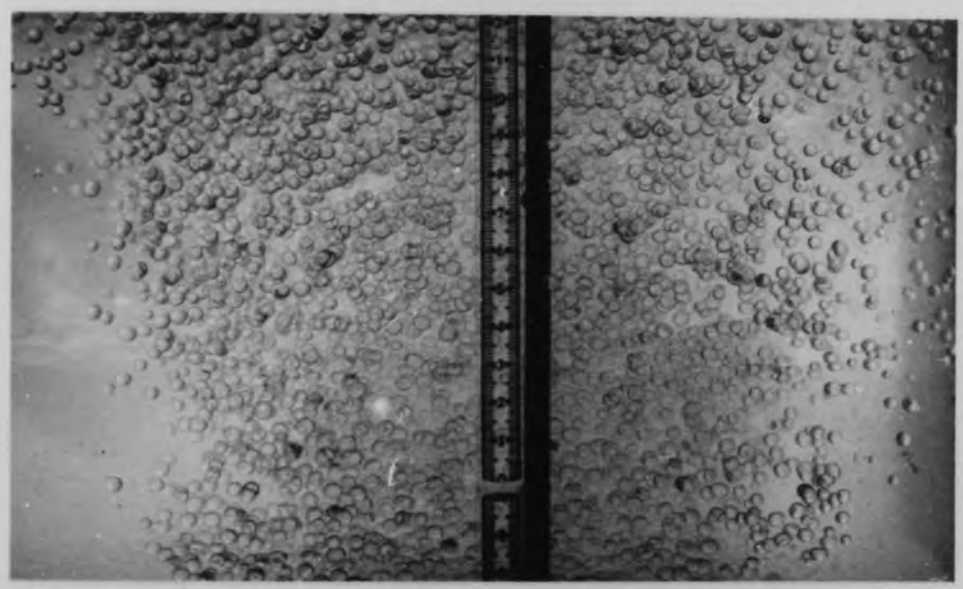

b) U_D = 17.64 cmsec^{-1} U''_C = 0.27 cmsec^{-1}

c) U_D = 28.29 cmsec^{-1} U''_C = 0.27 cmsec^{-1}

Fig. 8.1-3 Droplet dispersion between plates 2 and 3
1.588 mm i.d. hole size.

a) 3.175 mm i.d. hole size: U_D=0.85 cmsec^{-1} U''_C=0.44 cmsec^{-1}

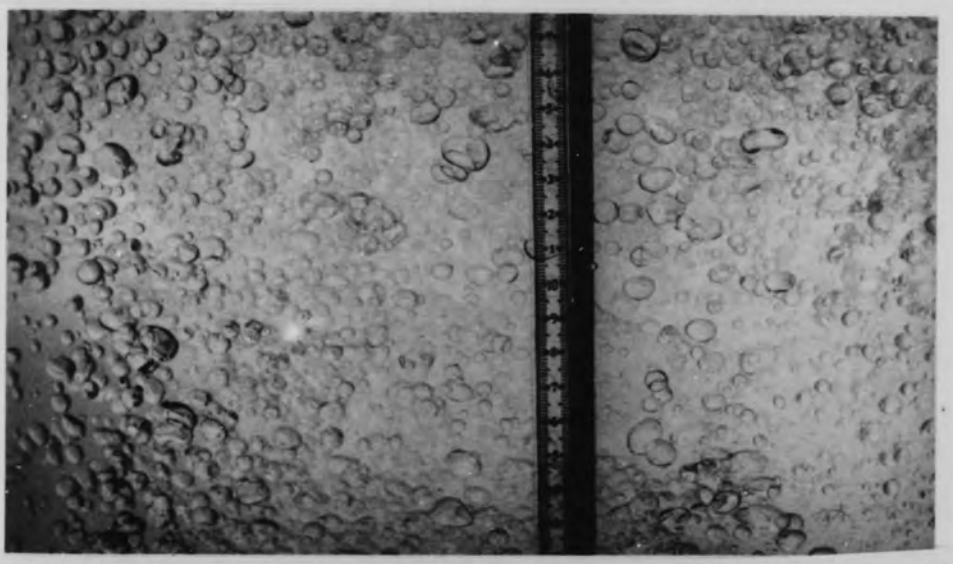

b) 4.763 mm i.d. hole size: U_D=0.85 cmsec^{-1} U''_C=0.44 cmsec^{-1}

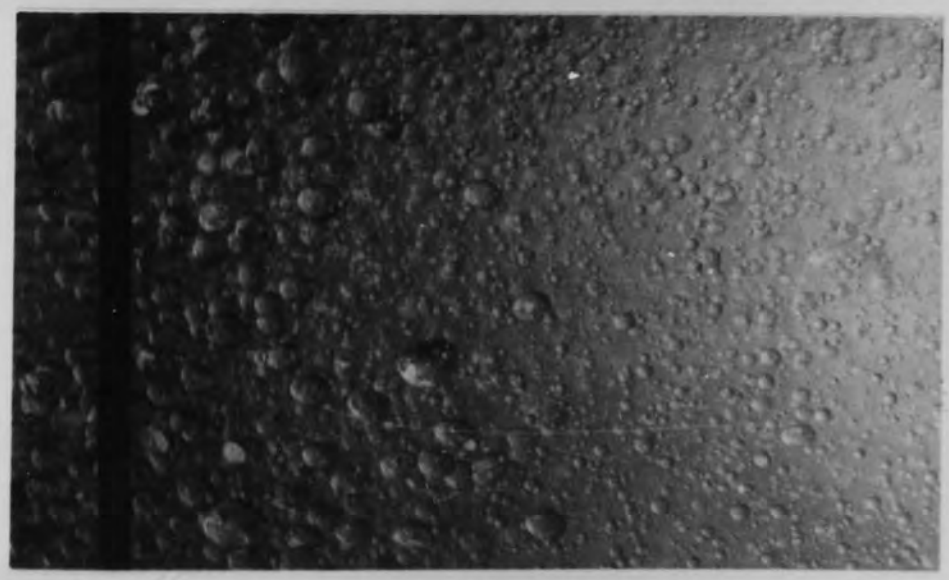

c) 6.350 mm i.d. hole size: U_D = 0.85 cmsec^{-1} U''_C=0.44 cmsec^{-1}

Fig. 8.1-4 Droplet dispersion between plates 2 and 3

to the fixed position of the camera. Correction factors for the diameter of the major and minor axes, d_1 and d_2 were subsequently applied to the drop size measurements. A Carl-Zeiss particle size analyser was used to analyse the photographs. Sauter mean drop diameter was evaluated from equation 3.2-2. The number of drops measured for each flow rate varied from approximately 200, when the drops were of uniform size, to approximately 500 when the drops varied in size considerably i.e. when $\frac{d_{max}}{d_{min}} \simeq 14.5$. Typical photographs are shown in Figures 8.1-3 and 8.1-4. Only drops with $\frac{d_1}{d_2} < 2$ were included in the counts. (In some photographs e.g. Figure 8.2-28, there were a few drops outside this range but not sufficient to affect the measured distribution).

8.2 EXPERIMENTAL RESULTS

8.2-1 DROP FORMATION MECHANISMS - JET LENGTH FROM PLATES

The jet length was measured for the system Clairsol '350' - water system using the photographic technique described in section 3.1-4. The jet lengths measured covered the range from the initial jetting velocity to the formation of turbulent jets. The results for the system are presented in Table 8.2-1 and in Figures 8.2-1(a) to (d) as jet length versus the dispersed phase superficial velocity.

The jet length measured was that length from the tip of the nozzles to the furthest point from the nozzle to which the liquid jet reached as a continuous stream. The lengths varied in fact, depending upon whether the end section of the jets were just about to break off as droplets. Regular pulsations of the jet length were also observed especially at high dispersed phase superficial velocities. It was necessary, therefore, to represent a jet length which was averaged out over these periodic fluctuations and over any other random fluctuations. The fluctuations in the jet length were fairly minor i.e. <5% over the lower flow rate range of the study. As the peak jet length was approached and then exceeded, however, the jet length became highly erratic. This was due

TABLE 8.2-1

RELATIONSHIP BETWEEN JET LENGTH AND DISPERSED PHASE SUPERFICIAL VELOCITY

PLATE HOLE SIZE cm	U''_C $cmsec^{-1}$	U_D $cmsec^{-1}$	U'_D $cmsec^{-1}$	AVERAGE JET LENGTH cm
0.1588	0.27	13.31	15.68	0.70
		17.64	18.32	1.80
		21.63	22.09	2.30
		28.29	29.00	1.90
0.3175	0.27	5.13	5.94	1.48
		6.80	6.98	2.47
		8.34	8.67	3.29
		10.90	11.21	2.58
0.4763	0.27	2.86	3.68	1.73
		4.08	5.11	2.52
		5.41	6.20	3.03
		6.64	7.31	3.78
		8.68	8.42	2.59
0.6350	0.27	2.33	3.92	1.65
		3.32	4.62	2.91
		4.40	5.11	4.26
		5.40	5.92	4.87
		7.06	7.81	3.18

to the countercurrent and crossflow effects of the more viscous continuous water phase. Between 7 and 18 jet lengths were averaged.

The plot of dispersed phase superficial velocity against jet length, shows that after passing through a critical dispersed phase superficial velocity, corresponding to a transition from direct droplet release to jetting, the length increased rapidly with increasing dispersed phase superficial velocity, reached a peak and thereafter declined less steeply. Typical photographs of the jet from the 0.6350 cm drilled and punched perforated hole plate during countercurrent operation are shown in Figure 8.1-c. It shows a change in the behaviour of the jet beyond the peak. Figures 8.1-1b and c show the change from the axisymetric nodal disturbance before the peak to a sinuous disturbance beyond the peak, as previously described by a number of investigators (83, 105, 142) for single nozzles.

Allowance was made for the non-jetting holes by introducing a correction factor to obtain actual jetting velocity as described in section 8.1. The experimental jet length data were then correlated and the result gave the equation

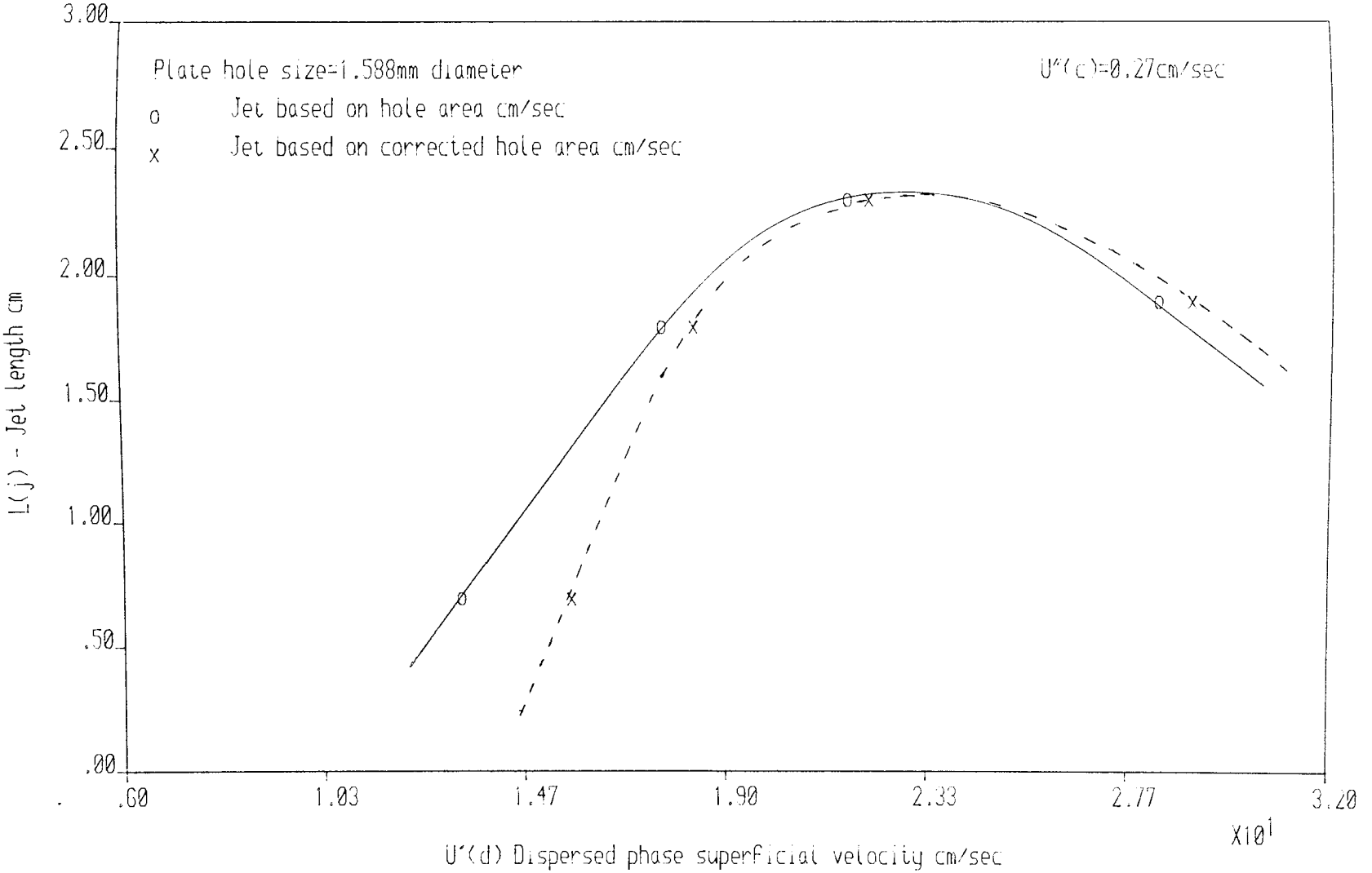

Fig.8.2-1a. Plot of dispersed phase superficial velocity against jet length

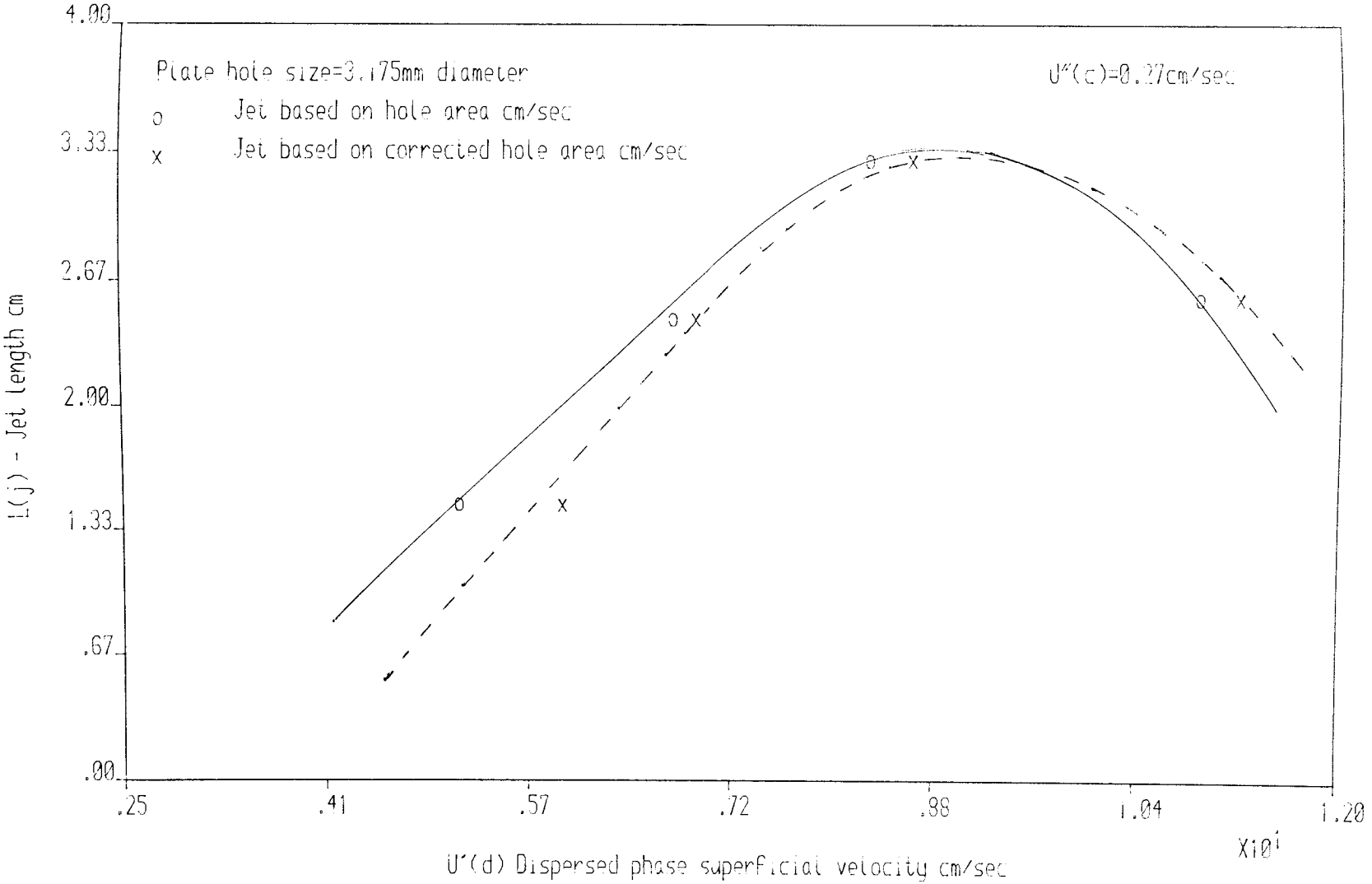

Fig.3.2-1b. Plot of dispersed phase superficial velocity against jet length

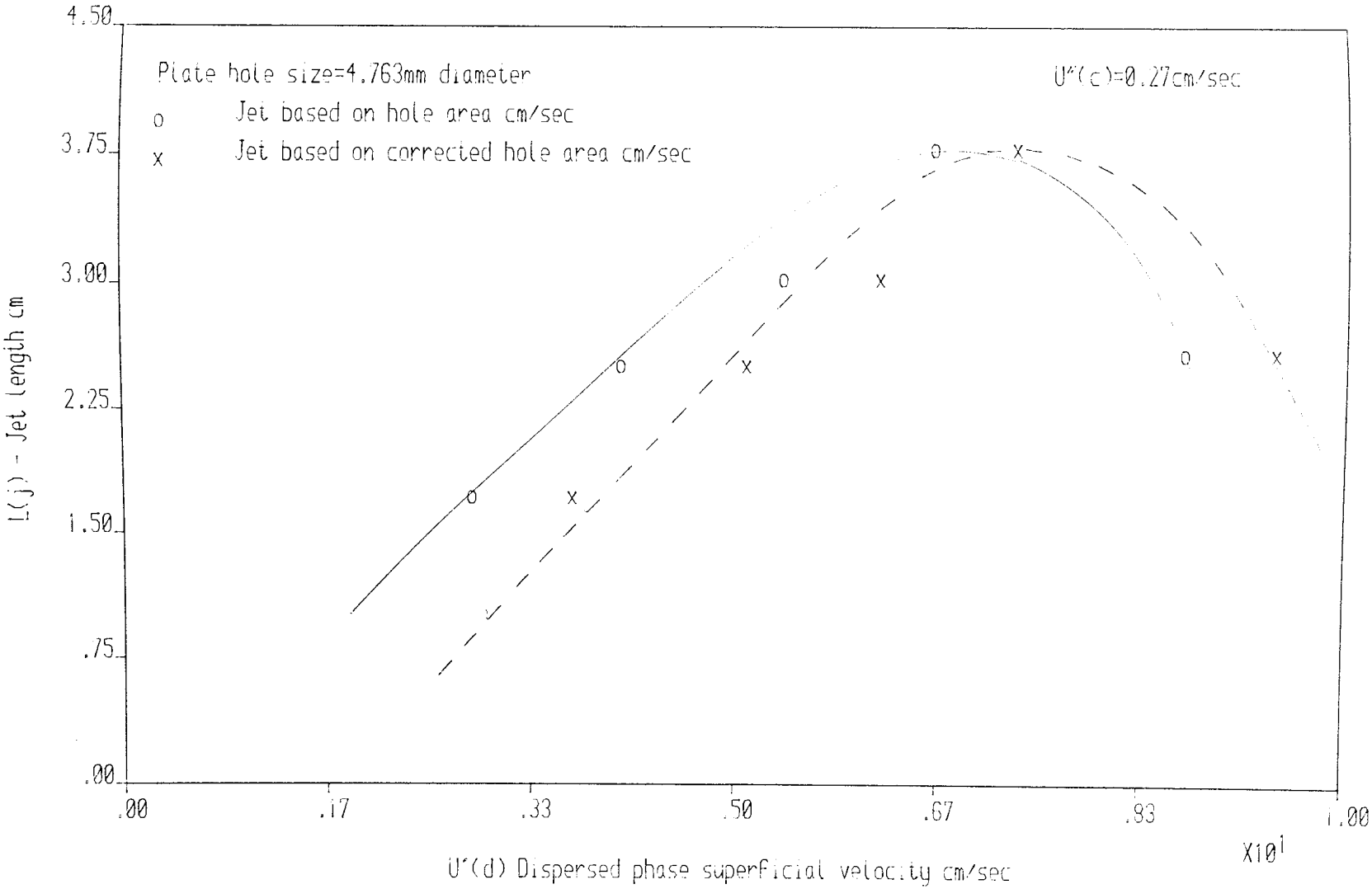

Fig.8.2-ic. Plot of dispersed phase superficial velocity against jet length

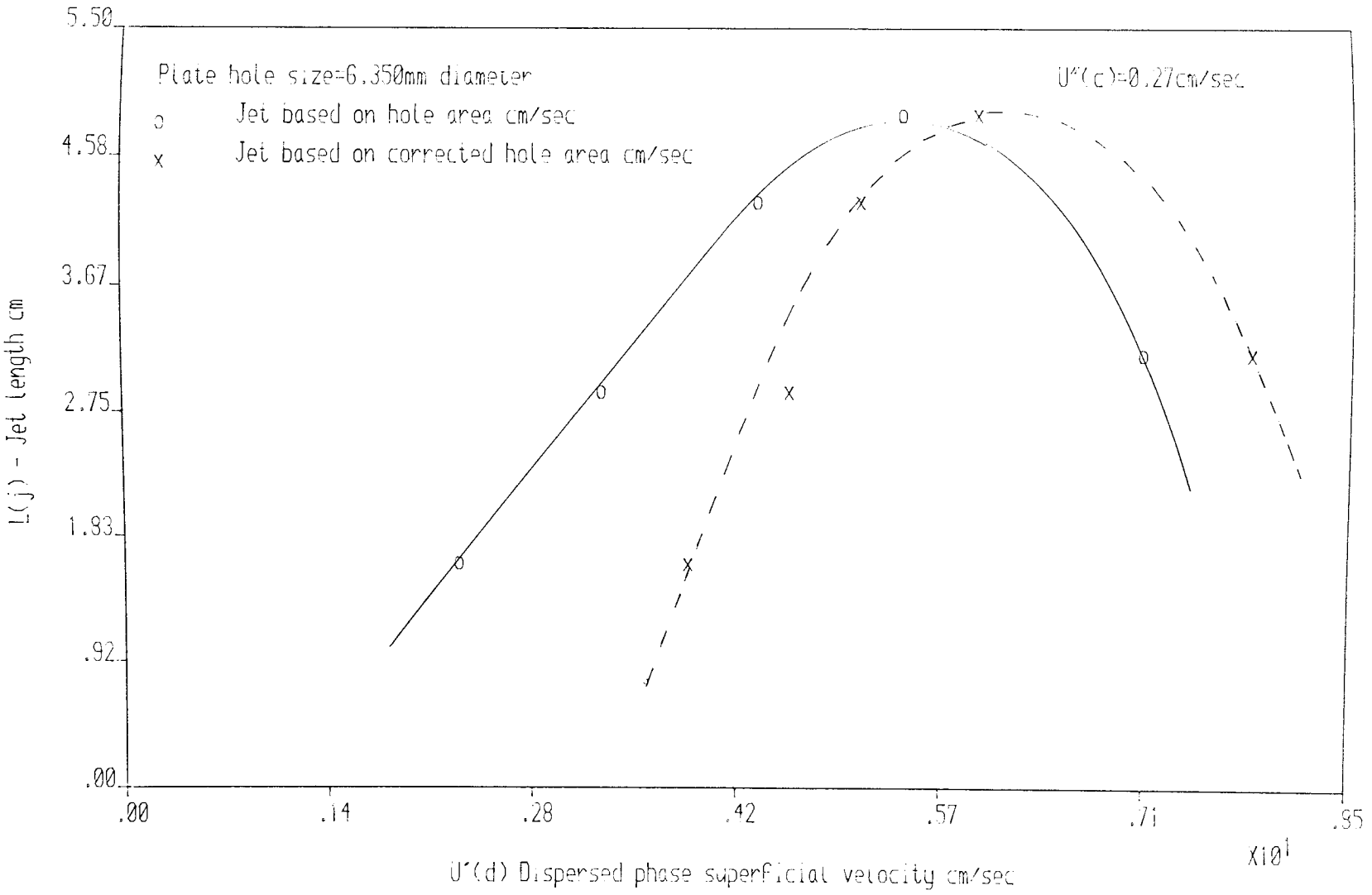

Fig.8.2-1d. Plot of dispersed phase superficial velocity against jet length

$$\frac{L_j}{D_N} = 22.2 \left(\frac{U_N^2 \rho_D D_N}{\sigma}\right)^{0.42} \left(\frac{U_N \rho_D D_N}{\mu_C}\right)^{-0.16} \qquad 8.2\text{-}1$$

The value of this correlation is discussed in Section 8.3-1.

8.2-2 HOLD-UP

The operating hold-up was determined by taking the difference between the total and the static hold-up as indicated by equation 3.2-3. The data are summarised in Table 8.2-2. The operating dispersed phase hold-up data was then used to calculate the characteristic velocity according to equation 3.2-6 proposed by Thornton(147) for spray columns. Figures 8.2-2 to 8.2-5 show the change in characteristic velocity U_S with plate hole size. An appreciable change in U_S from a value of 6.55 to 22.44 $cmsec^{-1}$ was observed with an increase in plate hole size from 0.1588 to 0.6350 cm. However, for an increase in plate hole size from 0.4763 to 0.6350 cm the change in U_S is small being in the range of 21.56 to 22.44 $cmsec^{-1}$, thereby showing a tendency for U_S to approach near constancy at these larger hole sizes. As discussed later in section 10.1 this should enable prediction of hold-up and residence time in industrial columns.

TABLE 8.2-2

PLATE HOLE HOLE SIZE cm	U''_C $cmsec^{-1}$	U''_D $cmsec^{-1}$	HOLD-UP %
0.1588	0.27	0.18	5.28
		0.33	7.91
		0.41	9.60
		0.54	12.81
	0.44	0.25	6.22
		0.41	9.35
		0.54	11.65
0.3175	0.27	0.18	2.50
		0.33	3.81
		0.41	4.70
		0.54	5.60
	0.44	0.25	3.00
		0.41	4.60
		0.54	5.26
0.4763	0.27	0.18	0.78
		0.33	1.45
		0.54	2.57
	0.44	0.41	1.65
		0.54	2.51
0.6350	0.27	0.18	0.69
		0.33	1.33
		0.54	2.41
	0.44	0.41	1.63
		0.54	2.39

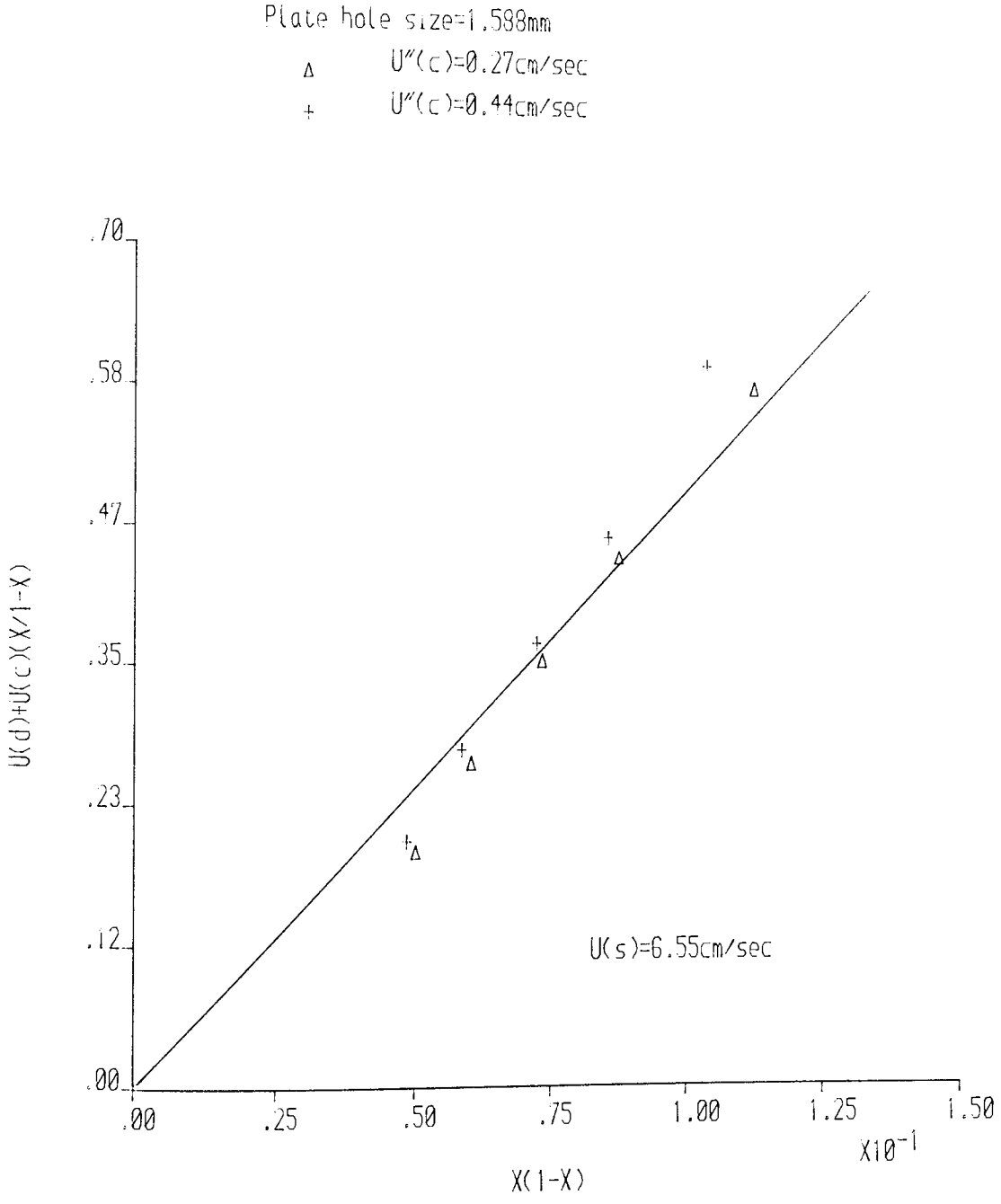

Fig.8.2-2. Plot of hold-up data for the system clairsol '350' dispersed in de-ionised water

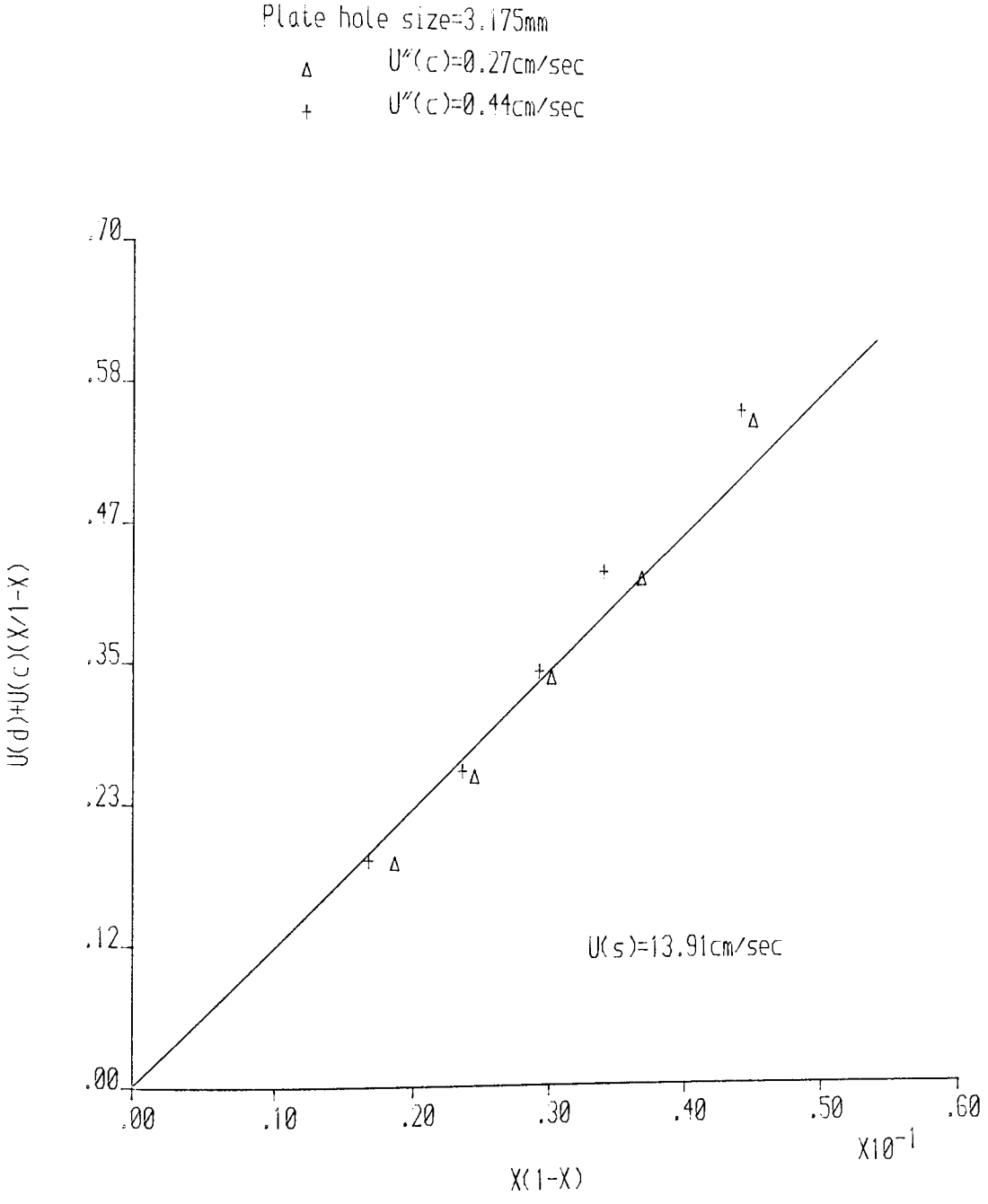

Fig.8.2-3. Plot of hold-up data for the system clairsol '350' dispersed in de-ionised water

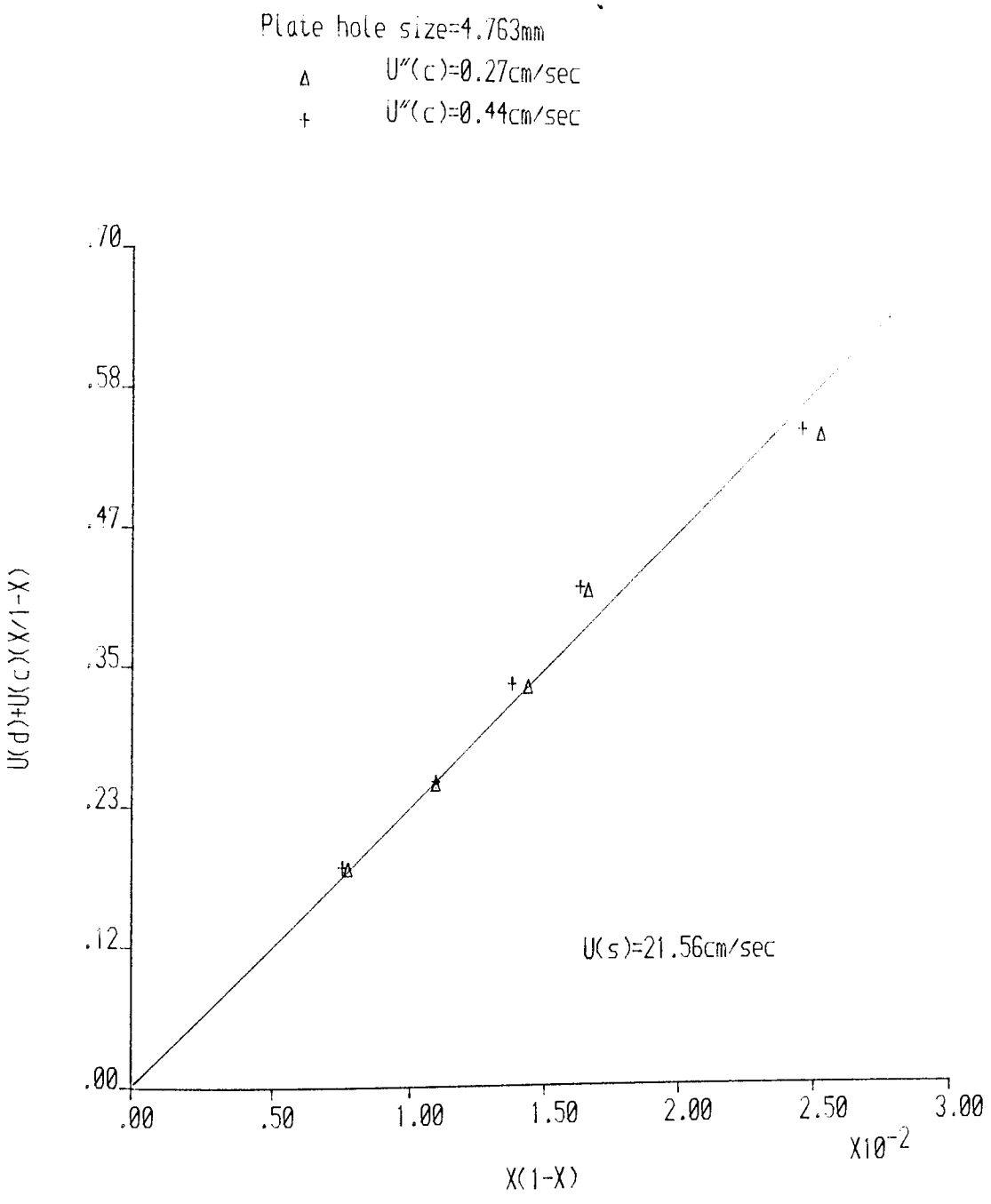

Fig.8.2-4. Plot of hold-up data for the system clairsol'350' dispersed in de-ionised water

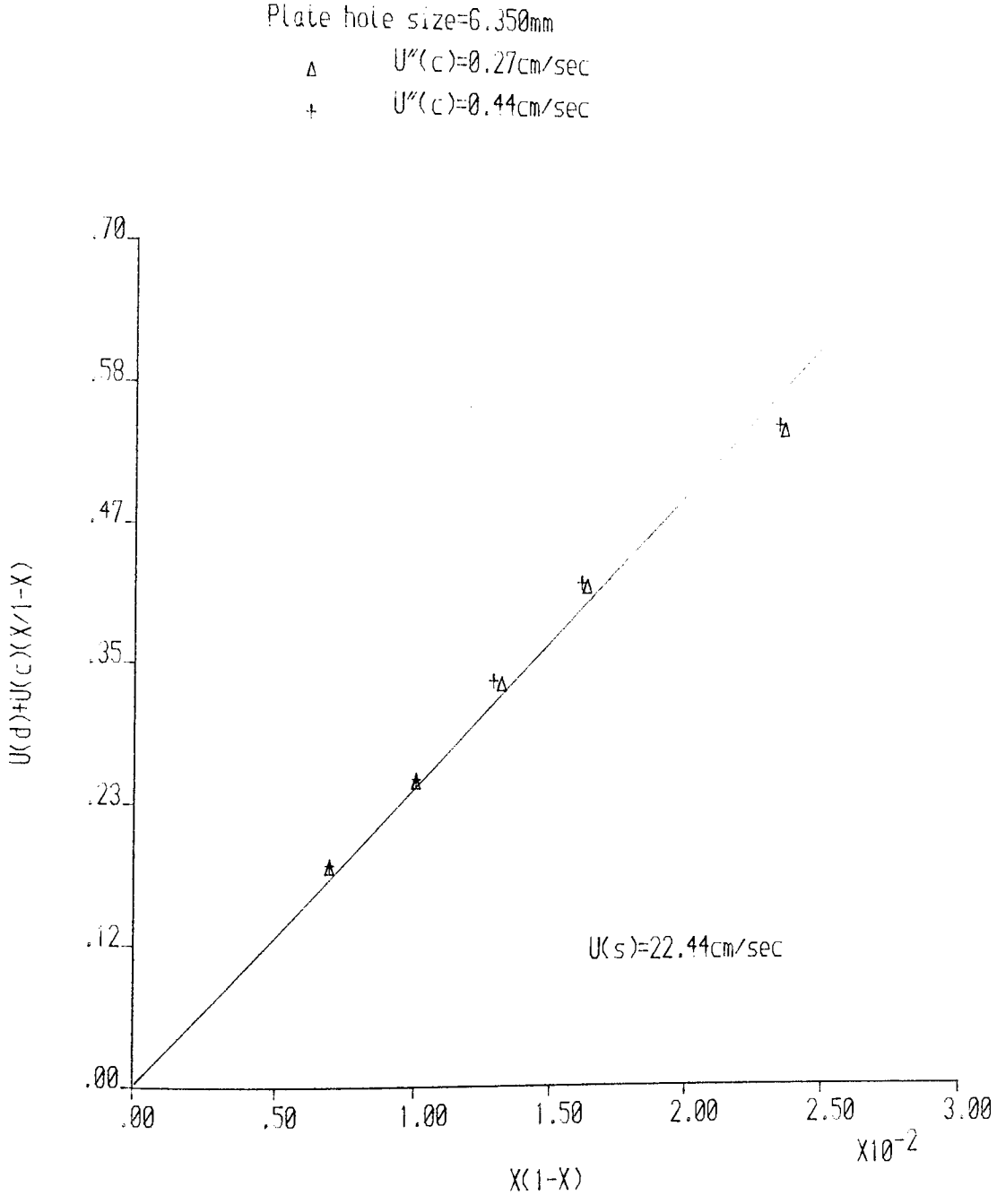

Fig.8.2-5. Plot of hold-up data for the system clairsol '350' dispersed in de-ionised water

Values of the equilibrium slip velocity U_S in the constant hold-up region of the column were calculated by equation 3.4-3. The results were then used to calculate the equilibrium slip velocity extrapolated to zero hold-up according to equation 3.4-4 proposed by Letan and Kehat(95) . The numerical constants in this work, Clairsol dispersed in de-ionised water at ambient temperature and with Sauter mean drop sizes between 0.30 to 0.67, were,

$$U_S^* = 23.93 \exp(-2.225H) \qquad 8.2\text{-}2$$

Subsequently experimental measurements of fractional hold-up of dispersed phase were made during mass transfer runs for the system Clairsol de-ionised water with acetone as solute and covering both directions of solute transfer viz., d→c i.e. solute transfer from dispersed phase (d) to continuous phase (c) and c→d i.e. solute transfer from continuous phase (c) to dispersed phase (d). The experiments are described in 8.1-2 and the data are summarised in Tables 9.4-1 and 9.4-2.

Comparison of the hold-up data in the absence of mass transfer and with transfer, albeit covering a limited concentration range (1 to 8% solute), showed that there was no significant difference i.e. <3%.

Furthermore, there was no appreciable variation with direction of mass transfer. Therefore, the experimental hold-up data obtained under both directions of solute transfer and with no transfer conditions was correlated and the result gave the equation

$$x=56.2\times10^{6}\left(\frac{\Delta\rho}{\rho_C}\right)^{0.32}\left(\frac{U''_D}{U''_C}\right)^{-0.12}\left(\frac{U''^{2}_D\ \rho_D\ D_C}{\sigma}\right)^{-1.23}\left(\frac{U''_D}{D_C g}\right)^{1.82}$$

8.2-3

where the terms are as defined in the Nomenclature. For this system, or presumably for systems of similar local interfacial tension effects due to solute, this equation enables a first estimate to be made of operating hold-up for column design as discussed later in Section 10.

8.2-3 DROPLET COLLECTION BENEATH PLATES

Figures 8.2-6 and 8.2-7 show the relationship between coalescence and flocculation zone height and dispersed phase superficial velocity at constant continuous phase superficial velocity for the 0.1588 cm and 0.3175 cm hole size plates. The coalescence and flocculation zone height - U''_D profiles show an upward trend of the coalesced and flocculation zone height

Plate hole size=1.588mm diameter
Plate type: drilled

Plate 1	Plate 2	
Δ	o	U″(c)=0
x	□	U″(c)=0.27cm/sec
▽	*	U″(c)=0.44cm/sec

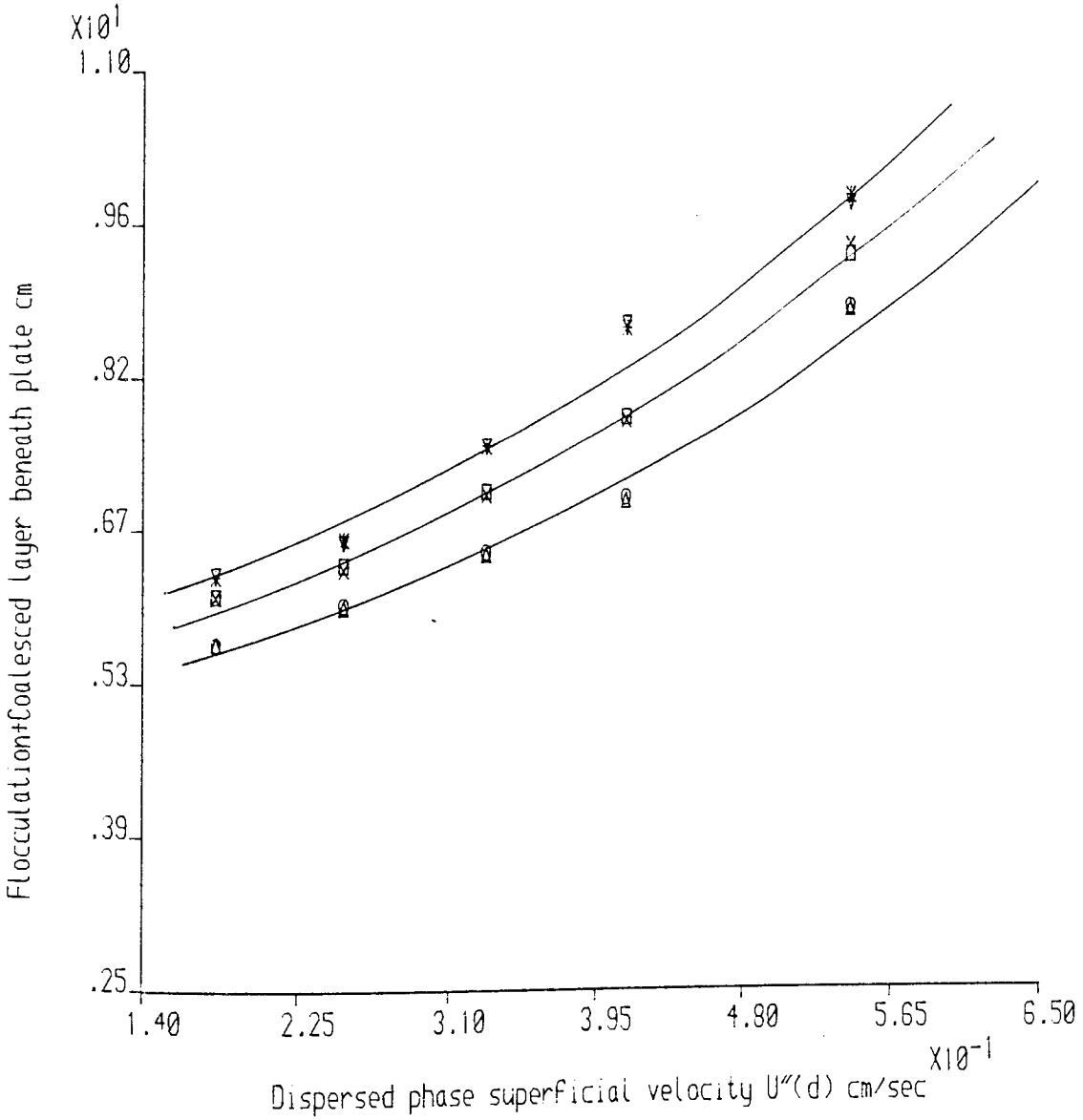

Fig.8.2-6. Flocculation zone beneath plates

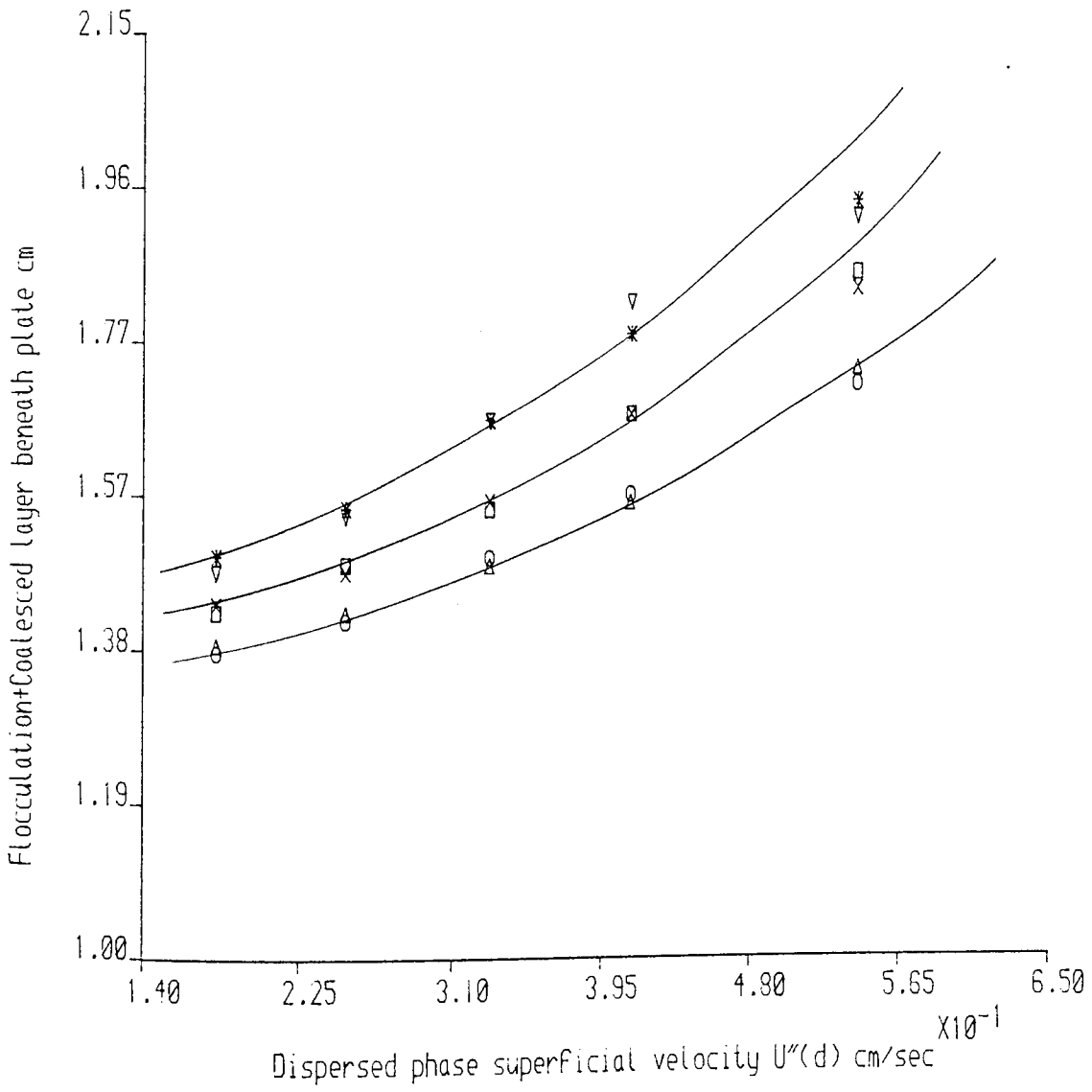

Fig.8.2-7. Flocculation zone beneath plates

Plate hole size=4.763mm diameter
Plate type: drilled and punched

Plate 1	Plate 2	
Δ	o	U″(c)=0
x	□	U″(c)=0.27cm/sec
▽	*	U″(c)=0.44cm/sec

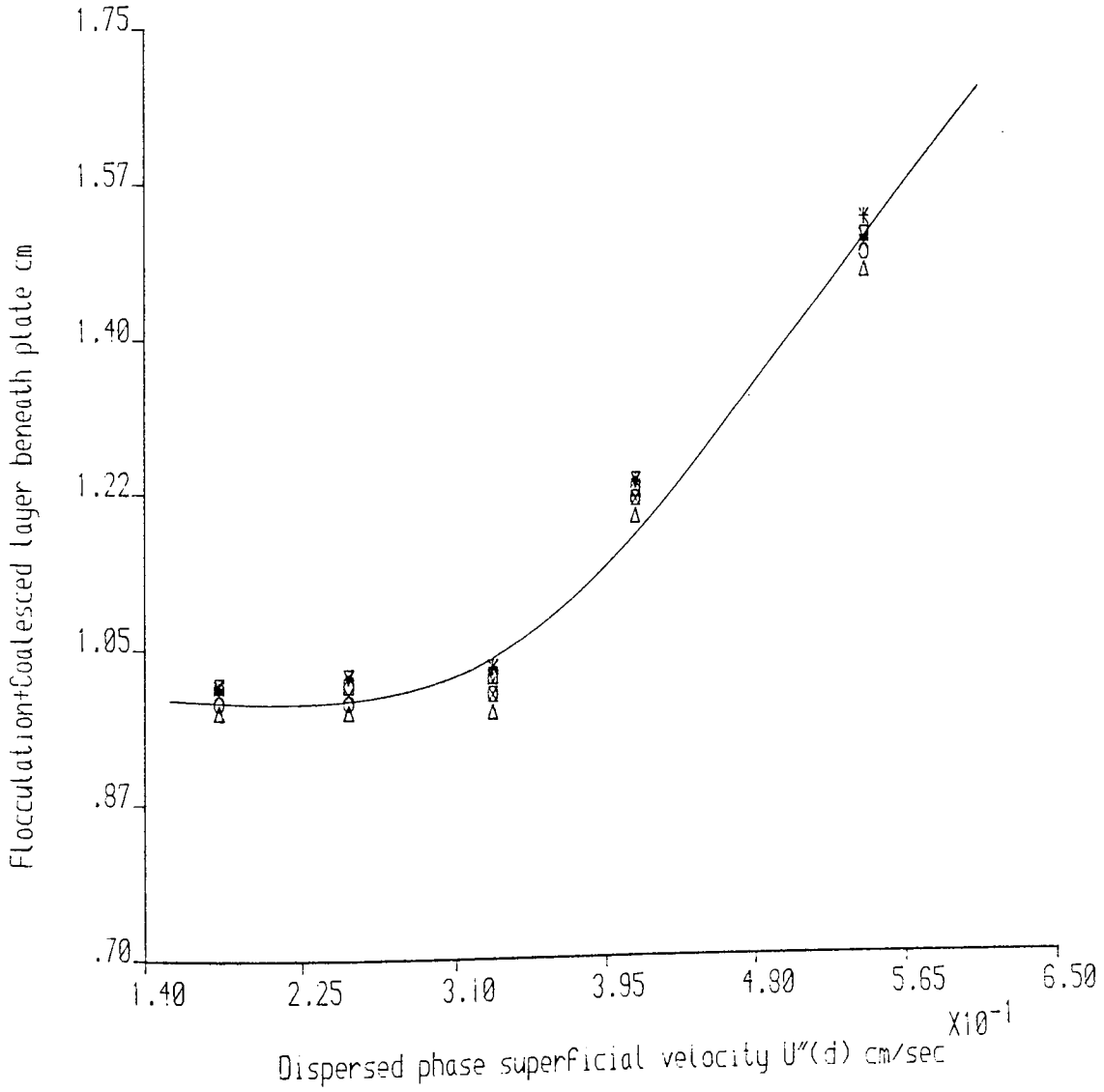

Fig.8.2-8a. Flocculation zone beneath plates

Plate hole size=6.350mm diameter
Plate type: drilled and punched

Plate 1	Plate 2	
Δ	o	U″(c)=0
x	□	U″(c)=0.27cm/sec
▽	*	U″(c)=0.44cm/sec

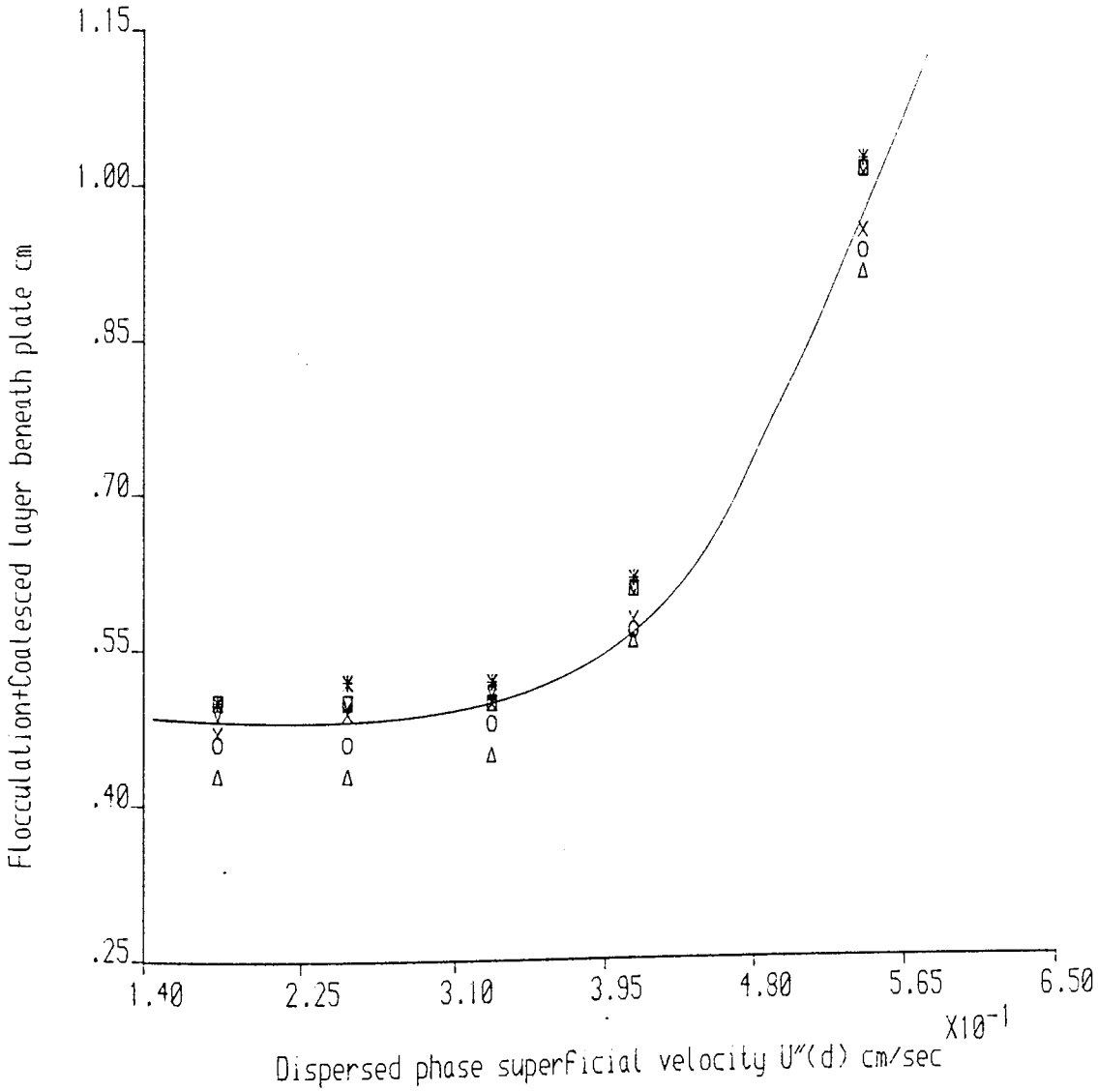

Fig.8.2-8b. Flocculation zone beneath plates

with increasing dispersed phase superficial velocity.

Also there is an upward shift in the profiles with higher values of continuous phase superficial velocity. Clearly the effect of countercurrent flow of the heavy continuous phase is to increase the hold-up beneath the plates. Since this hold-up is ineffective, increase in height will contribute to a reduction in contact time and effective interfacial area. A different situation was found with the 0.4763 cm and 0.6350 cm hole size plates as shown in Figure 8.2-8. Here the height remained approximately constant up to $U''_D = 0.33$ cmsec^{-1} then followed an appreciable thickening of the dispersed phase layer beneath the plates. The experimental data for all plates were correlated and the result gave the equation

$$\frac{h_{CF}}{D_N} = 93.6\times10^2\left(\frac{U''^2_N \rho_D d_{12}}{\sigma}\right)^{5.10}\left(\frac{U''^2_N}{d_{12} g}\right)^{4.93} \qquad 8.2\text{-}4$$

where h_{CF} = coalescence and flocculation zone height, cm.

d_{12} = mean drop diameter, cm.

8.2-4 (1) DROP SIZE

Figures 8.2-9 to 8.2-12 demonstrate the variation of mean drop size with superficial velocity of the dispersed phase (U_D) for plates with 0.1588 cm, 0.3175 cm, 0.4763 cm and 0.6350 cm hole sizes respectively. Inspection of these curves shows that there was a marked reduction in drop size at high dispersed phase or high water rates. It is convenient to discuss the results in terms of three separate regions albeit with different characteristics depending on the hole size. For the plate with D_N = 0.1588 cm, i.e. the smallest hole size, the drop size profiles obtained formed three separate regions. Region I in which the dispersed phase superficial velocity had little effect on the drops break down, i.e. little change in d_{32}.; Region II in which increase in dispersed phase superficial velocity caused an appreciable corresponding decrease in the mean drop size. In this region, turbulence controls the drop size directly through its effect on formation rates, rise and travel. Region III in which the drop size remains substantially constant with increasing dispersed phase superficial velocity. In this region at a constant value of U_C'' increase in U_D had no significant effect on the break down of the liquid droplets into smaller ones. For the plate with D_N = 0.3175 cm. the effect of dispersed phase

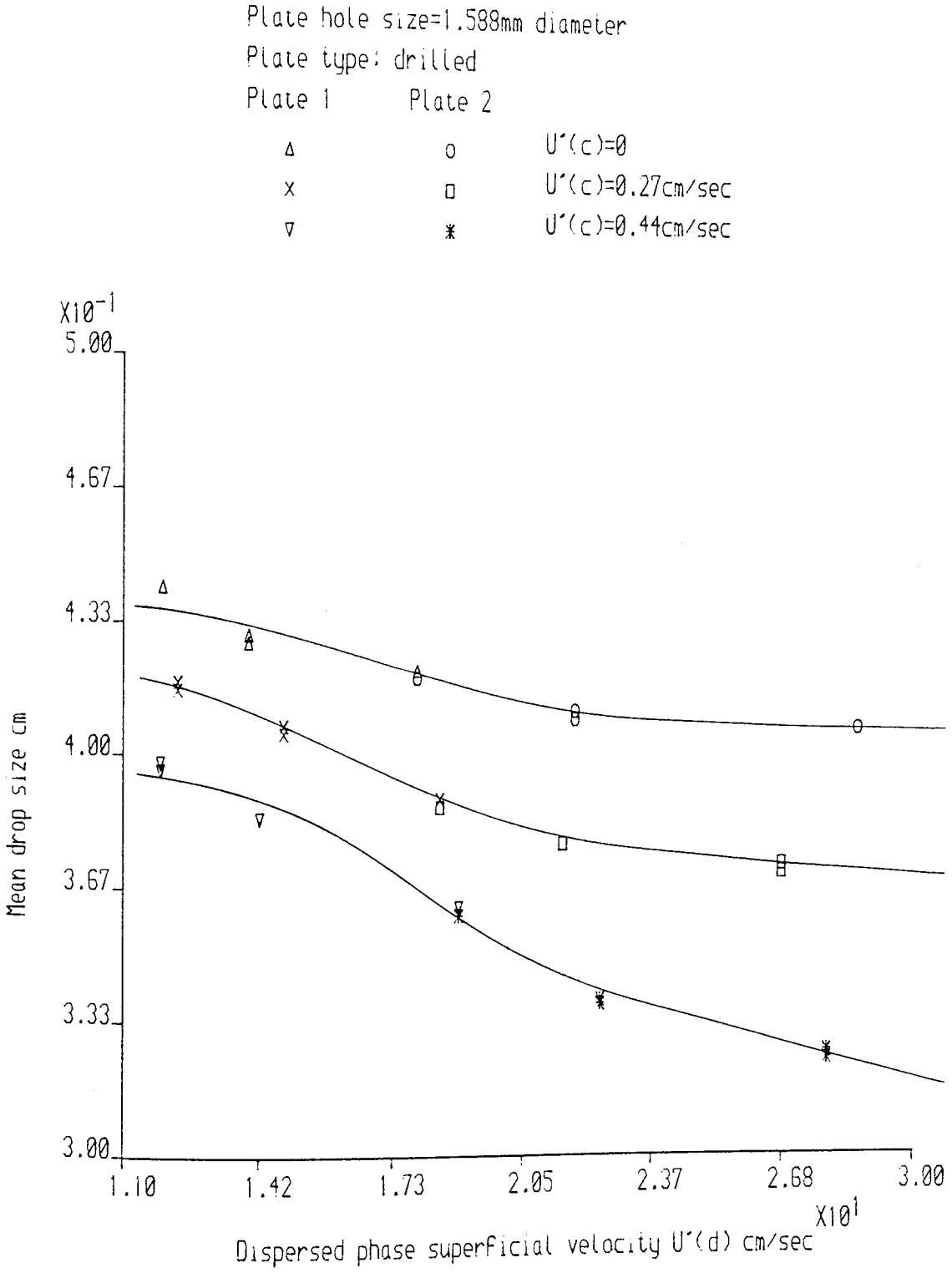

Fig.8.2-9. Plot of mean drop size against dispersed phase superficial velocity

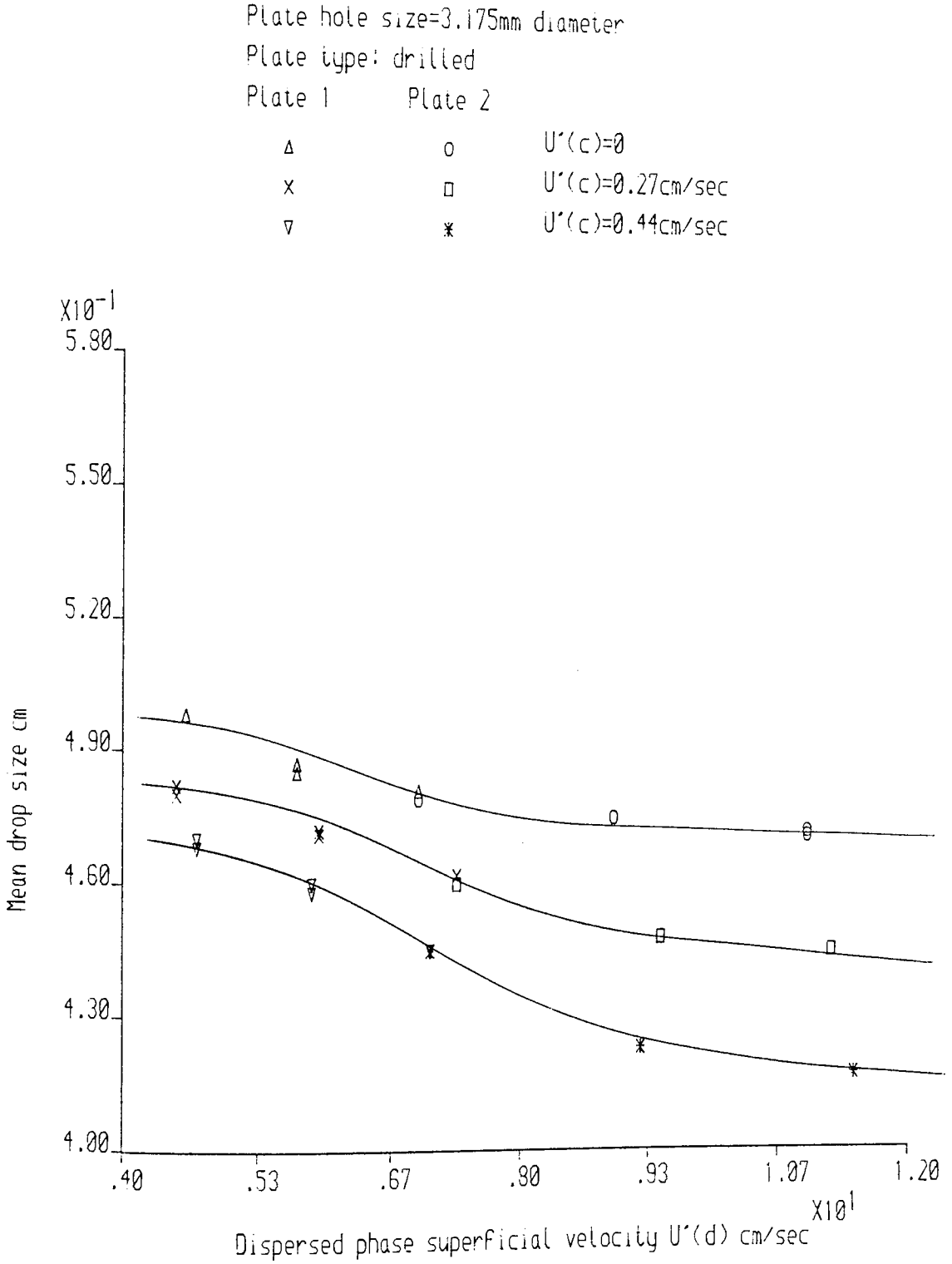

Fig.8.2-10. Plot of mean drop size against dispersed phase superficial velocity

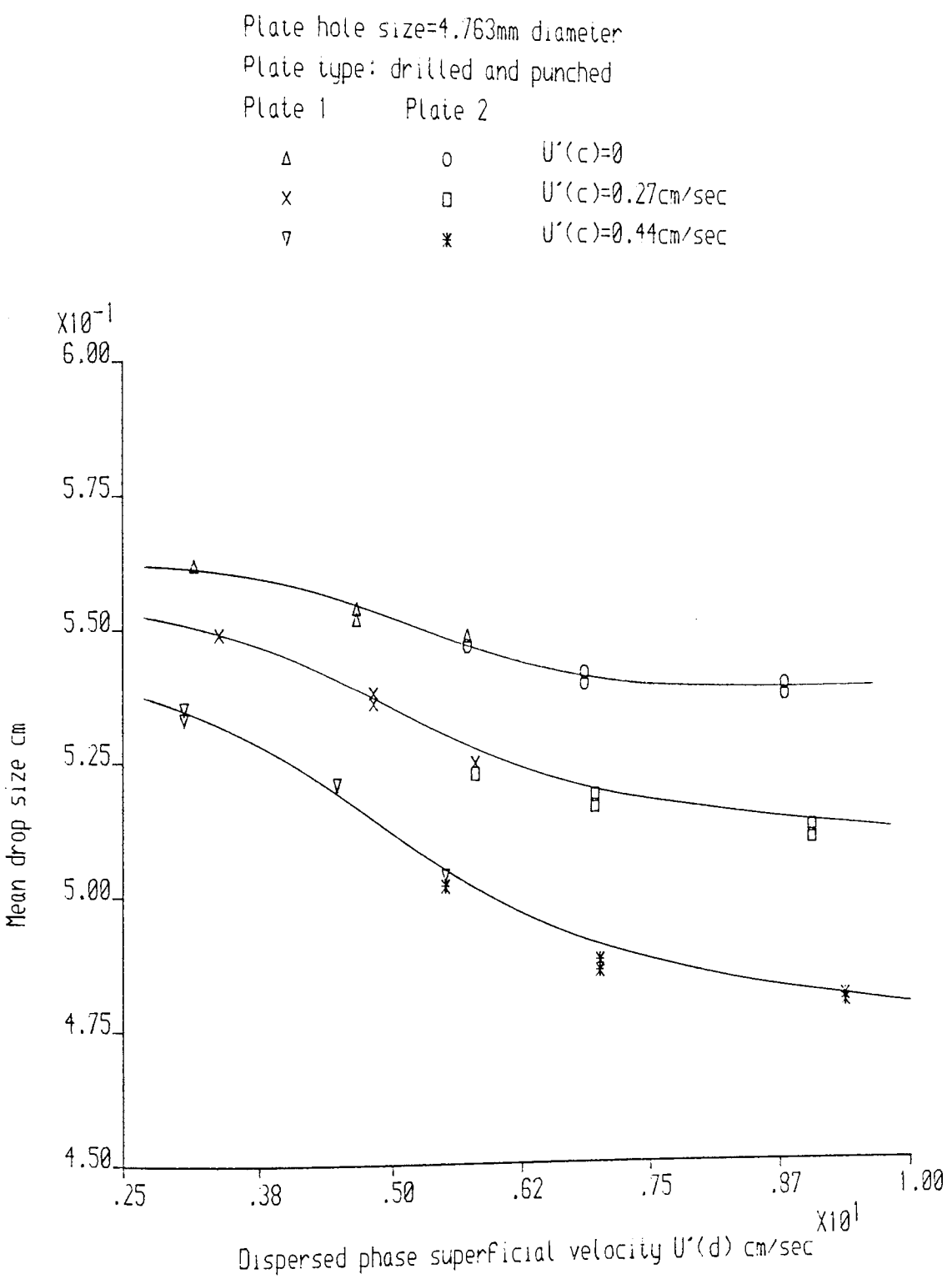

Fig.8.2-11. Plot of mean drop size against dispersed phase superficial velocity

Plate hole size=6.350mm diameter
Plate type: drilled and punched

Plate 1	Plate 2	
Δ	o	U'(c)=0
x	□	U'(c)=0.27cm/sec
▽	*	U'(c)=0.44cm/sec

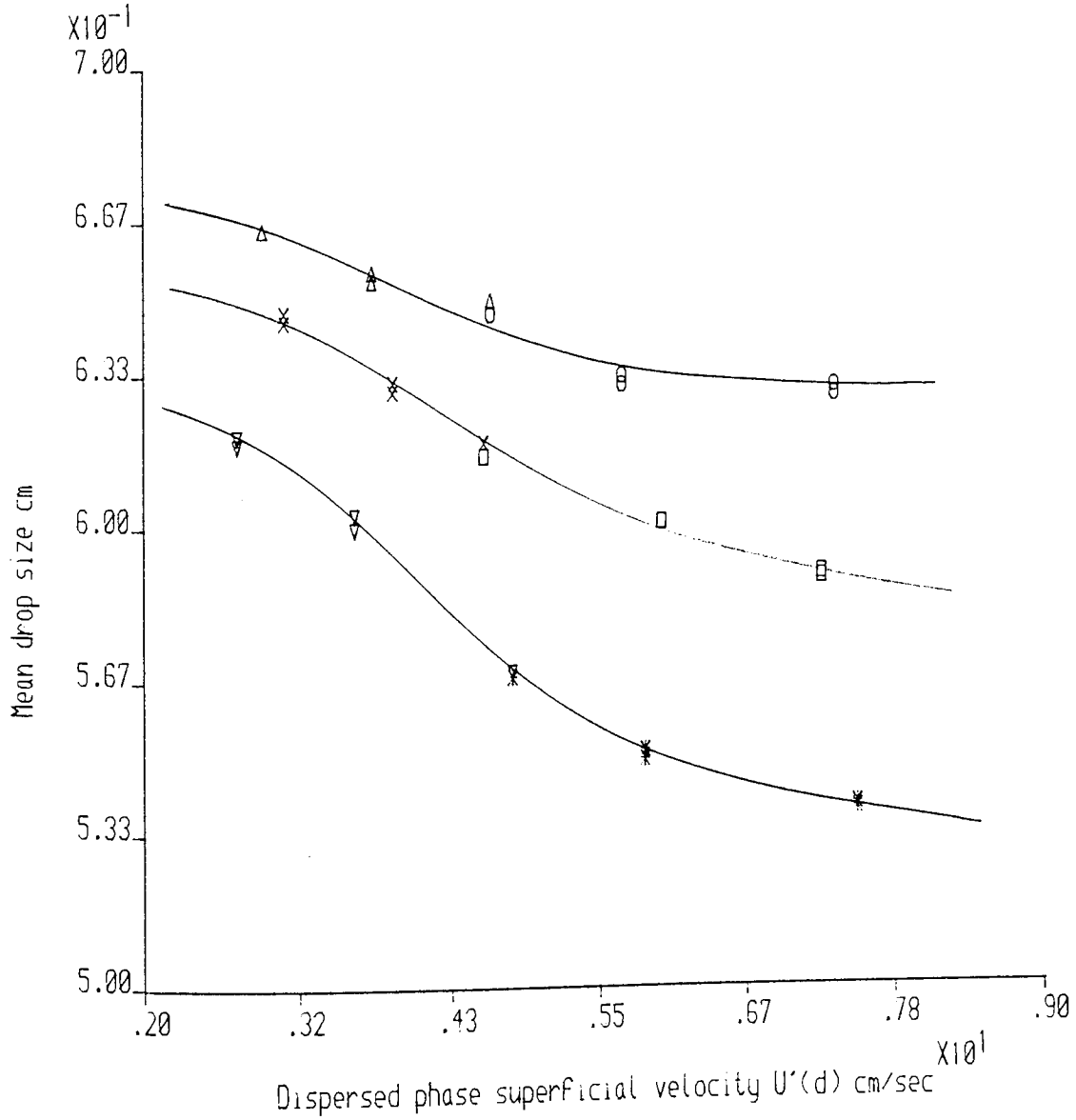

Fig.8.2-12. Plot of mean drop size against dispersed phase superficial velocity

superficial velocity on drop break down for the mean drop size profiles for $U''_C = 0$ and $U''_C = 0.27$ cmsec^{-1} in regions I, II and III are similar to that of D_N = 0.1588 cm. For $U''_C = 0.44$ cmsec^{-1}, there is a considerable decrease in the mean drop both in regions I and II because of the increase in continuous phase cross flow velocity. For the plate $D_N = 0.4763$ cm the dispersed phase has no significant effect in any of the regions I, II and III for $U''_C = 0$. For $U''_C = 0.27$ cmsec^{-1} and 0.44 cmsec^{-1} respectively, there is considerable effect of both dispersed and continuous phase superficial velocities on the drops break down in regions I and II, and hence a sharp decrease in the mean drop size. For the plate $D_N = 0.6350$ cm, the first mean drop size profile (i.e. for $U''_C = 0$), shows very little change in the mean drop size in the three regions. For $U''_C = 0.27$ cmsec^{-1} and 0.44 cmsec^{-1} there is sharp decrease in the mean drop size in regions I and II. This is because the much larger droplets which are produced by this plate hole size compared to the other plates are more vulnerable to break down into smaller droplets by increase in both continuous phase cross flow velocity and dispersed phase superficial velocity.

Figures 8.2-9 to 8.2-12 also demonstrate the reduction in mean drop size as U''_C is increased. This effect arises from

(i) Premature shearing at the orifice due to increased cross-flow of continuous phase.

(ii) Increased backmixing of drops with the smaller drop sizes being retained preferentially in the compartment above the plate from which they originated.

8.2-4 (2) CORRELATION OF VOLUME (SAUTER) MEAN DROP DIAMETER d_{32}

An analysis of the dependency of volume (Sauter) mean diameter upon the various column variables and liquid system variables was made by deriving a functional relationship between the mean diameter and variables such as column dimensions, plate hole size and the physical properties of the system. Because of the complexity of the problem hydrodynamically, it was necessary to base this correlation upon dimensional analysis using the π-theorem. Thus assuming that

$$d_{32} = \phi(U_N, \rho_c, \rho_d, \sigma, \mu_c, \mu_d, g, h, D_N, D_C)$$

and assuming the applicability of power functions to express the functional relationship of the dimensionless groups, it is found that:

$$\frac{d_{32}}{D_N} = K\left(\frac{\rho_c}{\rho_d}\right)^a \left(\frac{U_N^2\ \rho_d\ D_N}{\sigma}\right)^b \left(\frac{U_N\ \rho_d\ D_N}{\mu_c}\right)^p \left(\frac{U_N^2}{D_N g}\right)^q \left(\frac{D_N}{h}\right)^y \left(\frac{D_N}{D_C}\right)^z$$

The usual meaning of the symbols are as defined in the nomenclature. The exponents a, b, p, q and z, and the constant K were determined by a multiple regression analysis using the experimental data from the system Clairsol de-ionised water with no mass-transfer. The exponents on the composite groups $\left(\frac{\rho_d}{\rho_c}\right)$ and $\left(\frac{D_N}{h}\right)$ were very low and therefore discarded, the final expressions obtained were then,

(i) Including the column geometry group

$$\frac{d_{32}}{D_N} = 0.64\left(\frac{U_N^2\ \rho_D\ D_N}{\sigma}\right)^{0.04} \left(\frac{U_N\ \rho_D\ D_N}{\mu_c}\right)^{-0.28} \left(\frac{U_N^2}{D_N g}\right)^{0.05} \left(\frac{D_N}{D_C}\right)^{-0.5} \qquad 8.2\text{-}5$$

(ii) Without the column geometry group

$$\frac{d_{32}}{D_N} = 14.0\left(\frac{U_N^2\ \rho_D\ D_N}{\sigma}\right)^{-0.14} \left(\frac{U_N\ \rho_D\ D_N}{\mu_c}\right)^{-0.36} \left(\frac{U_N^2}{D_N g}\right)^{0.27} \qquad 8.2\text{-}6$$

Comparisons of these equations with the experimental results are shown in Figures 8.2-13 and 8.2-14. In

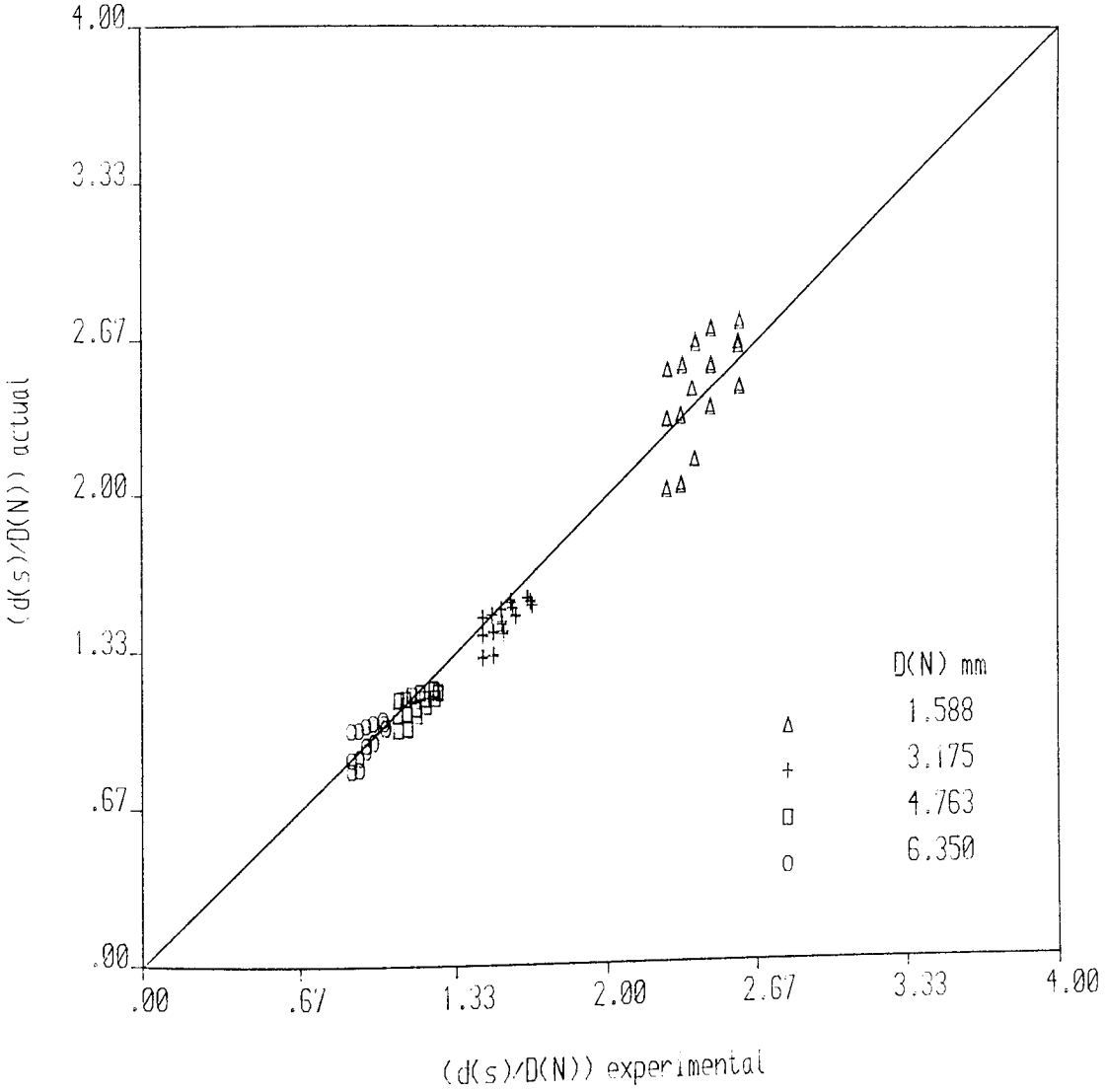

Fig.8.2-13. Comparison of actual values of d(s)/D(N) with experimental values

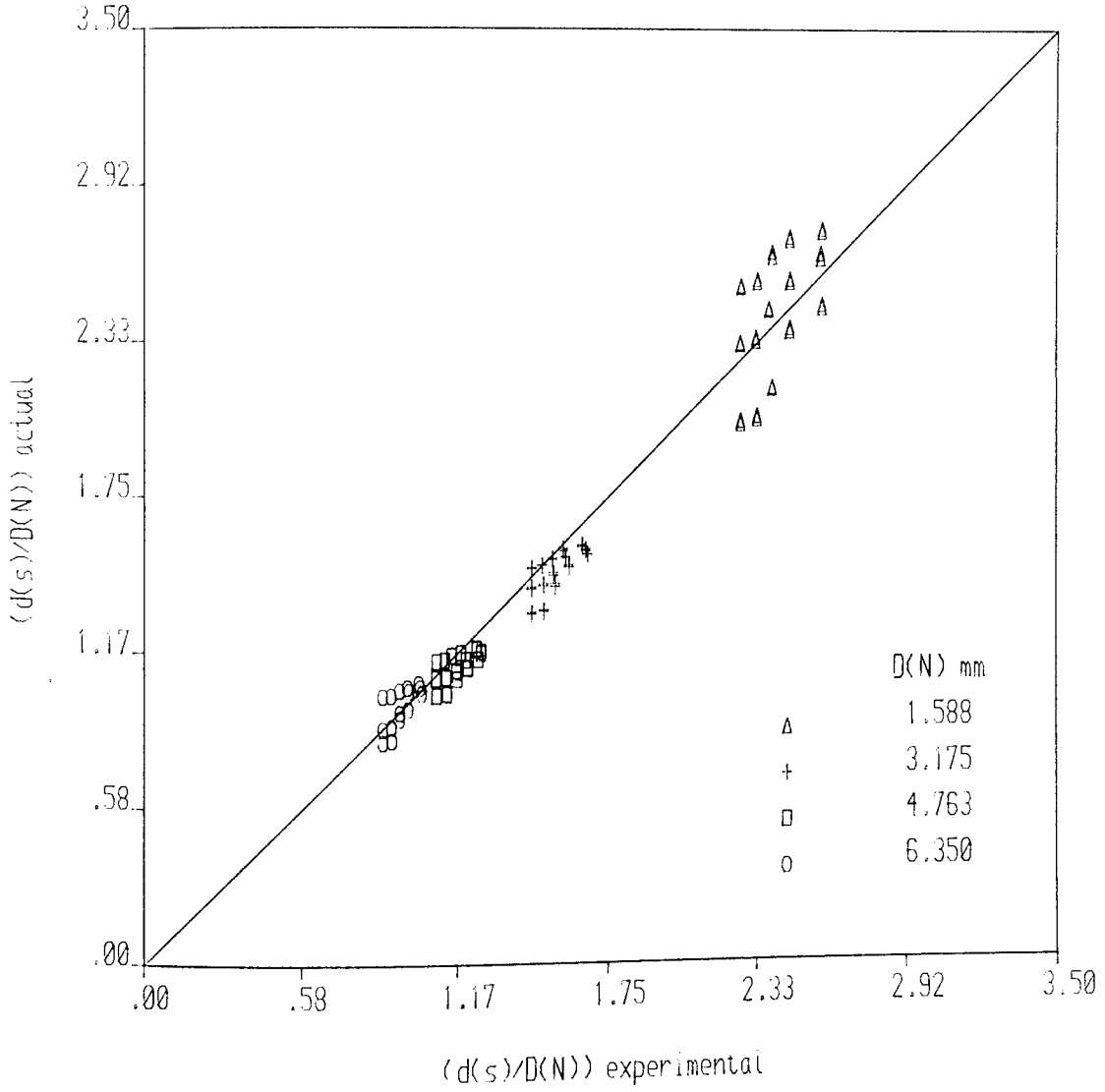

Fig.8.2-14. Comparison of actual values of d(s)/D(N) with experimental values

the equipment it was impossible to operate beyond a dispersed phase superficial velocity of U''_D = 0.60 $cmsec^{-1}$ because drop formation became irregular and considerable inter-droplet coalescence coupled with back mixing occurred during travel between plates. Nevertheless correlation within the range studied is satisfactory considering the complexity of the process. The correlation coefficient calculated by regression analysis for the equations 8.2-5 and 8.2-6 was 0.964 giving a standard deviation about regression of 0.113.

8.2-4 (3) DROP SIZE DISTRIBUTION

Tables 3.2-3 to 8.2-6 in Appendix 6-9 show the conditions under which drop size distributions were determined on the four types of plates. In all runs, droplets ranging from 0.68 mm diameter to, >12.00 mm diameter were observed. There were large numbers of small diameter droplets (<2.50 mm) but these accounted for a relatively small proportion (3-8 volume %) of the droplet size distributions. Figures 8.2-19 to 8.2-22 show the comparisons of the experimental size distribution with Mugele-Evans and the log-normal distributions. These are for 25% free area; 1.588 mm, 3.715 mm, 4.763 mm and 6.350 mm hole diameter plates respectively. A selection of data, in fact that plotted in Figures 8.2-19 to 8.2-22

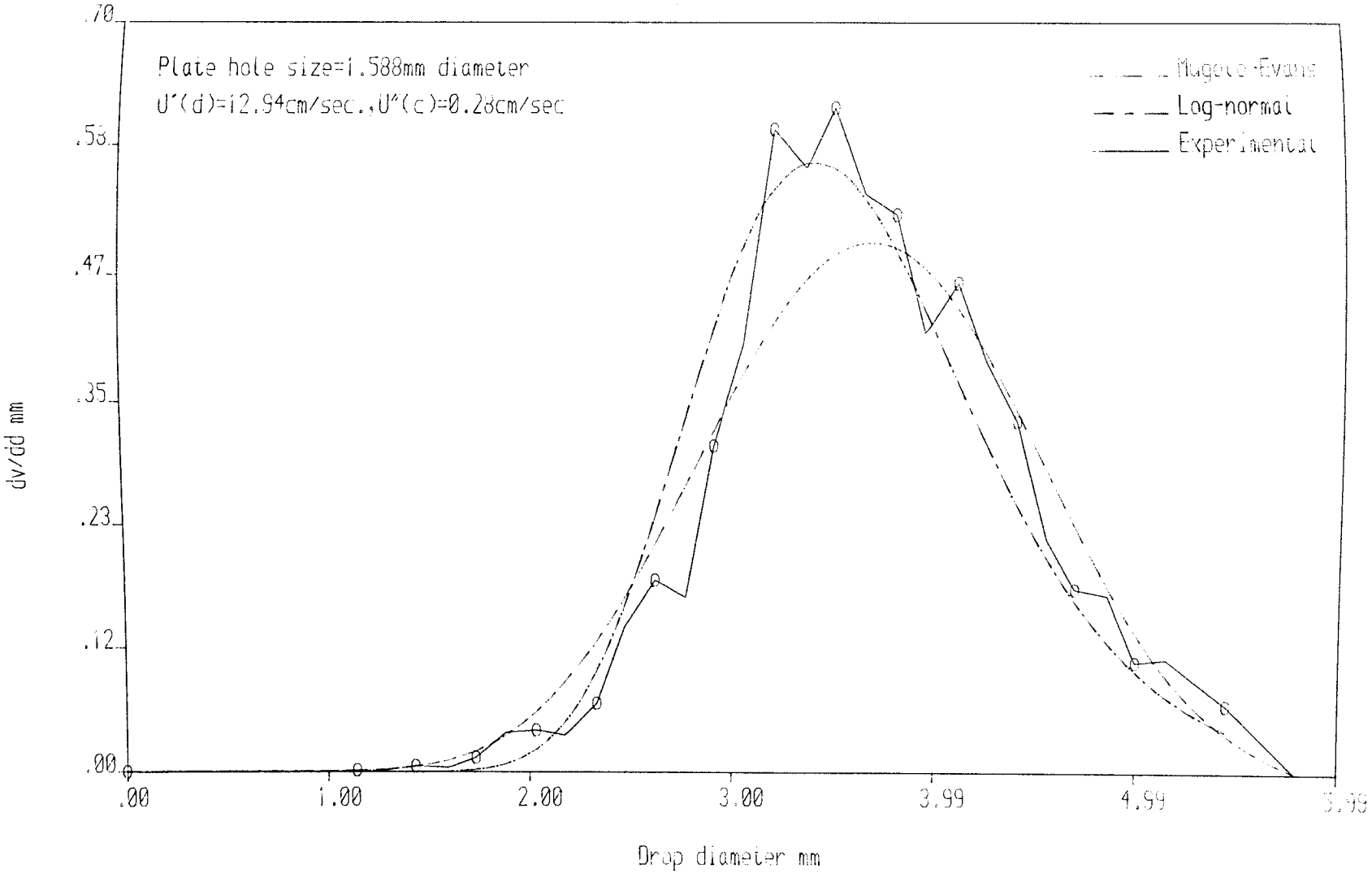

Fig.8.2-19. Comparison of experimental drop size distributions with Mugele-Evans and log-normal functions

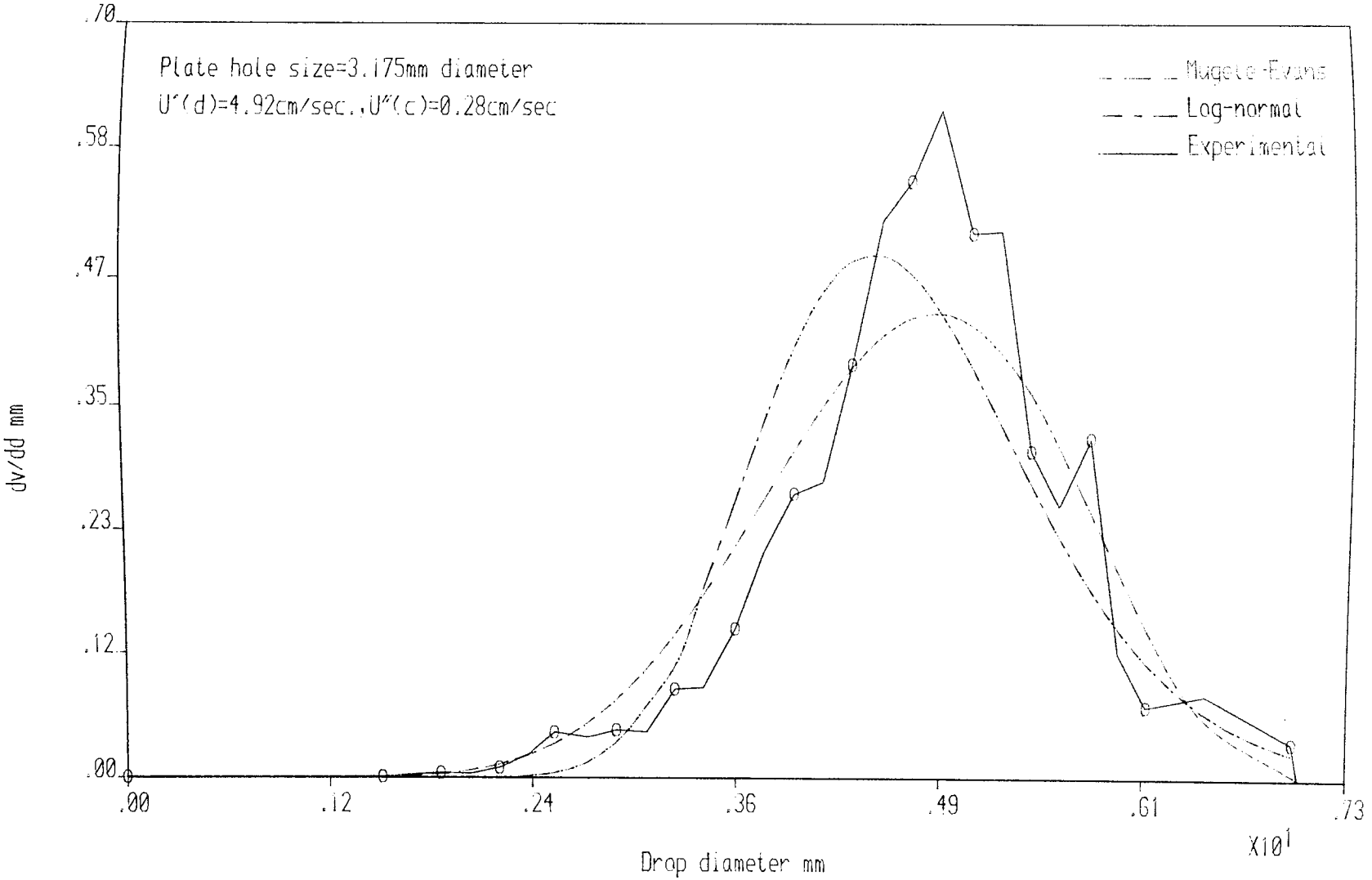

Fig.8.2-20. Comparison of experimental drop size distributions with Mugele-Evans and log-normal functins

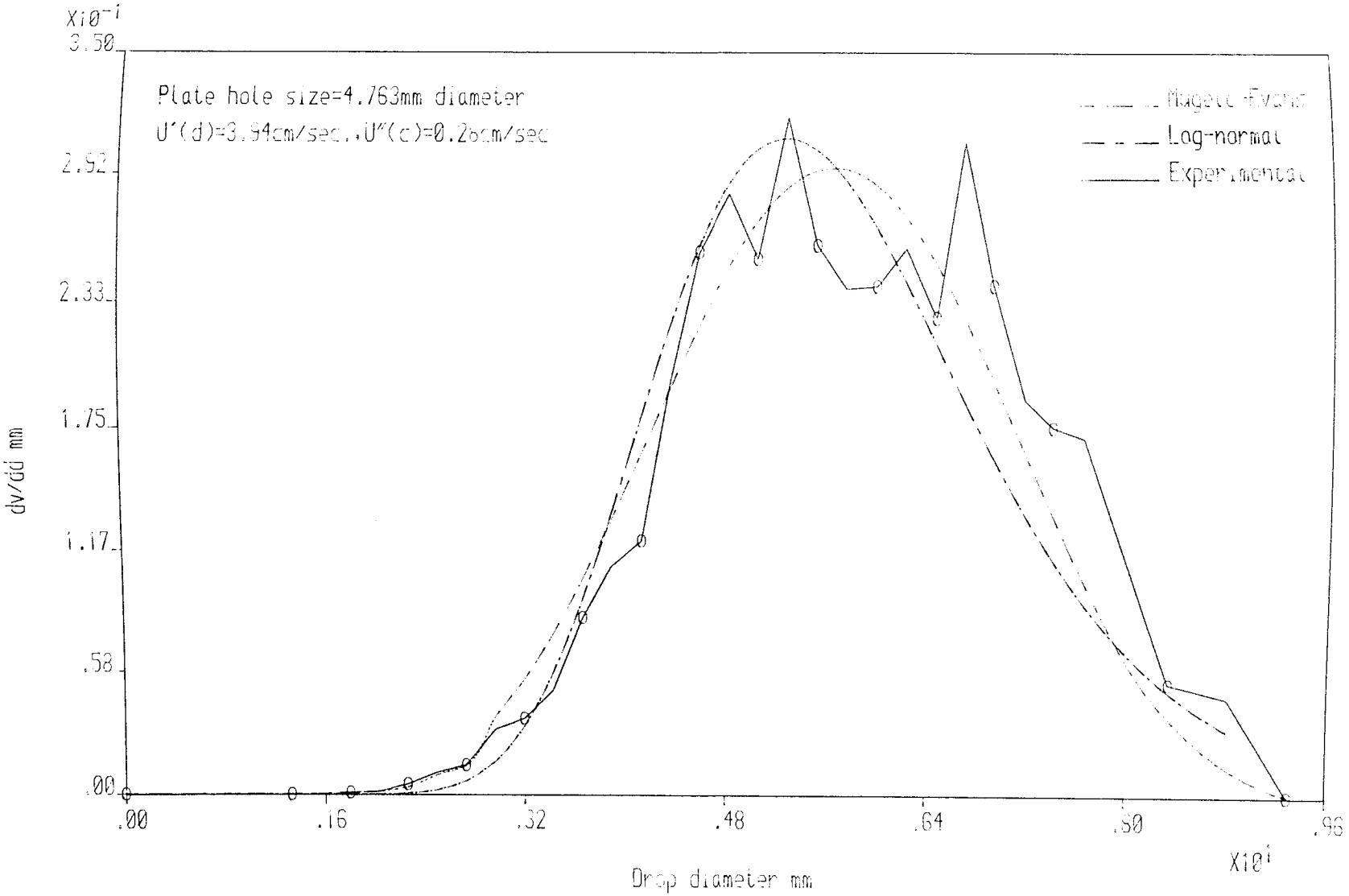

Fig.6.2-21. Comparison of experimental drop size distributions with Mugele-Evans and log-normal functions

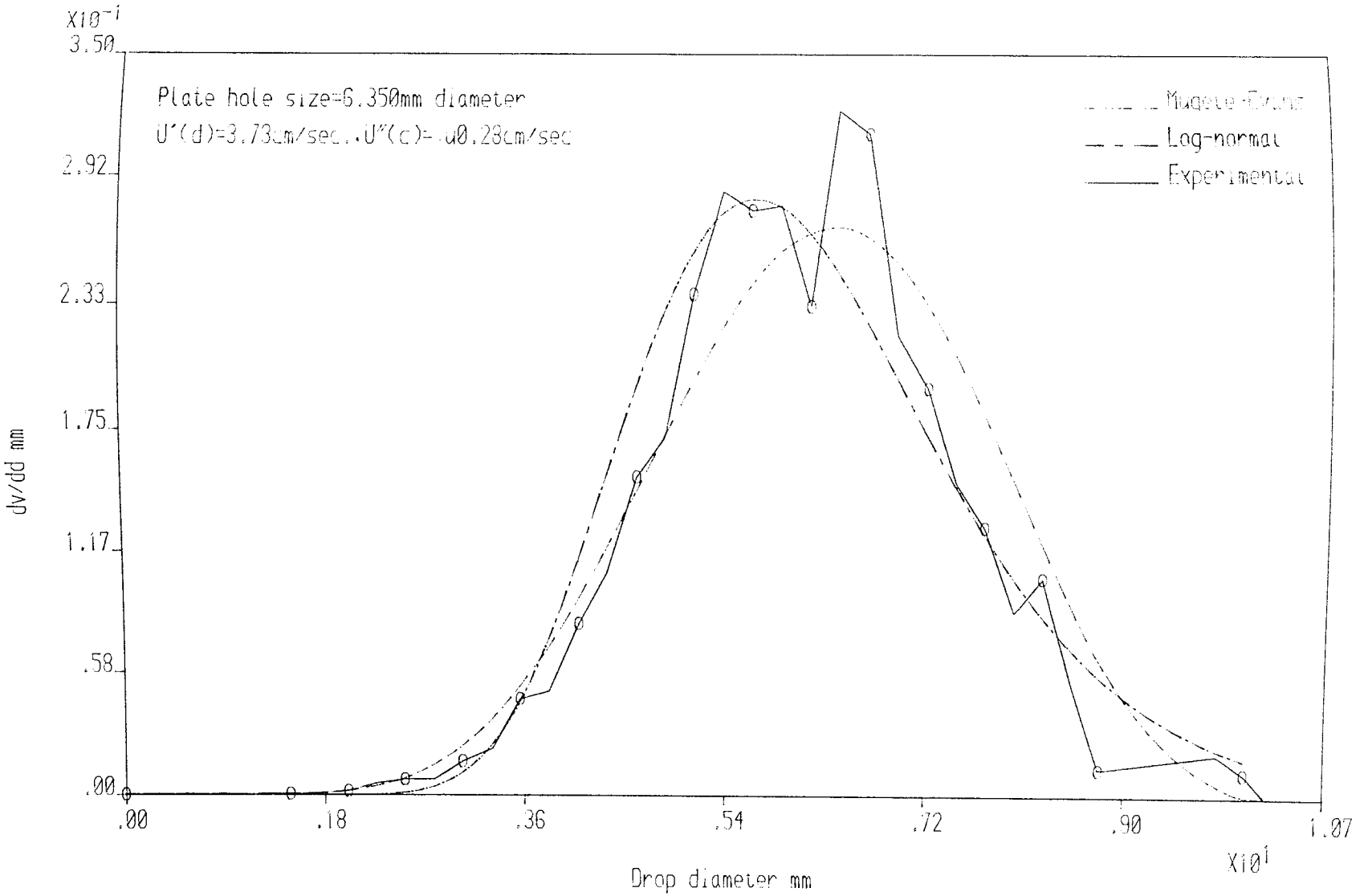

Fig.8.2-22. Comparison of experimental drop size distributions with Mugele-Evans and log-normal functions

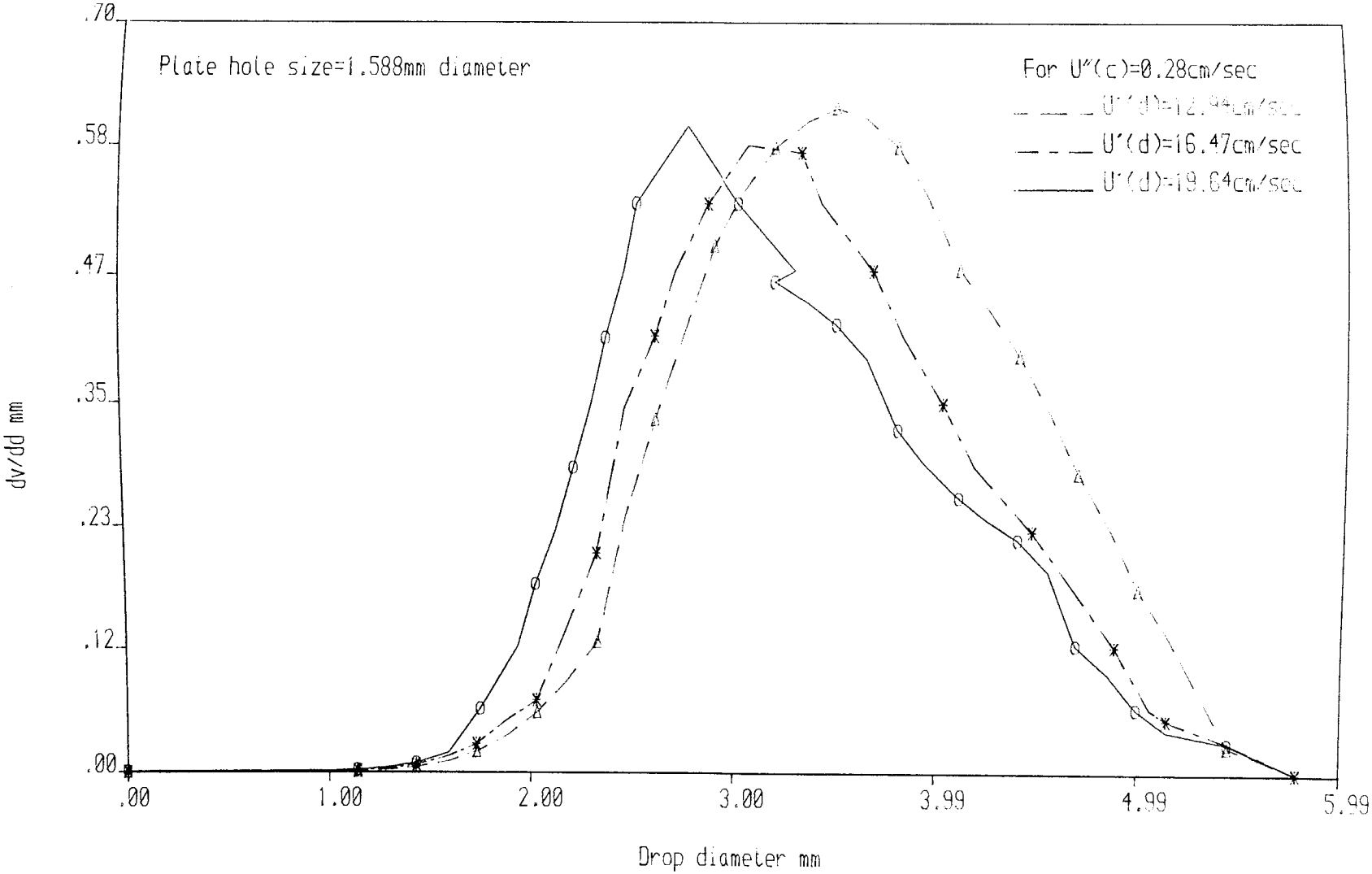

Fig 8.2-19a. Drop size distribution for clairsol'350' dispersed into de-ionised water

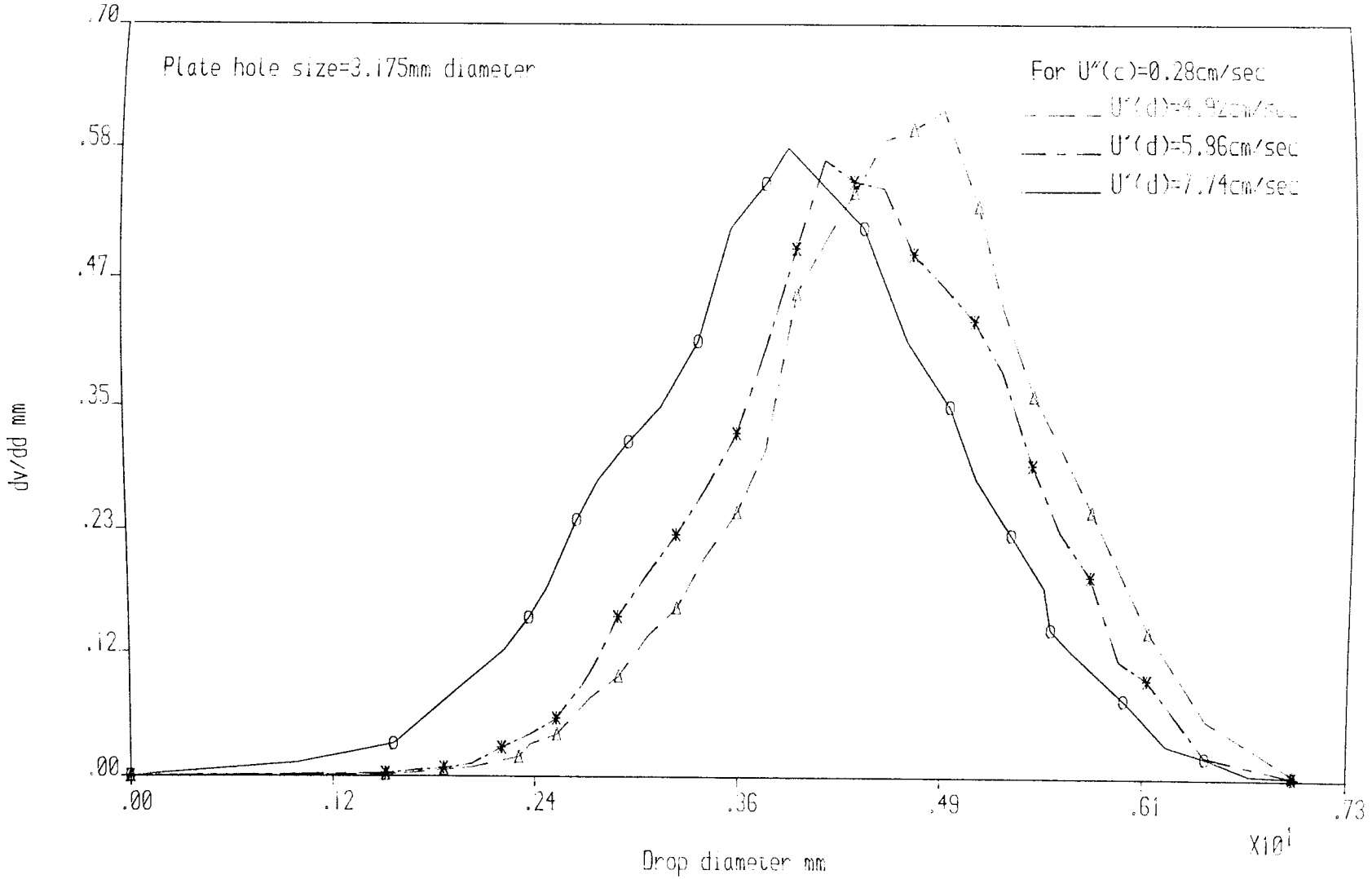

Fig 8.2-20a. Drop size distribution for clairsol '350' dispersed into de-ionised water

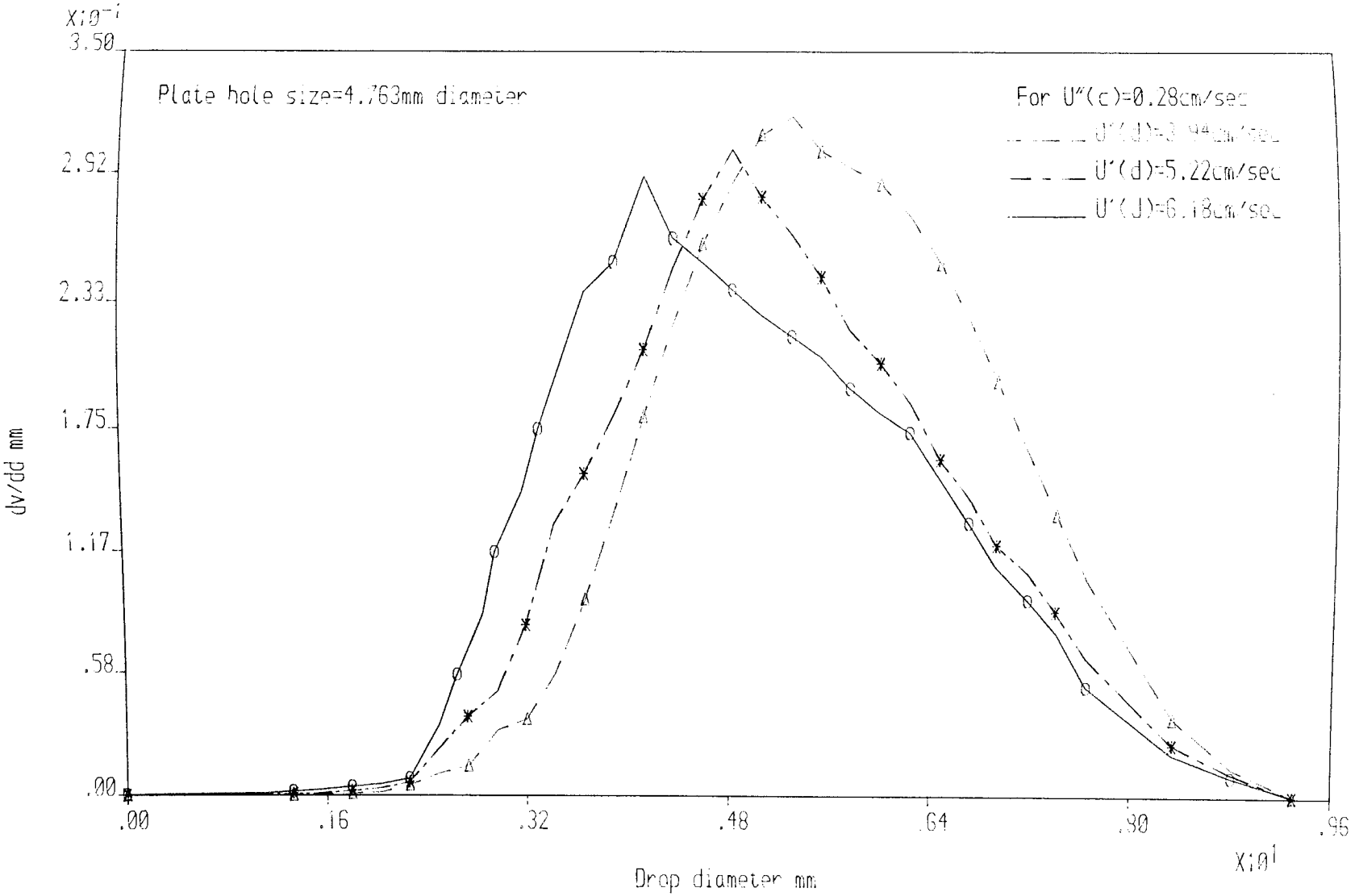

Fig 8.2-21a. Drop size distribution for clairsol'350' dispersed into de-ionised water

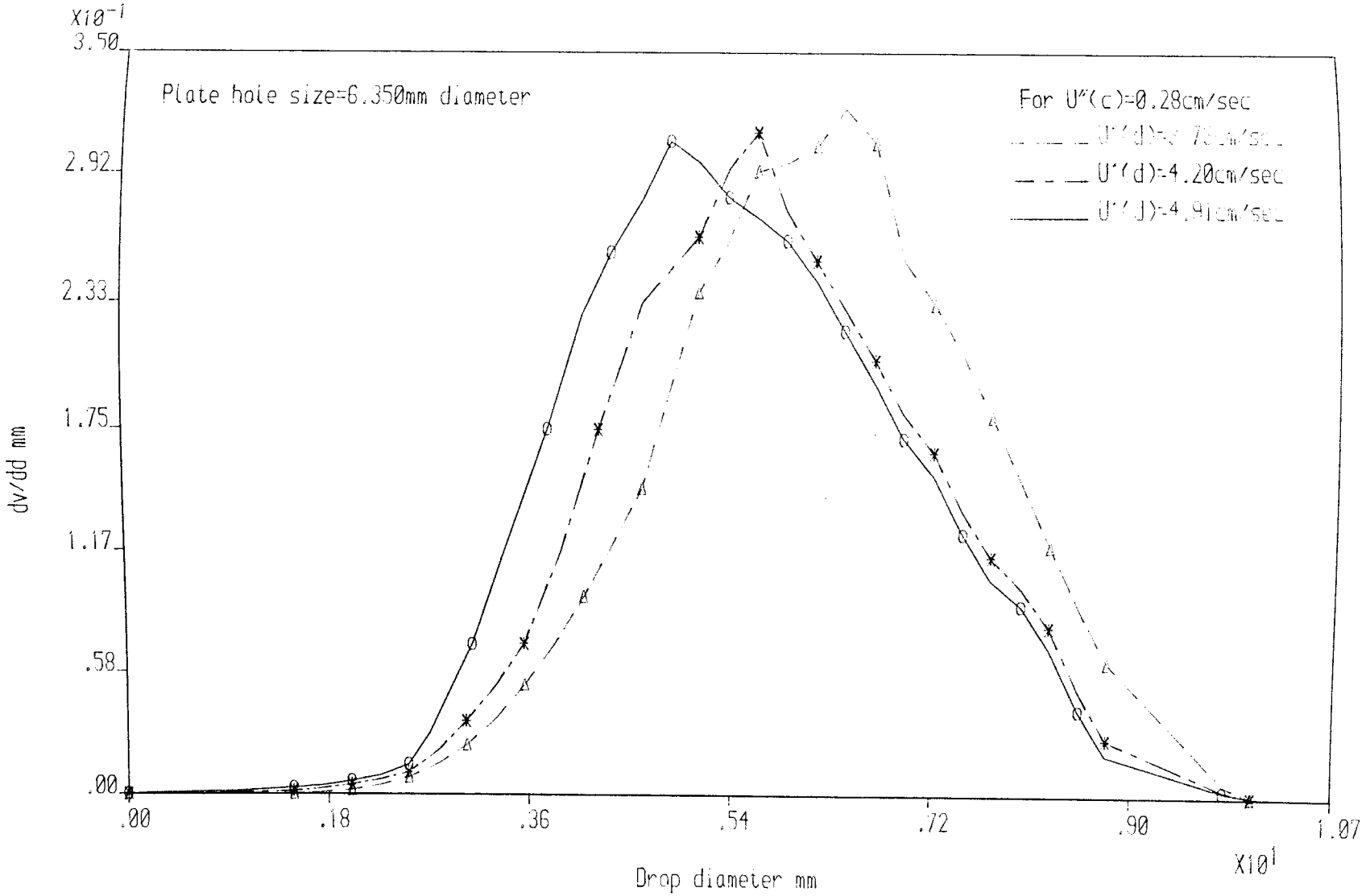

Fig 8.2-22a. Drop size distribution for clairsol '350' dispersed into de-ionised water

is shown as histograms of equivalent spherical diameter versus drop fraction in Figures 8.2-23 to 8.2-26.

Drop size cumulative volume plots, from which Figures 8.2-19 to 8.2-22 were derived are shown in Figures 8.2-15 to 8.2-18 (in Appendix 10-15)for the four different plates used. Several parameters of the size distribution are tabulated in Table 8.2-6 and 8.2-7. These include the maximum drop size d_m, the volume (Sauter) mean diameter d_{32}, the ratio of $\frac{d_{32}}{d_{50}}$ and the Skewness parameters δ and a.

The ratio of $\frac{d_{32}}{d_{50}}$ ranges from 3.67 to 6.27. Mugele-Evans(111) outline the range of $\frac{d_{32}}{d_{50}}$ to be expected for certain types of sprays and dispersions. The experimental d_{32} values determined from the drop photographs were compared with the calculated d_{32} values using both the log-normal and Upper Limit methods. The agreement is quite good with the Upper Limit method, the average deviation from the experimental values being ±2.11% compared to the average deviation of 11.86% using the log-normal method. The index δ determines the spread of the distribution, a smaller value indicating a wider range of drop sizes whilst a value of a greater than unity indicates a wider range of drops of sizes larger than d_{50}. The range

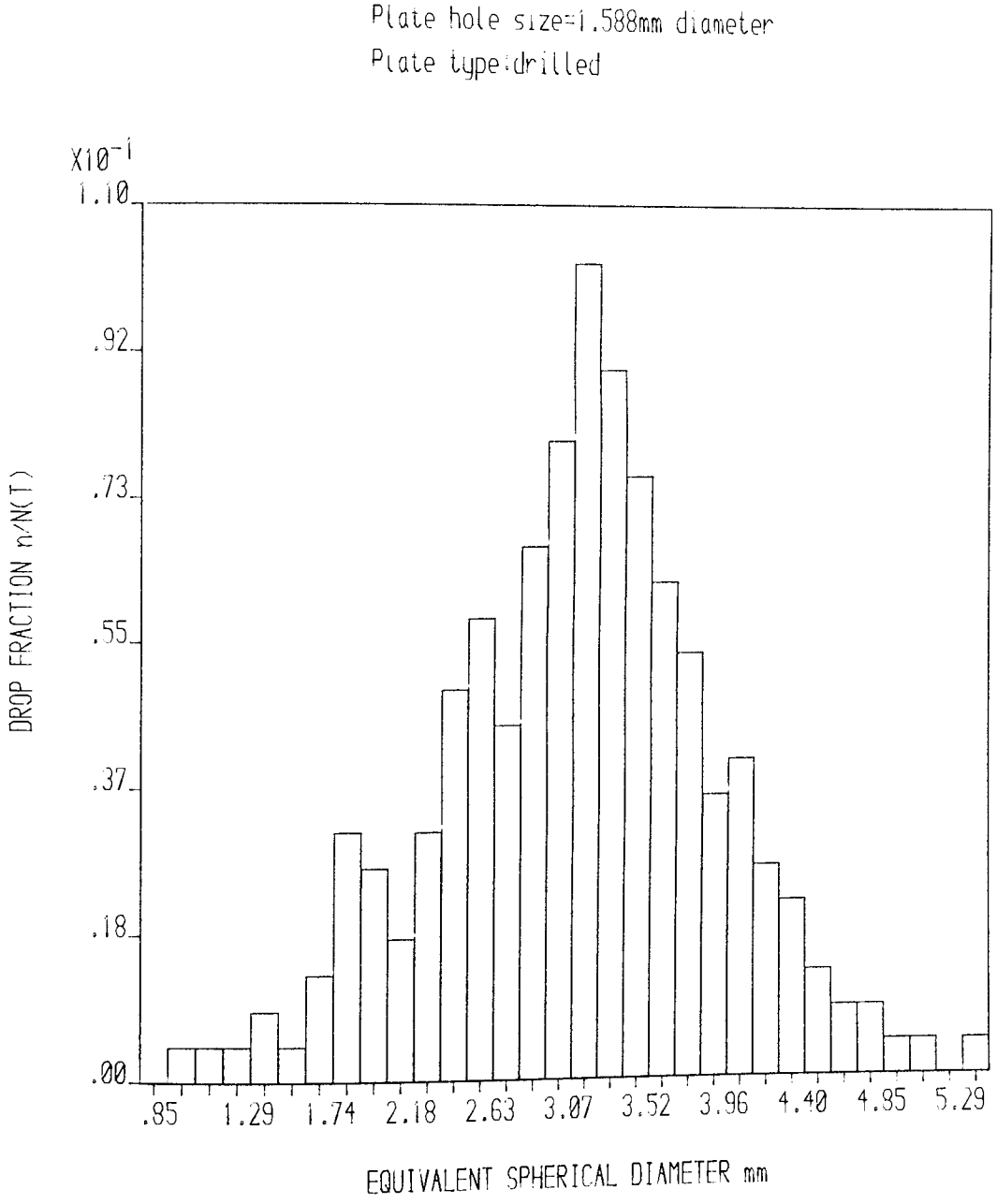

Fig.8.2-23. Drop size distribution in 450mm sieve-plate extractor column for clairsol '350' drops in de-ionised water at superficial velocity of 17.64cm/sec for clairsol and superficial velocity of 0.44cm/sec for water Total number of drops counted=224

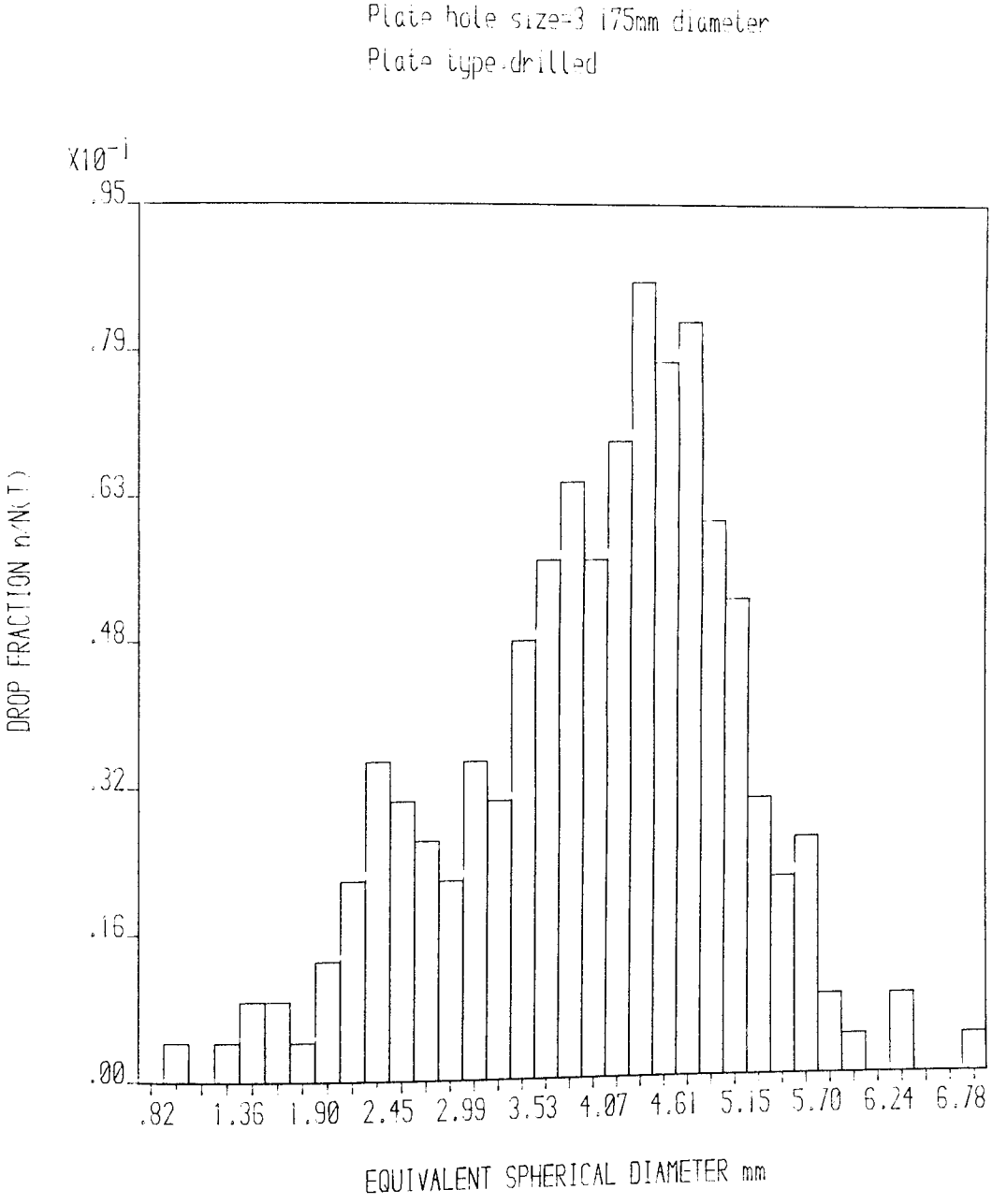

Fig.8.2-24. Drop size distribution in 450mm sieve-plate extractor column for clairsol '350' drops in de-ionised water at superficial velocity of 10.90cm/sec for clairsol and superficial velocity of 0.27cm/sec for water Total number of drops counted=231

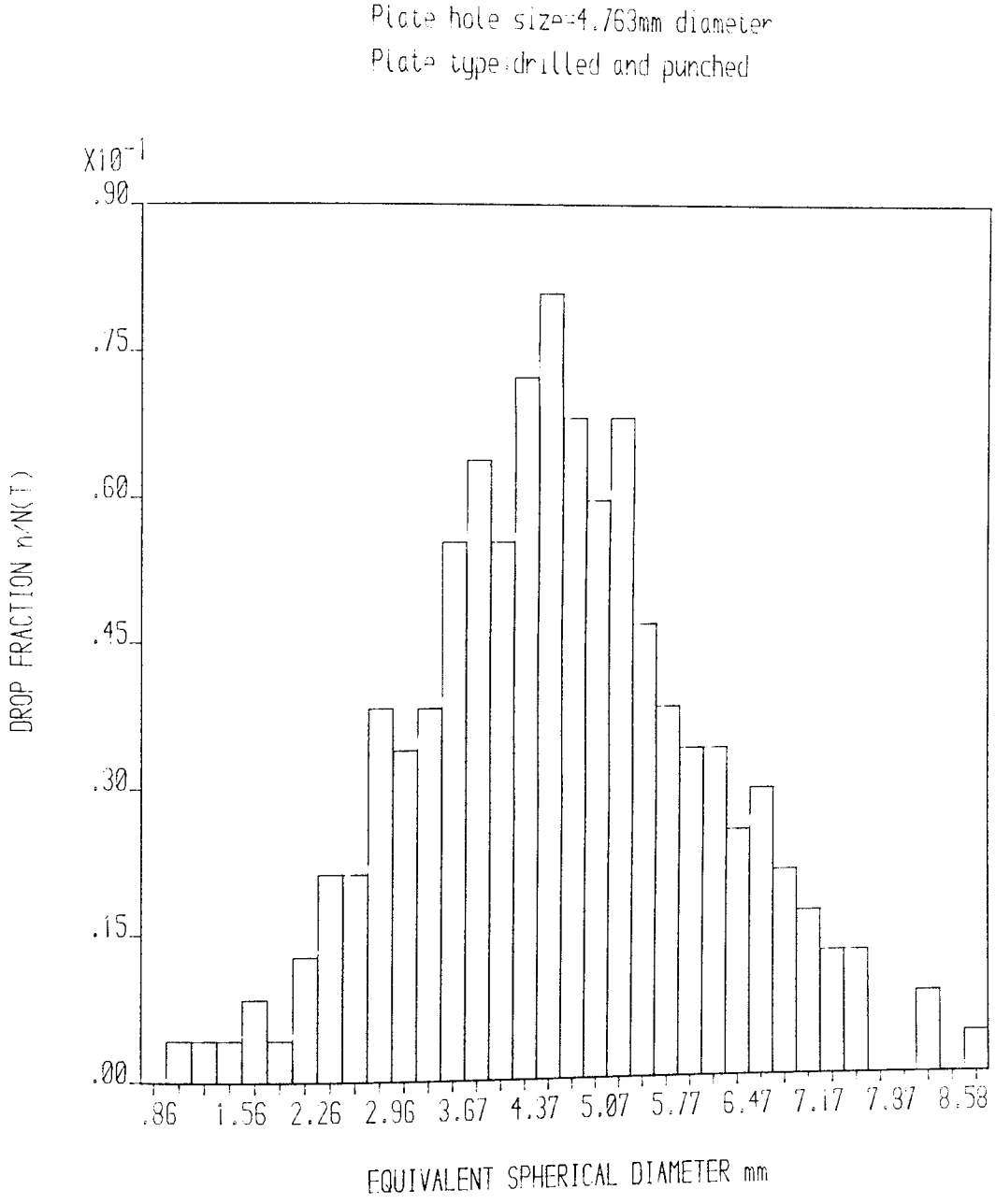

Fig.8.2-25. Drop size distribution in 450mm sieve-plate extractor column for clairsol'350' drops in de-ionised water at superficial velocity of 8.68cm/sec for clairsol and superficial velocity of 0.44cm/sec for water Total number of drops counted=235

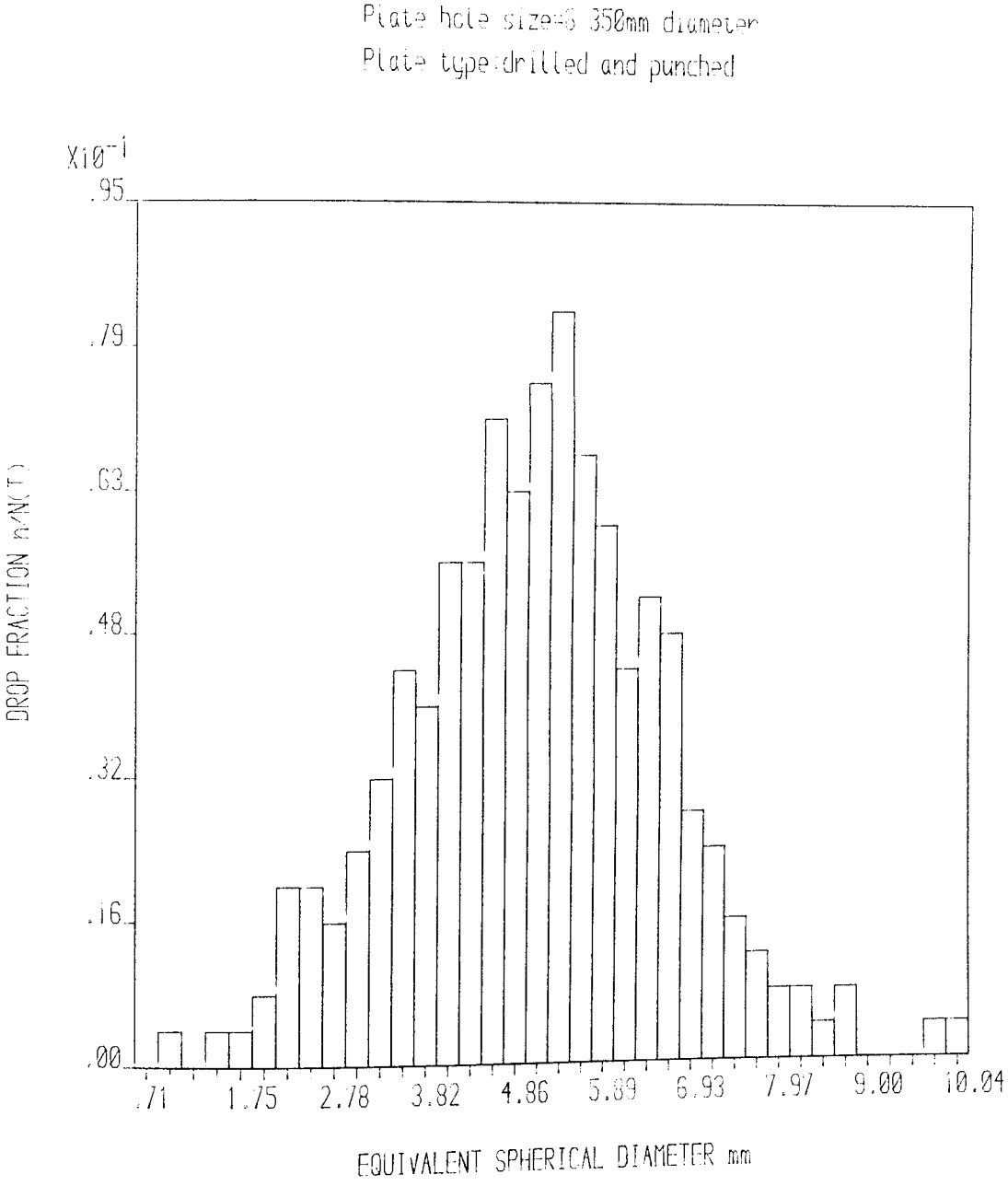

Fig.8.2-26. Drop size distribution in 450mm sieve-plate extractor column for clairsol '350' drops in de-ionised water at superficial velocity of 4.40cm/sec for clairsol and superficial velocity of 0.44cm/sec for water Total number of drops counted=353

TABLE 8.2-6

COMPARISON OF EXPERIMENTAL SAUTER MEAN DIAMETER WITH THAT CALCULATED VIA LOG NORMAL AND MUGELE-EVANS FUNCTIONS

PLATE HOLE SIZE (mm)	1.588	3.175	4.763	6.350
Log-normal (d_{32})	3.89	5.00	6.49	6.92
Experimental	3.54	4.62	5.50	5.93
% deviation	9.00	7.60	16.54	14.31
Upper-Limit (Mugele-Evans)	3.50	4.47	5.33	5.88
Average % Deviation	-1.14	-3.36	-3.09	-0.85

TABLE 8.2-7

DISTRIBUTION PARAMETERS IN SIEVE PLATE COLUMN

PLATE HOLE SIZE (mm)	LOG NORMAL		UPPER LIMIT		
	d_{GM}	δ	δ	a	$\frac{d_{32}}{d_{50}}$
1.588	3.55	3.50	1.58	0.96	3.67
3.175	4.60	3.91	1.45	0.67	4.71
4.763	5.60	2.97	1.46	0.98	5.66
6.350	6.00	2.90	1.35	0.83	6.27

of the uniformity parameter δ for the present work data is 1.35 to 1.58 for Mugele-Evans (Upper-Limit) and 2.90 to 3.91 for log-normal. The Upper Limit compares for example with a range of 0.60 to 1.50 tabulated by Mugele-Evans(111) for pressure and tangential nozzles and Venturi atomizers.

It may be concluded from this that, for systems of the general type studied, in sieve plate columns with plate holes in the range 1.588 mm to 6.350 mm and U_D between 2.33 and 28.30 $cmsec^{-1}$ the drop size distribution is most closely approximated by the Upper Limit of Mugele-Evans.

Also shown in Tables 8.2-3 to 8.2-6 in Appendices 6 to 9 are the estimated terminal velocities U_t for the drops of Clairsol 350 in water taken from the Hu-Kintner plot reproduced as Figure 3.1-6. From this values of N_{Re} were predicted; these give an indication whether single drops would be in the stagnant regime i.e. $N_{Re}<10$ (see Section 9.3) or in the more efficient circulating or oscillating drop regimes.

8.2-5 DISTRIBUTOR BEHAVIOUR

The same distributor, with 4.763 mm drilled and punched holes, was used throughout (Figure 7.2-6). The performance of this distributor is illustrated in Figure 8.2-27. At low velocities, i.e. U_D<0.40 cmsec^{-1}, drops formed at the tip of the orifice as described by Hayworth and Treybal(54). As the velocity was increased the drops ceased forming at the tip but broke away from a stream projected from the tip, doing so quite uniformly. At still higher velocities with the jet elongating and vibrating, and a non-uniformity of drop size resulted.

The behaviour differed from that of a single nozzle since there was inevitably mal-distribution of dispersed phase, i.e. some orifices were preferred and others 'starved' at low throughputs. The predominant tendency was for drops to form from holes at or near the centre and for holes at the outer periphery to be 'starved'.

The mean drop volume was compared with different correlations and the results were presented in terms of average percentage deviation in Table 8.2-8. The Scheele and Meister(106) and Kagan et al.(81) correlations showed an increase in drop volume with corresponding increase in dispersed phase superficial

U_D = 2.86 $cmsec^{-1}$

U''_C = 0.27 $cmsec^{-1}$

U_D = 2.86 $cmsec^{-1}$

U''_C = 0

U_D = 5.41 $cmsec^{-1}$

U''_C = 0.27 $cmsec^{-1}$

Mixed Regime

Drip Point and jetting

U_D = 5.41 $cmsec^{-1}$

U''_C = 0

Mixed Regime

Drip point and jetting

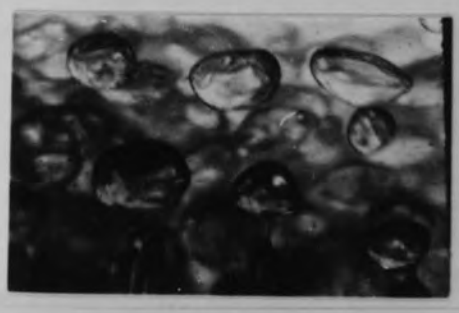

U_D = 8.68 $cmsec^{-1}$

U''_C = 0.27 $cmsec^{-1}$

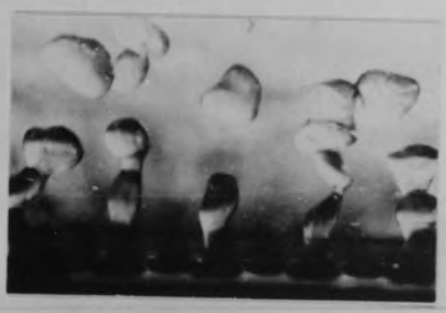

U_D = 8.68 $cmsec^{-1}$

U''_C = 0

Fig. 8.2-27 Drop formation mechanisms from distributor plate.

Distributor: 4.763 mm i.d. hole size x 558 drilled and punched holes.

TABLE 8.2-8

COMPARISON OF MEAN DROP VOLUME AS PREDICTED OF DIFFERENT CORRELATIONS IN TERMS OF THE AVERAGE PERCENTAGE DEVIATION

U_C'' $cmsec^{-1}$	U_D $cmsec^{-1}$	Schecle & Meister	Izard	Kagan et al	Present Work cm^3	Average Percentage Deviation
0.27	2.86	0.273 cm^3 (12.08)	0.249 cm^3 (3.61)	0.374 cm^3 (35.83)	0.240	17.17
	4.80	0.297 cm^3 (41.41)	0.246 cm^3 (29.27)	0.422 cm^3 (58.77)	0.174	43.15
	5.41	0.320 cm^3 (50.63)	0.242 cm^3 (37.71)	0.465 cm^3 (66.02)	0.158	51.45
	6.64	0.339 cm^3 (64.60)	0.237 cm^3 (49.37)	0.499 cm^3 (75.95)	0.120	63.31
	8.68	0.361 cm^3 (71.47)	0.226 cm^3 (54.43)	0.539 cm^3 (80.90)	0.103	68.93

velocity while the correlation of Izard (75)showed a decrease in drop volume for a corresponding increase in dispersed phase superficial velocity. Thus the Izard direction of change agreed fairly well with the present data.

The percentage deviation from the experimental work was highest for the correlation of Kagan et al; the Scheele and Meister correlation gave a high percentage deviation for high dispersed phase superficial velocity but the deviation at low dispersed phase superficial velocity was fairly low i.e. 12.08%. The Izard correlation gave a small deviation at low dispersed phase superficial velocity but the deviation at high dispersed phase rate was approximately 50%. Although none of the correlations compared well with the experimental data, the Izard correlation was best overall. Consideration of the hydrodynamics furthermore suggests that the trend observed in this work and by Izard is correct.

8.2-6 DROP SHAPE

Figure 8.2-28 shows typical shapes of rising droplets encountered during the experimental operation of the column. These photographs compared well with the results of Satapathy and Smith (152) shown in Figure 3.1-3 for immiscible liquid falling through a liquid in the Reynolds number range $100 \lesssim Re \lesssim 2000$. Figures 8.2-28(a) and (b) show a mixture of fluctuation and non-axial symmetry in the droplet shape. These correspond to Reynolds numbers greater than 100.

Figure 8.2-28(c) corresponds to Reynolds numbers greater than 300. In this case the drops followed the line of a helical spiral. This appeared to be induced by the alternate detachment of vortices at the rear of the droplet.

Evidently, under conditions where the surface of the drop is expanded and contracted the drop shape will depend upon the interfacial tension, drop velocity, as well as the Reynolds number.

a) U_D = 2.86 cmsec^{-1} U''_C = 0.27 cmsec^{-1} Re>800

b) U_D = 4.08 cmsec^{-1} U''_C = 0.27 cmsec^{-1} Re>800

c) U_D = 6.64 cmsec^{-1} U''_C = 0.27 cmsec^{-1} Re>800

Fig 8.2-28 Relationship between drop shapes, dispersed phase throughputs and Reynolds number - Plate ¼ 4.763 mm i.d. hole size.

8.3 DISCUSSION OF RESULTS

8.3-1 DROP FORMATION BY JETTING - PLATE

The photograph presented as Figure 8.1-1 indicates the change in jetting behaviour from an axisymmetric, nodal disturbance before the peak to a sinuous disturbance beyond the peak, as previously described by a number of investigators (21, 141, 163).

The plot of jetting velocity against jet length in Figure 8.2-1, does not show the marked discontinuities in jet length which Meister and Scheele (163) observed with a single nozzle, corresponding in their view to a very rapid lengthening of the jet through droplets merging. However, the curve showed a continuous steep rise almost immediately after initial jetting; this steep slope continued almost unchanged until the peak length was approached.

The single nozzle correlations of previous workers (21, 163), however did not accurately predict the jet length observed in the present work. This discrepancy may be due to the complex behaviour of multiple jets in a commercial size column compared to those from single nozzles. For example,

(1) The onset of jetting occurred at lower U_D values than for a single nozzle, as described in 8.2-1. This tended to give lower d_{32} values.

(2) Violent vibration of individual jets as the maximum jet length was approached and in a small percentage of cases, e.g. 10%, contacting adjacent jets at the maximum jet length. This resulted in inconsistent drop formation.

(3) Effects of countercurrent and cross-flow of the continuous phase. No difference was observed between drop formation from rows of nozzles where the continuous phase was accelerating or decelerating across the plate, but this would only be detectable, if at all, in a very large column. However, the horizontal velocity component of the continuous phase flow, which would if anything cause jet disruption and premature break-up giving smaller drops, and the vertical component, which would tend to result in thicker jets and hence larger drops, could be important factors. Infact, based upon the assumption that the continuous phase flows across the plate entirely in a section equivalent in height to the downcomer height and in width to the varying plate cross-section, values of U_C''' for cross-flow in this work were in the range 0.54 to 1.10 $cmsec^{-1}$ when $U_C''' = 0.27$ $cmsec^{-1}$ and 0.88 to

TABLE 8.3-1

COMPARISON OF DROP DIAMETER IN JETTING REGION AS PREDICTED BY DIFFERENT MODELS

IN TERMS OF THE AVERAGE PERCENTAGE DEVIATION

Plate Hole Size cm		Christensen and Hixson (21)	Perrut and Loutaly(122)	Kumar and (92) Hartland	Present Work
0.1588	Mean drop size (cm)	0.277	0.319	0.465	0.407
	Precentage Deviation	-46.93	-27.59	12.47	
0.3175	Mean drop size (cm)	0.510	0.581	0.687	0.461
	Percentage Deviation	9.61	20.65	32.90	
0.4763	Mean drop size (cm)	0.526	0.729	0.857	0.542
	Percentage Deviation	-3.04	25.65	36.76	
0.6350	Mean drop size (cm)	0.535	0.706	0.831	0.649
	Percentage Deviation	-21.31	8.07	21.90	
Average Percentage Deviation		-15.42	6.70	26.01	

TABLE 8.3-2

COMPARISON OF VELOCITY IN JETTING REGION AS PREDICTED BY DIFFERENT MODELS

IN TERMS OF THE AVERAGE PERCENTAGE DEVIATION

Plate hole size cm		Scheele and Meister (105	De Chazel and Ryan (30)	Fujinawa et al (36	Present Work
0.1588	Jetting velocity ($cm\,sec^{-1}$)	22.51	22.98	22.55	17.64
	Percentage Deviation	21.64	23.24	21.77	
0.3175	Jetting velocity ($cm\,sec^{-1}$)	11.55	14.24	15.95	6.80
	Percentage Deviation	41.13	52.25	57.37	
0.4763	Jetting velocity ($cm\,sec^{-1}$)	5.88	9.11	13.02	4.08
	Percentage Deviation	30.61	55.21	68.66	
0.6350	Jetting velocity ($cm\,sec^{-1}$)	2.15	7.74	11.28	3.32
	Percentage Deviation	-54.42	57.11	70.57	
Average Percentage Deviation		9.74	47.00	54.60	

1.76 $cmsec^{-1}$ when U''_C = 0.44 $cmsec^{-1}$. The effects could therefore be expected to vary from distortion of the jet, i.e. displacement from the vertical at relatively low U''_C' values to premature rupture of the jet at anti-node at the higher U''_C' values almost equivalent to average U_D values. Deviations were observed not to be symmetrical because of the cross flow effects.

(4) The drop-sizes in a practical column represent a population from a range of formation mechanisms, as 8.2-4, and ages, i.e. due to back-mixing. Thus the data represent average rather than 'point' values.

(5) Because of the method of construction, and operation practical plates inevitably have,

(a) some variation in hole size about the design value.

(b) some variation in projection height (if punched)

(c) some variation in smoothness of edges even after filing.

(d) a change in cleanliness with operating time and depending initially on the method of pre-cleaning.

(e) possible variations in flatness i.e. bowing.

(f) possible deviations from the horizontal.

Infact, if applicable these were minor features in the column described since fabrication was to high tolerances and cleanliness was maintained throughout. Deviation of plates from horizontal, which would have a serious effect on the height of dispersed reservoir beneath a plate and therefore upon drop formation, was not infact a feature of the column used in the present work because provision had been made along the length of the tie rods to hold plates in positions with collars for accurate alignment.

8.3-2 HOLD-UP

The results of the hold-up under non-mass transfer conditions indicate that equation 3.4-2 based on a hydrodynamically simplified model proposed by Thornton adequately relates the phase flow rates to the droplet characteristic velocity and the dispersed phase hold-up as in the case of Spray (147) and packed columns (148).

There was no significant change in the experimental hold-up determined in the absence of solute transfer when compared to the ease of solute transfer from dispersed Clairsol phase to the continuous water phase and vice-versa. This will clearly depend upon the liquid system in use, i.e. upon the variation of interfacial tension with solute concentration and hence the tendency for solute transfer to enhance or inhibit coalescence, and so alter the drop size distribution and terminal velocities.

The effect of hole size on characteristic velocity is shown in Figures 8.2-2 to 8.2-5 for the system Clairsol 350 - de-ionised water covering the 1.588, 3.175, 4.763 and 6.350 mm hole sizes used. The data for larger hole sizes (4.763 and 6.350 mm) gave a higher value of characteristic velocity than that obtained for smaller hole sizes; this was expected since as the hole size

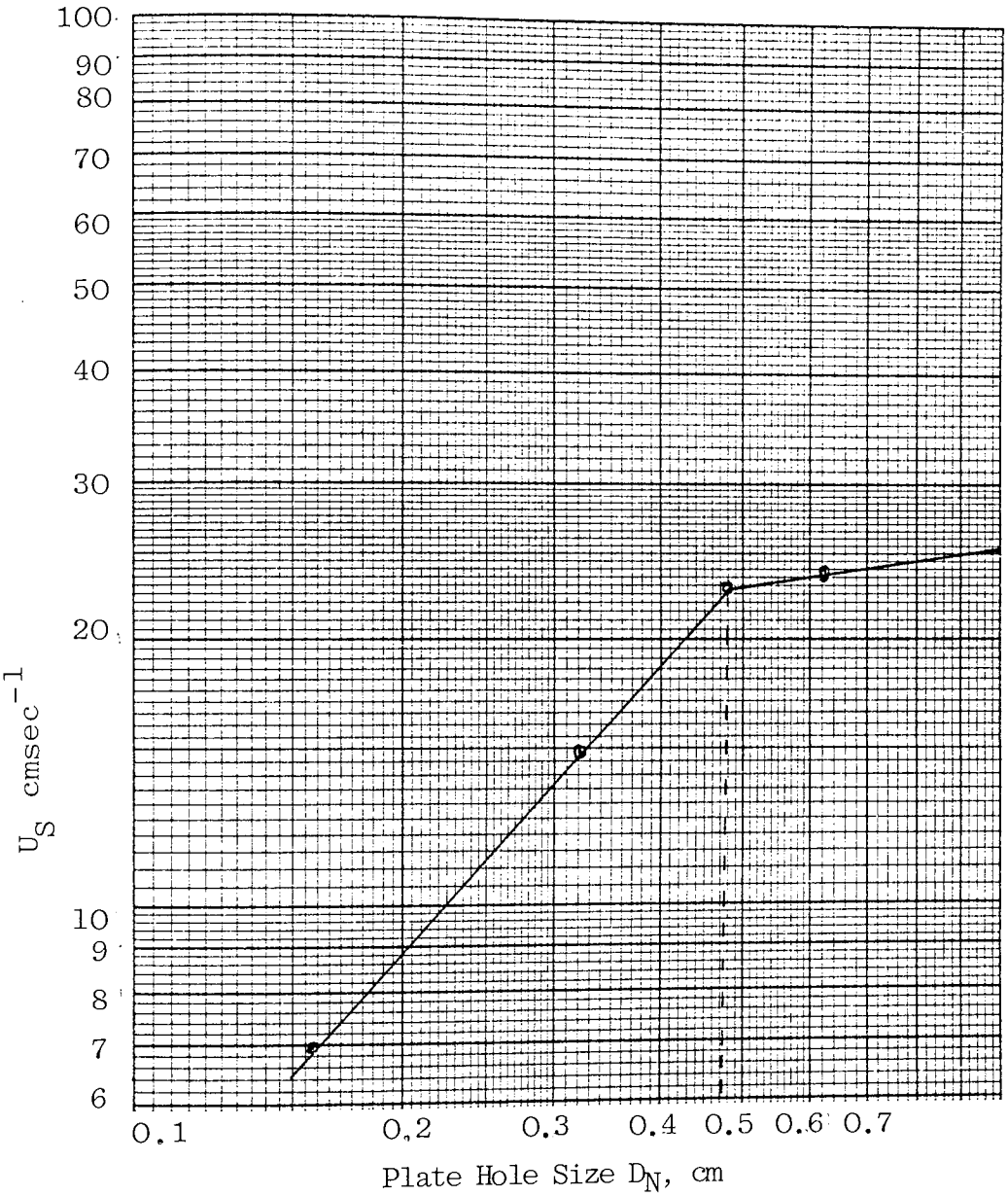

Fig. 8.3-1 Plot of characteristic velocity against plate hole size

increased, the mean drop size also increased and therefore the terminal velocity. Figure 8.3-1 shows a plot of U_S versus D_N for the system Clairsol 350 - de-ionised water. The plot demonstrates the average characteristic velocity $\bar{U}_S$ was dependent on D_N to a marked extent up to a critical hole size, beyond which $\bar{U}_S$ varied only slightly with increase in hole size. The critical hole size, D_{NC} is indicated by a break in the correlation line between regions I and II this occurs at a D_N value of approximately 0.47 cm. The critical hole size corresponding to the two hydrodynamic regimes of sieve plate column operation viz, the near constant characteristic velocity (Region I) and the varying characteristic velocity region (Region II), would however depend upon the column geometry as well as liquid physical properties.

A possible explanation for the distinct transition in Figure 8.3-1 is suggested by reference to the flocculation zone height results in Figures 8.2-6 to 8.2-8. Flocculation zone height decreased with increase in hole size. At the transition point, corresponding approximately to the plate hole size 4.763 cm, the flocculation zone height became insignificant.

8.3-3 DROPLET COLLECTION BENEATH PLATES

From Figures 8.2-6 and 8.2-7, the observation of Treybal and Dumoulin (155) that the thickness of the dispersed phase layer beneath each plate increased with continuous water flow rate was confirmed. The thickness was reasonably constant from plate to plate at any given combination of dispersed and water rate except at conditions approaching flooding when there was an appreciable thickening of one or more of the layers. This occurred when the water rate was considerably higher than the dispersed Clairsol rate. (This could also occur when the dispersed phase rate is much higher than water rate, although flooding was not reached in this work because of the size of the equipment used). This is because a finite time is required for the drop coalescence process. Hence although flooding proper would have involved complete rejection of one of the phases from the column (See Section 3.2-3) a condition of 'pseudo-flooding' could be reached, under which it would be impractical to operate an industrial column. This was characterised by,

(a) Increasing depth of flocculation layer, i.e. less useful column volume. With the smallest hole size plate this layer almost extended to the plate below.

(b) Cloudiness of the continuous phase due to back-mixing of the smallest drops.

Bussolari et al (15), observed that the total layer thickness beneath a plate is due to three different effects, viz

(i) the interfacial tension effect,

(ii) the orifice effect, and

(iii) the downcomer effect, as given below

$$h = (h_\sigma + h_o + h_{continuous}) \qquad 8.3\text{-}1$$

and

$$h_\sigma = \frac{6\sigma}{d\Delta\rho g} \qquad 8.3\text{-}2$$

$$h_o = \frac{\rho_D\left[1 - \left(\frac{S_o}{S_t}\right)^2\right]U_D^2}{2gC^2\Delta\rho} \qquad 8.3\text{-}3$$

$$h_{continuous} = \frac{4.5\, U_{C_1}^{'''2}\, \rho_C}{2g\Delta\rho} \qquad 8.3\text{-}4$$

where S_o = cross-sectional area of all perforations, cm^2

S_t = cross-sectional area of column less the downcomer area, cm^2

C = overall orifice coefficient, dimensionless.

d = drop diameter, cm

$U_{C_1}^{'''}$ = velocity of the continuous phase through the downcomer, $cmsec^{-1}$

When the plate hole size was changed from 0.1588 cm to 0.3175 cm for a particular set of volumetric flow rates of the dispersed and continuous phases, the velocity through the orifices was reduced and from equation 8.3-3 the layer thickness beneath the plates due to the orifice effect would have decreased. The continuous phase velocity being the same (since downcomer size was constant), the layer of thickness due to downcomer effect, equation 8.3-4, would be unaltered. The layer thickness which depends on the drop formation characteristics will alter as per equation 8.3-2 of Bussolari et al (15) because it is dependent upon the phase flow rates. Hence from the theoretical considerations, the layer thickness should decrease when the hole size is changed from 0.1588 cm to 0.3175 cm. The same trend has been observed from the experimental (measured) layer thickness data for any particular set of phase flow rates. One result is that when the data of the plates with 0.1588 cm and 0.3175 cm hole sizes are compared under identical flow rates, the effective travel length for the drops between plates is much less for 0.1588 cm hole size (because the layer thickness is greater) than that for 0.3175 cm; the useful interfacial contact area therefore becomes reduced.

Substitution of the parameters and physical properties applicable to this study into equations 8.3-2 to 8.3-4

showed that the predicted values equation 8.3-1 were in the range 1.65 cm to 6.15 cm whereas the experimental data was in the range 0.70 cm to 10.0 cm.

Therefore equation 8.2-3 was correlated from the experimental data. This represents measurements against which further developments could be tested.

8.3-4 (1) DROP SIZE - PLATES

The mean drop size - superficial velocity results are plotted in Figures 8.2-9 to 8.2-12 for a number of operating conditions. As summarised in Table 8.3-1 the mean drop diameters obtained for various injection velocities of Clairsol 350 in water showed significant deviations from values predicted from single nozzle correlations (21, 92, 122). In the jetting region of high superficial velocities (U_D>6.60 cmsec^{-1}) equation (A1) of Christensen and Hixson predicted a lower mean drop diameter value for the plates of 1.588 mm, 4.763 mm and 6.350 mm hole sizes and a slightly higher mean drop size value for the plate of 3.175 mm hole size. The equation (B1) of Perrut and Loutaty predicted a higher mean drop size value for the plates of 3.175 mm and 4.763 mm hole sizes and a lower value for the plate of 1.588 mm hole size but was in fairly good agreement with the experimental value for the plate of 6.350 mm hole size. The equation (C1) of Kumar and Hartland gave a systematic deviation for the four different hole sizes used (1.588 mm, 3.175 mm, 4.763 mm and 6.350 mm). The results are presented in terms of mean percentage deviation in Table 8.3-1. The deviations from the experimental values could be attributed to the way drops are formed from single nozzles (i.e. nozzle projection, pressure head, drop formation time and nozzle wettability) compared to the drop swarms

(i.e. shorter nozzles projection, low pressure head, and more competing droplets at break up) from perforated plate. With a single nozzle of the type shown in Section 3.1-1, Figure 3.1-2, high pressure head is a common phenomenon, thus jets would tend to form at a dispersed phase velocity much lower than from multi-orifices distributors or industrial scale plates. Single nozzles are of close tolerance on diameter and meticulously cleaned which are impracticable on a pilot or industrial scale.

With a perforated plate however, reproducibility is an important factor, therefore it is desirable for the plate to be wetted by the continuous phase to prevent reduction in interfacial area due to coalescence of the dispersed phase into globules. Drop formation at the plate orifice was unpredictable because pressure drop at the orifice was small compared to the local pressure fluctuations below and above the orifices.

Furthermore, these authors (92, 21, 122) established their correlations operating with a single nozzle under condition of maximum jet length ($U_M = U_{max}$) and the drops obtained had a maximum size. However, perforated plate produce jets of numerous different lengths (Section 8.1-1), the velocity U_M through each hole being different. The mean drop sizes obtained are smaller than predicted by these authors' correlations.

Generally, the main aim of correlations of mean drop diameter from a single nozzle was to extend accumulated data to the practical ease of a swarm of drops encountered in commercial equipment. These correlations, however, relied upon the basic assumption that drop swarms from a perforated plate are produced in the idealised manner from a single nozzle. The above results indicate that this assumption is invalid.

The velocities in the jetting region were also compared with those predicted by the single nozzle correlations of other workers (30, 36, 105). The results are summarised in Table 8.3-2. The correlations of Scheele and Meister (105), De Chazel and Ryan (30) and Fujinawa (36) agreed fairly well for the 0.1588 cm hole size plate with percentage deviations of 21.64, 23.24 and 21.77 respectively. For the 0.3175 cm, 0.4763 cm and 0.6350 cm hole sizes plates the correlations of these authors differ appreciably compared to the experimental data. However, the correlation of Scheele and Meister still proved the best. The wide deviation between these single nozzle correlations and the experimental data may be explained from the two mechanisms on which the prediction of the jetting velocity are based. The first mechanism considers that a jet will form if there is sufficient upward force at the nozzle exit to form the jet. If a drop is not large enough to detach from the nozzle, the kinetic force of the liquid leaving the nozzle can either enlarge the drop or raise

TABLE 8.3-1

Comparison of drop diameter in jetting region as predicted by different models in terms of the average percentage deviation

Plate hole size cm		Chrisfensen and Hixson (21)	Perrut and Loutaty (122)	Kumar and Hartland (92)	Present Work
0.1588	Mean drop size (cm)	0.277	0.319	0.465	0.407
	Percentage Deviation	-46.93	-27.59	12.47	
0.3175	Mean drop size (cm)	0.510	0.581	0.867	0.461
	Percentage Deviation	9.61	20.65	32.90	
0.4763	Mean drop size (cm)	0.526	0.729	0.857	0.542
	Percentage Deviation	-3.04	25.65	36.76	
0.6350	Mean drop size (cm)	0.535	0.706	0.831	0.649
	Percentage deviation	-21.31	8.07	21.90	
Average Percentage Deviation		-15.42	6.70	26.01	

TABLE 8.3-2

Comparison of velocity in jetting region as predicted by different models in terms of the average percentage deviation

Plate hole size cm		Scheele and Meister (105)	De Chazel and Ryan (30)	Fujinawa et al (36)	Present Work
0.1588	Jetting velocity ($cm\,sec^{-1}$)	22.51	22.98	22.55	17.64
	Percentage Deviation	21.64	23.24	21.77	
0.3175	Jetting velocity ($cm\,sec^{-1}$)	11.55	14.24	15.95	6.80
	Percentage Deviation	41.13	52.25	57.37	
0.4763	Jetting velocity ($cm\,sec^{-1}$)	5.88	9.11	13.02	4.08
	Percentage Deviation	30.61	55.21	68.66	
0.6350	Jetting velocity ($cm\,sec^{-1}$)	2.15	7.74	11.28	3.32
	Percentage Deviation	-54.42	57.11	70.57	
Average Percentage Deviation		9.74	47.0	54.60	

the drop up on a cylinder of liquid, thus forming a jet. It is postulated that if sufficient upward force exists to form a jet, this will occur in preference to further enlargement of the drop. This second mechanism considers that a jet will form when the initial rise velocity of a drop is sufficiently low that the drop will rise less than one drop diameter during the time of formation of the next drop. The drops will then merge to form a continuous jet. The first mechanism depends on

(1) projection of the multi-nozzles above the sieve plate, and

(2) pressure gradient across the plate.

The second mechanism, depends mostly on the system physical properties e.g. viscosity. Scheele and Meister (163) observed that a high viscosity paraffin oil dispersed in water exhibited earlier jetting than predicted. When a drop broke away from the nozzle the material was so cohesive that it tended to draw a jet of fluid out of the nozzle.

8.3-4 (2) DROP SIZE DISTRIBUTION - PLATES

Tables 8.2-6 and 8.2-7 show a comparison between the distribution parameters for the various plates. As expected, there was a considerable increase in d_{32} with increasing plate hole size, because a greater proportion of large drops were produced. However, because

(i) most large drops formed due to mal-distribution of the dispersed phase across the plate resulting in a significant number of holes, e.g. upto 25% being starved particularly at low throughputs of dispersed phase, and

(ii) large drops may obscure a number of smaller drop during the counting and consequently lead to considerable experimental error, particularly when both drop diameter d and Δn varied by a large factor, the reliability of drop counting was considered of paramount importance. Therefore, drop counts were made from two or three replicate photographs for most of the runs.

Figures 8.2-19 to 8.2-22 show comparisons of distribution functions with the experimental data. These plots show that the Upper-Limit of Mugele and Evans gave the proper trend in most cases, as well as a good quantitative fit. Alternatively, the log-normal gave a

good fit for the experimental data for plates of hole size 1.588 mm and 3.175 mm diameter but did so poorly for plates of hole size 4.763 mm and 6.350 mm.

When at a certain plane or section in the perforated plate column, there was little variation in the drop size, a number of different functions (including the normal) would describe the size distribution equally well. This situation occurred when the dispersed phase superficial velocity was low ($0<U_D<10$ cmsec^{-1}) for plate hole size 1.588 mm diameter. As the population aged and size change occurred, mainly through drop break-up, the distribution became skewed towards an excessive number of drops bigger than the arithemtic average.

The log-normal and the Upper-Limit of Mugele-Evans distribution described the experimental data equally well and for most practical purposes both are equally suitable. However, the Upper-Limit distribution is preferrable because of the satisfying way its observed parameter varied with population age and plates hole size.

8.3-5 DISTRIBUTOR BEHAVIOUR

Comparison of the distributor behaviour with that predic ted from single nozzle correlations show that the predicted mean drop volume of Izard(75) was in good agreement with the experimental result at low dispersed phase superficial velocity, $U_D < 3.0$ cmsec^{-1}, but deviated consistently with increase in dispersed phase flow rate, giving an average percentage deviation of 34.9. The mean drop volumes predicted by Scheele and Meister(105) and Kagan et al (81) showed an upward trend with dispersed phase flow rate with an appreciable deviation as it was increased, $U_D > 2.86$ cmsec^{-1}. These authors' correlations gave a much higher average percentage deviation (48.04% and 63.49% respectively) compared to that of Izard and to the experimental results. These deviations could be due to the way in which single nozzles are designed, i.e. fairly high with a sharp pointed outlet. Unlike single nozzles, perforated plate nozzles tend to be drilled and punched holes, i.e. short projected nozzles, which require a much lower pressure head to overcome the drag force effect induced by the heavy continuous phase, compared to the single nozzle. Multi-nozzles are also arranged on a triangular/rectangular pitch with a short distance between one nozzle and another, generally 12.71 to 19.05 mm apart. In this work this often resulted in adjacent jets coming into contact at

high jetting velocity, thus producing droplets greater than average diameter.

However, as discussed in 8.2-5 the unequal sharing of dispersed phase was a major problem resulting in premature jetting of liquid in the distributor. This was due to the change in pressure drop across the distributor plate i.e. the pressure head increased with distance away from the central dispersed phase inlet to the distributor ($\Delta P_{\text{liquid discharge through nearest holes}} < \Delta P_{\text{to nearest row of holes}}$). To account for this a correction was made in order to obtain the actual superficial velocities of the dispersed phase.

This phenomenon must be a feature of a commercial column and measures to overcome it are discussed in 10.2.

CHAPTER 9

MASS TRANSFER RESULTS AND DISCUSSION

9. MASS TRANSFER RESULTS AND DISCUSSION

9.1 PHASE EQUILIBRIA

The apparatus used to determine phase equilibria consisted of a glass vessel of 150 ml capacity surrounded by a glass jacket through which water was circulated to maintain the contents of the vessel constant at any desired temperature. The vessel was provided with an agitator, whose speed could be controlled, and a side arm near the top as in Figure 9.1-1 for charging the liquid components. The bottom of the vessel was provided with a screw type, PTFE stop cock for emptying the contents on completion of an experiment, or for discharging the heavy phase for sampling following an equilibration experiment. The water jacket was connected to a Tecam C-400 thermostatic system containing a circulating pump and temperature controller capable of maintaining the temperature at any desired level up to 85^{o}C. Experiments were in fact conducted at 20^{o}C±0.5^{o}C.

The water rich phase data were obtained by charging a homogeneous mixture of two components (de-ionised water and acetone) of known composition to the vessel. The mixture was continuously stirred at a speed of approximately 120 rpm to ensure uniform temperature conditions. The third component (Clairsol) was added using an auto-pipette until 'cloudiness' appeared and persisted and homogeniety prevailed when viewed against a beam of light arranged

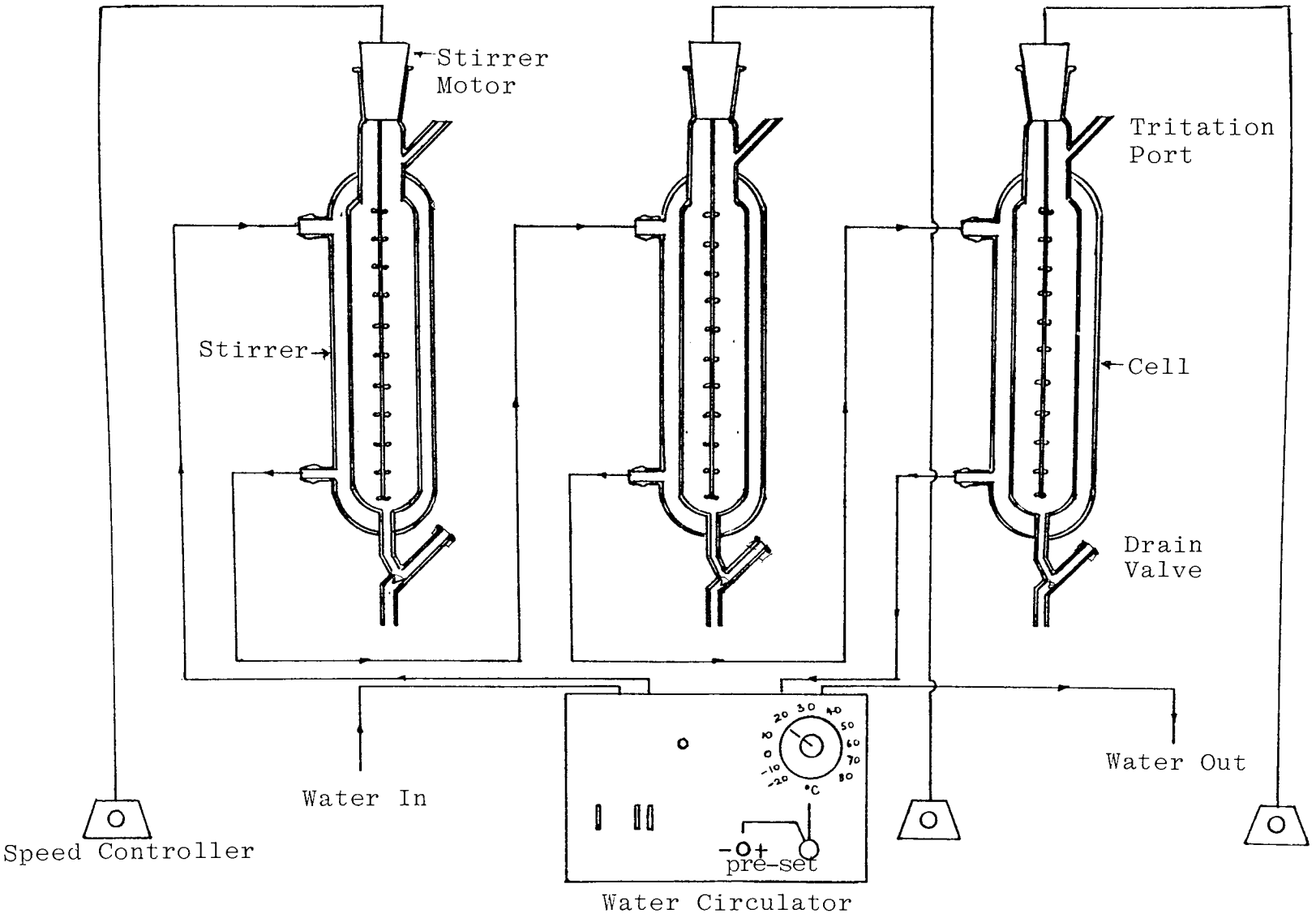

Fig. 9.1-1 Arrangement of Smith-Bonner Equilibrium Cells

at the rear. This identified the cloud point at which Clairsol saturated the ternary mixture i.e. the three components (Clairsol-acetone-water) were in equilibrium. This represents one point on the ternary solubility curve A sample of this mixture was analysed using a calibrated Abbey '60' refractometer; the cell was maintained at 20±0.5^{o}C by recirculation of water from the same thermostatic system as for the glass vessel. After an experiment was completed the vessel was emptied, rinsed several times with water and then with acetone and finally dried under vacuum. Each experiment was carried out three times to ensure reliability, and any result which deviated above or below 5% was discarded and the mean of the results taken. The experiment was repeated by varying the component composition to obtain more data points.

The Clairsol-rich phase data were obtained in a similar manner with Clairsol and acetone as the homogeneous mixture in the vessel and water as the addendum.

TIE LINE :

A heterogeneous ternary mixture of Clairsol 350-acetone-water was made directly in the vessel and stirred continuously for two hours to bring the layers to equilibrium. The mixture was then allowed to settle into two distinct clear layers with a sharp interface.

TABLE 9-1-1

WATER RICH PHASE

Volume (ml)			Weight (gm)			Percentage by Weight		
Water	Acetone	Clairsol	Water	Acetone	Clairsol	Water	Acetone	Clairsol
20	19.50	0.25	19.96	15.41	0.196	56.13	43.32	0.55
20	23.50	0.40	19.96	18.57	0.313	51.40	47.80	0.80
20	45.00	1.20	19.96	35.55	0.939	35.36	62.97	1.67
25	24.00	0.50	24.96	18.96	0.391	56.32	42.79	0.09
25	20.50	0.30	24.96	16.20	0.235	60.30	39.13	0.57
25	28.00	0.70	24.96	22.12	0.548	52.40	46.45	1.15
25	31.00	0.90	24.96	24.49	0.704	49.76	48.84	1.40
30	18.00	0.15	29.95	14.22	0.117	67.62	32.11	0.27
35	12.50	0.10	34.94	9.88	0.078	77.83	22.00	0.17
10	35.00	1.50	9.98	27.65	1.174	25.72	71.25	3.03
10	48.00	2.50	9.982	37.92	1.956	20.02	76.06	3.92

TABLE 9.1-2

CLAIRSOL RICH PHASE

Volume (ml)			Weight (gm)			Percentage by Weight		
Clairsol	Acetone	Water	Clairsol	Acetone	Water	Clairsol	Acetone	Water
10	37.00	1.20	7.82	29.23	1.198	20.45	76.41	3.14
15	35.50	0.70	11.74	28.05	0.699	28.99	69.28	1.73
15	40.00	0.90	11.74	31.60	0.898	26.53	71.44	2.03
20	12.40	0.10	15.65	9.80	0.100	61.26	38.35	0.39
20	31.00	0.45	15.65	24.49	0.449	38.55	60.34	1.11
20	36.50	0.60	15.65	28.84	0.599	34.71	63.96	1.33
25	33.50	0.30	19.56	26.47	0.300	42.22	57.13	0.65
30	16.50	0.15	23.47	13.04	0.150	64.03	35.56	0.41
40	32.00	0.26	31.30	25.28	0.260	55.06	44.48	0.46
10	54.00	2.00	7.82	42.66	2.00	14.91	81.28	3.81
25	9.50	0.05	19.56	7.51	0.05	72.14	27.68	0.18
5	37.00	2.00	3.912	29.23	2.00	11.13	83.18	5.69
2	47.50	7.00	1.57	37.53	6.99	3.41	81.43	15.16

TABLE 9.1-3 Tie-Line Data

Volume (ml)			Percent by Weight	
Clairsol	Acetone	Water	Clairsol Phase	Water Phase
20	3.5	25	1.50	10.99
15	10	25	2.50	22.97
10	15	25	3.50	30.66
10	20	20	5.00	41.82
10	28	10	8.50	68.60
7	32	7	12.50	78.20

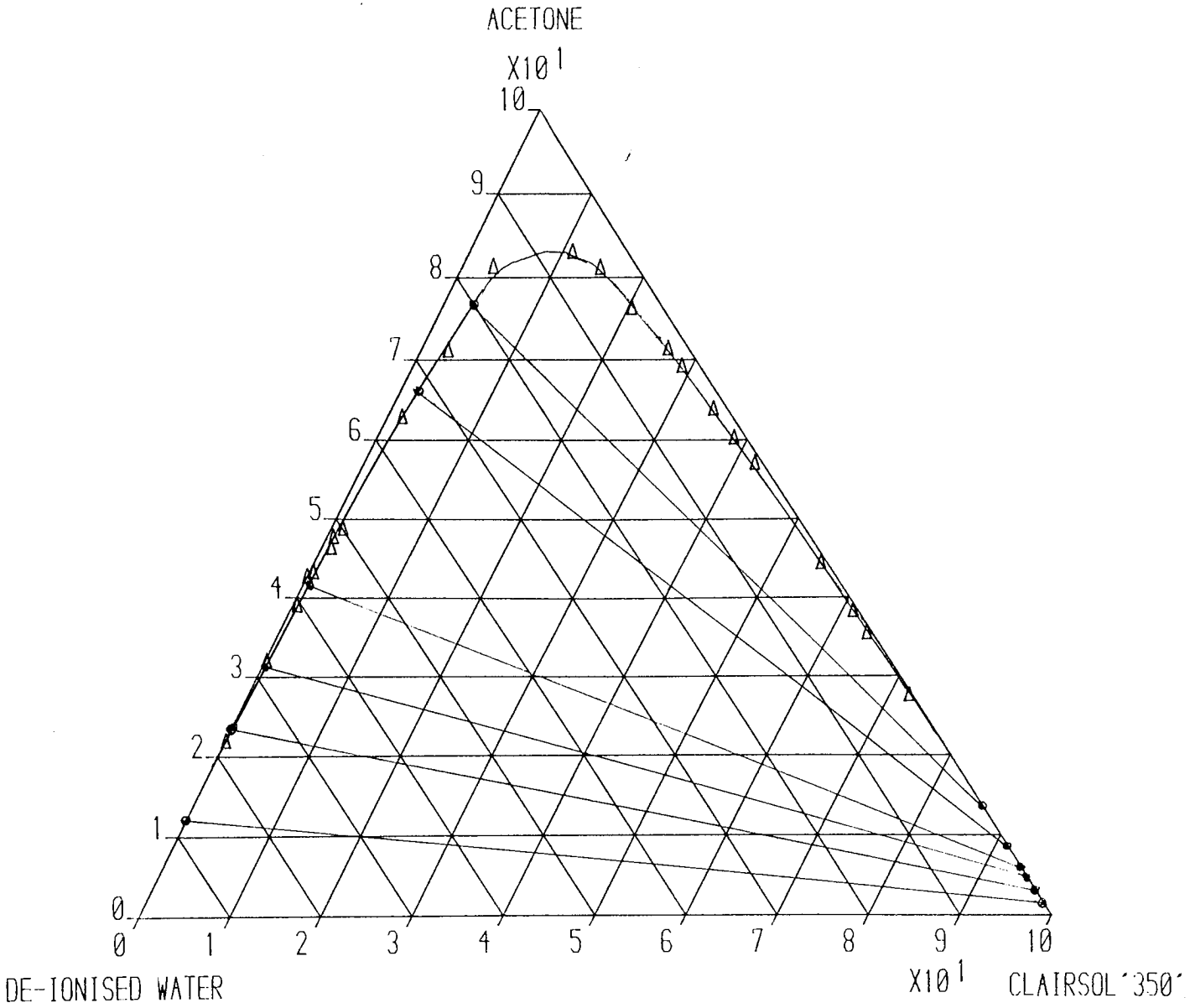

FIG.9.1-2. SOLUBILITY PLOT FOR CLAIRSOL-ACETONE-WATER SYSTEM

The settling time increased as the plait point was approached. The top Clairsol layer was taken for analysis with a pipette, care being taken to prevent the tip from touching the walls of the interface. The water layer was taken for analysis by opening the stop cock and letting the liquid run directly into the sample bottle. Because of the time required to attain phase equilibria and sufficient tie line data, it was more convenient to operate three vessels simultaneously. Each experiment was carried out two times and mean results taken.

The experimental data at 20°C are presented in Tables 9.1-1 and 9.1-2. The ternary solubility curve plotted on triangular graph paper is shown in Figure 9.1-2. For each tie line equilibria determination the concentration of acetone in each phase was plotted on the solubility curve. Each pair of points were joined by straight lines. Each straight line passed through the point within the unstable two phase region beneath the binoidal solubility curve corresponding to the composition of the heterogeneous mixture charged into the cell. The results show that the three points obtained for each component fall into a very good straight line; thus confirming the reproducibility of the experimental techniques.

9.2 MASS TRANSFER EXPERIMENTAL PROCEDURE

Mass transfer investigations were performed using only the two sets of plates with hole sizes at the ends of the range, i.e. 0.6350 cm and 0.1588 cm respectively. This enabled the range to be covered economically.

Initial experiments were made with mass transfer of acetone from the dispersed Clairsol 350 to the continuous water phase. In later experiments, transfer was in the reverse direction.

Prior to each experiment, the Clairsol in the reservoir was mutually saturated with de-ionised water; the water in the reservoir was also pre-saturated with Clairsol. This was to ensure that only transfer of solute, i.e. acetone, was investigated under reproducible conditions. The dispersed phase, i.e. the solvent solution having the desired solute concentration, was thoroughly mixed by means of the recycle system (interchangeable between the inlet and the outlet solvent tanks) incorporated into the equipment. The desired solute concentration was achieved by adding acetone to the Clairsol in the reservoir and consistent analysis of the Clairsol-acetone solution.

Water was fed to the top of the column and solvent

solution to the bottom distributor via their respective rotameters. The principal interface was adjusted and maintained steady at 18.0 cm below the top cover plate by regulating the control valves in both the solvent and water exit lines, and the flows were set and held at the desired rates. The height of the effective extraction section was measured from the bottom end of the column to the principal interface in the top disengaging section (The error due to inclusion of the final flocculation zone was considered negligible).

Samples of the inlet and outlet streams, and samples from the different compartments were taken at two, 15 minute intervals after sufficient time had elapsed for 2 to 3 complete changes of continuous phase to take place. The analyses were carried out using a calibrated Abbey '60' refractometer.

All runs were performed at ambient temperature which varied from 20°C to 18°C in the course of the experimental work. Therefore, since the temperature of both liquids did not vary by more than ±2°C, its effect on the equilibrium curve of the system studied was neglected. The range of the superficial velocities investigated was from 2.0 $cmsec^{-1}$ to 30.0 $cmsec^{-1}$ (based on plate hole size) for the dispersed phase and 0.2 $cmsec^{-1}$ to 0.51 $cmsec^{-1}$ (based on column cross-section) for the continuous phase.

9.3 ANALYSIS OF MASS TRANSFER DATA

The column performance is expressed in terms of overall height of transfer unit (HTU). In the present work (i) the two phases were essentially immiscible (ii) dilute solutions were used and (iii) the simple distribution law is approximately followed for the system over the concentration range involved. Therefore the following simplified equations, based on those discussed in sections 4.1-1, 4.2-1 and 4.3-1 earlier, were used for calculating the results

$$Ka = \frac{N}{V(\Delta C_m)} \qquad 9.3\text{-}1$$

$$HTU = \frac{Q}{Ka} \qquad 9.3\text{-}2$$

where Ka is the overall extraction coefficient in gm/sec cm^3 (ΔC_m)

N is the gm of solute transferred per sec.

ΔC_m is the mean concentration driving force gm/cm^3

V is the volume of the column, cm^3

Q is the flowrate of the phase offering maximum resistance.

The transfer coefficient (Ka) was analysed in terms of two limiting transfer mechanisms (i) transfer by molecular diffusion from stagnant drops (ii) transfer from circulating/ oscillating drops, with a Higbie type equation (or with a modified Higbie equation) for the

outside coefficient. This is the model proposed by Handlos and Baron (59) and later modified by other investigators (68, 69, 100).

The basis for this, and for determining which proportion were stagnant, oscillating or circulating was the calculation of the droplet Reynolds number for every U_D, U_C, d combination and comparison with the following transition values,

Stagnant drops	$Re < 10$
Circulating drops	$Re < 200$
Oscillating drops	$Re > 200$.

For the stagnant drop model k_{dSD} is obtainable from the Newman (117) relation,

$$k_{dSD} = 1 - \frac{6}{\pi^2} \sum_{n=1}^{\infty} \frac{1}{n^2} \exp\left(\frac{-4\mathscr{D}_d \pi^2 n^2 t}{d^2}\right) \qquad 9.3\text{-}3$$

$$= \left[1 - \exp\left(\frac{-4\mathscr{D}_d \pi^2 t}{d^2}\right)\right]^{0.5} \qquad 9.3\text{-}4$$

where k_{dSD} is the dispersed phase mass transfer coefficient for stagnant drops.

$$t = \frac{h_E X}{U_D} = \text{drop contact time, sec.}$$

Equation (9.3-3) is only approximate when a continuous phase resistance is present; various workers (152) have pointed out its limitations. Equation 9.3-4 is an empirical approximation (157). However, since most of the drops involved in this work were in the circulating and oscillating regions, and only a very small percentage, i.e. 1.0% of stagnant drops were involved; equation 9.3-4 was neglected.

CIRCULATING DROPS

(i) The model proposed by Handlos and Baron (59) was used to estimate dispersed and continuous phase mass transfer coefficients respectively.

$$k_{dCD} = \frac{0.00375U_s}{1 + \mu_D/\mu_C} + k_{dSD} \qquad 9.3\text{-}5$$

for the case of no continuous phase resistance, equation (9.3-5) becomes

$$k_{dCD} = \frac{0.00375U_s}{1 + \mu_D/\mu_C} \qquad 9.3\text{-}6$$

$$k_{CCD} = \left(\frac{4\mathscr{D}_c U_s}{\pi d}\right)^{0.5} \qquad 9.3\text{-}7$$

where $\mathscr{D}_d$ and $\mathscr{D}_c$ are the solute diffusivities in the drop phase and in the continuous phase, estimated via the Wilke and Chang (162) correlation, k_{dCD} and k_{CCD} are the dispersed and continuous phase mass transfer coefficients for circulating drops, μ_D and μ_C are the dispersed and continuous phase viscosities and the characteristic drop slip velocity U_s is defined by

$$U_s = \frac{U_D}{X} + \frac{U_C}{1-X} \qquad 9.3\text{-}8$$

where X = volume fraction hold-up of dispersed phase

(ii) Dispersed phase mass transfer coefficient was also estimated using the Kronig and Brink (91)

correlation

$$k_{dCD} = 1 - \frac{3}{8} \sum_{n=1}^{\infty} A_n^2 \exp\left(1 - \frac{\psi_n 64 \mathcal{D}_d t}{d^2}\right) \qquad 9.3\text{-}9$$

$$= \left\{1 - \exp\left[\frac{-2.25(4)\mathcal{D}_d \pi^2 t}{d^2}\right]\right\}^{0.5} \qquad 9.3\text{-}10$$

or

$$k_{dCD} = \frac{17.9\mathcal{D}_d}{d} \qquad 9.3\text{-}11$$

where A_n and ψ_n are eigenvalue.

The second half of equation (9.3-10) is an empirical approximation (16). Continuous phase mass transfer coefficient was estimated by Garner et al (40) correlations

$$Sh = -126 + 1.8\ Re^{0.5}\ Sc^{0.42} \qquad 9.3\text{-}12a$$

The overall mass transfer coefficient in an extraction process is related to the continuous phase mass transfer coefficient and the dispersed phase mass transfer coefficient by the relation given in equations 9.3-12a or 9.3-7. Therefore for circulating drops

$$\frac{1}{K_{OCD}} = \frac{1}{k_{dCD}} + \frac{m}{k_{CCD}} \qquad 9.3\text{-}12$$

OSCILLATING DROPS

Dispersed phase mass transfer coefficient was estimated firstly using the correlation of Rose and Kintner (129) who expressed ω in terms of the drop size and the physical property of the system by

$$k_{dOD} = 0.45\ (\mathcal{D}_d\omega)^{0.5} \qquad 9.3\text{-}13$$

$$\text{where } \omega^2 = \frac{\sigma b}{r^3}\left[\frac{n(n-1)(n+1)(n+2)}{(n+1)\rho_d + n\rho_c}\right] \qquad 9.3\text{-}14$$

r = drop radius, cm

n = an interger = 2.0

b = constant depending on drop size; $b = 1.052 d_o^{0.225}$

d_o = drop size, cm

k_{dOD} = dispersed phase mass transfer coefficient for oscillating drop.

Secondly the Angelo et al (4) correlation was used

$$k_{dOD} = \left[\frac{4\mathcal{D}_d\omega}{\pi}(1+\delta+0.375\delta^2)\right]^{0.5} \qquad 9.3\text{-}15$$

$$\text{where } \delta = 0.434\left(\frac{\omega d_o}{U_s}\right)^{-0.46}\left(\frac{d_o U^2 \rho_c}{\sigma}\right)^{-0.53}\left(\frac{\mu_c U_s}{\sigma}\right)^{-0.11} \qquad 9.3\text{-}16$$

Continuous phase mass transfer coefficient was estimated by Garner et al (40) correlation

$$\frac{k_{dOD} d_o}{\mathcal{D}_c} = 50 + 0.0085\ Re Sc^{0.7} \qquad 9.3\text{-}17$$

The overall mass transfer coefficient of oscillating drops was estimated by the following correlations

(i) Rose and Kintner (129) and Garner et al (40)

$$\frac{1}{K_{O.OD}} = \frac{1}{k_{d.OD}} + \frac{m}{k_{c.OD}} \qquad 9.3\text{-}18$$

(ii) Angelo et al (4)

$$\frac{1}{K_{O.OD}} = k_{d.OD}\left[\frac{1}{1+m\left(\frac{\phi_d}{\phi_c}\right)^{0.5}}\right] \qquad 9.3\text{-}19$$

where m = slope of the equilibrium curve.

The mean driving force Δy_m was estimated by applying Simpson's rule based on y_{top}, y_{bottom} and on the equilibrium concentration in the water phase, corresponding to the observed concentration in the Clairsol phase.

$$\Delta y_m = \frac{1}{12}\left[y_{top} + y_{bottom} + 4(y_1+y_3) + 2y_3\right] \qquad 9.3\text{-}20$$

The rate of extraction was estimated from the rate of flow of the dispersed phase and from the change in the concentration of water or the dispersed phase. Elgin and Browning (31) took the mean of the two estimated values as the rate of extraction while Allerton et al (3) took that value for the rate of extraction in which the percentage change of concentration in two liquids was larger. The rate of extraction in the present work was taken as the mean of the two estimated values and readings which agreed within 10% of the two estimated values were taken.

A specimen calculation for one set of data is given in Appendix 22.

9.4 MASS TRANSFER RESULTS

A summary of the experimental results is presented in Tables 9.4-1 and 9.4-2. The mass transfer coefficients were calculated by applying Simpson's rule to determine the actual mean concentration driving force ($\Delta C_M'$) using the acetone concentration profile along the column. Acetone concentration was measured in samples of the continuous phase taken from compartments 1, 2, 3 and 4. The calculation of mass transfer coefficients based on the single drop mass transfer correlations of other workers (4, 40, 43, 91) involved the novel use of the drop size distribution diagram to determine the volume percentage of the stagnant, circulating and oscillating drops in the drop sample population. Compartment No. 3 was taken as the representative compartment for the whole column. A specimen calculation is given in Appendix 22.

The solute concentration range was 0.5 - 8.0% in order to avoid the formation of an emulsion which could occur at higher acetone concentrations because of lowering of the interfacial tension (In a trial experiment at 15% acetone concentration in the dispersed phase small droplets were produced between plates and the continuous phase become cloudy due to secondary haze formation.)

The dispersed phase and continuous phase superficial velocities were varied from $0.20 > U_D'' < 0.54$ cmsec^{-1} and

$0.20 > U''_C < 0.44$ cmsec^{-1} respectively, the upper limits of which were well within the flooding rates.

Figures 9.4-1 and 9.4-2 show plots of $K_{O.D}.a$ values against U''_D at constant U''_C values. At a particular continuous phase superficial velocity, the values of $K_{O.D}.a$ increased markedly with increase in the dispersed phase superficial velocity. This was due to an increase in the number of drops, resulting in increased interfacial area of contact and also due to vigorous turbulence in the column. From the data presented in Tables 9.4-1 and 9.4-2, it is evident that at a particular dispersed phase superficial velocity the values of $K_{O.D}.a$ are almost constant, with minor variations, independent of the continuous phase superficial velocity. This arose because the number of drops in a compartment did not increase significantly with increase in the continuous phase superficial velocity. (However, there was increased back-mixing of the droplets.) Hence there was little increase in the contact area and consequently in the value of $K_{O.D}.a$. The effect of varying flow rates on $K_{O.D}.a$ has been studied by some earlier workers (3, 50, 126) and their observations have been similar (see Section 5.2).

The effect of plate hole size on mass transfer coefficients was compared from the data of Tables 9.4-1 and 9.4-2. At any value of U''_D with increase in hole size the number of drops formed at the plate decreases at any

TABLE 9.4-1

Results of Mass Transfer Experiments - Plate Hole Size = 0.6350 cm

Run No.	Direction of Transfer	U'_C cmsec^{-1}	U'_D cmsec^{-1}	Acetone Concentrations gm acetone/100gm aqueous solution				$K_{O,D}a$ x 10^{-5} gm / sec cm^3 ΔC_m	Hold-up %
				Water in	Water out	Clairsol in	Clairsol out		
1	D→C	0.28	0.22	0.00	0.67	2.50	1.60	6.20	1.20
2		0.35	0.30	0.00	1.07	3.80	2.50	7.80	1.33
3		0.44	0.37	0.90	1.67	4.38	2.08	9.03	1.30
4		0.21	0.23	0.90	2.13	4.34	3.81	5.91	1.01
5		0.28	0.33	1.65	3.00	4.47	2.60	7.94	1.34
6		0.32	0.37	1.65	3.40	4.90	2.71	9.80	1.30
7		0.21	0.37	1.82	3.51	4.52	2.67	9.72	1.10
9		0.28	0.40	1.82	3.56	4.67	2.73	10.25	2.35
11		0.28	0.48	2.83	4.07	4.86	3.05	10.91	2.46
13		0.51	0.45	2.67	3.88	4.60	2.85	10.60	2.39
14	C→D	0.28	0.22	1.00	0.68	0.00	0.20	3.27	1.29
15		0.35	0.30	2.30	1.33	0.17	0.31	4.14	1.34
16		0.44	0.37	2.73	2.34	0.33	0.43	4.21	1.38
18		0.21	0.23	3.29	2.78	0.41	0.26	3.07	1.05
19		0.28	0.33	3.73	3.30	0.67	0.49	4.32	1.39
20		0.32	0.37	4.43	4.09	0.89	0.88	5.04	1.37

TABLE 9.4-2

Results of Mass Transfer Experiments - Plate Hole Size = 0.1588 cm

Run No.	Direction of Transfer	U'_C $cm\,sec^{-1}$	U'_D $cm\,sec^{-1}$	Acetone Concentrations gm acetone/100 gm aqueous solution				$K_{O.D}a$ $\times 10^{-5}$ gm / sec $cm^3 \Delta C_m$	Hold-up %
				Water in	Water out	Clairsol in	Clairsol out		
21	D→C	0.28	0.22	0.00	1.00	2.30	1.02	12.0	6.41
22		0.35	0.30	0.00	1.24	3.23	1.65	11.30	7.79
23		0.44	0.37	0.98	2.08	3.44	1.90	12.40	9.35
24		0.21	0.23	0.98	2.73	3.50	1.70	11.38	6.41
25		0.28	0.33	1.93	3.60	3.48	1.95	13.10	7.91
26		0.32	0.37	1.93	3.65	5.33	3.38	12.10	7.80
28		0.21	0.37	2.27	3.59	5.17	3.41	13.51	8.74
29		0.28	0.40	2.27	3.68	5.24	3.53	13.97	11.25
30		0.28	0.48	3.08	4.61	5.89	4.19	15.41	12.07
32		0.51	0.45	3.05	3.98	4.80	3.53	11.25	11.65
33	C→D	0.28	0.22	1.01	0.67	0.00	0.25	5.90	6.49
34		0.35	0.30	1.70	1.13	0.23	0.34	4.37	7.83
35		0.44	0.37	2.43	2.00	0.31	0.39	6.35	9.41
37		0.21	0.23	3.00	2.35	0.51	0.29	3.84	6.47
38		0.28	0.33	3.67	3.02	0.79	0.58	6.20	7.96
39		0.32	0.37	4.23	3.67	0.86	1.07	4.78	7.85

TABLE 9.4-3

Comparison of Experimental Mass Transfer Coefficients with Correlations

Run No.	Direction of Transfer	Rose-Kintner and Garner et al $K_{O.D} \cdot ax10^{-4}$	Angelo et al $K_{O.D} \cdot ax10^{-4}$	Experimental $K_{O.D} \cdot ax10^{-5}$	Run No.	Direction of Transfer	Rose-Kintner and Garner et al $K_{O.D} \cdot ax10^{-4}$	Angelo et al $K_{O.D} \cdot ax10^{-4}$	Experimental $K_{O.D} \cdot ax10^{-5}$
1	D→C	2.17	3.30	6.20	21	D→C	5.74	24.40	12.0
2		2.96	3.96	7.80	22		4.28	4.97	11.30
3		4.10	4.39	9.03	23		5.93	25.10	12.40
4		1.76	2.84	5.91	24		3.14	3.34	10.10
5		3.37	3.74	7.94	25		6.26	27.10	13.10
6		4.27	5.31	9.80	26		5.87	23.50	12.10
7		4.03	4.87	9.72	28		5.90	24.10	13.97
9		3.91	4.46	10.25	29		5.64	23.92	13.97
11		4.16	4.92	10.91	30		6.45	29.20	15.41
13		3.91	4.33	10.60	32		4.03	4.77	11.25
14	C→D	1.33	2.17	3.27	33	C→D	3.18	17.70	5.90
15		2.07	2.91	4.14	34		2.67	3.34	4.37
16		2.45	3.11	4.21	35		3.47	18.20	6.35
18		1.07	2.03	3.07	37		2.09	2.78	3.84
19		2.54	2.87	4.32	38		3.26	17.90	6.20
20		2.92	3.44	5.04	39		2.83	3.74	4.78

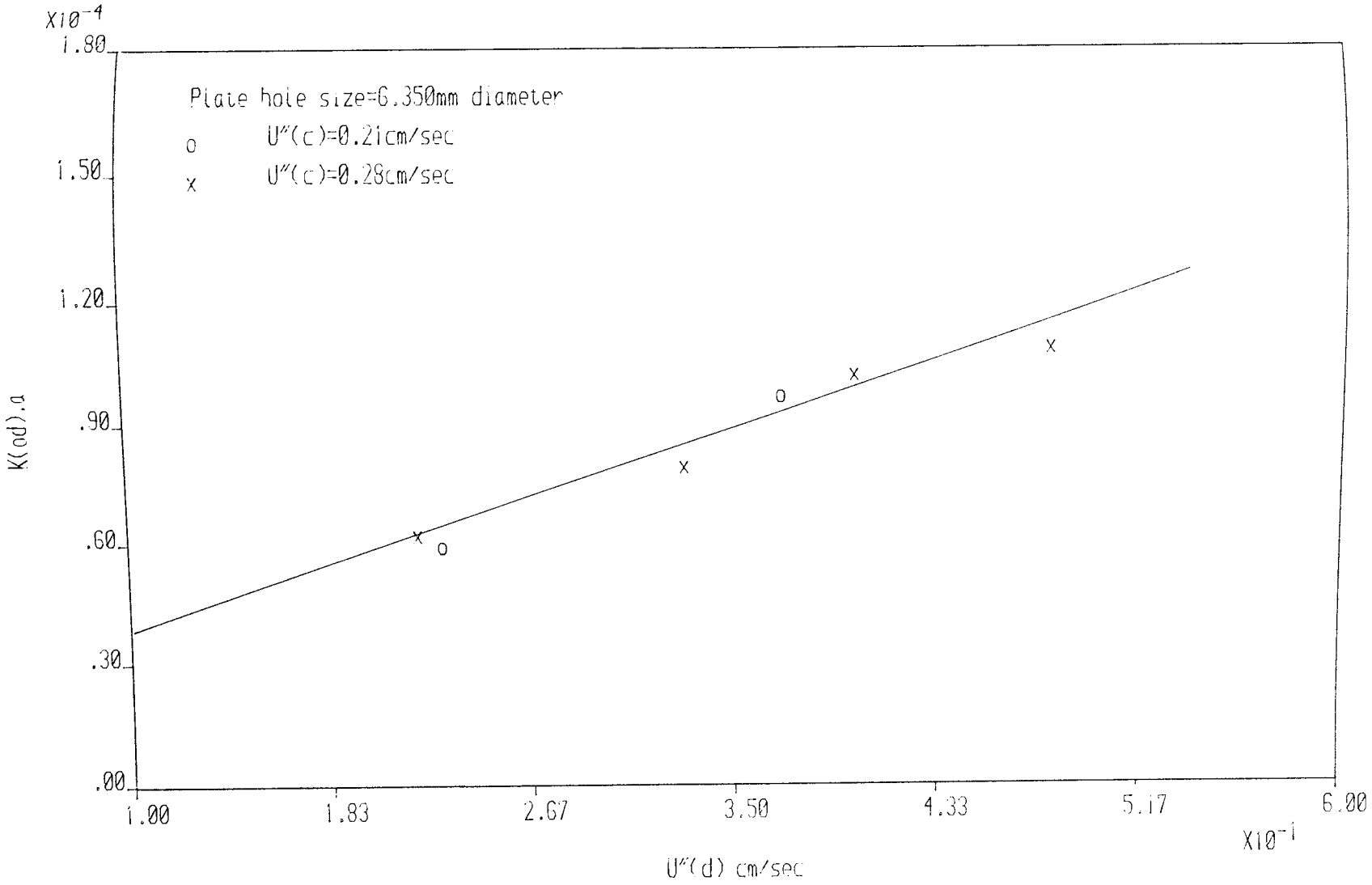

Fig.9.4-1 Plot of K(od).a Vs U"(d) at constant U"(c)

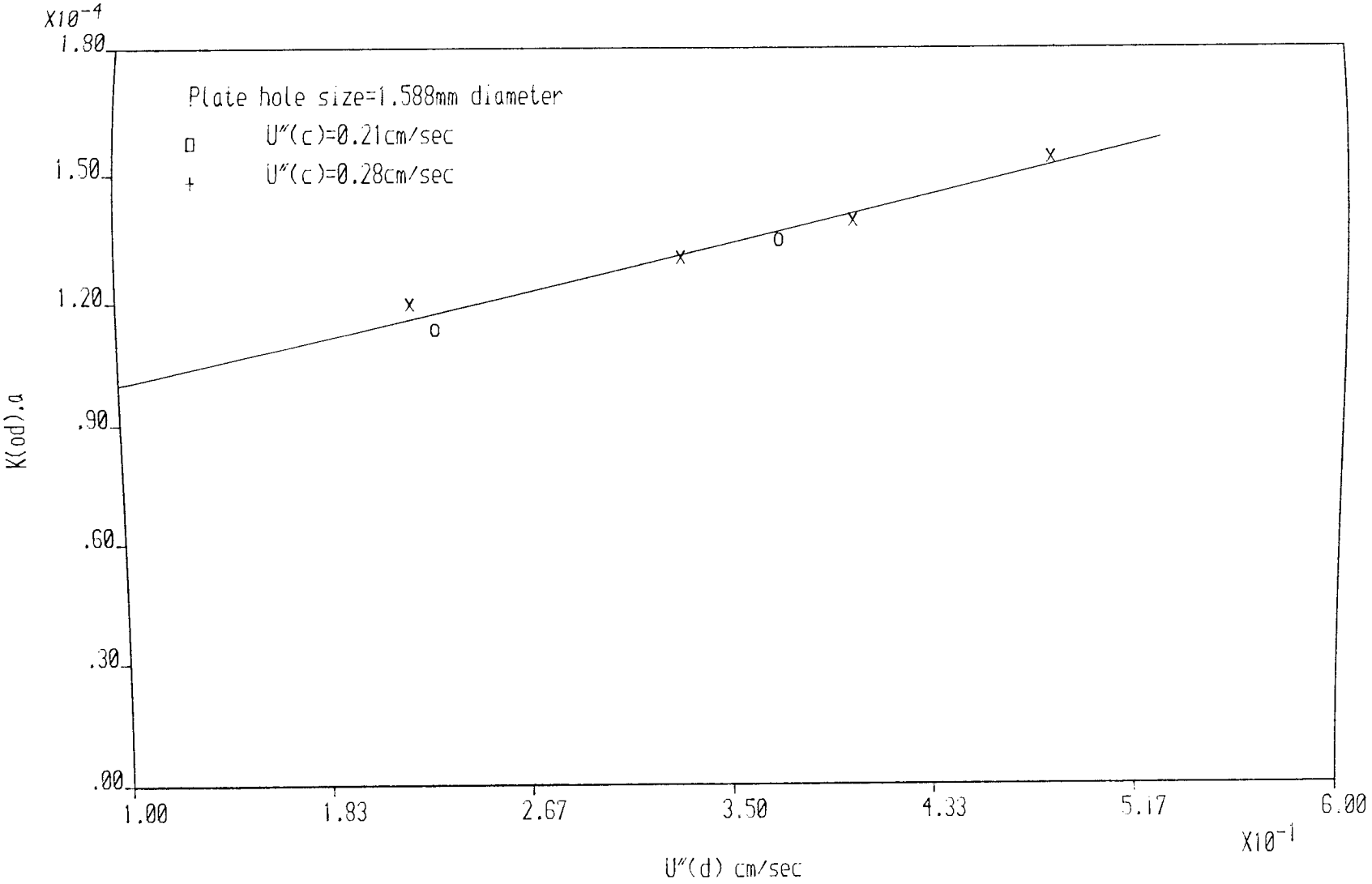

Fig.9.4-2 Plot of K(od).a Vs U″(d) at constant U″(c)

instant in the column, which resulted in decrease in the interfacial area of mass transfer and hence decreased values of mass transfer coefficients. The drops formed with 0.6350 cm diameter hole are bigger in size than those formed with 0.1588 cm diameter hole but any advantage gained from the bigger drops for mass transfer is more than offset by the formation of larger number of drops at the plate with 0.1588 cm diameter hole.

For the system Clairsol-acetone-water with Clairsol dispersed, the path taken by droplets rising from one plate to the next depended on the water rate. When the continuous phase superficial velocities U''_C were more than 0.40 $cmsec^{-1}$, however a considerable amount of dispersed phase was entrained in the high velocity stream of continuous phase in the downcomer (about 3-5% of the total), and circulated back to the plate through which it had just passed. This "downcomer recirculation" effect increases the overall extraction residence time of the dispersed phase in the column. No allowance for this effect was made when calculating $K_{O.D}.a$.

The change (i.e. increase or decrease) in the mass transfer coefficient $K_{O.D}.a$ with concentration for both directions of solute transfer may be connected with the interfacial tension which has a marked effect on the Reynolds number at which circulation begins within a droplet. Interfacial tension can be considered as one

aspect of surface forces which may give rise to more or less regular orientation of all molecules near the interface. Such orientation, and the resultant increased viscosity at the interface, may modify solute transfer from droplets in two ways firstly by directly obstructing the passage of solute molecules, and secondly by reducing the intensity of circulation within the drop because of interference with the movement of the interface.

Average hold-up was measured for each mass transfer run. Slightly higher hold-ups (i.e. 2% higher) were recorded when acetone was transferred from the continuous to the dispersed, and lower when acetone was transferred from dispersed phase to continuous phase (i.e. 2% lower) compared with the non-mass transfer results. This effect is normally attributed in extraction columns to the enhanced, or inhibited, coalescence effects related to the direction of transfer of a solute which tends to lower the interfacial tension. However, in this work there was little observable interdrop coalescence between release and the flocculation layer.

9.5 MASS TRANSFER DISCUSSION

The overall mass transfer coefficients calculated by Rose-Kintner and Garner et al correlations and Angelo et al correlations are compared with the experimental overall mass transfer coefficients $K_{O.D}.a$ in Table 9.4-3. The Rose-Kintner and Garner et al correlations gave a higher average factor of 4 and the correlations of Angelo et al gave an average factor of 5 compared with the experimental results for the 0.6350 cm plate hole size. These high factor values may be due to the following effects:

(1) the phase flow rates which are not properly allowed for in any of the correlations used in the calculations. The only implicit inclusion of flow rates are in equations 9.3-12a and 9.3-17 through the droplet Reynolds number i.e. $\rho_D U_S D/\mu_C$. The drop's characteristic velocity U_S is calculated by Thornton's correlation of equation 4.2-3 which relates the phase velocities with hold-up and the resulting figure gives no indication whatsoever of phase flow rates used.

(2) the axial mixing or longitudinal mixing between plates which are caused by

(a) coalescence and break-up of droplets,

(b) droplet velocity distribution across the column radius, and

(c) turbulent velocity fluctuations of the continuous phase which affect the pattern of movement of the dispersed phase droplets. These occur due to non-ideal flow in which random movement of fluid is super-imposed on the main flow. They tend to destroy the true counter-current flow pattern and also decrease the concentration driving force.

(3) the concentration driving force was evaluated by Simpson's rule as described in Section 9.3. . Simpson's rule has a great advantage over the log mean driving force in the sieve plate column for a very obvious reason, that is it allows for the shape of the operating line resulting from the flow pattern of the phases within the column not being plug flow.

(4) the fact that oscillations are super-imposed on the circulating droplets due to the existence of a swarm of drops in close proximity inducing adjacent drops to oscillate in highly turbulent regions within plates. On the other hand, the use of industrial grade solvent and the scale of operation may have an opposite effect on the circulating drops making them behave as stagnant drops with very low mass transfer coefficients.

For the 0.1588 cm hole size plate, Rose-Kintner and Garner et al correlations gave a greater average

factor of 6. In addition to the above mentioned effects, the high value of the coefficients predicted from the Rose-Kintner and Garner et al correlations may be due to the single drop theoretical assumptions on which these authors based their models, i.e. drops formed from single nozzle behave the same way as in big column; while that of Angelo et al was based on drop swarms but on a smaller scale column compared to the present work.

The effect of hole diameter, with constant hole area was previously studied by Pyle et al (126) and Nandi and Ghosh (50). Pyle et al used a partially miscible system whereas the systems used by Nandi and Ghosh were immiscible. Nandi and Ghosh found that when the hole size was changed from 0.16 to 0.32 cm with constant hole area, slightly higher mass transfer coefficients were obtained with smaller size perforations. Thus the results of the present work are in conformity with that of Nandi and Ghosh.

Tables 9.4-1 and 9.4-2 show a decrease in the experimental mass transfer coefficient $K_{O.D.}a$ when solute transfer was from C→D compared to transfer from D→C. These decreases in values of $K_{O.D.}a$ for transfer from C→D may be due to

(i) the large proportion of the circulating drops predicted by the drop distribution diagram actually

oscillating and persisting for larger time in the high turbulent regions between plates.

(ii) the hydrogen bond between acetone and water is probably considerably weaker (i.e. weaker Van der Waals forces) than that between Clairsol and water. This effect has been studied by Licht and Conway (164) and Garner et al (38). The work of Garner et al shows that, the transfer rate of diethylamine in alternate directions between toluene and water was several fold greater when it was from toluene to water than from water to toluene. Thus the experimental results are in conformity with that of Garner et al.

In all the theoretical overall mass transfer coefficients calculated, no stagnant drops were included because of the limitation of the photographic technique used in measuring the drop size and drop size distribution. However, they exist in the dispersion but their contribution to the overall mass transfer coefficient will be insignificant because the proportion will be very small compared to the whole drop population.

A problem inherent in the prediction of theoretical single drop mass transfer coefficients, and one possible explanation for the wide divergence with the experimental data for the drop swarms in this work, is the estimation of the velocity term in Reynolds number Re. In Appendices

6 to 9 the velocity was estimated from the Hu-Kintner plot and in Appendix 22 it was calculated as U_S. However, the majority of drops did not rise vertically but followed a circulatory path. Therefore, it is strictly the lesser resultant velocity which should be inserted in Re; this would have the effect of bringing more drops into the circulatory region from the oscillatory region and causing an increased, although small proportion, to be stagnant. The need to study flow patterns to allow for this is discussed in section 10.3.

CHAPTER 10

CONCLUSIONS AND RECOMMENDATIONS

10. CONCLUSIONS AND RECOMMENDATIONS

10.1 CONCLUSIONS

The following major conclusions arise from this study:

1. For drop formation from drilled holes, there is a jet distruption velocity above which the jet length decreases with increasing velocity and the drop formation process becomes erratic. In this work, the transition velocity was at $U_D'' = 0.54$ cmsec^{-1}.

Experimental data obtained for the liquid-liquid system studied show good agreement with the correlation given in Equation 8.2-1.

2. The dispersed phase hold-up was satisfactorily correlated, within ±7% by equation 8.2-2 for the range 0.1588 to 0.6350 cm plate hole sizes.

The critical hole size demarcating the two hydrodynamic regimes of sieve plate operation viz, the near constant characteristic velocity region (Region II) and the varying characteristic velocity (Region I) is dependent upon the column geometry as well as liquid physical properties, e.g. interfacial tension.

3. As would be expected the hold-up of the dispersed

phase beneath the perforated plates decreased with increase in the hole size but increased with increase in the superficial velocity of either phase.

4. The Sauter mean drop diameter obtained when Clairsol 350 was dispersed in a continuum of de-ionised water phase that preferentially wetted plates and under conditions of no mass transfer can be correlated by equations 8.2-5 and 8.2-6 within ±5%. A comparison of the experimental results and the correlations are shown in Figures 8.2-11 and 8.2-12.

5. The photographic analysis of the drop size distribution results show that the Sauter mean drop diameter (d_{32}) depends markedly on the plate hole size and the superficial velocity of either phase i.e. increasing D_N increases d_{32} in the range 0.316 to 0.650 cm.

Mugele-Evans Upper Limit distribution function accurately represents the experimental drop size distribution and should be used in preference to the log-normal distribution function.

MASS TRANSFER

1. The Ka obtained from the experimental results was 4 to 5 times less than predicted from single drop correlations using conventionally estimated velocities.

2. Interplate recirculation tended to destroy the true flow pattern between plates.

3. The effect of dispersed phase superficial velocities on mass transfer coefficient was approximately direct and linear. The effect of continuous phase superficial velocities on the mass transfer coefficients was direct but small, although not negligible. The values of Ka also decreased when mass transfer of acetone was from C→D compared with D→C; the magnitude of this affect was a 10 to 20% reduction when transfer was from C→D.

4. Increase in plate hole size caused a decrease in the values of mass transfer coefficient (Ka) under similar operating conditions (See Tables 9.4-1 and 9.4-2).

5. The use of concentration driving force along the column to calculate the mean concentration driving force viz. Simpson's Rule results in a more precise experimental overall mass transfer coefficients (Ka) compared to the traditional method often used.

6. The use of drop size distribution in the calculation of the theoretical mass transfer coefficients gave results, not very comparable with the experimental coefficients, but the method of calculation in Section 9.3 represents the first step in making calculation more rigorous. This method of calculation has the added advantage that the mean diameter and the surface area of the forming drop can be obtained readily.

All these conclusions tend to cast doubt on liquid-liquid extraction data obtained in small plate columns or extrapolated from single drop experiments. Therefore further work is recommended in 10.2.

In addition, a number of useful minor conclusions are summarised below

(a) Recirculation of droplets was quite pronounced within the stage.

(b) Channelling of drops was frequently very severe and drop velocities were always in excess of individual drop terminal velocities.

10.2 APPLICATION TO THE DESIGN AND OPERATION OF SIEVE PLATE COLUMNS

10.2-1 PLATE DESIGN AND SPACING

The velocity through the holes should be such that drops do not form slowly at the holes, but rather that the dispersed phase streams through the openings to be broken up into droplets at a slight distance from the plate. This generally requires average linear velocities through the holes of from $U_D' = 15.24$ to $30.48\ cmsec^{-1}$. Maldistribution of dispersed phase from the holes in a plate only becomes a problem at relatively low flow rates, i.e. $U_D'' < 0.25\ cmsec^{-1}$; these are unlikely to be used in industrial columns. However some improvement at the lowest rates could be achieved as described for the distributor in 10.2-3. The preferred hole size range is 0.1588 cm to 0.6350 cm and the preferred hole type is the drilled and punched.

The distance between trays should be larger than the coalescence and flocculation zone height h_{CF}, so that

(1) the dispersed liquid from the holes break-up into drops before coalescing into the layer of liquid beneath the next plate (i.e. there is enough time lag between drop break-up and coalescence).

(2) The linear velocity of the continuous liquid is not greater than that in the downcomer to avoid excessive entrainment. There is scope for reducing the conventional plate spacing to an optimum value based upon minimising the droplet recirculation patterns described in 9.5 to which reduced efficiency was attributed in 9.4.

The depth of the coalesced layer beneath each plate can be estimated from the correlation of equation 8.2-4. Subtraction of this depth from the specified height between plates gives the height of rise of the drops between consecutive plates.

10.2-2 DOWNCOMER DESIGN

Downcomers are best set flush with the plate from which they lead. The desirable velocity of the continuous phase in the downcomer U''_C, which determines the downcomer cross-section, should be set at a value lower than the terminal velocity of some arbitrarily small droplet of dispersed phase 0.08 or 0.16 cm diameter, otherwise recirculation of entrained dispersed phase around a plate will result in premature flooding. The downcomer should extend beyond the accumulated layer of dispersed phase on the plate.

10.2-3 DISTRIBUTOR DESIGN

As described in 8.3-5, efficient initial distribution of dispersed phase cannot be relied on in industrial columns using convectional distributor designs. The problems of variation of supply to the orifices may be overcome by either,

(a) Division of the distributor into four or more equal quadrants individually fed from the inlet line;

(b) Packing the volume beneath the distributor plate with knitted mesh or raschig rings.

The raschig rings would need to be selected so as to be preferentially wetted by the dispersed phase, so that an even reservoir of this phase was maintained beneath the plate. The knitted mesh could be Knitmesh D.C. which would be equally applicable to aqueous dispersed systems.

Treatment of the under side only of the plate to render it preferentially wettable by the dispersed phase e.g. thin plastic spray coating for organic dispersed systems.

Whatever design is used the distributor must be as horizontal as practicable using a spirit level i.e. it is not necessarily satisfactory to ensure only that the column is vertical.

10.3 RECOMMENDATIONS FOR FURTHER WORK

Flow patterns in both phases were highly sensitive to flow conditions, the most serious effect of this being by-passing. The causes of pattern changes may be closely connected to the insertion of the continuous phase leaving the downcomer. Drop formation at the orifices was also unpredictable because many holes were not working and the pattern of working holes was not consistent. This is because the pressure drop in the orifice is small compared to the local pressure fluctuations below and above the orifices. It may be connected to the continuous phase patterns and is certainly due to drop patterns below the trays.

From the above observations, it appears that the major uncertainty relates to the flow patterns. Therefore improvement of sieve plate column performance would depend upon improvement of flow patterns within the equipment. This may be achieved in part by some modifications to the existing design such as,

(1) Shortening the downcomer length so as to (a) reduce the velocity of the incoming continuous phase as it enters the test stage, and (b) decrease the residence time of the continuous phase, but at the same time increase the amount of mixing.

(2) More attention should be given to hole design, since it is believed that entrance effects are important in obtaining effective use of all orifices. This may provide more uniform dispersion and less segregation of the drop phase after formation. Both drilled and punched and drilled only plate orifices were used in this work; experience showed that the drilled and punched plate orifices work well with a smooth entrance region.

(3) A critical review of proposed non-mass transfer and mass transfer models is also needed to assess their usefulness to practical column design some, e.g. the Fujanawa single nozzle droplets hydrodynamic model and the Handlos and Baron model seem inapplicable on close inspection, others may be directly useful or susceptible to useful modification.

(4) It would be useful to test the distributor designs recommended above (10.2-3). This would simply involve modification of the existing distributor to include the proposed improvements in turn, operation over the range of flow rates given in 8.2-5, and a comparison of the numbers of operating holes and the drop size distributions.

(5) An investigation can be made of the optimum plate spacing as discussed in 9.4 and 10.2-1 above. The preferred way of doing this would be to use 0.1588 cm hole size plate

with spacing of 30.0, 38.0 and 46.0 cm .

(6) It would be useful to extend the work to cover different systems i.e. a range of interfacial tension σ = 2 to 50 dynes/cm and viscosity μ = 0.6 to 3.5 cp. A check could then be made on correlations, equations 8.2-1 to 8.2-6 and recommendations 10.2-1 and 10.2-2. These studies could include operation with Clairsol continuous by simply using water as the solvent over the flowrate range U''_D = 0 to U''_D = 0.44 $cmsec^{-1}$.

(7) The fundamentals of plate design could be studied further by testing the optimum plate design as described in 10.2-1, by varying available parameters e.g. blocking of holes to reduce plate free area. The best design of orifice could be checked using a single holed plate (e.g. using drilled and punched orifices of different entrance dimensions and projection height).

APPENDICES

APPENDIX 1

FLOW MEASURING INSTRUMENT

TYPE: Q.V.F. Rotameter

LIGHT PHASE:

Rotameter Tube: 47F; Float: Stainless Steel

Capacity: 1.67 litre sec^{-1}

Rotameter Tube: 65F: Float: Stainless Steel

Capacity: 3.83 litre sec^{-1}

HEAVY PHASE:

Rotameter Tube: 47F; Float: Stainless Steel

Capacity: 1.67 litre sec^{-1}

F = Flanges

ELGASTAT

B224

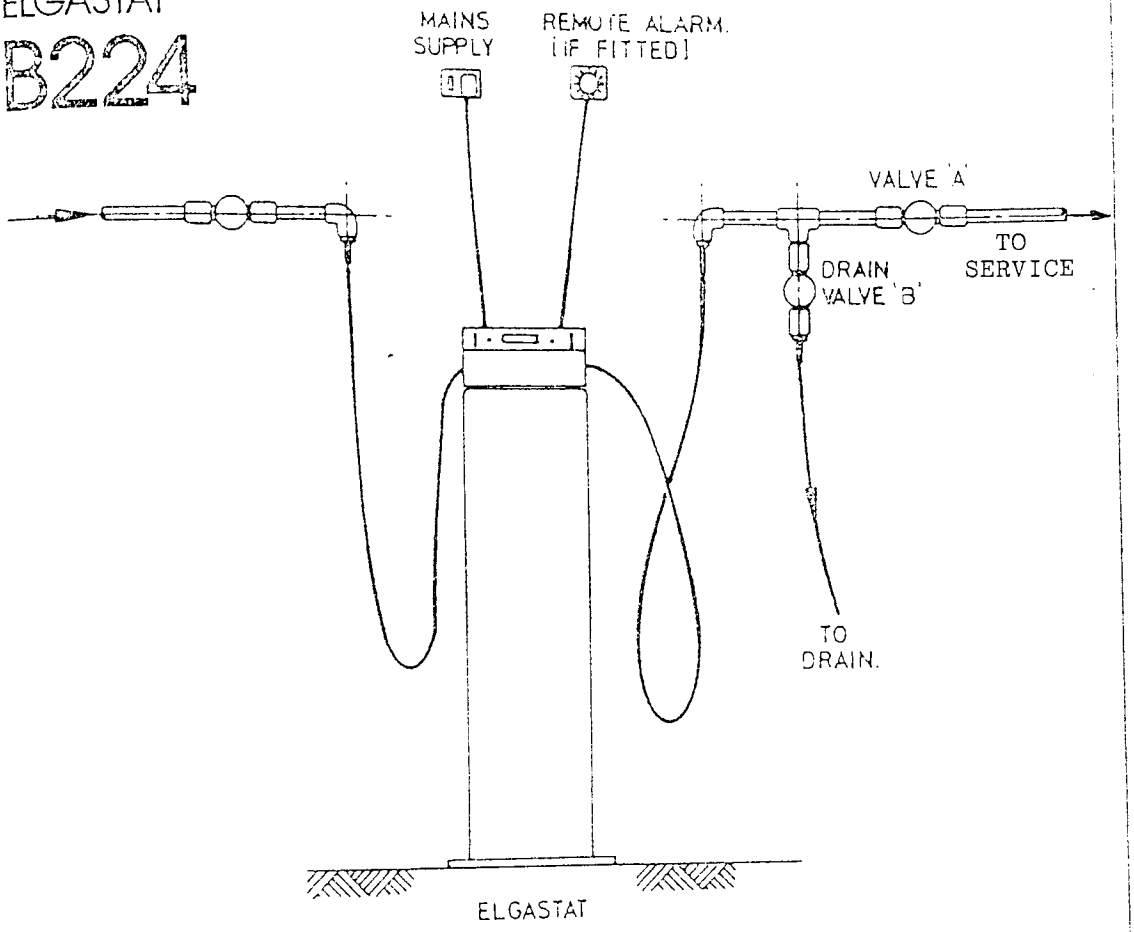

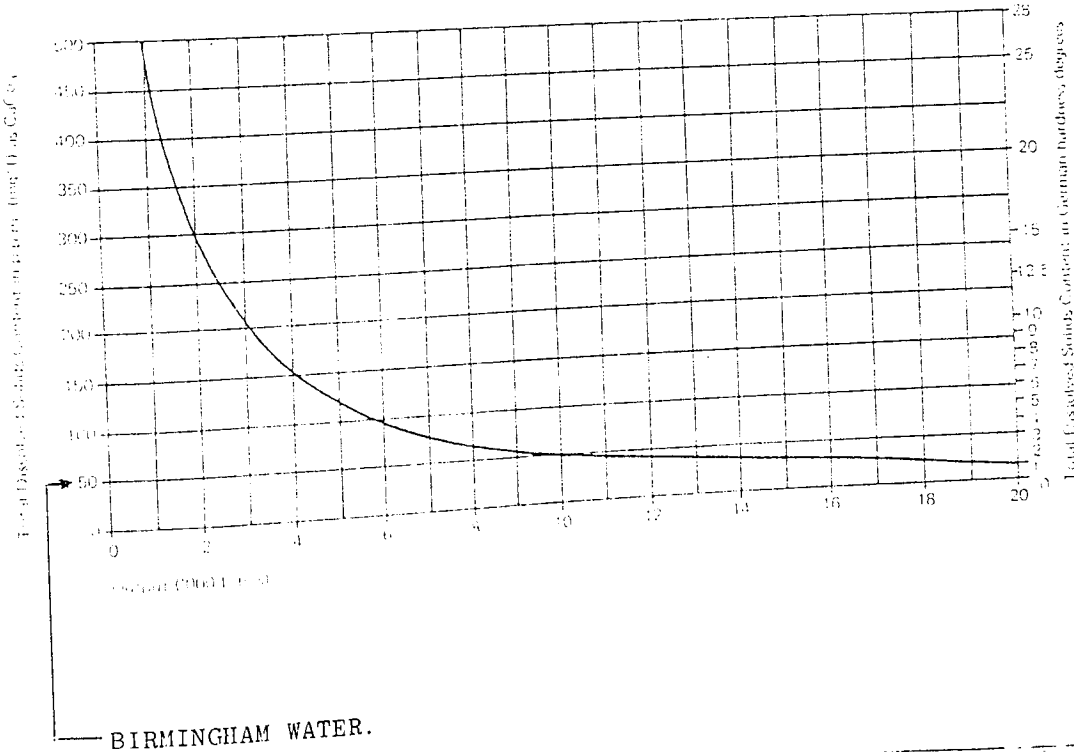

APPENDIX 2a

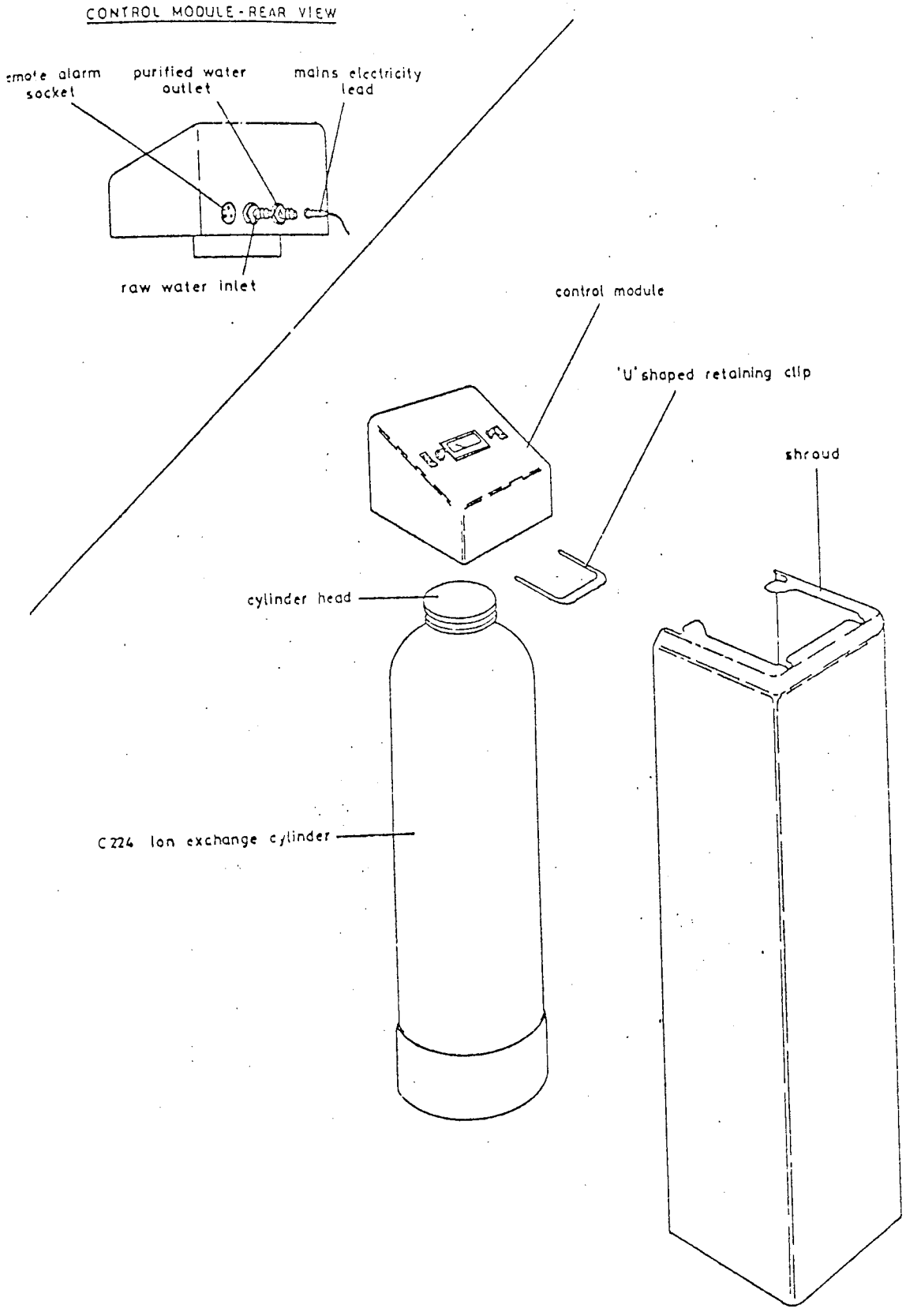
CONTROL MODULE - REAR VIEW
emote alarm socket
purified water outlet
mains electricity lead
raw water inlet
control module
'U' shaped retaining clip
shroud
cylinder head
C 224 Ion exchange cylinder

APPENDIX 3

ELGASTAT B224

SPECIFICATION

Dimensions	Height 1095mm
	Depth 225mm
	Width 225mm
Weight	23.0kg
Electrical Supply	240 Volts (50HZ single phase)

RAIN WATER SUPPLY

Cold polable water free of suspended solids. Maximum input pressure 4.5 bar (70 p.s.i.)

TYPICAL TREATED WATER ANALYSIS IN P.P.M. (mg/i)

Copper, lead, trace metals	0.0006
Iron	0.0005
Ammonia, sulphate	0.002
Chloride	0.015
Sodium	1.0
Silica	As influent
Free carbon dioxide	As influent
T.D.S.	5-10
pH	5.0-6.0
Electrical resistivity	50-15 µS (0.02-0.07 meg ohm cm)

FLOWRATE

Up to 360 litre per hour

CLAIRSOL SPECIFICATION

CLAIRSOL TYPE	SPECIFIC GRAVITY AT 15°C	CLAIRSOL RANGE °C	FLASH POINT °C	AROMATIC CONTENT % W/W	KAURI BUTANOL VALUE	THRESHOLD LIMIT VALUE P.P.M.	RELATIVE VENTILATION REQUIREMENT
250 (C_7)	0.725	87-106	-23	0.01	38	450	2.1
280 (C_8)	0.740	110-135	7	0.02	36	450	0.9
300 (C_9)	0.765	140-156	24	0.05	35	450	0.3
310 (C_{10})	0.774	155-200	42	0.05	34	500	0.1
315 (C_{10})	0.775	160-180	43	0.05	34	500	0.1
330 (C_{11})	0.780	180-205	60	0.05	30	500	0.03
350 (C_{12})	0.785	205-230	71	0.1	28	500	0.01

APPENDIX 5a

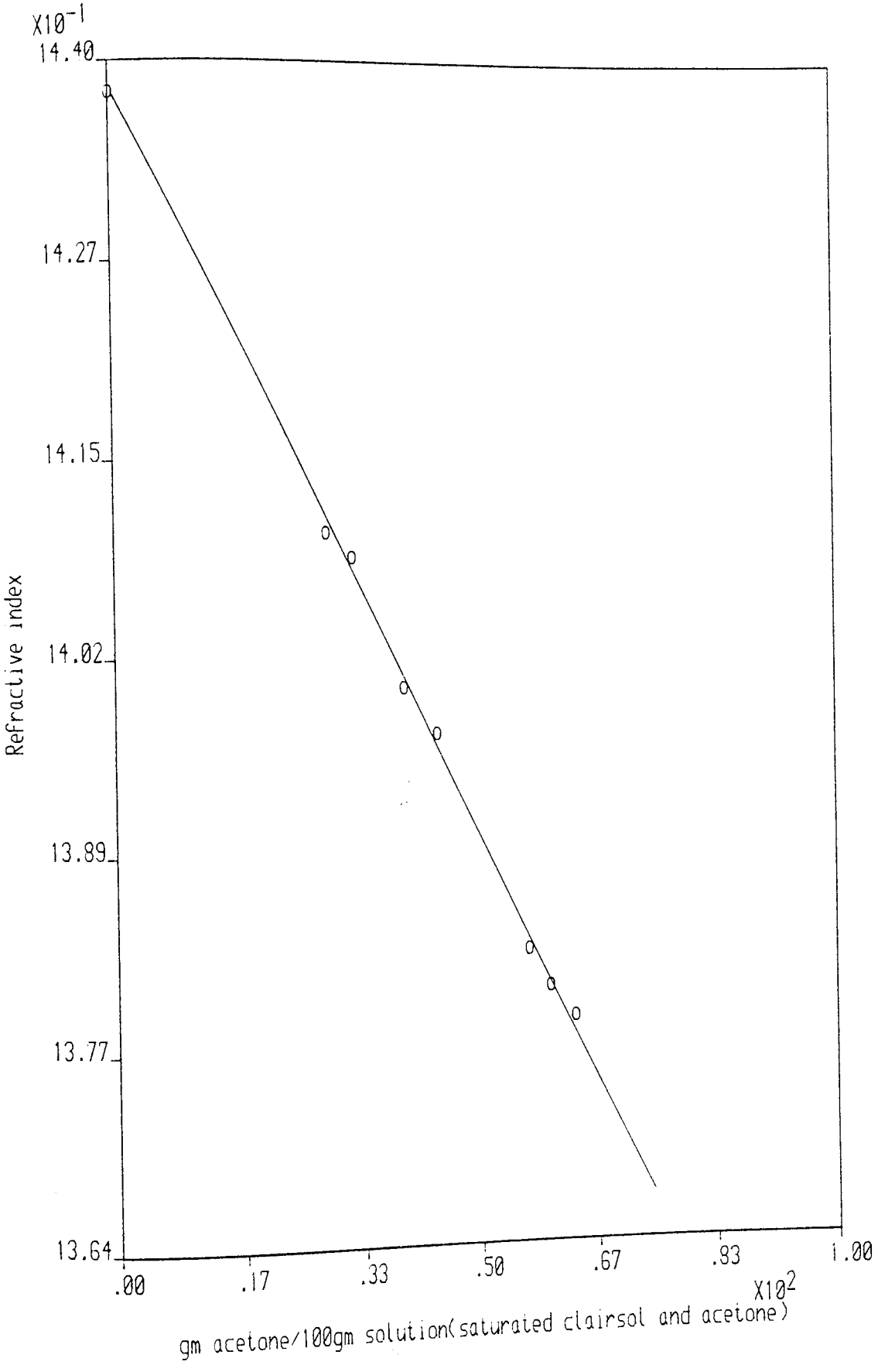

Fig.7.1-2a. Calibration curve for refractive index vs weight percent water saturated clairsol and acetone solution

APPENDIX 5b

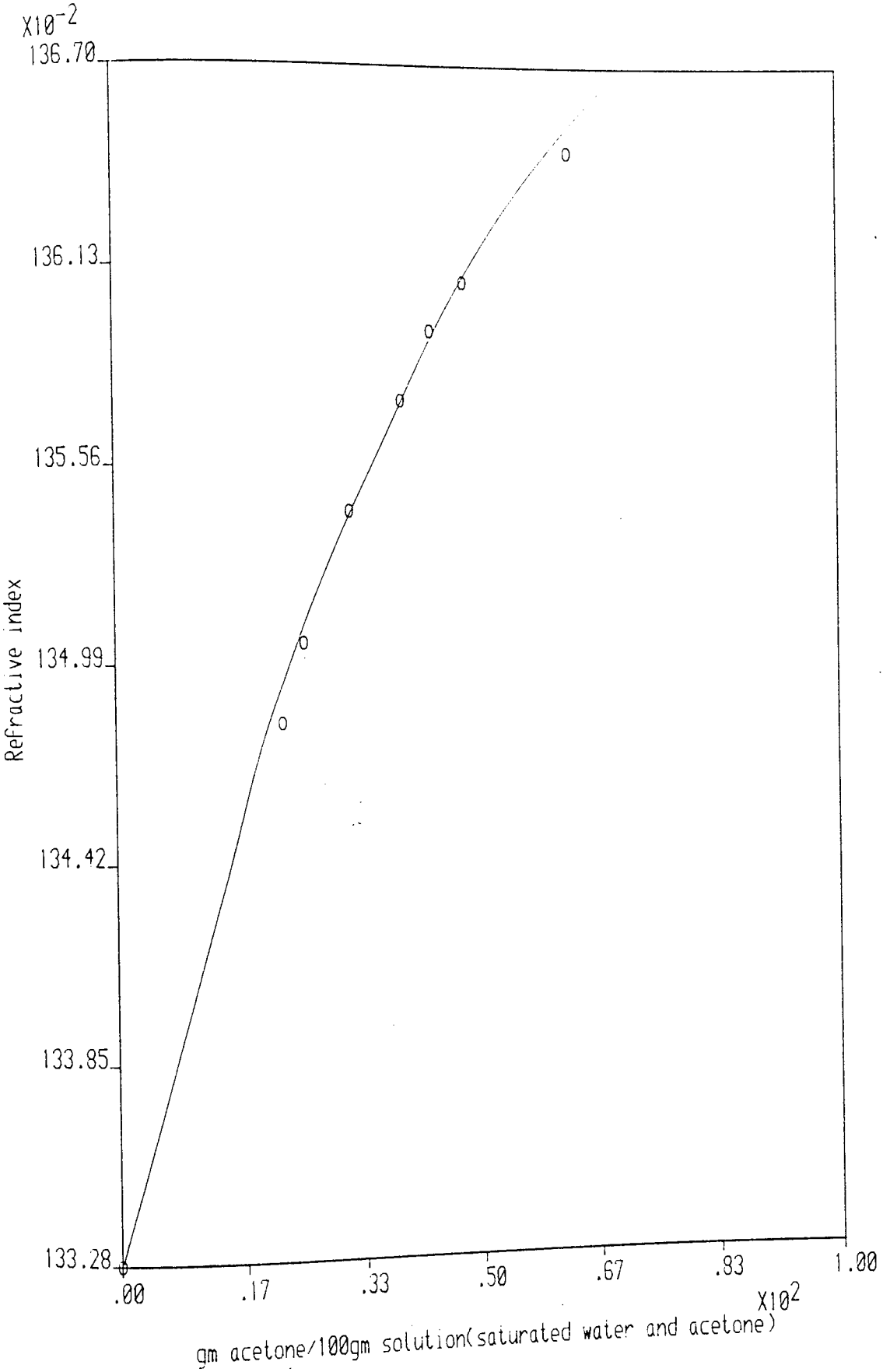

Fig.7.1-2b. Calibration curve for refractive index vs weight percent clairsol saturated water and acetone solution

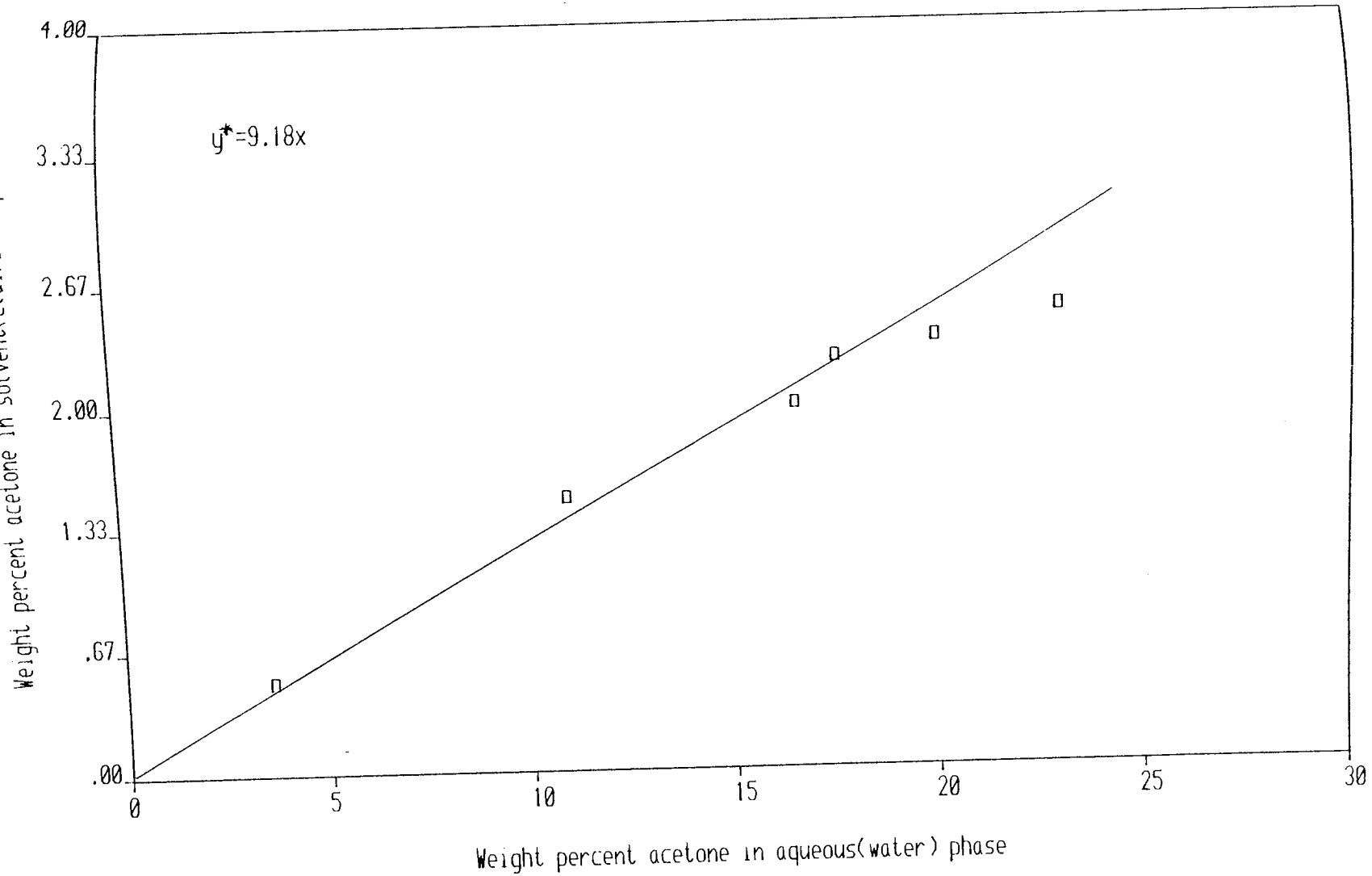

Equilibrium distribution of acetone between waterand clairsol'350' at 20 C

APPENDIX 6

TABLE 8.2-3 Plate Hole Size = 1.588 mm diameter

Photo-graph d mm	Actual d mm	n	$n\frac{\pi}{6}d^3$	Cumu-lative Vol. Fraction v	$U=\frac{d}{d_m-d}$	Experimental	N_{Re}	U_t cmsec^{-1}
1.05	—	-	—	—	—	—	—	—
1.23	0.99	1	0.5081	0.0001	0.1594	0.000	35	4.47
1.42	1.14	1	0.7757	0.0003	0.1881	0.001	48	5.35
1.60	1.29	1	1.1240	0.0005	0.2183	0.001	64	6.31
1.78	1.43	2	3.0622	0.0012	0.2478	0.005	80	7.11
1.97	1.59	1	2.1047	0.0017	0.2834	0.003	99	7.96
2.15	1.73	3	8.1331	0.0035	0.3163	0.013	120	8.73
2.34	1.88	7	24.3540	0.0090	0.3534	0.037	141	9.59
2.52	2.03	6	26.2808	0.0149	0.3927	0.039	162	10.20
2.70	2.17	4	21.4012	0.0197	0.4314	0.034	184	10.83
2.89	2.33	7	46.3622	0.0301	0.4784	0.065	206	11.27
3.07	2.47	11	86.7925	0.0496	0.5222	0.139	227	11.71
3.26	2.62	13	122.4182	0.0771	0.5721	0.183	251	12.25
3.44	2.77	10	111.2853	0.1021	0.6253	0.167	273	12.58
3.62	2.91	15	193.5392	0.1455	0.6783	0.310	298	13.08
3.81	3.06	18	270.0445	0.2061	0.7391	0.404	321	13.38
3.99	3.21	23	398.3287	0.2956	0.8045	0.597	348	13.85
4.18	3.37	20	400.7913	0.3855	0.8799	0.562	370	14.01
4.36	3.51	17	384.9186	0.4719	0.9512	0.617	397	14.45
4.54	3.66	14	359.3933	0.5526	1.0339	0.538	422	14.73
4.73	3.81	12	347.5000	0.6306	1.1239	0.520	439	14.71
4.91	3.95	8	258.1546	0.6886	1.2154	0.414	464	14.99
5.10	4.11	9	327.1648	0.7620	1.3301	0.459	494	15.34
5.28	4.25	6	241.1663	0.8162	1.4407	0.387	517	15.52
5.46	4.40	5	223.0111	0.8662	1.5714	0.333	531	15.41
5.65	4.55	3	147.9633	0.8994	1.7170	0.221	559	15.69
5.83	4.69	2	108.0307	0.9237	1.8685	0.174	573	15.61
6.02	4.85	2	119.4686	0.9505	2.0638	0.168	602	15.84
6.20	4.99	1	65.0579	0.9651	2.2579	0.104	619	15.85
6.38	5.14	1	71.1031	0.9811	2.4952	0.107	639	15.87
6.57	—	-	—	—	—	—	—	—
6.75	5.44	1	84.2937	1.0000	3.0709	0.063	683	16.03
-	-	224	4454.5317	-	-	-	-	-

APPENDIX 7

TABLE 8.2-4 Plate Hole Size = 3.175 mm diameter

Photo-graph d mm	Actual d mm	n	$n\frac{\pi}{6}d^3$	Cumu-lative Vol. Fraction v	$U=\frac{d}{d_m-d}$	Experimental	N_{Re}	U_t cmsec^{-1}
0.86	—	—	—	—	—	—	—	—
1.05	1.00	1	0.5236	0.0001	0.1456	0.0000	44	5.65
1.42	—	—	—	—	—	—	—	—
1.60	1.53	1	1.8753	0.0002	0.2413	0.0002	94	7.83
1.78	1.70	2	5.1449	0.0007	0.2755	0.0022	114	8.53
1.97	1.88	2	6.9583	0.0014	0.3139	0.0039	141	9.59
2.15	2.05	1	4.5109	0.0019	0.3522	0.0029	166	10.36
2.34	2.23	3	17.4195	0.0035	0.3954	0.0089	190	10.86
2.52	2.40	5	36.1912	0.0071	0.4388	0.0212	216	11.49
2.70	2.56	8	70.2762	0.0139	0.4821	0.0425	242	12.05
2.89	2.76	7	77.0591	0.0214	0.5401	0.0375	274	12.69
3.07	2.93	6	79.0229	0.0290	0.5931	0.0447	297	12.96
3.26	3.11	5	78.7499	0.0367	0.6534	0.0428	331	13.57
3.44	3.28	8	147.8122	0.0510	0.7146	0.0841	358	13.96
3.62	3.45	7	150.5061	0.0656	0.7805	0.0859	386	14.28
3.81	3.64	11	277.7765	0.0926	0.8605	0.1421	415	14.56
3.99	3.81	13	376.4583	0.1291	0.9384	0.2147	439	14.71
4.18	3.99	15	498.8943	0.1775	1.0284	0.2689	465	14.89
4.36	4.16	13	490.0292	0.2251	1.1213	0.2800	495	15.19
4.54	4.33	16	680.1149	0.2911	1.2232	0.3882	528	15.57
4.73	4.51	20	960.6346	0.3842	1.3422	0.5172	541	15.33
4.91	4.68	18	966.0702	0.4780	1.4671	0.5518	566	15.45
5.10	4.86	19	1141.9867	0.5889	1.6146	0.6161	602	15.81
5.28	5.04	14	938.4654	0.6799	1.7809	0.5056	621	15.74
5.46	5.21	12	888.5729	0.7662	1.9587	0.5077	648	15.87
5.65	5.39	7	573.9353	0.8218	2.1647	0.3089	674	15.97
5.83	5.56	5	449.9798	0.8655	2.4069	0.2571	708	16.26
6.02	5.74	6	594.1356	0.9232	2.6948	0.3206	738	16.42
6.20	5.92	2	217.2670	0.9443	3.0359	0.1172	747	16.12
6.38	6.09	1	118.2634	0.9557	3.4214	0.0671	778	16.32
6.57	—	—	—	—	—	—	—	—
6.75	6.44	2	279.6960	0.9829	4.5035	0.0777	819	16.24
6.94	—	—	—	—	—	—	—	—
7.12	—	—	—	—	—	—	—	—
7.30	6.96	1	176.5332	1.0000	7.6484	0.0329	899	16.49
		231	10304.8634					

APPENDIX 8

TABLE 8.2-5 Plate Hole Size = 4.763 mm diameter

Photo-graph d mm	Actual d mm	n	$n\frac{\pi}{6}d^3$	Cumu-lative Vol. Fraction v	$U=\frac{d}{d_m-d}$	Experimental	N_{Re}	U_t cmsec^{-1}
0.68	—	—	—	—	—	—	—	—
0.86	1.09	1	0.6781	0.0000	0.0000	0.0000	44	5.14
1.05	1.33	1	1.2318	0.0001	0.1348	0.0000	71	6.80
1.23	1.56	1	1.9878	0.0002	0.1618	0.0004	97	7.97
1.42	1.80	2	3.0536	0.0004	0.1915	0.0008	131	9.29
1.60	2.03	1	4.3801	0.0007	0.2214	0.0013	166	10.46
1.78	2.26	3	18.1320	0.0018	0.2528	0.0048	200	11.30
1.97	2.50	5	40.9062	0.0043	0.2874	0.0104	234	11.93
2.15	2.73	5	53.2668	0.0075	0.3223	0.0139	273	12.75
2.34	2.97	9	123.4555	0.0150	0.3609	0.0313	311	13.39
2.52	3.20	8	137.2583	0.0234	0.4000	0.0365	350	13.98
2.70	3.43	9	190.1619	0.0349	0.4414	0.0500	382	14.23
2.89	3.67	13	336.4652	0.0554	0.4874	0.0854	419	14.59
3.07	3.90	15	465.8903	0.0837	0.5342	0.1100	458	15.01
3.26	4.14	13	482.9954	0.1130	0.5864	0.1221	494	15.23
3.44	4.37	17	742.8341	0.1582	0.6398	0.1965	528	15.44
3.62	4.60	19	968.3352	0.2170	0.6970	0.2557	564	15.67
3.81	4.84	16	949.8493	0.2747	0.7610	0.2821	596	15.73
3.99	5.07	14	955.3237	0.3328	0.8271	0.2526	637	16.04
4.18	5.31	16	1254.3022	0.4090	0.9015	0.3175	671	16.13
4.36	5.54	11	979.3109	0.4685	0.9788	0.2587	708	16.31
4.54	5.77	9	905.2501	0.5235	1.0626	0.2391	732	16.21
4.73	6.01	8	909.3101	0.5788	1.1580	0.2404	771	16.39
4.91	6.24	8	1017.7530	0.6406	1.2581	0.2575	814	16.66
5.10	6.48	6	854.8204	0.6926	1.3729	0.2261	844	16.63
5.28	6.71	7	1107.2973	0.7599	1.4944	0.3059	885	16.84
5.46	6.93	5	871.3012	0.8128	1.6230	0.2405	917	16.90
5.65	7.18	4	775.2325	0.8599	1.7861	0.1884	941	16.74
5.83	7.40	3	636.5244	0.8986	1.9474	0.1759	971	16.76
6.02	7.65	3	703.2410	0.9413	2.1549	0.1708	1005	16.78
6.20	—	—	—	—	—	—	—	—
6.38	—	—	—	—	—	—	—	—
6.57	8.34	2	607.4727	0.9782	2.9161	0.0535	1097	16.80
6.75	—	—	—	—	—	—	—	—
6.94	8.81	1	358.0357	1.0000	3.6862	0.0464	1164	16.86
		235	16456.0568					

APPENDIX 9

TABLE 8.2-6 Plate Hole Size = 6.350 mm diameter

Photo-graph-d mm	Actual d mm	n	$n\frac{\pi}{6}d^3$	Cumu-lative Vol. Fraction v	$U=\frac{d}{d_m-d}$	Experimental	N_{Re}	U_t cmsec^{-1}
0.50	—	—	—	—	—	—	—	—
0.68	0.96	1	0.4633	0.0000	0.0000	0.0000	33	4.40
0.86	—	—	—	—	—	—	—	—
1.05	1.48	1	1.6974	0.0001	0.1482	0.0002	86	7.39
1.23	1.73	1	2.7111	0.0002	0.1776	0.0004	120	8.73
1.42	2.00	2	8.3776	0.0006	0.2112	0.0015	153	9.78
1.60	2.26	5	30.2200	0.0020	0.2454	0.0054	191	10.80
1.78	2.51	5	41.4000	0.0038	0.2801	0.0072	234	11.88
1.97	2.78	4	44.9980	0.0058	0.3199	0.0074	276	12.68
2.15	3.03	6	87.3932	0.0098	0.3590	0.0160	319	13.42
2.34	3.30	8	150.5326	0.0166	0.4039	0.0222	359	13.90
2.52	3.55	11	257.6774	0.0282	0.4482	0.0464	400	14.38
2.70	3.81	10	289.5833	0.0412	0.4974	0.0500	442	14.82
2.89	4.08	14	497.8599	0.0636	0.5521	0.0830	478	14.95
3.07	4.33	14	595.1005	0.0904	0.6064	0.1072	527	15.55
3.26	4.60	18	917.3702	0.1318	0.6696	0.1533	564	15.67
3.44	4.85	16	955.7489	0.1748	0.7326	0.1720	602	15.84
3.62	5.10	19	1319.6621	0.2342	0.8006	0.2376	635	15.91
3.81	5.37	21	1702.7103	0.3109	0.8803	0.2841	672	15.99
3.99	5.63	17	1588.4470	0.3825	0.9640	0.2754	715	16.21
4.18	5.89	15	1604.8549	0.4547	1.0556	0.2777	754	16.34
4.36	6.15	11	1339.7281	0.5151	1.1560	0.2323	793	16.46
4.54	6.40	13	1784.3576	0.5955	1.2623	0.3216	832	16.59
4.73	6.67	12	1864.4785	0.6794	1.3892	0.3107	869	16.63
4.91	6.92	7	1214.5487	0.7341	1.5209	0.2188	906	16.72
5.10	7.19	6	1167.7142	0.7867	1.6799	0.1948	945	16.78
5.28	7.45	4	866.0190	0.8257	1.8532	0.1500	977	16.74
5.46	7.70	3	717.1204	0.8580	2.0424	0.1292	1008	16.73
5.65	7.97	2	530.1559	0.8819	2.2771	0.0885	1047	16.78
5.83	8.22	2	581.6264	0.9081	2.5292	0.1048	1079	16.77
6.02	8.49	1	320.4215	0.9225	2.8490	0.0533	1111	16.71
6.20	8.74	2	699.1380	0.9540	3.2015	0.0126	1139	16.65
6.38	—	—	—	—	—	—	—	—
6.57	—	—	—	—	—	—	—	—
6.75	—	—	—	—	—	—	—	—
6.94	9.79	1	491.2999	0.9748	5.8274	0.0198	1249	16.29
7.12	10.04	1	529.9071	1.0000	9.3832	0.1008	1309	16.65
		253	22203.3230					

APPENDIX 10

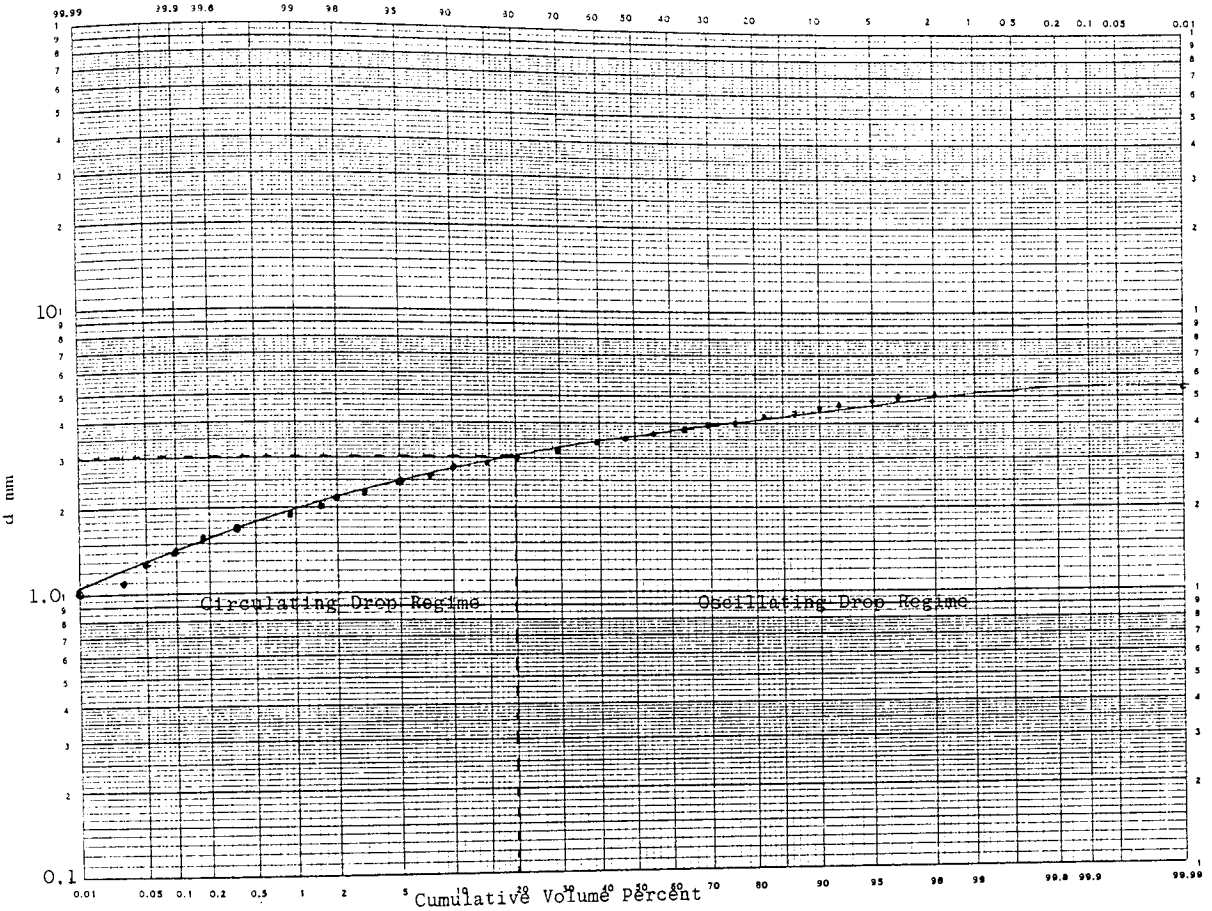

Fig. 8.2-15a Plot of cumulative-drop size for plate hole size = 0.1588 cm

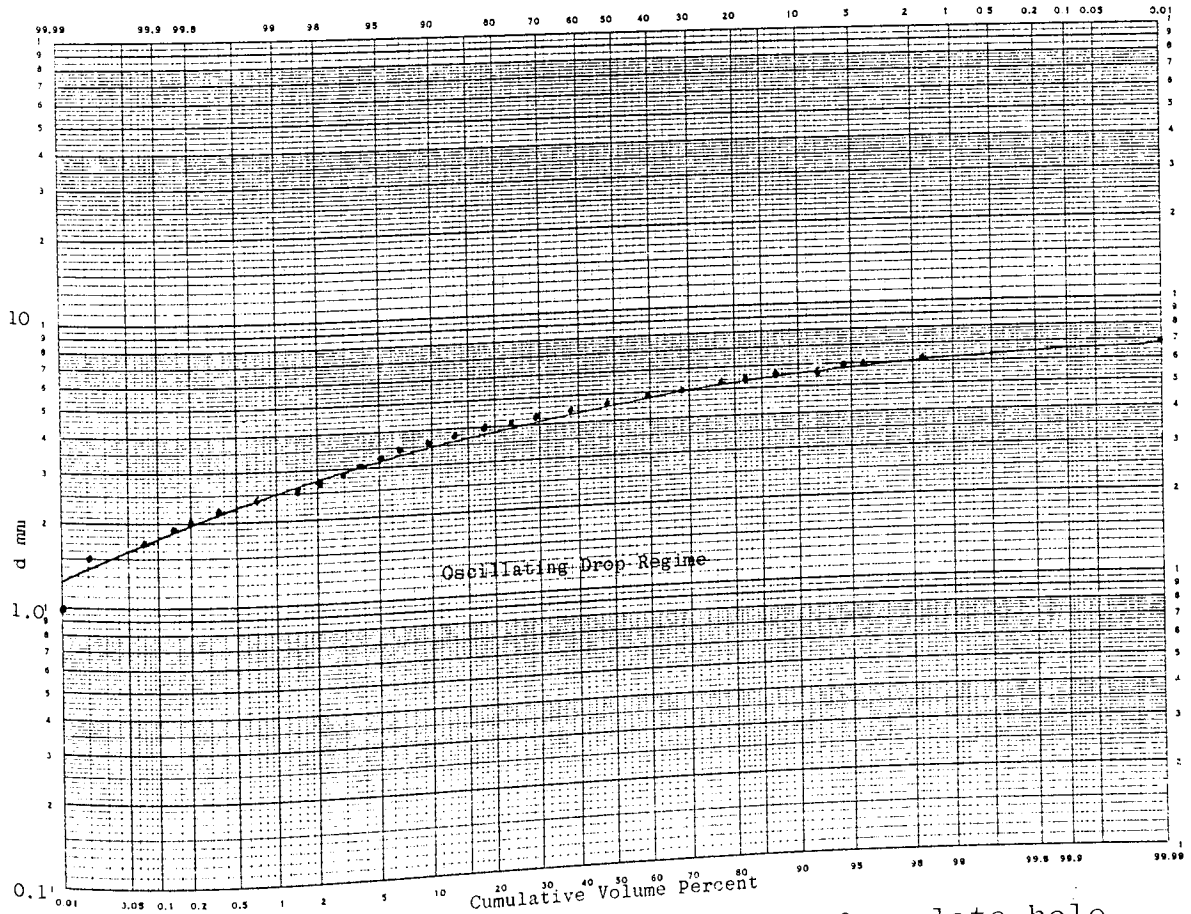

Fig. 8.2-16a Plot of cumulative-drop size for plate hole size = 0.3175 cm

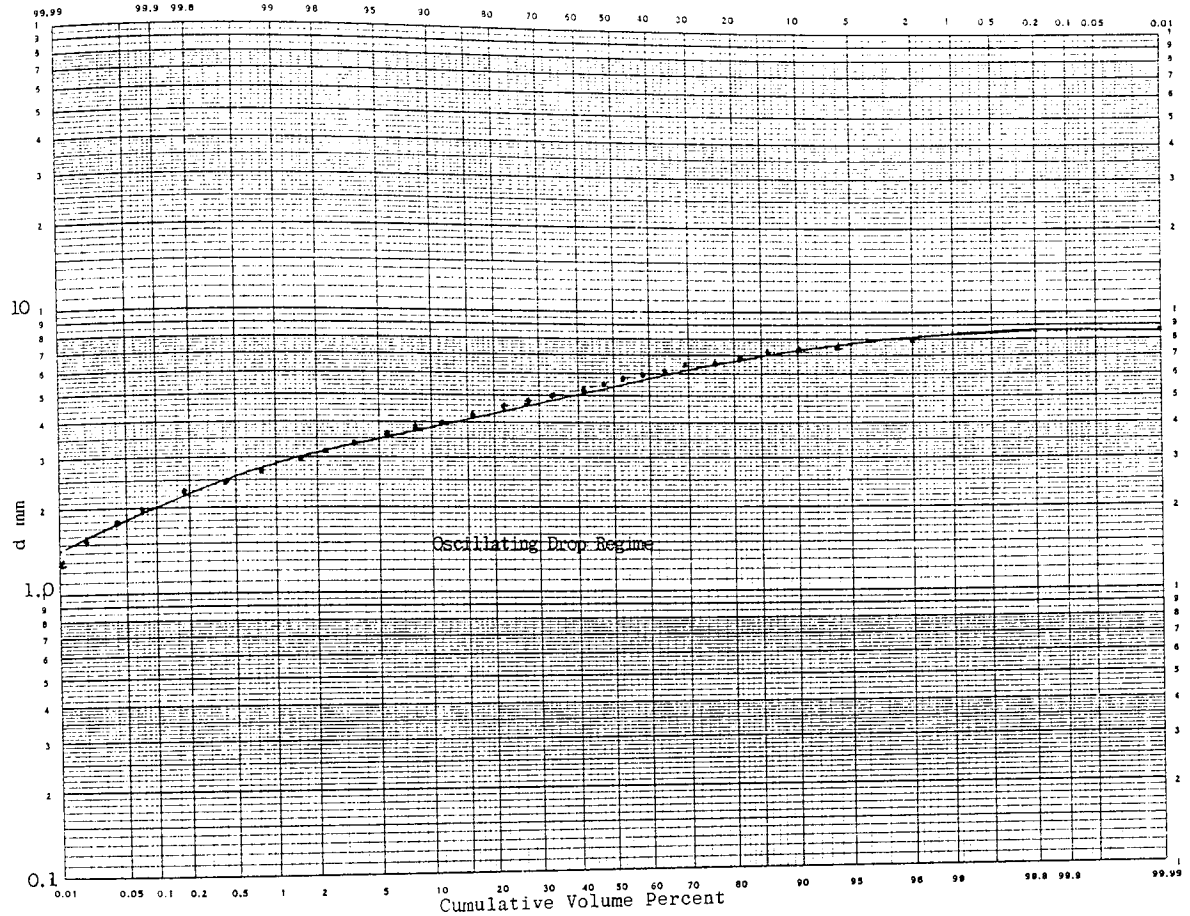

Fig. 8.2-17a Plot of cumulative-drop size for plate hole size = 0.4763 cm

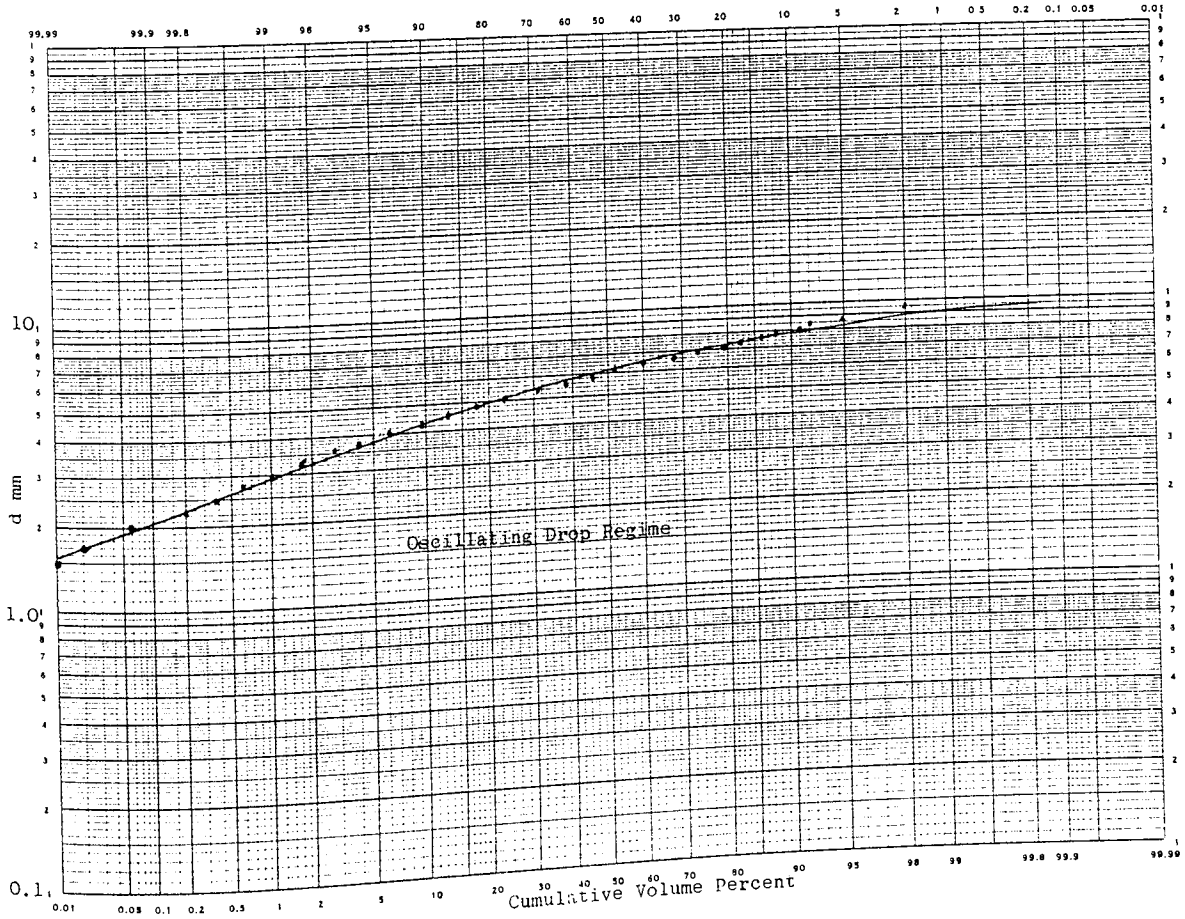

Fig. 8.2-18a Plot of cumulative-drop size for plate hole size = 0.6350 cm

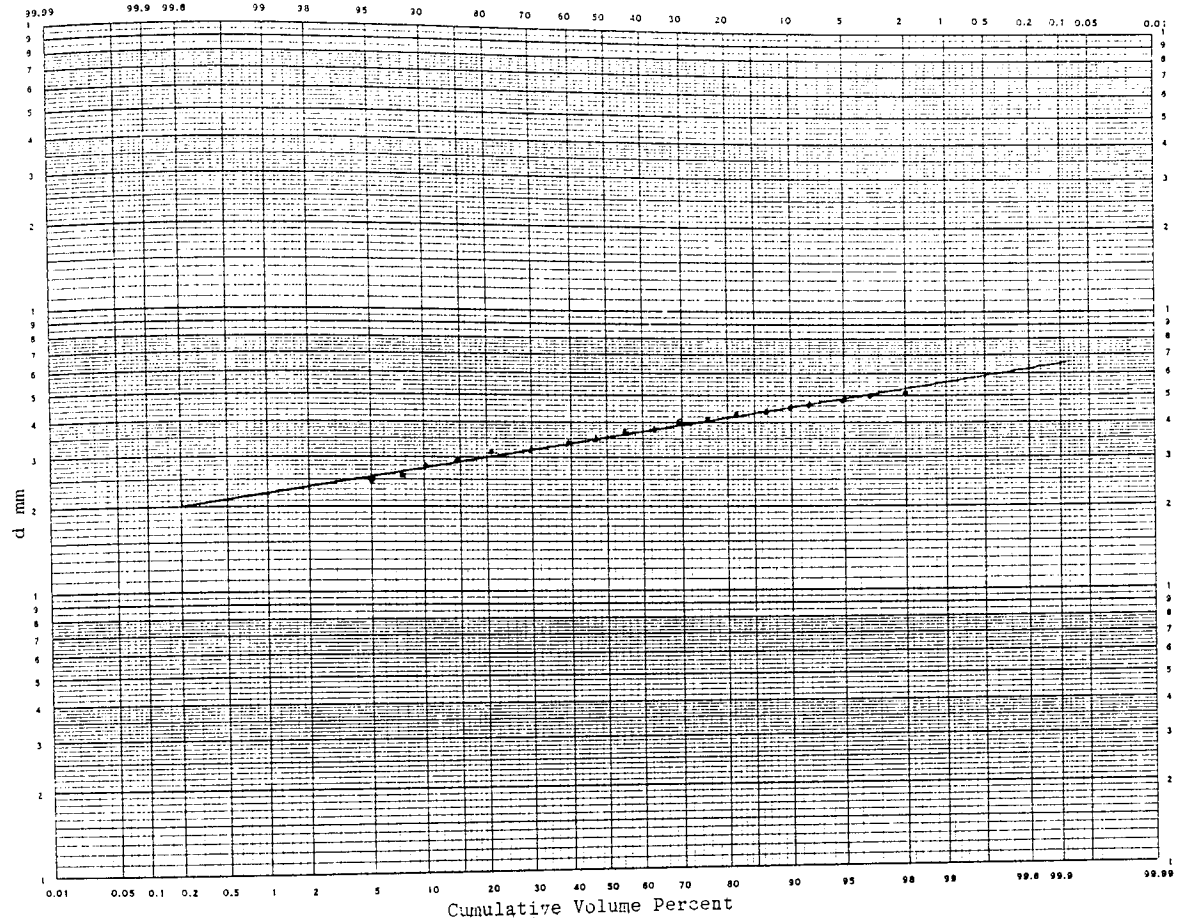

Fig 8.2-15b Log probability analysis of experimental data for plate hole size = 0.5188 cm

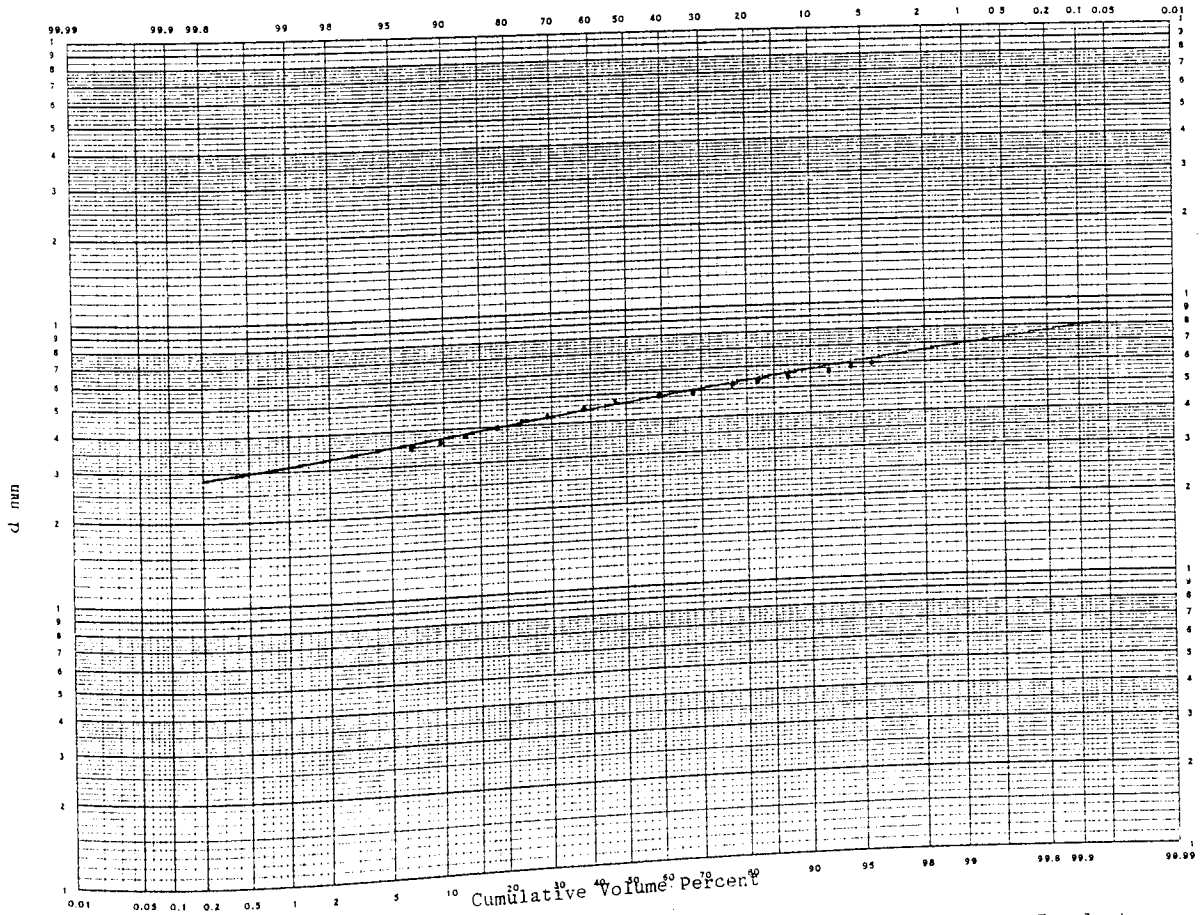

Fig. 8.2-16b Log probability analysis of experimental data for plate hole size = 0.3175 cm

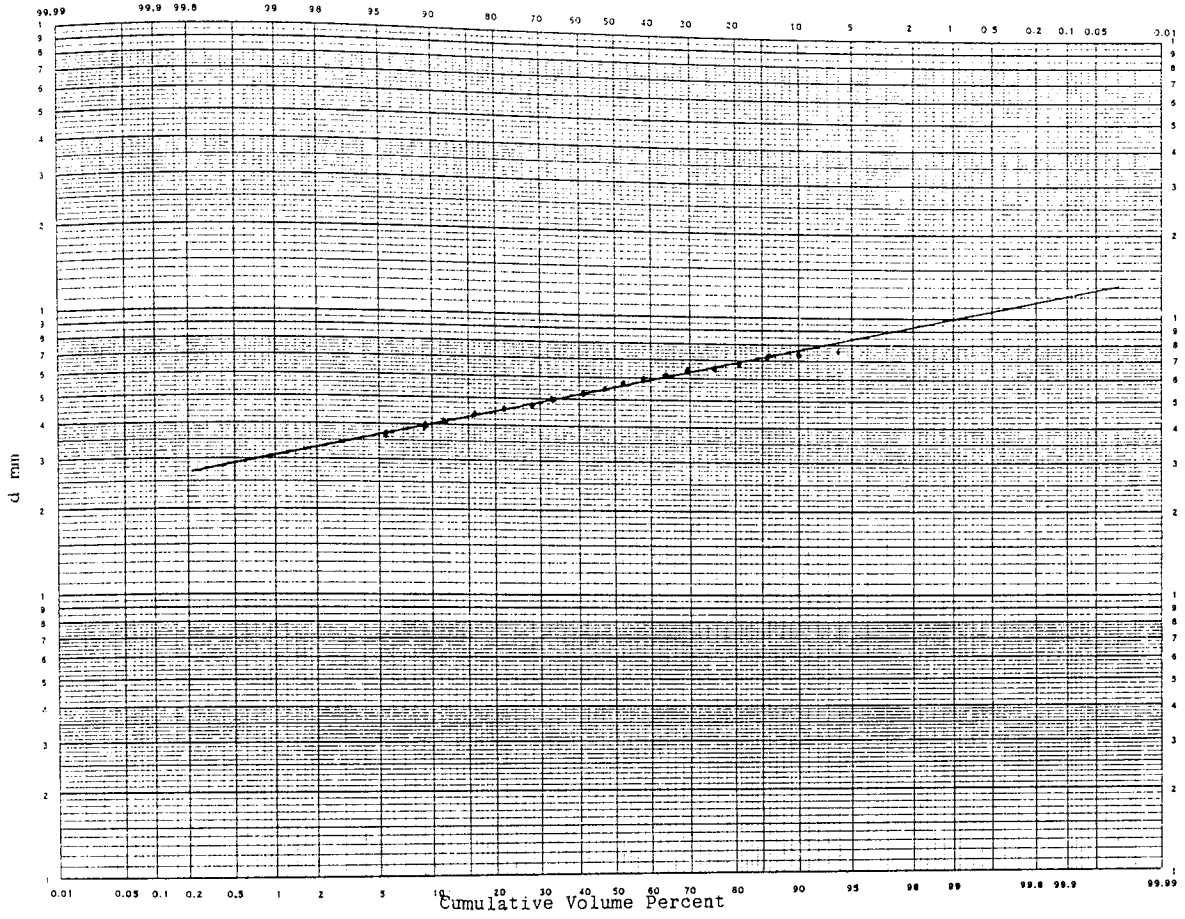

Fig. 8.2-17b Log probability analysis of experimental data for plate hole size = 0.4763 cm

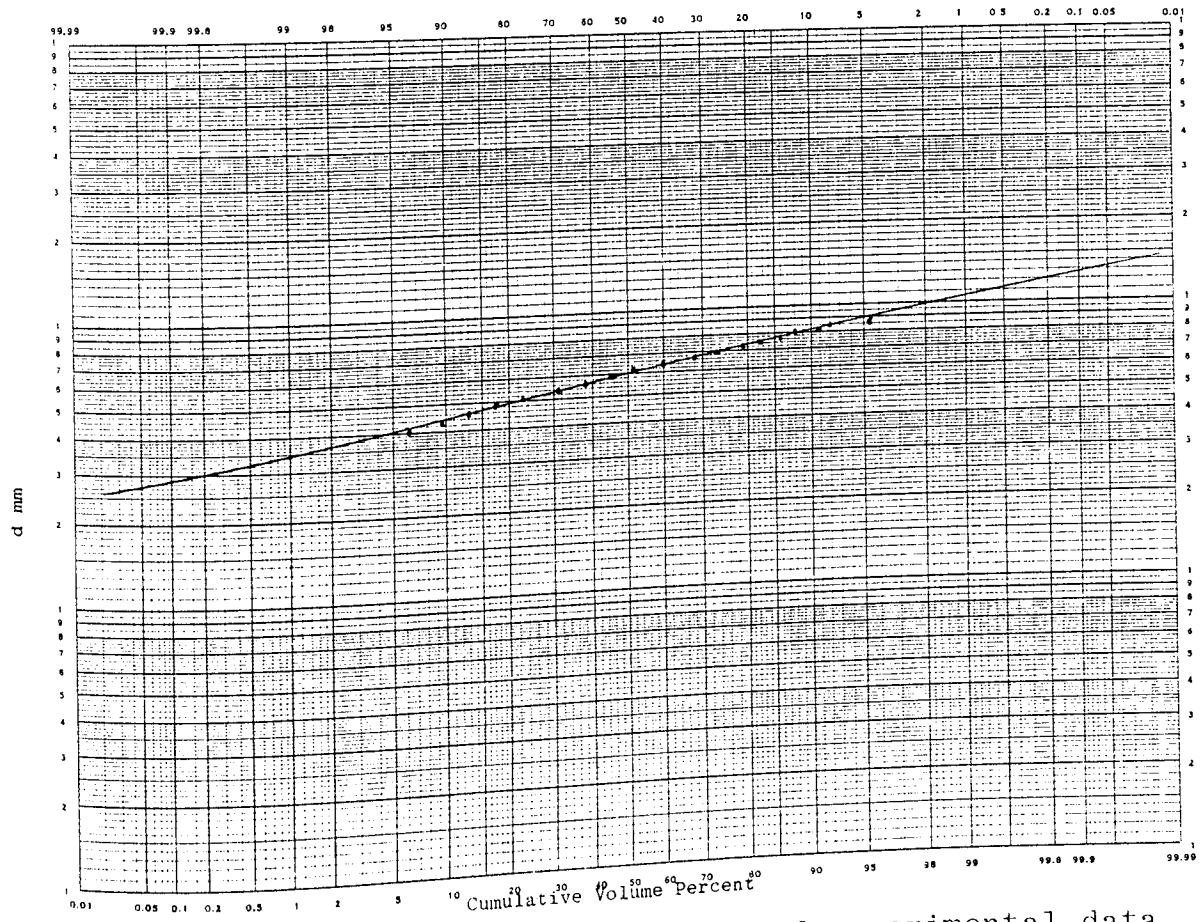

Fig. 8.2-18b Log probability analysis of experimental data for plate hole size = 0.6350 cm

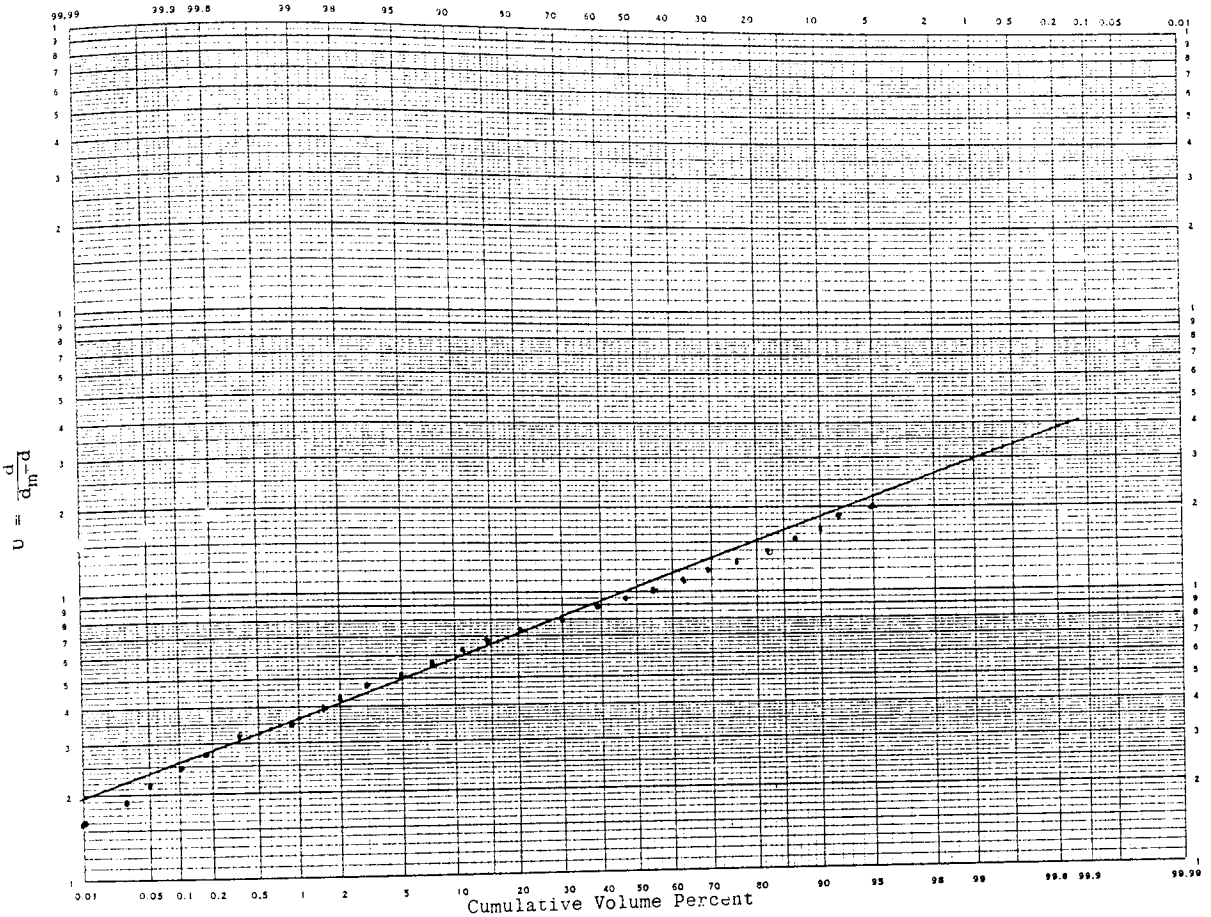

Fig. 8.2-15c Upper limit analysis of experimental data for plate hole size = 0.5188 cm

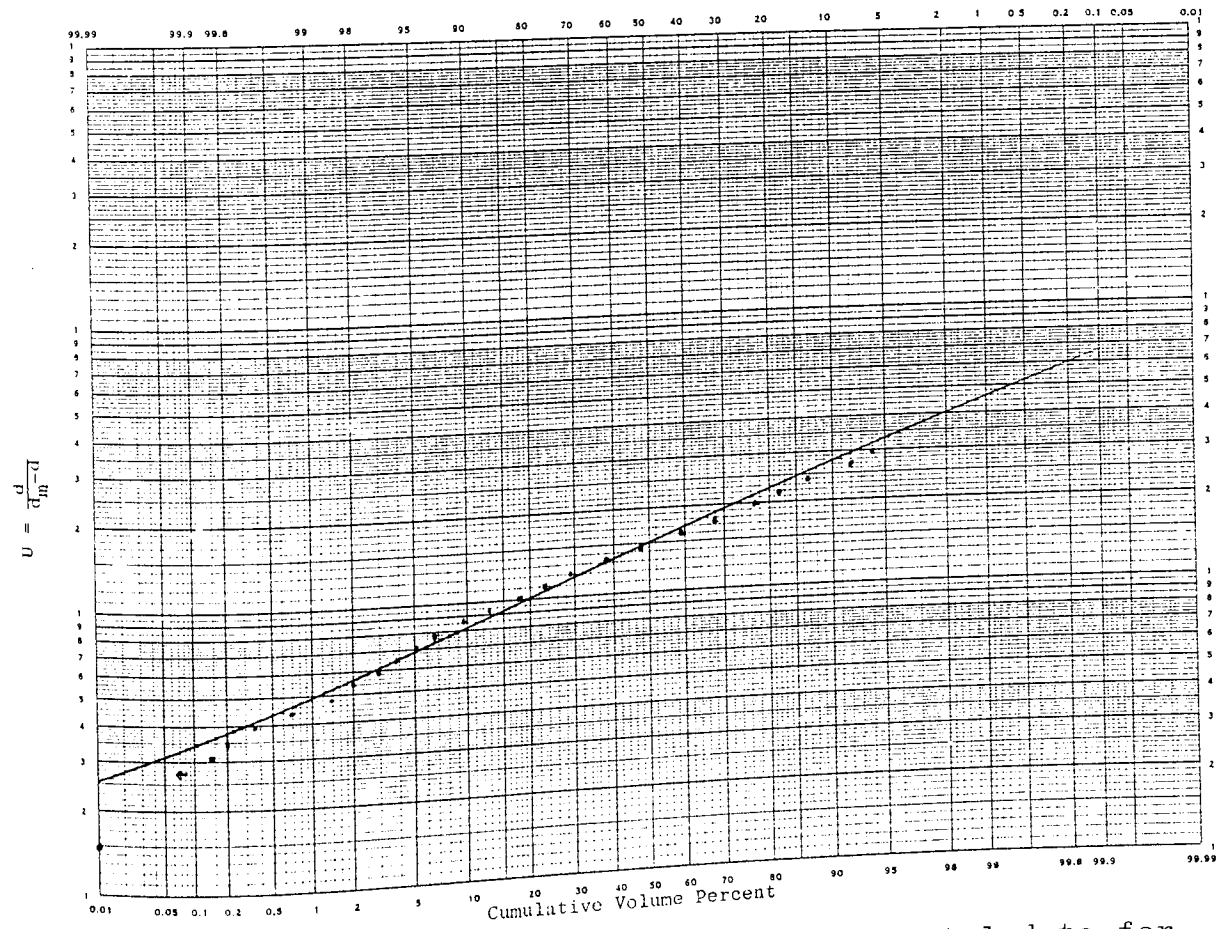

Fig. 8.2-16c Upper limit analysis of experimental data for plate hole size = 0.3175 cm

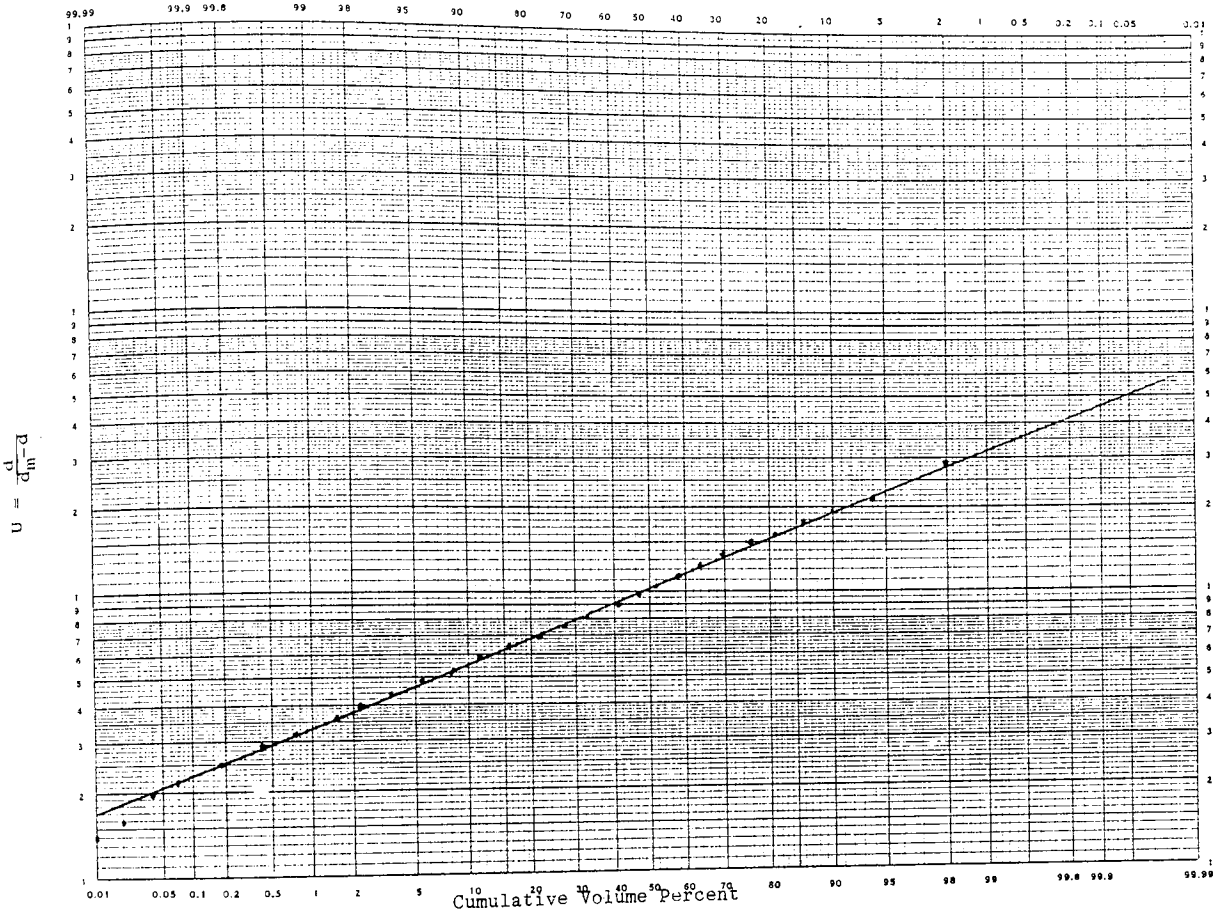

Fig. 8.2-17c Upper limit analysis of experimental data for plate size = 0.4763 cm

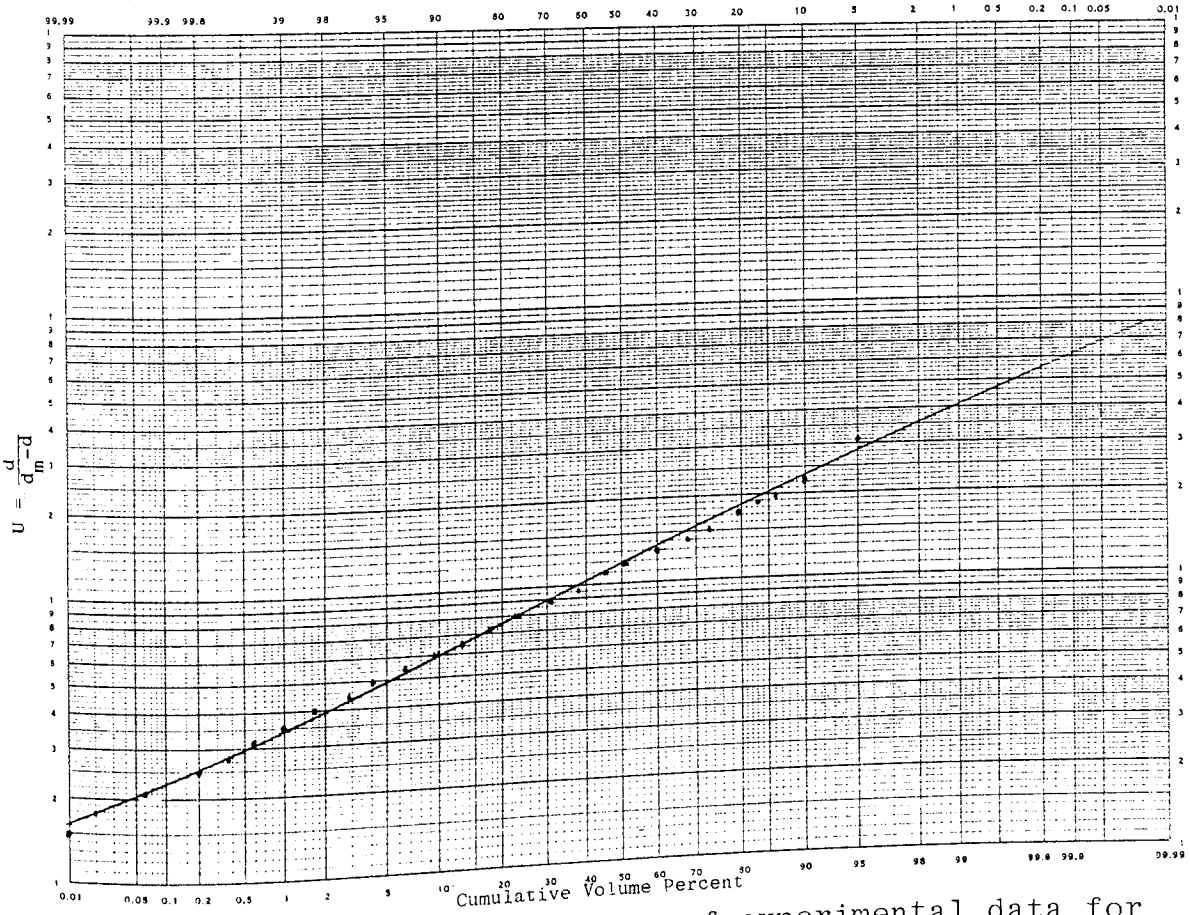

Fig. 8.2-18c Upper limit analysis of experimental data for plate hole size = 0.6350 cm

APPENDIX 16

CALCULATION OF MEAN DROPSIZE USING LOG-NORMAL DISTRIBUTION

D1: From graph Fig. 8.2-15b

Geometric mean diameter $d_{GM} = d_{50\%} = 3.55\text{mm}$

Geometric standard deviation $S_G = \frac{d_{84.14\%}}{d_{50\%}}$

$$= \frac{4.30}{3.55}$$

$$= 1.21$$

Volume-surface (Sauter) mean is given as

$$\text{In } d_{32} = \text{In } d_{GM} + 2.5 \text{ In}^2 S_G$$

$$\log_{10} d_{32} = \log_{10}(3.55) + 2.5 + 2.303 \log_{10}^2(1.21)$$

$$= 0.5502 + 0.0395$$

$$= 0.5897$$

$$\therefore d_{32} = 3.89\text{mm}$$

D2: From graph Fig. 8.2-16b

$$d_{GM} = 4.6\text{mm}$$

$$S_G = \frac{5.5}{4.6} = 1.20$$

$$\log_{10} d_{32} = \log_{10}(4.6) + 2.5 \times 2.303 \log_{10}^2(1.20)$$

$$= 0.6628 + 0.0361$$

$= 0.6983$

$\therefore\ d_{32} = 5.0$ mm

D3 : From graph Fig. 8.2-17b

$d_{GM} = 5.60$ mm

$S_G = \frac{7.20}{5.60} = 1.29$

$$\log_{10} d_{32} = \log_{10}(5.60) + 2.5 \times 2.303 \log_{10}^{2}(1.29)$$

$$= 0.742 + 0.0704$$

$$= 0.8186$$

$\therefore\ d_{32} = 6.59$ mm.

D4 : From graph Fig. 8.2-18b

$d_{GM} = 6.00$ mm

$S_G = \frac{7.60}{6.00} = 1.27$

$$\log_{10} d_{32} = \log_{10}(6.00) + 2.5 \times 2.303 \log_{10}^{2}(1.27)$$

$$= 0.7782 + 0.0620$$

$$= 0.8402$$

$\therefore\ d_{32} = 6.92$ mm

$$\delta = \frac{0.394}{\log_{10}(d_{90}/d_{GM})}$$

From graph Fig. 8.2-15b

$d_{90} = 4.60$ mm, $d_{GM} = 3.55$ mm

$$\delta = \frac{0.394}{\log_{10}(\frac{4.60}{3.55})} = 3.50$$

From graph Fig. 8.2-16b

$d_{90} = 5.80$ mm, $d_{GM} = 4.60$ mm

$$\delta = \frac{0.394}{\log_{10}(\frac{5.80}{4.60})} = 3.91$$

From graph Fig. 8.2-17b

$d_{90} = 7.60$ mm, $d_{GM} = 5.60$ mm

$$\delta = \frac{0.394}{\log_{10}(\frac{7.60}{5.60})} = 2.97$$

From graph Fig. 8.2-18b

$$d_{90} = 8.20 \text{ mm}, \qquad d_{GM} = 6.0 \text{ mm}$$

$$\delta = \frac{0.394}{\log_{10}(\frac{8.20}{6.0})} = 2.90$$

APPENDIX 17

CALCULATION OF MEAN DROP SIZE USING UPPER-LIMIT DISTRIBUTION

$$\frac{d_m}{d_{50}} = \frac{d_{50}(d_{90}+d_{10})-2d_{90}d_{10}}{d_{50}^2 - d_{90}d_{10}}$$

D1: From graph Fig. 8.2-15a

d_{10} = 2.80 mm; d_{50} = 3.60 mm; d_{90} = 4.40 mm

$$\frac{d_m}{3.60} = \frac{3.60(4.40+2.80)-2x4.40x2.80}{(3.60)^2 - 4.40x2.80}$$

$$= \frac{25.92-24.64}{12.96-12.32}$$

$$= \frac{1.28}{0.64} = 2.0$$

$\therefore d_m$ = 7.20 mm

D2: From graph Fig. 8.2-16a

d_{10} = 3.5 mm; d_{50} = 4.60 mm; d_{90} = 5.60 mm

$$\frac{d_m}{4.60} = \frac{4.60(5.60+3.50)-2x5.60x3.5}{(4.60)^2-5.60x3.5}$$

$$= \frac{41.86-39.2}{21.16-19.60}$$

$$= \frac{2.66}{1.56} = 1.71$$

$\therefore d_m$ = 7.87

D3: From graph Fig. 8.2-17a

$$d_{10} = 4.00 \text{ mm}; \quad d_{50} = 5.60 \text{ mm}; \quad d_{90} = 7.20 \text{ mm}$$

$$\frac{d_m}{5.60} = \frac{5.60(7.20+4.0)-2x7.20x4.0}{(5.60)^2-7.20x4.0}$$

$$= \frac{62.72-57.60}{31.36-28.80}$$

$$= \frac{5.12}{2.56} = 2$$

$$\therefore d_m = 11.20 \text{ mm}$$

D4: From graph Fig. 8.2-18a

$$d_{10} = 4.30 \text{ mm}; \quad d_{50} = 6.20 \text{ mm}; \quad d_{90} = 8.00 \text{ mm}$$

$$\frac{d_m}{6.20} = \frac{6.20(8.00+4.30)-2x8.0x4.30}{(6.20)^2-8.0x4.30}$$

$$= \frac{76.26 - 68.80}{38.44 - 34.40}$$

$$= \frac{7.46}{4.04} = 1.85$$

$$\therefore d_m = 11.47 \text{ mm}$$

$$\delta = \frac{0.394}{\log_{10}(U_{90}/U_{50})}$$

From Graph Fig. 8.2-15c

U_{50} 1 1.04; $U_{90} = 1.85$

$$\delta = \frac{0.394}{\log_{10}(\frac{1.85}{1.04})} = 1.85$$

$$d_{32} = \frac{d_m}{(1+aR^{\frac{1}{4\delta^2}})} \qquad d_m = 7.20 \text{ mm}$$

where $a = \frac{d_m - d_{50}}{d_{50}}$

but $U = \frac{d}{d_m - d}$

$\therefore$ $a = \frac{1}{U_{50}}$

Thus $a = \frac{1}{1.04} = 0.96$

$$d_{32} = \frac{7.2}{(1+0.96\ e^{\frac{1}{4(1.58)^2}})}$$

$$= \frac{7.2}{(1+0.96 \times e^{0.1001})} = \frac{7.2}{(1+0.96 \times 1.1053)}$$

$$= \frac{7.2}{2.06}$$

$\therefore$ $d_{32} = 3.50$ mm

$$\delta = \frac{0.394}{\log_{10}(U_{90}/U_{50})}$$

From graph D1-3

$$U_{50} = 1.04; \qquad U_{90} = 1.85$$

$$\delta = \frac{0.394}{\log_{10}(\frac{1.85}{1.04})} = 1.58$$

$$d_{32} = \frac{d_m}{(1+aR^{\frac{1}{48^2}})} \qquad d_m = 7.20 \text{ mm}$$

where $a = \frac{d_m - d_{50}}{d_{50}}$

but $U = \frac{d}{d_m - d}$

$\therefore \quad a = \frac{1}{U_{50}}$

Thus $a = \frac{1}{1.04} = 0.96$

$$d_{32} = \frac{7.2}{(1+0.96\ e^{\frac{1}{4(1.58)^2}})}$$

$$= \frac{7.2}{(1+0.96 \times e^{0.1001})} = \frac{7.2}{(1+0.96 \times 1.1053)}$$

$$= \frac{7.2}{2.06}$$

$\therefore \quad d_{32} = 3.50$ mm

$$\delta = \frac{0.394}{\log_{10}(U_{90}/U_{50})}$$ D2

From graph Fig. 8.2-16c

$$U_{50} = 1.50; \qquad U_{90} = 2.8$$

$$\delta = \frac{0.394}{\log_{10}(\frac{2.8}{1.50})} = 1.45$$

$$d_{32} = \frac{d_m}{(1 + ae^{4\delta^{\frac{1}{2}}})} \qquad d_m = 7.87 \text{ mm}$$

where $a = \frac{d_m - d_{50}}{d_{50}}$

but $U = \frac{d}{d_m - d}$

$\therefore \quad a = \frac{1}{U_{50}}$

Thus $a = \frac{1}{1.50} = 0.67$

$$d_{32} = \frac{7.87}{(1+0.67e^{\frac{1}{4(1.45)^2}})}$$

$$= \frac{7.87}{(1+0.67e^{0.1189})} = \frac{7.87}{(1+0.67 \times 1.1263)}$$

$$= \frac{7.87}{1.76}$$

$\therefore \quad d_{32} = 4.47$ mm

$$\delta = \frac{0.394}{\log_{10}(U_{90}/U_{50})}$$ D3

From graph Fig. 8.2-17c

$U_{50} = 1.02; \quad U_{90} = 1.90$

$$\delta = \frac{0.394}{\log_{10}(\frac{1.90}{1.02})} = 1.46$$

$$d_{32} = \frac{d_m}{(1+ae^{\frac{1}{4\delta^2}})} \qquad d_m = 11.20 \text{ mm}$$

where $a = \frac{d_m - d_{50}}{d_{50}}$

but $U = \frac{d}{d_m - d}$

$\therefore \quad a = \frac{1}{U_{50}}$

Thus $a = \frac{1}{1.02} = 0.98$

$$d_{32} = \frac{11.20}{(1+0.98\ e^{\frac{1}{4(1.46)^2}})}$$

$$= \frac{11.20}{(1+0.98e^{0.1173})} = \frac{11.20}{(1+0.98 \times 1.1244)}$$

$$= \frac{11.20}{2.10}$$

$\therefore \quad d_{32} = 5.33$ mm

$$\delta = \frac{0.394}{\log_{10}(U_{90}/U_{50})}$$

From graph Fig. 8.2-18c

$U_{50} = 1.2$; $U_{90} = 2.35$

$$\delta = \frac{0.394}{\log_{10}(\frac{2.35}{1.20})} = 1.35$$

$$d_{32} = \frac{d_m}{(1+ae^{\frac{1}{4\delta^2}})} \qquad d_m = 11.47 \text{ mm}$$

where $a = \frac{d_m - d_{50}}{d_{50}}$

but $U = \frac{d}{d_m - d}$

$\therefore \quad a = \frac{1}{U_{50}}$

Thus $a = \frac{1}{1.2} = 0.83$

$$d_{32} = \frac{11.47}{(1+0.83e^{\frac{1}{4(1.35)^2}})}$$

$$= \frac{11.47}{(1+0.83e^{0.1372})} = \frac{11.47}{(1+0.83 \times 1.1470)}$$

$$= \frac{11.47}{1.95}$$

$\therefore \quad d_{32} = 5.88$ mm

APPENDIX 18

CALCULATION OF DROP DIAMETER IN JETTING REGION

USING DIFFERENT MODELS

(1) Christensen and Hixson

$$\frac{d}{D_N} = 2.07 \frac{1}{0.485 Eö^{0.5}+1} \qquad Eö = \frac{g\Delta\rho D_N^2}{\sigma}$$

$$= 2.07 \frac{1}{0.485(0.1499)^{0.5}+1} \qquad = \frac{980.7 \times 0.2152 \times (0.1588)^2}{35.5}$$

$\therefore$ d = 0.277 cm $\qquad$ = 0.1499

$$\% \text{ deviation} = \frac{0.277-0.407}{0.277} \qquad = -46.93$$

(2) Perrut and Loutaky

$$\frac{d}{D_N} = 2.07(1 - 0.193 Eö)$$

$$= 2.07(1 - 0.193 \times 0.1499)$$

$\therefore$ d = 0.319 cm

$$\% \text{ deviation} = \frac{0.319-0.407}{0.319} \qquad = -27.59$$

(3) Kumar and Hartland

$$\frac{d}{D_N} = 1.591\left(\frac{\Delta\rho D_N U_N^2}{\sigma}\right)^{-0.068} \left(\frac{\Delta\rho D_N^2 g}{\sigma}\right)^{-0.278}$$

$$= 1.591\left(\frac{0.2152 \times 0.1588 \times (17.64)^2}{35.5}\right)^{-0.068} (0.1499)^{-0.278}$$

$\therefore$ d = 0.465

$$\% \text{ deviation} = \frac{0.465-0.407}{0.465} = 12.47$$

APPENDIX 19

CALCULATION OF VELOCITY IN JETTING REGION

USING DIFFERENT MODELS

(1) Scheele and Meister

$$U_j = \sqrt{3}\left(\frac{\sigma}{\rho_d D_N}\right)^{0.5}\left(1-\frac{D_N}{d}\right)^{0.5}$$

$$= \sqrt{3}\left(\frac{35.5}{0.783 \times 0.1588}\right)^{0.5}\left(1-\frac{0.1588}{0.389}\right)^{0.5}$$

$$= 22.51 \text{ cm sec}^{-1}$$

$$\% \text{ deviation} = \frac{22.51-17.68}{22.51} = 21.64$$

(2) De Chazel and Ryan

$$U_j = \sqrt{\frac{2\sigma}{\rho_d D_N}}\left(1.07-0.75\sqrt{\frac{\Delta\rho g D_N^2}{4\sigma}}\right)$$

$$= \sqrt{\frac{2 \times 35.5}{0.783 \times 0.1588}}\left(1.07-0.75\sqrt{\frac{0.2152 \times 980.7 \times 0.1588^2}{4 \times 35.5}}\right)$$

$$= 22.98 \text{ cm sec}^{-1}$$

$$\% \text{ deviation} = \frac{22.98-17.64}{22.98} = 23.24$$

(3) Fujinawa et al.

$$U_j = 4.4\sigma^{0.2} D_N^{-0.5}$$

$$= 4.4(35.5)^{0.2} \times (0.1588)^{-0.5}$$

$$= 22.55 \text{ cm sec}^{-1}$$

$$\% \text{ deviation} = \frac{22.55 - 17.64}{22.55} = 21.77$$

APPENDIX 20

CALCULATION OF DROP VOLUME FROM DISTRIBUTOR

1. Scheele and Meister

$$V = \psi\left[\frac{\theta\pi D_N}{\Delta\rho g} + \frac{5\mu_c \pi D_N^3 U_N}{d^2 \Delta\rho g} - \frac{\rho_D \pi D_N^2 U_N^2}{3\Delta\rho g} + 4.5\left(\frac{\sigma\pi^2 \rho_D D_N^2 U_N^2}{16(\Delta\rho)^2 g^2}\right)^{1/3}\right]$$

$$\frac{\sigma\pi D_N}{\Delta\rho g} = \frac{35.5 \times \pi \times 0.4763}{0.2152 \times 980.7} = 0.2517$$

$$\frac{5\mu_c \pi D_N^3 U_N}{d^2 \Delta\rho g} = \frac{5 \times 0.01 \times \pi (0.4763)^3 \times 6.64}{(0.771)^2 \times 0.2152 \times 980.7} = 0.0009$$

$$\frac{\rho_D \pi D_N^2 U_N^2}{3\Delta\rho g} = \frac{0.783 \times \pi (0.4763)^2 (6.64)^2}{3 \times 0.2152 \times 980.7} \; 1 \; 0.0389$$

$$4.5\left(\frac{\sigma\pi^2 \rho_D D_N^2 U_N^2}{16(\Delta\rho)^2 g^2}\right)^{1/3} = 4.5\left(\frac{35.5 \times \pi^2 \times 0.783 \times (0.4563)^6 (6.64)^2}{16(0.2152)^2 (980.7)^2}\right)$$

$$= 0.2631$$

$$V = \psi(0.2517 + 0.0009 - 0.0389 + 0.2631)$$

$$V = \psi(0.47684) \text{ cm}^3$$

$$\left(\frac{\psi}{V}\right)^{1/3} D_N = \left(\frac{1}{0.47684}\right)^{1/3} D_N$$

$$= \left(\frac{1}{0.47684}\right)^{1/3} \times 0.4763$$

$$\therefore D_N\left(\frac{\psi}{V}\right)^{1/3} = 0.6095$$

From the Harkin-Brown correction factor plot, $\psi \doteq 0.71$. The size of drops formed at the distributor $V \doteq \psi(0.47684)$

$$V = 0.71 \times 0.47684$$

$$d = \left(\frac{6V}{\pi}\right)^{1/3} = \left(\frac{6 \times 0.339}{\pi}\right)^{1/3} = 0.865 \text{ cm}$$

Present work $d = 0.771$ cm

$$\therefore V = \frac{\pi d^3}{6} = \frac{(0.771)^3}{6} \simeq 0.24 \text{ cm}^3$$

$$\% \text{ deviation} = \frac{0.339 - 0.240}{0.339} = 29.20$$

2. Izard

$$V = \left| \frac{\pi D_N}{\Delta\rho g} + \frac{\pi D_N U_N \mu_C}{2\Delta\rho g}\left(\frac{\mu_C + 1.5\mu_D}{\mu_C + \mu_D}\right) - \frac{\pi D^2 U_N^2 \rho_D}{3\Delta\rho g}\left(1 - \frac{2\rho_D}{2\rho_D + \rho_C}\right) \right|$$

$$\frac{\pi D_N \sigma}{\Delta\rho g} = \frac{35.5 \times 0.4763 \times \pi}{0.2152 \times 980.7} = 0.2517$$

$$\frac{\pi D_N U_N \mu_C}{2\Delta\rho g}\left(\frac{\mu_C + 1.5\mu_D}{\mu_C + \mu_D}\right) = \frac{\pi \times 0.4763 \times 6.64 \times 0.01}{2\ 0.2152 \times 980.7}\left(\frac{0.01 + 1.5 \times 0.017}{0.01 + 0.017}\right)$$

$$= 0.00031$$

$$\frac{\pi D_N^2 U_N^2 \rho_D}{3\Delta\rho g}\left(1 - \frac{2\rho_D}{2\rho_D + \rho_C}\right)$$

$$\frac{\pi (0.4763)^2 (6.64)^2 \times 0.783}{3 \times 0.2152 \times 980.7}\left(1 - \frac{2 \times 0.783}{2 \times 0.783 \times 0.9982}\right)$$

$$= 0.015128$$

$$V = 0.2517 + 0.00031 - 0.015128$$

$$= 0.237 \text{ cm}^3$$

$$\% \text{ deviation } \frac{0.237 - 0.240}{0.237} = -1.27$$

$$\therefore d = \left(\frac{6V}{\pi}\right)^{1/3} = 0.768 \text{ cm}$$

3. Kagan, Kovaleu and Zakherychev

$$V = \pi\psi a^3 R(1+2.39W^{1/3}-0.485W)$$

$$a = \left(\frac{2\sigma}{\Delta\rho g}\right)^{0.5} = \left(\frac{2x35.5}{0.2152x980.7}\right)^{0.5} = 0.5800$$

$$\therefore \quad a^3 = 0.19513$$

$$W = \frac{(\rho_c+\rho_D)U_N^2 D_N}{2\sigma} = \frac{(0.9982+0.783)(6.64)^2(0.4763)}{2x35.5}$$

$$= 0.52683$$

$$W^{1/3} = 0.8078$$

$$R = \frac{D_N}{2a} = \frac{0.4763}{2x0.5800} = 0.4106$$

$$V = \psi x\pi x0.19513x0.4106(1+2.39x0.8078-0.485x0.52683)$$

$$\frac{V}{\psi} = 0.67335 \qquad \simeq 0.6734$$

$$\frac{\psi}{V} = \frac{1}{0.6734}$$

$$\left(\frac{\psi}{V}\right)^{1/3} D_N = \left(\frac{1}{0.6734}\right)(0.4763)$$

$$= 1.4303$$

From the Harkin-Brown correction factor plot, $\psi = 0.59$

The size of drops formed at the distribution $V = \psi x0.6734$

$$V = 0.59x0.6734$$

$$= 0.397 \text{ cm}^3$$

$$\% \text{ deviation} = \frac{0.397-0.240}{0.397}$$

$$\therefore \quad d = \left(\frac{6V}{\pi}\right)^{1/3} = 0.912 \text{ cm}$$

APPENDIX 21

CALCULATION OF EXPERIMENTAL MASS TRANSFER

$U''_C = 0.28\ cmsec^{-1}$ $U''_D = 0.22\ cmsec^{-1}$

Hold-up = 0.0641 $H_E = 190.0$ cm $d_{32} = 0.389$

$y^* = 9.2x$

where 9.2 is the slope of the equilibrium line shown in Appendix 12.

	y	x	y*	$\Delta y = y^* - y$
Bottom	1.00	2.30	21.16	20.16
Comp 1	0.34	1.49	13.71	13.37
Comp 2	0.30	1.39	12.79	12.49
Comp 3	0.28	1.35	12.42	12.14
Top	0.00	1.02	9.38	9.38

where y = acetone concentration in the aqueous phase

Δy = driving force in each compartment

The mean driving force Δy_m was estimated by applying Simpson's Rule and then converted to the mean concentration driving force (ΔC_m)

$$\Delta y_m = \frac{1}{12}\left[\Delta y_{bottom} + \Delta y_{top} + (\Delta y_1 + \Delta y_3) + 2 \times \Delta y_2\right]$$

$$= \frac{1}{12}\left[20.16 + 9.38 + (13.37 + 12.14) + 2 \times 12.49\right]$$

$$\Delta y_m = 13.0467 \ \frac{\text{gm. acetone}}{\text{100gm aqueous solution}}$$

or

$$\Delta y_m = 0.1305 = \frac{\text{gm acetone}}{\text{gm aqueous solution}}$$

Density of aqueous phase solution $\simeq 0.9983$ gm/cm^3

$$\Delta C_m = \frac{0.1305}{0.9982} = 0.1307 \frac{\text{gm acetone}}{\text{cm}^3 \text{ solution}}$$

Effective volume of the column = $H_E \times A_C$

$$= 190 \times \frac{\pi}{4} (45)^2$$

$$= 302181.94 \text{ cm}^3$$

where A_C = cross-section area of column.

Total downcomer volume = 17690 cm^3.

∴ Actual effective volume of the column = 302181.94-17690

$$= 284491.94 \text{ cm}^3$$

The specific interfacial area $a = \frac{6x}{d_{32}}$

where x = fractional hold-up

$$a = \frac{6 \times 0.0641}{0.389} = 0.9887 \text{ cm}^2/\text{cm}^3$$

∴ Total interfacial area A = aV

$$= 284491.94 \times 0.9887$$

$$= 281277.18 \text{ cm}^2$$

Rate of mass transfer $N = Q_C\rho_C(y_{OUT}-u_{IN}) = Q_D\rho_D(X_{IN}-X_{OUT})$

or

$$N = U''_C A_C \rho_C (Y_{OUT}-Y_{IN}) = U''_D A_C \rho_D (X_{IN}-X_{OUT})$$

$$= 0.28\times1590.43\times0.9882\ (0.01-0.00)$$

$$= 4.4452\ \text{gm/sec}$$

$$K_{Expt.} = \frac{N}{A(\Delta C_m)}$$

$$= \frac{4.4452}{281277.18\times0.1307} = 1.21\times10^{-4}\ \text{cmsec}^{-1}$$

or

$$K_{Expt.}\cdot a = \frac{N}{V(\Delta C_m)}$$

$$= \frac{4.4452}{284491.24\times0.1307}$$

$$= 1.20\times10^{-4}\ \text{gm/sec cm}^3(\Delta C_m)$$

APPENDIX 22

CALCULATION OF MASS TRANSFER COEFFICIENT USING CORRELATIONS

The characteristic velocity of drops U_S in the sieve plate column was determined by applying Thornton correlation (148).

$$U_S = \frac{U_D}{X} + \frac{U_C}{1-X}$$

$$= \frac{0.22}{0.0641} + \frac{0.28}{1-0.0641}$$

$$\therefore \quad U_S = 3.73 \text{ cmsec}^{-1}$$

1. STAGNANT DROPS REGIME

The maximum diameter of the stagnant drop in the whole drop population when droplet Reynolds number R_e =10 was found from

$$R_e = \frac{\rho_D U_S d_s}{\mu_C}$$

$$d_s = \frac{10 \times 0.01}{0.783 \times 3.73}$$

$$d_s = 0.034 \text{ cm}$$

The minimum diameter of the oscillating drops regime when R_e = 200 was

$$d_o = \frac{200 \times 0.01}{0.783 \times 3.73}$$

$\therefore d_o = 0.685$ cm

From the cumulative drop size of Figure 8.2-15a in Appendix 12, the drop size for stagnant drops d_s was found to be too small to be included in the calculation Hence, the drop population for 0.1588 cm hole size was considered to contain only circulating and oscillating drops regime with d_o as boundary between the two regimes. Therefore, from Figure 8.2-15a the fractional proportion of the circulating drops $\varepsilon=0.20$ and the oscillating drops fractional proportion - $1-\varepsilon=0.8$.

2. CIRCULATING DROPS REGIME

(a) Dispersed and continuous phase mass transfer coefficient was estimated by Handlos and Baron (59) correlations.

$$k_{d.c} = \frac{0.00375 U_s}{1+\mu_d/\mu_c}$$

$$= \frac{0.00375 \times 3.73}{1+\frac{0.01}{0.017}} = 8.81\times10^{-3} \text{ cmsec}^{-1}$$

$$k_{c.c} = \left(\frac{4\varnothing_c U_s}{\pi \bar{d}_c}\right)^{0.5}$$

where $\bar{d}_c = 0.28$ cm from Figure 8.2-15a

$$= \left(\frac{4\times1.1\times10^{-5}\times3.73}{\pi\times0.28}\right)^{0.5} = 1.37\times10^{-2} \text{ cmsec}^{-1}$$

Overall mass transfer coefficient

$$\frac{1}{K_{o.c}} = \frac{1}{k_{a.c}} + \frac{m}{k_{c.c}}$$

$$= \frac{1}{0.00881} + \frac{9.2}{0.0137}$$

$$\therefore K_{o.c(1)} = 1.27\times10^{-3} \text{ cmsec}^{-1}$$

(b) Dispersed phase mass transfer coefficient was estimated by Kronig and Brink (91) equation

$$K_{d.c} = \frac{17.9\mathscr{D}_d}{\bar{d}_c}$$

$$= \frac{17.9\times1.37\times10^{-5}}{0.28} = 8.76\times10^{-4} \text{ cmsec}^{-1}$$

Continuous phase mass transfer coefficient was estimated by Garner et al. (40) correlations

$$Sh = -126 + 1.8\, R_e^{0.5}\, S_c^{0.42}$$

$$\frac{k_{c.c}\ 0.28}{1.1\times10^{-5}} = -126+1.8\left(\frac{0.9982\times3.73\times0.28}{0.01}\right)^{0.5}\left(\frac{0.01}{0.9882\times1.1\times10^{-5}}\right)^{0.42}$$

$$\therefore k_{c.c} = 6.02\times10^{-4} \text{ cmsec}^{-1}$$

$\therefore$ Overall mass transfer coefficient

$$\frac{1}{K_{o.c}} = \frac{1}{8.76\times10^{-4}} + \frac{9.2}{6.02\times10^{-4}}$$

$$\therefore K_{o.c(2)} = 6.10\times10^{-5} \text{ cmsec}^{-1}$$

3. OSCILLATING DROPS REGIME

(a) Dispersed phase mass transfer coefficient was firstly estimated by Rose and Kintner (129) correlation

$$k_{d.o} = 0.45(\mathcal{D}_d\omega)^{0.5}$$

$$\omega^2 = \frac{\sigma b}{r^3}\left[\frac{n(n-1)(n+1)(n+2)}{(n+1)\rho_d + n\rho_c}\right]$$

$$n = 2; \qquad b = \frac{\bar{d}_o^{0.225}}{1.242}$$

$$b = \frac{(0.39)^{0.225}}{1.242} = 0.6514; \qquad r^3 = \left(\frac{0.39}{2}\right)^3 = 0.0074$$

$$\omega^2 = \frac{35.5\times0.6514}{0.0074}\left[\frac{2(1)(3)(4)}{3\times0.783+2\times0.9982}\right]$$

$$\therefore \omega = 131.38 \text{ sec}^{-1}$$

$$\therefore k_{d.o} = 0.45(1.37\times10^{-5}\times131.38)^{0.5}$$

$$= 1.91\times10^{-2} \text{ cmsec}^{-1}$$

Continuous phase mass transfer was estimated by Garner et al (43) correlation

$$Sh = 50+0.0085\ R_e S_c^{0.7}$$

$$\frac{k_{c.o}\ \bar{d}_o}{\mathcal{D}_c} = 50 + 0.0085\left(\frac{\rho_c U_s \bar{d}_o}{\mu_c}\right)\left(\frac{\mu_c}{\rho_c\ c}\right)^{0.7}$$

$$\frac{k_{c.o}\times 0.39}{1.1\times 10^{-5}} + 50 + 0.0085\left(\frac{0.998\times 3.73\times 0.39}{0.01}\right)\left(\frac{0.01}{0.9982\times 1.1\times 10^{-5}}\right)^{0.7}$$

$$\therefore\ k_{c.o} = 5.52\times 10^{-3}\ \text{cmsec}^{-1}$$

Overall mass transfer coefficient

$$\frac{1}{K_{O.O(1)}} = \frac{1}{0.0191} + \frac{9.2}{0.00552}$$

$$\therefore\ K_{O.O(1)} = 5.81\times 10^{-4}\ \text{cmsec}^{-1}$$

(b) Angelo et al (4) correlations

$$k_{d.o} = \left[\frac{4\phi_d\omega(1+\delta+\frac{3}{8}\delta^2)}{\pi}\right]^{0.5}$$

$$\delta = 0.434\left(\frac{\omega\bar{d}_o}{U_s}\right)^{-0.46}\left(\frac{\rho_c U_s^2 \bar{d}_o}{\sigma}\right)^{-0.53}\left(\frac{\mu_c U_s}{B}\right)^{-0.11}$$

$$= 0.434\left(\frac{131.38\times 0.39}{3.73}\right)^{-0.46}\left(\frac{0.01\times(3.73)^2\times 0.39}{35.5}\right)^{-0.53}\left(\frac{0.01\times 3.73}{35.5}\right)^{-0.11}$$

$$\therefore\ \delta = 1.90$$

$$k_{d.o} = \left[\frac{4\times 1.37\times 10^{-5}\times 131.38(1+1.90+\frac{3}{8}(1.90)^2}{\pi}\right]^{0.5}$$

$$\therefore\ k_{d.o} \simeq 0.099$$

$$K_{O.O} = k_d \left[\frac{1}{1+m\left(\frac{\phi_d}{\phi_c}\right)^{0.5}} \right]$$

$$\therefore \quad K_{O.O(2)} = 0.099 \left[\frac{1}{1+9.2\left(\frac{1.37\times10^{-5}}{1.10\times10^{-5}}\right)^{0.5}} \right]$$

$$\simeq 8.80\times10^{-3}$$

Therefore, the overall mass transfer coefficient for the whole drop population (i.e. circulating and oscillating drops) is

$$K_{correlation} = K_{O.c} \times \varepsilon + K_{O.O}(1-\varepsilon)$$

(1) For Handlos and Baron, Rose and Kintner and Garner et al

$$K_{correlation} = 1.27\times10^{-3}\times0.2+5.81\times10^{-4}\times0.8$$

$$= 7.19\times10^{-4} \text{ cmsec}^{-1}$$

(2) For Kronig and Brink, Rose and Kintner and Garner et al

$$K_{correlation} = 6.10\times10^{-5}\times0.2+5.81\times10^{-4}\times0.8$$

$$= 4.77\times10^{-4} \text{ cmsec}^{-1}$$

(3) For Handlos and Baron and Angelo et al

$$K_{correlation} = 1.27\times10^{-3}\times0.2+2.47\times10^{-3}\times0.8$$

$$= 2.23\times10^{-3} \text{ cmsec}^{-1}$$

(4) For Kronig and Brink and Angelo et al

$$K_{correlation} = 6.10\times10^{-5}\times0.2+2.47\times10^{-3}\times0.8$$

$$= 1.99\times10^{-3} \text{ cm sec}^{-1}$$

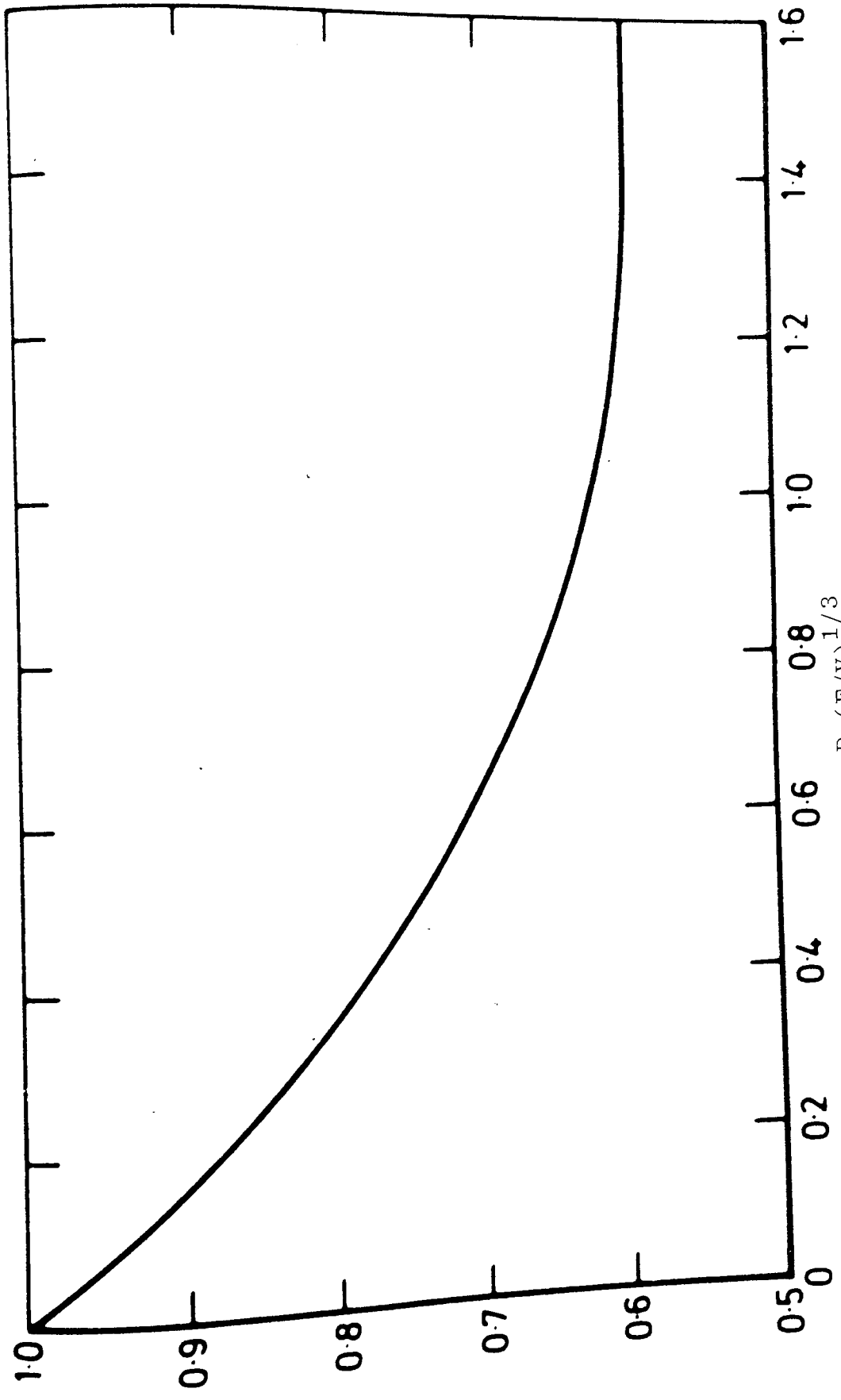

Harkin-Brown Correction Factor

F

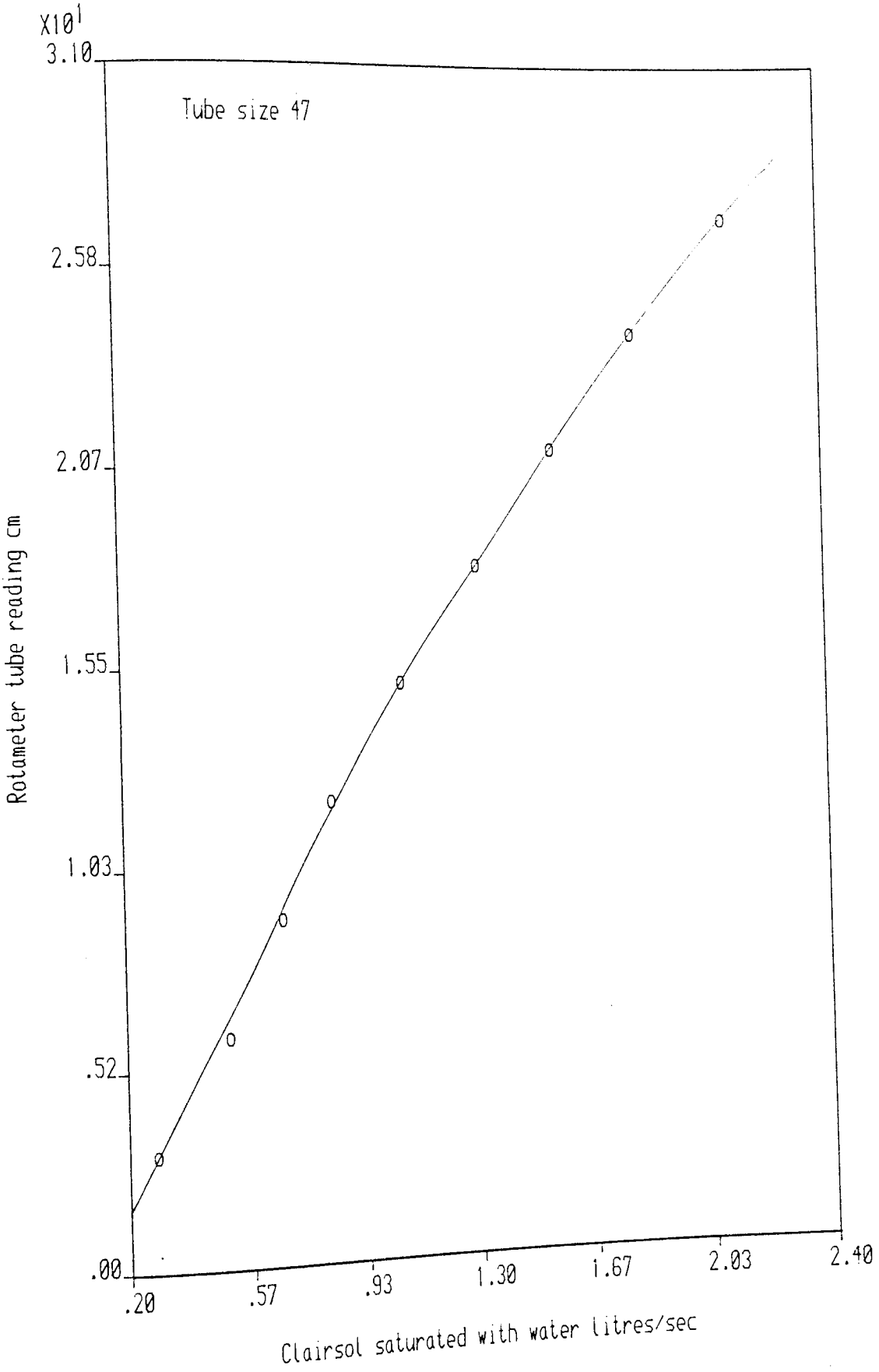

Calibration curve for saturated clairsol '350' at 20 c

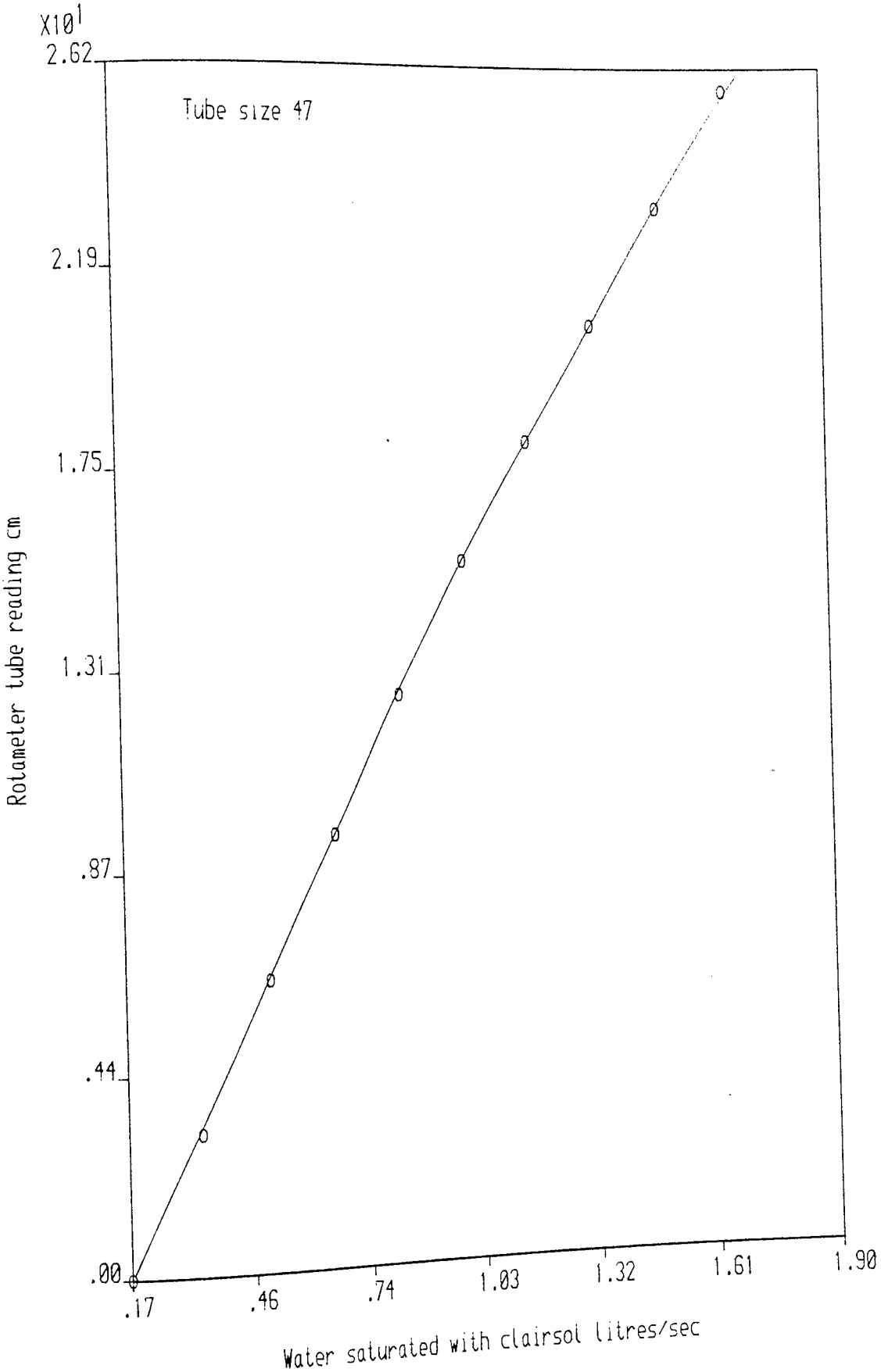

Calibration curve for saturated de-ionised water at 20 C

APPENDIX 25

```
0          TRACE 2
1          MASTER EQUILIB
2          REAL X(150),Y(150),XX1(2),YY1(2)
3          READ(1,50)N
4          DO 60 I=1,N
5          READ(1,40) X(I),Y(I)
6       60 CONTINUE
7          CALL APPLE(X,Y,N,B,A,R,S,XX1,YY1)
8          CALL PLOT(X,Y,N,XX1,YY1)
9       50 FORMAT(I0)
10      40 FORMAT(2F0.0)
11         STOP
12         END
13         SUBROUTINE APPLE(X,Y,N,B,A,R,S,XX1,YY1)
14 C       LINEAR REGRESSION
15         DIMENSION X(150),Y(150),XX1(2),YY1(2)
16         SUMX=0.0
17         SUMY=0.0
18         SUMX2=0.0
19         SUMY2=0.0
20         SUMXY=0.0
21         DO 750 I=1,N
22         SUMX=SUMX+X(I)
23         SUMY=SUMY+Y(I)
24         SUMX2=SUMX2+X(I)**2
25         SUMY2=SUMY2+Y(I)**2
26         SUMXY=SUMXY+X(I)*Y(I)
27      750 CONTINUE
28         V=N
29         XM=SUMX/V
30         YM=SUMY/V
31         B=(SUMXY-V*XM*YM)/(SUMX2-V*XM**2)
32         A=YM-B*XM
33         XX1(1)=3.50
34         YY1(1)=A
35         XX1(2)=18.0
36         YY1(2)=A+18.0*B
37         WRITE(2,780) XX1,YY1
38         WRITE(2,800) A,B
39      780 FORMAT(2F10.4)
40      800 FORMAT(1H ,'INTERCEPT A=',F10.4,20X,'GRADIENT B=',F10.4)
41 C       CORRELATION COEFFICIENT R
42         R1=(SUMXY-SUMX*SUMY/V)**2
43         R2=SUMX2-SUMX**2/V
44         R3=SUMY2-SUMY**2/V
45         R=R1/(R2*R3)
46 C       STANDARD DEVIATION
47         S=SQRT((SUMY2-A*SUMY-B*SUMXY)/(V-2))
48         WRITE(2,840) S,R
49      840 FORMAT(1H ,'STANDARD DEVIATION=',F8.3/,1H ,
50        *'CORRELATION CO-EFFICIENT=',F8.3)
51         WRITE(2,860)
52      860 FORMAT(1H ,'AVERAGE VALUES')
53         RETURN
54         END
```

```
      SUBROUTINE PLOT(X,Y,N,XX1,YY1)
      REAL XX1(2),YY1(2)
      DIMENSION X(N),Y(N)
      CALL OPENGINOGP
      CALL SOFCHA
      CALL UNITS(0.60)
      CALL CHASIZ(3.0,5.0)
      CALL SHIFT2(100.0,100.0)
      CALL AXIPOS(1,0.0,0.0,200.0,1)
      CALL AXIPOS(1,0.0,0.0,200.0,2)
      CALL AXISCA(3,6,0.0,30.0,1)
      CALL AXISCA(3,6,0.0,4.0,2)
      CALL AXIDRA(1,1,1)
      CALL AXIDRA(-1,-1,2)
      CALL GRASYM(X,Y,6,5,0)
   35 CONTINUE
      CALL MOVTO2(-17.0,-50.0)
      CALL CHAHOL(80HE*LQUILIBRIUM DISTRIBUTION OF ACETONE BETWEEN WATER
     +AND CLAIRSOL'350' AT *U20 C*.)
      CALL MOVTO2(110.0,30.0)
      CALL CHAHOL(16H*LY =*U9.18*LX*.)
      CALL MOVTO2(31.0,-25.0)
      CALL CHAHOL(50HW*LEIGHT PERCENT ACETONE IN AQUEOUS(WATER) PHASE*.)
      CALL CHAANG(90.0)
      CALL MOVTO2(-25.0,26.5)
      CALL CHAHOL(53HW*LEIGHT PERCENT ACETONE IN SOLVENT(CLAIRSOL) PHASE
     +*.)
      CALL DEVEND
      RETURN
      END
      FINISH
```

NOMENCLATURE

NOMENCLATURE

A	interfacial area
a	Laplace constant
a_c	surface area per drop of coalescence, cm^2
a_f	surface area per drop of formation, cm^2
a_s	surface area per unit volume
B_n	eigenvalue
C	concentration of solute in one of the two phases, gmoles/ml
C_D	drag coefficient
C_o	concentration of solute at t = o, gmoles/ml
C_x	concentration distribution of centinuous phase in the column
C_{x1}, C_{x_o}	concentration of continuous phase inside and outside the column
C_y	concentration distribution of dispersed phase in the column
C^*	concentration of solute in equilibrium with the other phase, gmoles/ml
D, d	diameter of a solid sphere; equivalent diameter of a drop, cm
d_c	critical droplet size, cm
d_{32}	equilibrium value of the mean droplet size
	volumetric diffusivity, $cm^2 s^{-1}$
d	dispersed phase volumetric diffusivity, $cm^2 s^{-1}$

D_e	equivalent droplet diameter = $6V_D/\pi^{\frac{1}{3}}$, cm
D_F	diameter of detached drop, cm
D_H	horizontal diameter of droplet, $D_e E^{\frac{1}{3}}$
D_j	jet diameter, cm
D_N	inside diameter of nozzle, cm
D_V	vertical diameter of droplet, $D_e F^{-2/3}$
E	droplet eccentricity = D_H/D_V
Eö	Eötvös number = $\Delta\rho d^2 g/\sigma$
F_{HB}, f	Harkins and Brown correction factor
F_R	flow ratio at flooding
g	gravitational acceleration (980.7)cm s^{-2}
g_c	conversion factor
h	column height, cm
h_E	effective height of the column; height between injection point and the principal interphase
h_t	total depth of dispersed phase beneath the plates
H_c	plate spacing, cm
I_F	raffinate oil refractive index for the feed
I_f	intercept on the ϕ-axis of the two stage runs
I_N	raffinate oil refractive index for the top stage N of the entrained extractor
k	average individual mass transfer coefficient, cm/sec
k'	instantaneous individual mass transfer co-efficient cm/sec
k_c	continuous phase film coefficient, cm/sec

k_d	dispersed phase film coefficient, cm/sec
k_{cf}	average individual mass transfer coefficient for continuous formation
k_{df}	mass transfer at formation; dispersed phase mass transfer coefficient based on the final area of the drop, cm/sec
K	overall mass transfer coefficient
K_{ox}	overall mass transfer coefficient related to phase x
L	mixing section length or distance
m	distribution coefficient; solute partition coefficient or equilibrium line slope
$m_{A(t)}$	total amount of solute transferred during formation
n	mode of oscillation
N	solute transferred across phase boundary in a given time, gmoles/cm^2,
N'	instantaneous flow across phase boundary, gmoles/cm^2
N_{Fr}	Froude number = U_D^2/gD
N_{M1}	mass transfer group, $(k_{df}t_f/D)$ and $(k_{dc}t_f/D)$
$(NTU)_{ox}$	true value of number of transfer unit to phase x
N_{oxp}	piston flow values
N_{Re}, R_e	Reynolds number for drops $(\rho_D U_D D/\mu_C)$
N_{Sc}	Schmidt number = μ/ρ_D

N_T	number of theoretical stages for a given feed improvement
N_{We}, We	Weber number = $\rho_D U_D^2 D/\sigma$
Q	dimensionless intercept in the plot of equilbrium concentrations
γ	radius of sphere
S	area of time dependent surface, cm^2
S_o	characteristic reference area for constant surface, cm^2
s	operating line slope
t	time, drop contact time, sec
t_f	formation time, sec
U_c	continuous phase superficial velocity based on total hole area, cm sec^{-1}
U_D, U_d	dispersed phase superficial velocity based on total hole area, cm sec^{-1}
U_c'	continuous phase superficial velocity based on corrected hole area, cm sec^{-1}
U_d'	dispersed phase superficial velocity based on corrected hole area, cm sec^{-1}
U_c''	continuous phase superficial velocity based on column cross-sectional area, cm sec^{-1}
U_d''	dispersed phase superficial velocity based on column cross-sectional area, cm sec^{-1}
$U_{c(f)}$	continuous phase velocity at flooding
$U_{d(f)}$	dispersed phase velocity at flooding

U_N average velocity through the nozzle, cms^{-1}

U_{NM} nozzle velocity at maximum velocity

U_S slip velocity in nozzle, cm/sec

U_t terminal velocity with no wall effect

U_x superficial volumetric flowrate of x phase

V drop volume after break off from the nozzle, cm^3

V_o, V_D volume of drop during and after formation respectively, cm^3

x fractional hold-up of the dispersed phase

x_f hold-up at flooding

Z physical property group = $\sigma^3 \rho_c / g \Delta \rho \mu_c^4$

GREEK LETTERS

ρ_c	continuous phase density, gm cm^{-3}
ρ_D	dispersed phase density, gm cm^{-3}
$\Delta\rho$	density difference, gm cm^{-3}
σ	interfacial tension, dynes cm^{-1}
μ_c	viscosity of continuous phase gm $cm^{-1}s^{-1}$
μ_d	viscosity of dispersed phase
ψ	Harkins and Brown correction factor
δ	skewness parameter, dimensionless amplitude factor
λ	wave length of disturbance, cm
λ_n	eigenvalue
ϕ	$I_F - I_N/I_F$
ϕ_{op}	operational hold-up
ϕ_s	static hold-up
ϕ_t	total hold-up
f	entrainment factor
η_a	apparent efficiency
ω	dimensionless time variable defined as $= t/_{to}$ where t_o is constant with units of time characteristic of the system being considered
	frequency of oscillation, t^{-1}

REFERENCES

REFERENCES

1 Akell, R.B.
Chem. Eng. Progr. 62 No. 9, 50 (1960)

2 Allak, A.M.A. and Jeffreys, G.V.
AIChE. J. 20 No. 3, 564 (1974)

3 Allerton, J., Strom, B.O. and Treybal, R.E.
Trans. Am. Instn. Chem. Engrs. 39, 361 (1943)

4 Angelo, J.B. and Lightfoot, E.N.
AIChE. J. 14 No. 4, 531 (1968)

5 Angelo, J.B., Lightfoot, E.N. and Howard, D.W.
AIChE. J. 12, 751 (1966)

6 Baird, M.I.H.
Chem. Eng. Sci. 9, 267 (1959)

7 Baird, M.I.H. and Hamielec, A.E.
Can. J. Chem. Eng. 40, 119 (1962)

8 Bashforth, F. and Adams, J.C.
"An Attempt to Test the Theories of Capillarity"
University Press Cambridge, 1883

9 Beek, W.J. and Kramers, H.
Chem. Eng. Sci. 16, 909 (1962)

10 Boussinesq, M.J.
Ann. Chem. Phys. 29, 349 (1913)

11 Boye-Christensen, C. and Terjesen, S.G.
Chem. Eng. Sci. 7, 222 (1958)

12 Boye-Christensen, C. and Terjesen, S.G.
Chem. Eng. Sci. 9, 225 (1958)

13 British Petroleum

14 Brown, H. and Hanson, C.
Brit. Chem. Eng. 11 No. 7, 695 (1966)

15 Bussolari, R.J., Schiff, S. and Treybal, R.E.
Ind. Eng. Chem. 45 No. 11, 2413 (1953)

16 Calderbank, P.H. and Korchinski, I.J.O.
Chem. Eng. Sci. 6, 65, 78 (1956)

17 Chao, B.T.
Phys. Fluids 5, 69 (1962)

18 Charles, G.E. and Mason, S.G.
J. Colloid Sci. 15, 105 (1960)

19 Charles, G.E. and Mason, S.G.
J. Colloid Sci. 15, 236 (1960)

20 Chartres, R.H. and Korshinsky, W.J.
Trans. Instn. Chem. Eng. 56, 91 (1978)

21 Christensen, E.G. and Hixson, A.N.
Ind. Eng. Chem. 49 No. 6, 1017 (1957)

22 Cockbain, E.G. and McRoberts, T.S.
J. Colloid Sci. 8, 440 (1953)

23 Crawford, J.W. and Wilke, C.R.
Chem. Eng. Progr. 47, 423 (1951)

24 Damon, K.G., Angelo, J.B. and Park, R.W.
Chem. Eng. Sci. 21, 813 (1966)

25 Davies, G.A. and Jeffreys, G.V.
"Filtration Separation" p349 (1969)

26 Davies, G.A., Jeffreys, G.V. and Afzal, M.
Chem. Eng. (London) p392 (1972)

27 Davies, G.A., Jeffreys, G.V. and Afzal, M.
Brit. Chem. Eng. Proc. Tech. 17 No. 9, 709 (1972)

28 Davies, J. and Vose, R.W.
Proc. Roy. Soc. A286, 218 (1965)

29 Dawodu, F.A.
University of Aston 12th Annual Chem. Eng.
Departmental Symposuim 1981

30 De Chazel, L.E.M. and Ryan, J.T.
AIChE. J. 17, 1226 (1971)

31 Elgin, J.C. and Browning, F.M.
Trans. Am. Instn. Chem. Engrs. 31, 639 (1935),
32, 105 (1936)

32 Elzinga, E.R. and Banchero, J.T.
AIChE. J. 7 No. 3, 394 (1961)

33 Eyring, H.
J. Chem. Phys. 4, 283 (1936)

34 Felix, J.R. and Holder, C.H.
AIChE. J. 1 No. 3, 296 (1955)

35 Friedlander, S.K.
AIChE. J. 3, 43 (1957)

36 Funijawa, K., Maruyama, T. and Nakeike, Y.
Kagaku Kikai, 21, 194 (1957)

37 Gal-Or, B. and Hoescher, H.E.
AIChE. J. 12, 499 (1966)

38 Garner, F.H., Ellis, S.R.M. and Fosbury, D.W.
Trans. Instn. Chem. Engrs. 31, 348 (1953)

39 Garner, F.H., Ellis, S.R.M. and Hill, J.W.
Trans. Instn. Chem. Engrs. 34, 223 (1956)

40 Garner, F.H., Foord, A. and Tayeban, M.
J. Appl. Chem. 9, 313 (1959)

41 Garner, F.H. and Hale, A.B.
Chem. Eng. Sci. 2, 157 (1953)

42 Garner, F.H. and Haycock, P.J.
Proc. Roy. Soc. A252, 457 (1959)

43 Garner, F.H., Nutt. C.W. and Nature, M.F.
Nature 175, 603 (1955)

44 Garner, F.H. and Skelland, A.H.P.
Trans. Instn. Chem. Engrs. 29, 315 (1951)

45 Garner, F.H. and Skelland, A.H.P.
Ind. Eng. Chem. 46, 1255 (1954)

46 Garner, F.H. and Skelland, A.H.P.
Chem. Eng. Sci. 4, 149 (1955)

47 Garner, F.H. and Skelland, A.H.P.
Chem. Eng. Sci. 4 No. 4, 149 (1965)

48 Garwin, L. and Smith, B.D.
Chem. Eng. Progr. 49, 591 (1953)

49 Gayler, R., Roberts, N.W. and Pratt, H.R.C.
Trans. Instn. Chem. Engrs. 31, 57 (1953)

50 Ghosh, S.K. and Nandi, S.K.
J. Indian Chem. Soc. Ind. and News Edition 12
No. 2, 213 (1950)

51 Gier, T.E. and Hougen, J.O.
Ind. Eng. Chem. 45, 1362 (1953)

52 Gillespie, T. and Rideal, E.K.
Trans. Faraday Soc. 52, 173 (1956)

53 Goldberger, W.M. and Benenati, R.F.
Ind. Eng. Chem. 51, 641 (1959)

54 Griffith, R.M.
Chem. Eng. Sci. 17, 1057 (1962)

55 Grober, H.Z.
Ver. deut. Ing. 69, 705 (1925)

56 Groothius, H. and Kramers, H.
Chem. Eng. Sci. 4, 17 (1955)

57 Groothius, H. and Zuiderweg, F.J.
Chem. Eng. Sci. 19, 63 (1964)

58 Hadamard, M.I.
Academic des Sciences Comptes Reudus 152, 1735 (1911)

59 Handlos, A.E. and Baron, T.
AIChE. J. 3, 127 (1957)

60 Harkins, W.D. and Brown, F.E.
J. Am. Chem. Soc. 41, 499 (1919)

61 Hartland, S.
Chem. Eng. Sci. 22, 1675 (1967)

62 Hartland, S.
Trans. Instn. Chem. Engrs. 46, T275 (1968)

63 Hartland, S. and Wise, G.D.
Trans. Instn. Chem. Eng. 45, T353 (1967)

64 Haydon, D.Z.
Nature 176, 839 (1955)

65 Haydon, D.Z.
Proc. Roy. Soc. A243, (I) 483; (II) 492 (1958)

66 Haynes, L.G., Himmelblau, D.M. and Schecter, R.S.
I and EC. Proc. Des. Dev. 7 No. 4, 508 (1968)

67 Hayworth, C.B. and Treybal, R.E.
Ind. Eng. Chem. 42 No. 6, 1174 (1950)

68 Heertjes, P.M. and De Nie, L.H.
Chem. Eng. Sci. 21, 755 (1966)

69 Heertjes, P.M., Holve, W.A. and Talsma, H.
Chem. Eng. Sci. 3, 122 (1954)

70 Higbie, R.
Trans. Am. Instn. Chem. Engrs. 31, 365 (1935)

71 Hou, H.L. and Franke, N.W.
Chem. Eng. Progr. 45 No. 1, 65 (1949)

72 Hu, S. and Kintner, R.C.
J. Am. Instn. Chem. Engrs. 1, 42 (1955)

73 Hughes, R.R. and Gilland, E.R.
Chem. Eng. Progr. 48, 497 (1952)

74 Ilkovic, D.
Coll. Czech. Chem. Commum. 6, 498 (1934)

75 Izard, J.A.
AIChE. J. 18, 634 (1972)

76 Jeffreys, G.V. and Hawskley, J.L.
AIChE. J. 11, 413 (1965)

77 Jeffreys, G.V. and Lawson, G.B.
Trans. Instn. Chem. Engrs. 42, T294 (1965)

78 Jeffreys, G.V., Mumford, C.J. and Al-Aswad, K.M.
2nd Symposuim of Separation Science and
Technology for Energy Application 16 No. 9, 1217
(1981)

79 Johnson, A.I. and Braida, L.
Can. J. Chem. Eng. 35 No. 4, 165 (1957)

80 Johnson, A.I. and Hamielec, A.E.
AIChE. J. 6, 145 (1960)

81 Kagan, S.Z., Kovalev, Y.U.N. and Zakharychev, A.P.
Theoretical Foundations Chem. Eng. 7, 514 (1973)

82 Katalinic, M.A.
Physik, 38, 511 (1926)

83 Keith, F.W. and Hixson, A.N.
Ind. Eng. Chem. 47 No. 2, 258 (1955)

84 King, C.J., Hsuch, I. and Mao, K.W.
Chem. Eng. Data 10, 348 (1965)

85 Kintner, R.C.
Adv. Chem. Eng. 4, 83 (1963)

86 Klee, A.J. and Treybal, R.E.
AIChE. J. 2, 444 (1956)

87 Krishna Murty, R., Jagannadha Rao, R. and
Venkata Rao, V.C.
Indian J. Technol. 5, 271 (1967)

88 Krishna Murty, R. and Venkata Rao, C
Chem. Age of India 19 No. 2, 106 (1968)

89 Krisma, P.M., Venkanteswarlu, D. and
Narasimharmurty, G.S.R.
J. Chem. Eng. Data 4, 336, 340 (1959)

90 Krishna, R. and Venkata Rao, C.
I & EC. Proc. Des. Dev. 7 No. 2, 166 (1968)

91 Kronig, R. and Brink, J.C.
Appl. Sci. Res. A-2, 142 (1950)

92 Kumar, A. and Hartland, S.
Trans. Instn. Chem. Engrs. 60 No. 1, 35 (1982)

93 Lamb, H.
Hydrodynamic, Dover New York (1945), 6th Edition

94 Lang, S.B. and Wilke, C.R.
Ind. Eng. Chem. Fundamentals 10, 341 (1971)

95 Letan, R. and Kehat, E.
AIChE. J. 13 No. 3, 443 (1967)

96 Levich, V.G.
Physico Chemical Hydrodynamics (Prentice Hall)
Englewood Cliffs. N.J. (1962)

97 Levich, V.G. and Frunkin, A.
Zhur. Fiz. Khim. 21 No. 10, 1183 (1947)

98 Lewis, J.B.
Chem. Eng. Sci. 8, 295 (1958)

99 Lewis, J.B., Jones, I. and Pratt, H.R.C.
Trans. Instn. Chem. Engrs. 29, 136 (1951)

100 Licht, W. and Pansing, W.F.
Ind. Eng. Chem. 45 No. 9, 1885 (1953)

101 Licht, W. and Narasimharmurty, G.S.R.
AIChE. J. 1 No. 3, 366 (1955)

102 Lindland, K.P. and Terjesen, S.G.
Chem. Eng. Sci. 5, 1 (1956)

103 Lochiel, A.C.
Can. J. Chem. Engr. 43, 40 (1965)

104 Mayfield, D.F. and Church, W.L.
Ind. Eng. Chem. 44, 2253 (1952)

105 Meister, B.J. and Scheele, G.F.
AIChE. J. 14 (I) 9; (II) 15 (1968)

106 Meister, B.J. and Scheele, G.F.
AIChE. J. 15 No. 5, 689 (1968)

107 Middleman, S.
Chem. Eng. Sci. 20, 1037 (1965)

108 Misek, T. and Marek, J.
Brit. Chem. Eng. 15, 202 (1970)

109 Morello, V.S. and Poffenberger, N.
Ind. Eng. Chem. 42 No. 6, 1021 (1950)

110 Moulton, R.W. and Walkey, J.E.
Trans. Am. Instn. Chem. Engrs. 40, 695 (1944)

111 Mugele, R.A. and Evans, H.D.
Ind. Eng. Chem. 43 No. 6, 1317 (1951)

112 Mumford, C.J.
Brit. Chem. Eng. 13 No. 7, 961 (1968)

113 Mumford, C.J. and Al-Hemiri, A.A.A.
Proc. Intern. Solvent Extrn. Conf. Lyon (ISEC)
2, 1591 (1974)

114 Murall, K. and Rao, M.J.R.
J. Chem. Eng. Data 7, 468 (1962)

115 Muyanchi, T.
AIChE. J. 11, 395 (1965)

116 Muyanchi, T. and Vermeulen, T.
Ind. Eng. Chem. Fundamentals 2, 304 (1963)

117 Newman, A.B.
Trans. Am. Instn. Chem. Engrs. 27, 203 (1931)

118 Nielson, L.E., Wall, R. and Adams, G.
J. Colloid Sci. 13, 441 (1958)

119 Null, H.R. and Johnson, H.F.
AIChE. J. 4 No. 3, 273 (1958)

120 Olander, D.R.
AIChE. J. 7, 175 (1961)

121 Olney, R.B.
AIChE. J. 10, 827 (1964)

122 Perrut, M. and Loutaty, R.
Chem. Eng. J. 3, 286 (1972)

123 Perry, R.H. and Chilton, C.H.
Chem. Eng. hand book McGrawhill 5th Edition 1973

124 Popovich, A.T., Jervis, R.E. and Trass, O.
Chem. Eng. Sci. 19, 357 (1964)

125 Pratt, H.R.C.
Ind. Eng. Chem. Proc. Des. Dev. 15 No. 4, 554 (1976)

126 Pyle, C., Colburn, A.P. and Duffey, H.R.
Ind. Eng. Chem. 42, 1042 (1950)

127 Rayleigh, Lord. "On the Instability of Jets",
Proc. London Math. Soc. 10, 4 (1879)

128 Rod, V.
Brit. Chem. Eng. 11 No. 6, 483 (1966)

129 Rose, P.M. and Kintner, R.C.
AIChE. J. 12 No. 3, 530 (1966)

130 Row, S.B., Koffolt, J.H. and Withrow, J.R.
Trans. Am. Instn. Chem. Engrs. 37, 559 (1941)

131 Ruby, C.L. and Elgin, J.C.
Chem. Eng. Progr. Symp. Ser. 51 No. 16, 17 (1955)

132 Satapathy, R. and Smith, W.
J. Fluid Mechanics 19, 561 (1961)

133 Savic, P.
Nat. Res. Council Can. Rept. No. MT.22 Ottawa (1953)

134 Sawistowski, H. and Goltz, G.E.
Trans. Instn. Chem. Engrs. 41, 174 (1963)

135 Schecter, R.S. and Farley, R.W.
Can. J. Chem. Eng. 41, 103 (1963)

136 Schroeder, R.R. and Kintner, R.C.
AIChE. J. 11, 5 (1965)

137 Schiebel, E.G.
Ind. Eng. Chem. 46, 2007 (1954)

138 Scriven, L.E. and Sternling, C.V.
Nature 187, 186 (1960)

139 Sherwood, T.K. and Wei, I.C.
Ind. Eng. Chem. 49, 1030 (1957)

140 Skelland, A.H.P. and Caenepeel, C.L.
AIChE. J. 18 No. 6, 1134 (1972)

141 Skelland, A.H.P. and Huang, Y.F.
AIChE. J. 23 No. 5, 701 (1977)

142 Skelland, A.H.P. and Huang, Y.F.
AIChE. J. 25 No. 1, 80 (1979)

143 Skelland, A.H.P. and Minhas, S.S.
AIChE. J. 17 No. 6, 1316 (1971)

144 Sleicher, C.A.
AIChE. J. 5, 145 (1959)

145 Smith, A.R., Caswell, J.E., Larson, P.P. and Carvers, S.D.
Can. J. Chem. Eng. 41, 150 (1963)

146 Thakar, N.S. and Othmer, D.F.
Ind. Eng. Chem. 45, 589 (1953)

147 Thornton, J.D.
Chem. Eng. Sci. 5, 201 (1956)

148 Thornton, J.D.
Trans. Instn. Chem. Engrs. 35, 316 (1957)

149 Thornton, J.D. and Ramshaw, C.
Instn. Chem. Engrs. Symp. Series No. 26, 73 (1967)

150 Thornton, J.D. and Ramshaw, C.
Instn. Chem. Engrs. Symp. Series No. 26, 86 (1967)

151 Tomotika, S.
Proc. Roy. Soc. A150, 322 (1935)

152 Treybal, R.E.
AIChE. J. 4, 202 (1958)

153 Treybal, R.E.
Liquid Extraction, McGraw Hill, 2nd Edition (1963)

154 Treybal, R.E.
"Mass Transfer Operation" p378-9 McGrawhill, N.Y. 1955, 1st Edition.

155 Treybal, R.E. and Dumoulin, F.E.
Ind. Eng. Chem. 34 No. 6, 709 (1942)

156 Van de Akker, H.E.A.
Chem. Eng. J. 19, 255 (1980)

157 Vermeuleu, T.
Ind. Eng. Chem. 45, 1664 (1953)

158 Wagner, C.
Metal Trans. 4, 91 (1952)

159 Warshay, M., Boguez, E., Johnson, M. and Kintner, R.C.
Can. J. Chem. Engr. 37, 29 (1959)

160 Weber, C. and Angew, Z.
Math. Mech. 11, 136 (1931)

161 Wellek, R.M., Agrawal, A.K. and Skelland, A.H.P.
AIChE. J. 12 No. 5, 854 (1966)

162 Wilke, C.R. and Chang, P.
AIChE. J. 1, 264 (1955)

163 Meister, B. J. and Scheele, G. F.
AIChE. J. 15, No. 5, 689 (1969)

164 Licht, W. and Conway, J. B.
Ind. Eng. Chem. 42, No. 6, 1151 (1950)